

Remote C-H Functionalization and Photochromic Properties Investigation of 3*H*-Naphthopyrans

vorgelegt von
Master of Science
Longying Qi

von der Fakultät II - Mathematik und Naturwissenschaften
der Technischen Universität Berlin
zur Erlangung des akademischen Grades

Doktor der Naturwissenschaften
- Dr. rer. nat. -

genehmigte Dissertation

Promotionsausschuss:

Vorsitzender: Prof. Dr. Michael Gradzielski

Gutachterin: Prof. Dr. Karola Rück-Braun

Gutachter: Prof. Dr. Bernd Schmidt

Tag der wissenschaftlichen Aussprache: 04. Dezember 2020

Berlin 2020

Die vorliegende Arbeit wurde
unter der Leitung von Frau Prof. Dr. Karola Rück-Braun
in der Zeit von Sep. 2016 bis Sep. 2020
im Institut für Chemie der Fakultät II
der Technischen Universität Berlin angefertigt

Abstract

Naphthopyrans, as an important class of organic photochromic compounds, have a wide application in ophthalmic lenses and other fields, such as molecular electronic devices, photochromic thin films, etc. The substituents have a great influence on the photochromic behaviors of naphthopyrans. Hence, the research about relationship between substituents and photochromic properties as well as the methods on introducing different substituents to naphthopyrans will lead to a better understanding on the design of naphthopyrans in the industry.

Selective C-H functionalization is a significant organic synthesis method, but it has not been adopted on naphthopyrans. Especially the distant selective C-H functionalization, it is still a challenge for naphthalenes. Thus, the first part of this thesis is exploring selective C-H functionalization of naphthopyrans involving two different methods. The first method is directed C-H functionalization. Selective *meta*-C-H (C4-H) and C5-H functionalization of naphthalenes were achieved with route 1. Selective C6-H functionalization of naphthopyrans was carried out with route 2. However, the second method, nondirected C-H functionalization lead to a mixture of different substituted products.

The second part of this thesis is the investigation on photochromic properties of different substituted 3*H*-naphthopyrans, which is focused on the effects of 8-, 6- and 3-substituents. Room temperature UV/Vis absorption spectroscopy and low temperature *in-situ* NMR measurements were applied. Kinetic analysis was conducted successfully in different solvents during UV irradiation, thermal relaxation and irradiation with visible light. The rate constants of different processes were calculated and demonstrated to be impacted greatly by substituents.

Kurzzusammenfassung

Naphthopyrane sind eine wichtige Klasse organischer photochromer Verbindungen mit weitreichenden Anwendungen in augenoptischen Gläsern und Linsen sowie auf anderen Gebieten, z.B. in molekularen elektronischen Instrumenten, photochromen dünnen Filmen usw.. Substituenten haben einen großen Einfluss auf das photochrome Verhalten von Naphthopyranen. Somit führen experimentelle Untersuchungen, die eine Beziehung zwischen Substituenten und photochromen Eigenschaften herstellen, und Methoden zur Einführung von verschiedenen Substituenten an Naphthopyranen, zu einem besseren Verständnis für das Design industriell relevanter Naphthopyrane.

Die selektive C-H Funktionalisierung ist eine signifikante organisch-synthetische Methode, die bislang auf Naphthopyrane kaum angewendet wurde. Insbesondere die weitreichende selektive C-H Funktionalisierung ist im Fall von Naphthalinen noch eine Herausforderung. Im ersten Teil der vorliegenden Promotionsschrift werden daher selektive C-H-Funktionalisierungen von Naphthopyranen über zwei verschiedene Methoden beschrieben. Die erste Methode ist eine dirigierende C-H Funktionalisierung. Hierbei wurde die *meta*-C-H (C4-H) und C5-H Funktionalisierung von Naphthalinen über Route 1 untersucht. Die selektive C6-H Funktionalisierung von Naphthopyranen wurde über Route 2 ebenfalls untersucht und erfolgreich ausgeführt. Außerdem wurde über die zweite Methode die nicht-dirigierende C-H Funktionalisierung von Naphthalinen erprobt, die allerdings eine Mischung verschiedener Verbindungen ergab.

Im zweiten Teil der Promotionsarbeit werden die photochromen Eigenschaften verschiedener 3*H*-Naphthopyrane untersucht und vorgestellt, wobei der Fokus auf den Einflüssen von 8-, 6- und 3-Substituenten liegt. UV/Vis-spektroskopische Untersuchungen bei Raumtemperatur und Tieftemperatur *in-situ* NMR Untersuchungen wurden durchgeführt. Kinetische Untersuchungen und Analysen wurden in verschiedenen Lösungsmitteln unter UV-Bestrahlung, thermischer Relaxation und unter Bestrahlung mit sichtbarem Licht ausgeführt. Die Geschwindigkeitskonstanten wurden ermittelt, und es konnte gezeigt werden, dass die Substituenten eine große Auswirkung auf die verschiedenen Prozesse zeigen.

Abbreviations

A	Absorbance
AP	Allenyl-naphthol
Ar	Aryl
APCI	Atmospheric pressure ionisation
ⁱ Bu	<i>iso</i> -butyl
^t Bu	<i>tert</i> -butyl
c	Concentration
CF	Closed form
COSY	Correlation spectroscopy
d	Doublet
DCE	1,2-Dichloroethane
DCM	Dichloromethane
DEPT	Distortionless enhancement by polarization transfer
DG	Directing group
DMF	Dimethylformamide
DMS	Dimethyl sulfide
DMSO	Dimethyl sulfoxide
EA	Ethyl acetate
eq.	Equivalent
ESI	Electrospray ionization
Et	Ethyl
h	Hour
HFIP	Hexafluoroisopropanol
HMBC	Heteronuclear multiple bond correlation
HMQC	Heteronuclear multiple-quantum correlation
HRMS	High resolved mass spectrometry
LDA	Lithium diisopropylamide
m	Multiplet
<i>m</i> -	<i>meta</i> -
M	mol/L

Me	Methyl
min	Minute
MOMCl	Chloromethyl methyl ether
Mp	Melting point
NBS	<i>N</i> -bromosuccinimide
NFSI	<i>N</i> -fluorobenzenesulfonimide
NMR	Nuclear magnetic resonance
ppm	Parts per million
PPTS	Pyridinium <i>p</i> -toluenesulfonate
PSS	Photostationary state
q	Quartet
R _f	Retention factor
r.t.	Room temperature
s	Singlet
t	Triplet
t _{1/2}	half-life (azobenzenes etc), or the time taken from absorbance to reduce by 1/2 of the initial absorbance (naphthopyrans)
t _{3/4}	The time taken from absorbance to reduce by 3/4 of the initial absorbance
t _{pss}	The time to arrive at the PSS
TC	<i>Transoid-cis</i>
TCE	Tetrachloroethene
THF	Tetrahydrofuran
TLC	Thin layer chromatography
TMS	Trimethylsilyl group
TT	<i>Transoid-trans</i>
UV	Ultraviolet
Vis	Visible
λ _{iso}	The wavelength at the isosbestic point
λ _{max}	The absorption maximum

Table of Contents

Abstract.....	i
Kurzzusammenfassung.....	ii
Abbreviations	iii
1. Introduction.....	1
1.1 Photochromism.....	1
1.1.1 Naphthopyrans.....	3
1.1.2 Synthesis of Naphthopyrans	6
1.1.3 Structure and Characterisation of 3 <i>H</i> -Naphthopyrans	8
1.1.4 Photochromic Properties of 3 <i>H</i> -Naphthopyrans Varied with Substituents.....	15
1.1.5 Applications of 3 <i>H</i> -Naphthopyrans	22
1.2 <i>Meta</i> -C-H Functionalization of Benzene	23
1.3 Distant Selective-C-H Functionalization of Naphthalene.....	27
2. Aim and Strategy	31
3. Synthesis of Remote Selective C-H Functionalization of Naphthopyrans.....	33
3.1 Method I : Directed Selective C-H Functionalization	33
3.1.1 Route 1 of the Synthesis	34
3.1.2 Route 2 of the Synthesis	47
3.2 Method II : Nondirected <i>Meta</i> -C-H Functionalization	54
3.3 Discussion.....	58
3.3.1 The Selection for C-H Functionalization of Naphthopyran N6	58
3.3.2 The Failure for Formation of Naphthopyran 21 in Route 1 of Method I	59
4. UV/Vis Spectroscopy	61
4.1 UV/Vis Studies of Two States System: Naphthopyrans N1, N2, N3 and N4.....	61
4.1.1 UV Irradiation	61
4.1.2 Thermal Back Reaction.....	63
4.1.3 Visible Light Irradiation	67
4.1.4 Solvent Effect on the Photochromic Properties	68
4.2 UV/Vis Studies of Three States System: Naphthopyrans N5 and N6.....	72

4.2.1 UV Irradiation	72
4.2.2 Thermal Back Reaction.....	73
4.2.3 Visible Light Irradiation	76
4.3 UV/Vis Studies of C-H Functionalization Product N7.....	78
4.3.1 UV Irradiation	78
4.3.2 Thermal Back Reaction.....	79
4.3.3 Visible Light Irradiation	80
4.4 UV/Vis Studies of Naphthopyrans N8, N9 and N10	82
4.5 Discussion.....	84
4.5.1 The Effect of 8-Substituent on the Photochromic Properties of Naphthopyrans.	84
4.5.2 Comparison between Two States System and Three States System	85
4.5.3 The Effect of 6-Substituent on Photochromic Properties of Naphthopyran.....	86
5. <i>In-situ</i> NMR Analysis	89
5.1 <i>In-situ</i> ¹ H NMR Analysis of Two States System: Naphthopyran N1, N3 and N4	89
5.1.1 Structural Identification of Different Isomers of N1.....	89
5.1.2 Structural Identification of Different Isomers of N3.....	92
5.1.3 Structural Identification of Different Isomers of N4.....	94
5.1.4 Kinetic Analysis of N1, N3 and N4 during Different Processes.....	96
5.2 <i>In-situ</i> ¹⁹ F NMR analysis of Three States System: Naphthopyran N5 and N6.....	100
5.3 Investigation of Visible Light Wavelength Influence on PSS _{vis} of N7 by <i>In-situ</i> ¹⁹ F NMR analysis.....	105
5.4 <i>In-situ</i> ¹ H NMR analysis of Naphthopyrans N8, N9 and N10	109
5.5 Discussion	111
5.5.1 The Different Performance between Two States System and Three States System during the Low Temperature <i>in-situ</i> NMR Measurements.....	111
5.5.2 The Effect of 6-Substituent on Photochromic Properties of Naphthopyran during the Visible Light Irradiation in Low Temperature <i>in-situ</i> NMR Measurements.....	113
6. Summary and Outlook	115
6.1 The Synthesis of Naphthopyrans by Selective C-H Functionalization.....	115
6.2 The Photochromic Properties of 3 <i>H</i> -Naphthopyrans	118
6.3 Outlook.....	124
7. Experimental Section.....	125

7.1 Synthesis	125
7.1.1 General Information	125
7.1.2 Procedure	126
7.2 UV/Vis Absorption Spectroscopy	150
7.2.1 General Information	150
7.2.2 Time-Resolved Experiments and Exponential Fitting	154
7.3 <i>In-situ</i> NMR Measurement	161
8. Appendix	163
8.1 ^1H and ^{13}C NMR Spectra	163
8.2 2D NMR Spectra	189
8.3 UV Absorption Spectra	195
8.4 <i>In-situ</i> NMR Spectra	204
9. Reference	213

1. Introduction

1.1 Photochromism

“Photochromism” was used firstly in 1950, when Hirshberg proposed the term “Photochromism” [from the Greek words: *phos* (light) and *chroma* (color)] to depict the phenomenon that compounds changed color under light irradiation and returned to the initial color in the dark.^[1] However, at present, “Photochromism” is defined as “a reversible transformation of a chemical species induced in one or both directions by absorption of electromagnetic radiation between two forms, which have different absorption spectra” (Figure 1.1).^[2] For most photochromic compounds, $\lambda_{\max}(A) < \lambda_{\max}(B)$ and the phenomenon is regarded as positive photochromism. Otherwise, it is negative (reverse) photochromism.

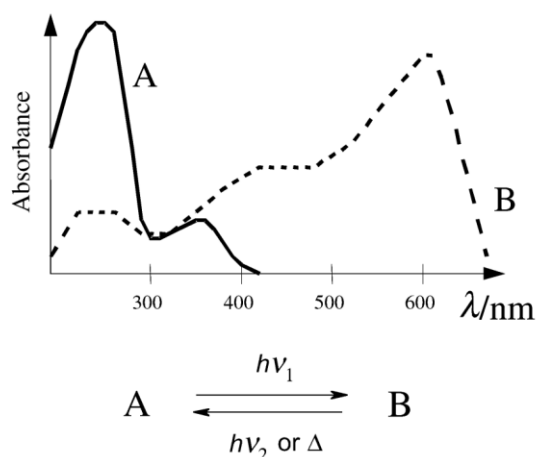


Figure 1.1 General photochromic behavior according to the definition of positive photochromism.
Copyright © 2001, International Union of Pure and Applied Chemistry.

Light is an excellent stimulus due to its several advantages: it is non-toxic, an unlimited energy source and can be delivered fast with high spatial and temporal control. Since the first example of Photochromism was reported in 1867,^[3] all kinds of photochromic compounds have been published. Based on the back reaction, they can be divided into two types. If the compounds are thermally reversible, they are T-type photochromic compounds (or photoswitches). If the photochromic molecules are thermally irreversible but photochemically reversible, they are P-type photochromic compounds. Various prevalent photochromic compounds of these two types are demonstrated in Figure 1.2.

1.1 Photochromism

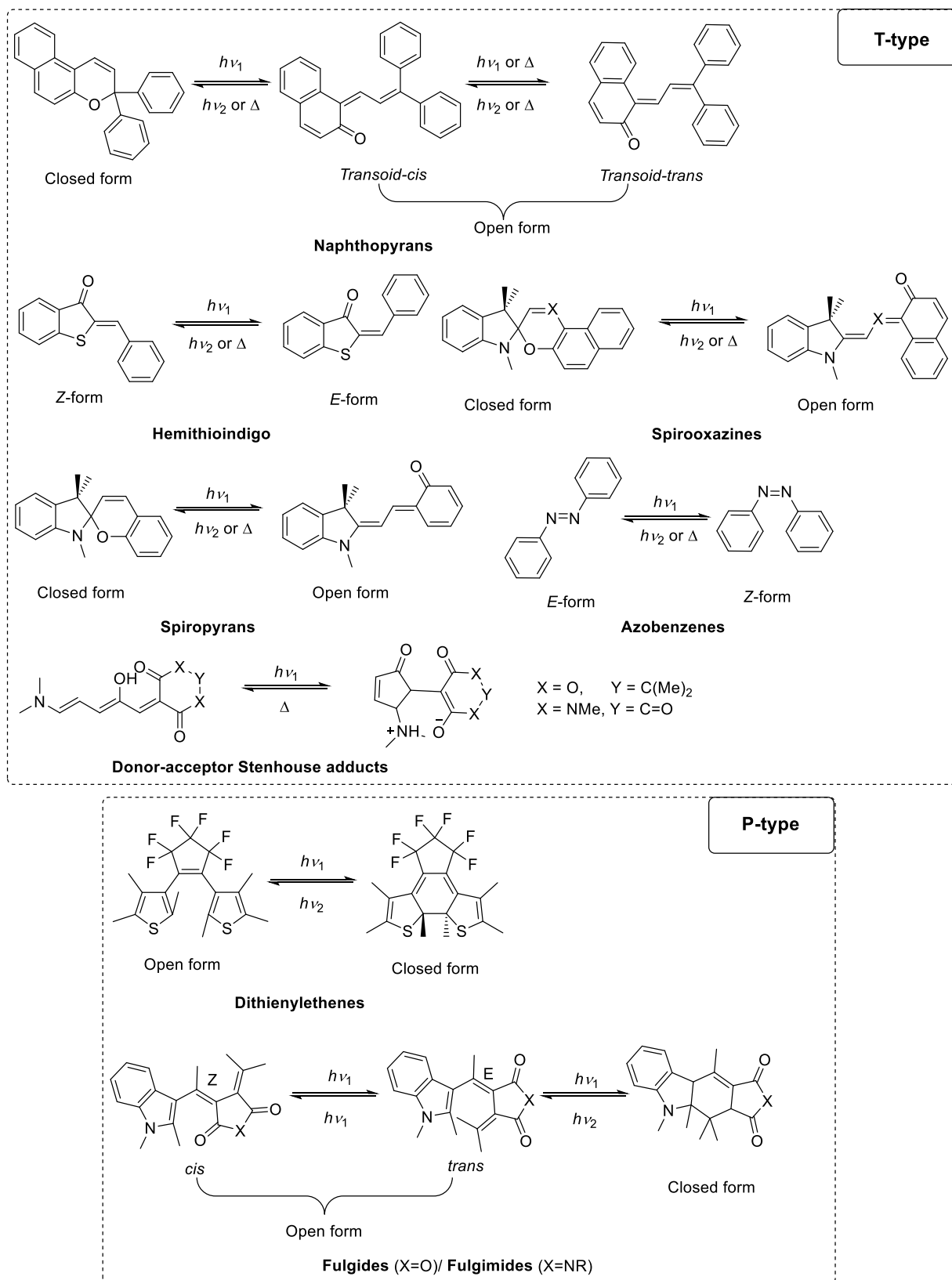


Figure 1.2 Different photochromic compounds of T-type and P-type.

Six different chemical processes are found during photochromism, including pericyclic reaction, *cis-trans* (*E/Z*) isomerizations, intramolecular hydrogen transfer, intramolecular group transfers, dissociation processes and electron transfer (oxido-reduction),^[2] wherein pericyclic reactions and *cis-trans* (*E/Z*) isomerizations are involved in the prevalent photochromic compounds presented in Figure 1.2 upon irradiation with light. For T-type photochromic compounds, spiropyrans and spirooxazines undergo 6π six atom electrocyclization ring opening reactions; hemithioindigo and azobenzenes go through *cis-trans* (*E/Z*) isomerizations; naphthopyrans undergo 6π six atom electrocyclization ring opening reactions followed by *cis-trans* (*E/Z*) isomerizations; donor-acceptor Stenhouse adducts (DASA) go through 4π electrocyclization ring closure reactions, which are also a kind of negative photoswitches. For P-type photochromic compounds, closed forms of dithienylethenes are obtained through 6π six atom electrocyclization ring closure reactions; Fulgides and related compounds go through *cis-trans* (*E/Z*) isomerizations followed by ring closure reaction.

Photochromic compounds have wide applications, such as optical data storage, fluorescence microscopy imaging, ophthalmic lenses, smart windows and biomaterials by incorporation into surfaces, peptides, polymers, enzymes, proteins and amino acids, because of the variation in photophysical and photochemical properties between isomers of photochromic compounds.^[4-10]

1.1.1 Naphthopyrans

Naphthopyrans, as a kind of chromene derivatives, were firstly reported by Becker and Michl in 1966.^[11] Chromenes are a kind of T-type photochromic compounds. As reported in the literature, photochromism of chromenes was observed and it was also found that the lifetime of colored isomers of chromenes was enhanced by the annulation of an additional benzene ring. In addition, it was reported that the stability of colored isomers was also increased by the conjugation substituents at the sp^3 -C-atom adjacent to the oxygen atom. Afterwards, the naphthopyrans with two aryl substituents attached to sp^3 -C-atom developed into currently the popular system of photochromic naphthopyrans.

There are three types of naphthopyrans, wherein *2H*-naphtho[1,2-*b*]pyrans and *3H*-naphtho[2,1-*b*]pyrans are the main research objects of photochromic behavior, resulting from few useful photochromic responses demonstrated for *2H*-naphtho[2,3-*b*]pyran.^[12]

1.1 Photochromism

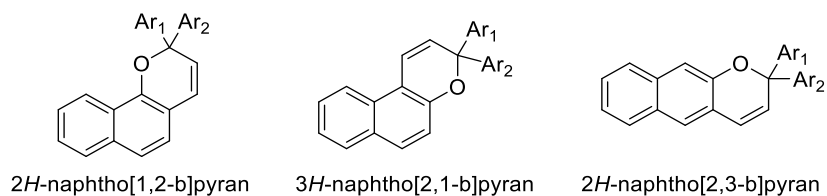


Figure 1.3 Different types of naphthopyrans.

After UV irradiation, the colorless naphthopyrans can change into colored open forms, resulting from the more bathochromic absorption spectrum of these colored open forms (Figure 1.4).^[13,14] Based on the mechanism investigation using femo-to-picosecond transient absorption spectroscopy by Guglielmetti and co-workers^[15,16], UV light excites the ground state (A) of the closed form of 3*H*-naphthopyran into one of its singlet excited states (ⁿA*). Then it decays to the first excited state (¹A*). The molecular conversion into a primary isomer (B₁) through a conical intersection and the cleavage of the C-O bond is observed in 450 fs. B₁ is short-lived and converts into the one of the trans-isomers (B₂) in 2 ps. At last, another trans-isomer (B₃) is formed through isomerization in 21 ps (Figure 1.5).

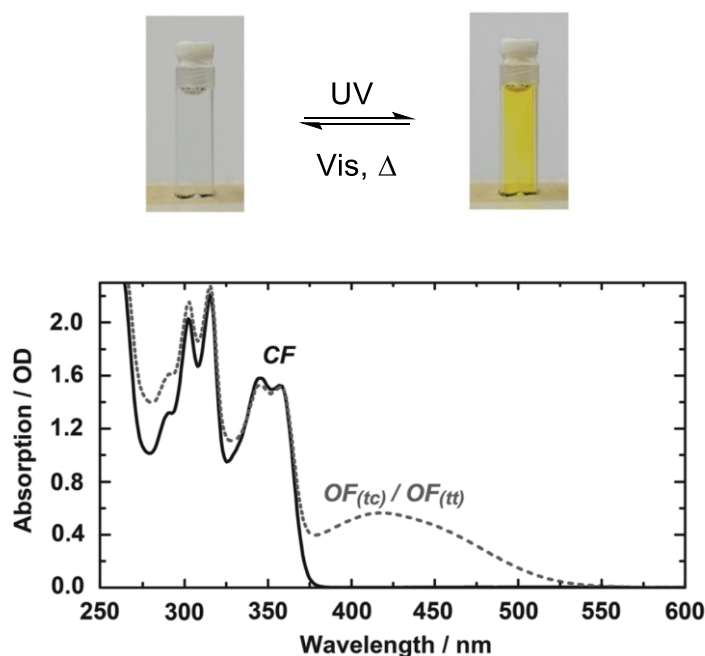


Figure 1.4 Color change (up) and absorption spectral changes of 2,2-diphenyl-3*H*-naphtho[2,1-*b*]pyran in acetonitrile after UV irradiation (down). Copyright © 2013, The Royal Society of Chemistry.

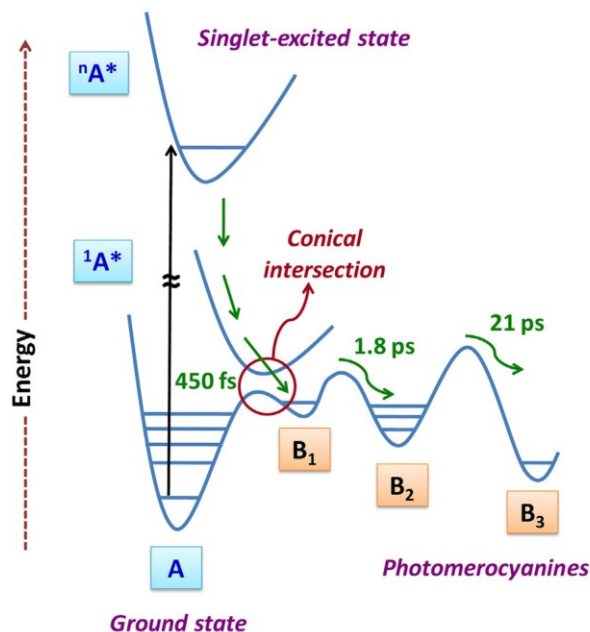


Figure 1.5 The energy diagram of the ring opening mechanism^[16]. Copyright © 2016, Elsevier B.V.

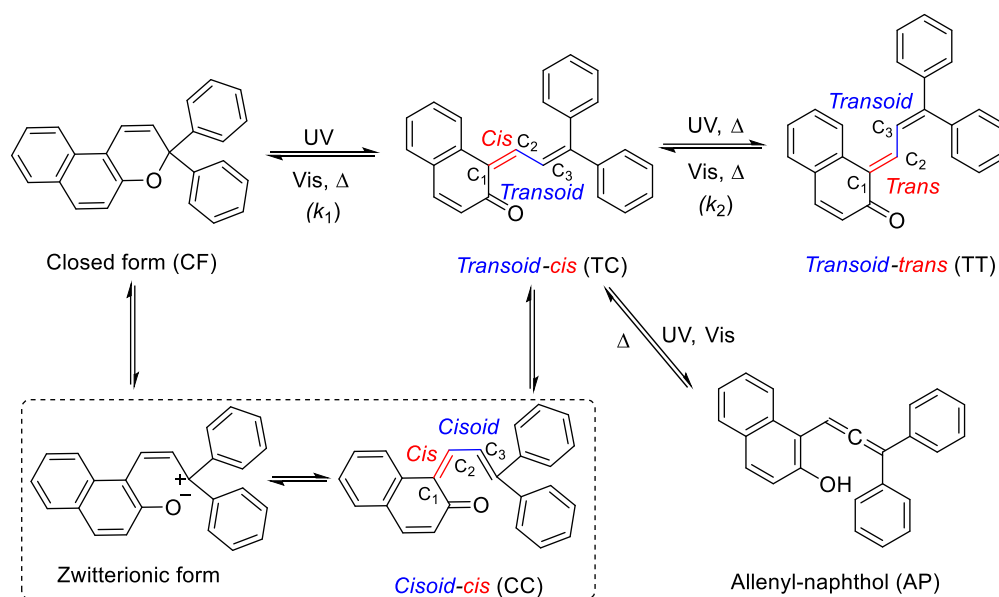


Figure 1.6 Generic photochromic and thermal relaxation processes of naphthopyrans.

Further mechanisms have also been studied.^[16] Upon UV irradiation, the cleavage of the C(sp³)-O bond appears, resulting in the short-lived CC form and was followed by the formation of the colored thermally unstable TC (*transoid-cis*) form through rotation of the single C₂-C₃ bond (from *cisoid* to *transoid*). Meanwhile, the TC form can revert to the long-lived TT (*transoid-trans*) form through rotation of the C₁=C₂ double bond under UV irradiation. If the aryl substituents attached

to the C(sp³)-atom are different, there will exist TTC, TTT, TCC and TCT forms. In addition, the allenyl-naphthol (AP) isomer was detected by Delbaere and co-workers,^[17,18] and the AP form can be reverted from the TC form under irradiation with UV or visible light. On the other hand, in the dark, the AP form can be reverted back to the TC form easily, and the TC form can be reverted back to the CF form (closed form) rapidly. By contrast, the thermal transformation from TT to TC is much slower. But faster conversion is observed under visible light irradiation (Figure 1.6).

1.1.2 Synthesis of Naphthopyrans

The earliest publication about the synthesis of naphthopyrans with two aryl substituents was reported by Livingstone and co-workers in 1960, in which aryl Grignard reagents were employed and 3*H*-naphthopyrans were obtained in moderate yield. But a byproduct was also detected at the same time (Figure 1.7).^[19–21]

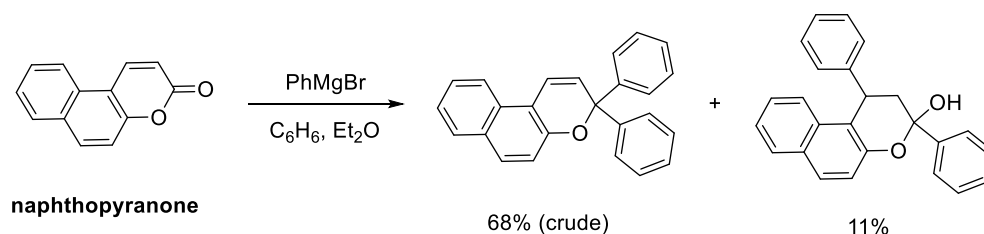


Figure 1.7 The synthesis of naphthopyrans from naphthopyranones.

In 1983, Talley reported a synthetic method for dimethyl substituted 3*H*-naphthopyrans from α,β -unsaturated aldehydes and ketones in the presence of *n*-BuLi.^[22] Afterwards, this method was developed by Heller to synthesize diaryl substituted 2*H*-naphthopyrans with different substituents (R¹) at 1-position. But the method is limited by the nature of the α,β -unsaturated aldehydes (Figure 1.8).^[23] Similar methods were also used for the synthesis of naphthopyrans with a benzothiophene ring in the presence of *n*-BuLi.^[24–26]

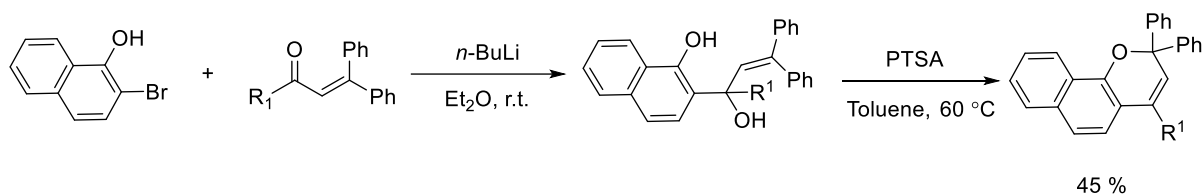


Figure 1.8 The synthesis of naphthopyrans from α,β -unsaturated aldehydes.

The most successful method is based on Claisen rearrangement of naphthyl propargyl ethers. The first publication about synthesis of naphthopyrans involving this method was reported by Iwai and Ide in 1962.^[27,28] Naphthopyrans were prepared from naphthol and propargyl bromide in two steps (Figure 1.9).

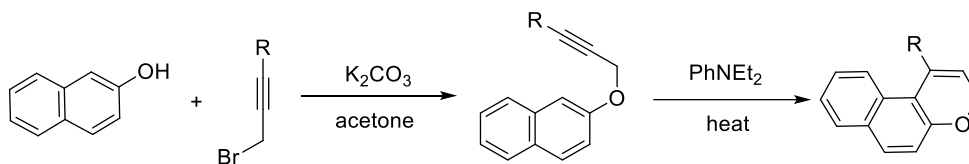


Figure 1.9 The two steps synthesis from propargyl bromide and naphthol.

In 1991, synthesizing diaryl naphthopyrans in a single step was achieved from naphthol and propargyl alcohol catalyzed by *p*-toluenesulfonic acid (PTSA) (Figure 1.10).^[29] In this method, naphthyl propargyl ethers were formed *in-situ* from naphthol and propargyl alcohol under acid catalysis, then naphthopyrans were generated through Claisen rearrangement.

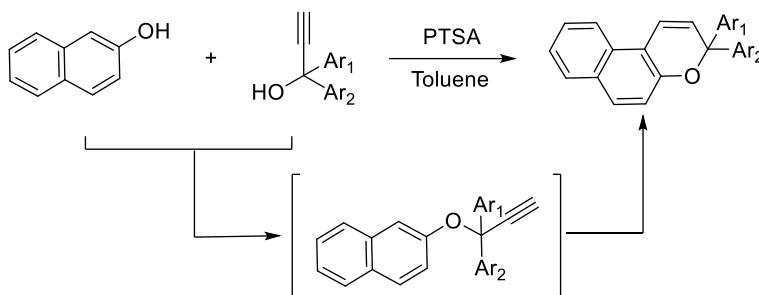


Figure 1.10 The one pot-multi step synthesis from propargyl alcohol and naphthol.

This method was adopted and developed by many other groups. Solid-state synthesis of naphthopyrans was achieved.^[30] The acid aluminium oxide and pyridinium *p*-toluenesulfonate (PPTS) as the catalyst can also work well.^[31,32] However, the yields were always low or moderate due to the formation of by-products (Figure 1.11). Wherein byproduct **A** was generated through Meyer-Schuster rearrangement of the propargyl alcohol and byproduct **B** was generated through [1,7]-H-shift.^[31,33] Surprisingly, the addition of (MeO)₃CH as a dehydrating agent improved the reaction to an excellent yield under the PPTS catalysis and the scope of this method is very wide (Figure 1.12).^[34]

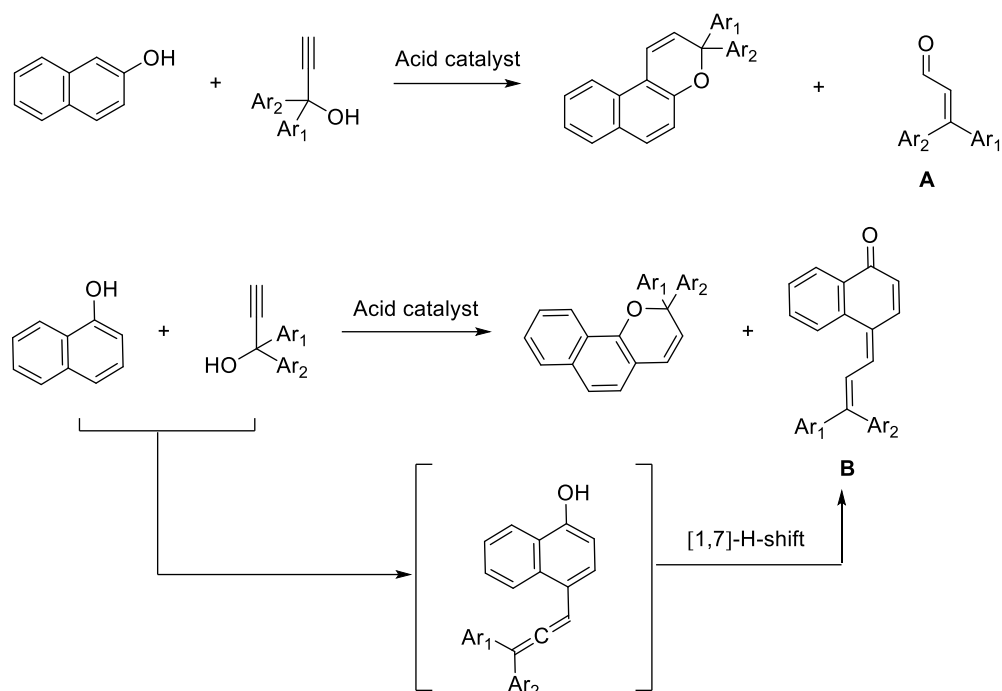


Figure 1.11 Generation of by-products through acid catalyzed synthesis of naphthopyrans.

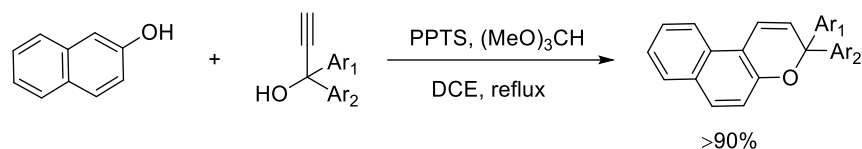


Figure 1.12 The synthesis of naphthopyrans with addition of (MeO)₃CH.

1.1.3 Structure and Characterisation of 3*H*-Naphthopyrans

1.1.3.1 UV/Vis Spectroscopy

There exist totally different UV absorption spectra for naphthopyrans before and after UV irradiation, hence UV/Vis spectroscopy is the main method to investigate the photochromic properties of naphthopyrans. The UV absorption spectra of closed and open forms can be obtained and maxima wavelengths of absorption (λ_{\max}) can be observed. Therefore, we can get the colorability, half-life ($t_{1/2}$) of different substituted naphthopyrans and then proceed to the kinetic investigation.

- Colorability

Colorability is the ability to produce coloration for a colorless or slightly colored photochromic material.^[2]

$$A_0(\lambda) = k \Phi_{\text{col}} \varepsilon_B C_A$$

$A_0(\lambda)$ is the initial absorbance at a given irradiation wavelength, Φ_{col} is the coloration quantum yield, ε_B is the molar absorption coefficient of the colored form, C_A is the concentration of the colorless form and k is the proportionality constant.^[35]

- Half-life

Half-life ($t_{1/2}$) is defined as the time taken from absorbance to reduce by $\frac{1}{2}$ of the initial absorbance during thermal relaxation.

- Kinetic investigation

When the λ_{max} of open forms are detected after UV irradiation, time resolved absorbance curves can be recorded at λ_{max} . Then the speed of ring opening and ring closure reaction can be calculated. For thermal fading rate, we are considering two processes: a. $\text{TC} \rightarrow \text{CF}$ and b. $\text{TT} \rightarrow \text{TC}$, which exist in the procedure at the same time, thermal back rate constants k_1 and k_2 can be calculated by fitting the absorbance curve to a biexponential decay (**Equation 1**).^[36–42]

$$A(t) = A_1 \exp(-k_1 t) + A_2 \exp(-k_2 t) + A_{\text{th}} \quad (1)$$

Where $A(t)$ is the absorbance at the λ_{max} , A_1 and A_2 are contributions to the initial absorbance A_0 , k_1 and k_2 are rate constants of fast and slow components, respectively. A_{th} is the residual absorbance when time approaches infinity. In addition, Abe group thinks the ratios of TT forms in the photostationary state (PSS) can be calculated through $A_2 / (A_1 + A_2)$.^[43,44]

However, if k_2 is far slower than k_1 ($k_2 \ll k_1$), there will be residual color left after thermal relaxation until prolonging enough thermal time due to the long-lived TT form. Correspondingly, the thermal fading curve is a monoexponential decay in the beginning stage of thermal back period, and k_1 can be obtained through fitting absorbance curves to a first order exponential decay (**Equation 2**).^[45,46]

$$A(t) = A_1 \exp(-kt) + A_{th} \quad (2)$$

Where $A(t)$ is the absorbance at the λ_{max} , A_1 is the contributions to the initial absorbance A_0 , k is rate constants of fast components, and A_{th} is the residual absorbance at the termination of testing time.

Furthermore, to explore the photochromic properties of different naphthopyrans, the measurements should be carried out in the same solvent and at the same temperature, considering temperature and solvent will influence the photochromic behaviors a lot.^[12,47] The photochromic properties vary with substituents through UV/Vis spectroscopy and will be discussed in Chapter 1.1.4.

1.1.3.2 *In-Situ NMR Spectroscopy*

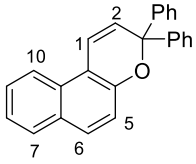
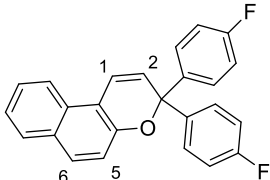
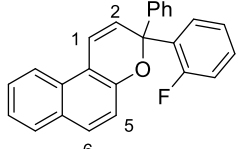
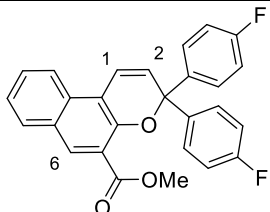
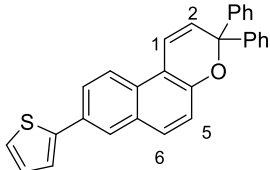
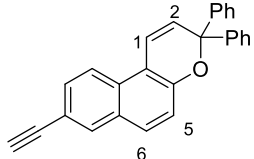
Because at least two new isomers are formed in the system of naphthopyrans after UV irradiation, spectral overlapping between different isomers makes it difficult to explore the photochromic properties of every isomer with UV/Vis spectroscopy. Thus, *in-situ* NMR spectroscopy is a more powerful method to investigate the photochromic behavior of naphthopyrans.^[48] Meanwhile, low temperature *in-situ* NMR measurements provide us a viable method for the detection of naphthopyrans which have a very fast thermal fading rate.

The chemical shifts of different substituted 3*H*-naphthopyrans are depicted in Table 1.1. It is revealed that the identifiable peaks of open forms are 1-position, 2-position and 5-position of protons. In general, the H-2 of TC forms appears at the lowest field around 9 ppm because of the deshielding caused by C=O, and H-1 of TT form is at the lowest field in its spectrum. The H-2 and H-1 are used as fingerprint for the presence of TC and TT form, respectively.^[48] The H-5 of both open isomers moves to a higher field around 6.4 ppm from a low field in the closed form.

Moreover, the allenyl-naphthol (AP) isomer of 3*H*-naphthopyrans was discovered by Delbaere and co-workers via NMR spectroscopy at low temperature.^[17,18] Its identifiable peak is the –OH, which generally appears at approximately 10 ppm.

1 Introduction

Table 1.1 Selected chemical shifts of reported 3*H*-naphthopyrans.

Naphthopyran	Chemical shift/ ppm			
	CF	TC	TT	AP
 NP1^a	H1 = 7.47 H2 = 6.56 H5 = 7.31 H6 = 7.81 H7 = 7.83 H10 = 8.08	H1 = 7.75 H2 = 8.43 H5 = 6.41 H6 = 7.59 H7 = 7.49 H10 = 7.59	-	H1 = 7.84 H5 = 7.44 H6 = 7.97 H7 = 8.02 H10 = 8.52 OH = 10.06 ^b
 NP2^a	H1 = 7.48 H2 = 6.46 H5 = 7.28 H6 = 7.81 F = -114.98	H1 = 7.68 H2 = 8.40 H5 = 6.41 H6 = 7.64 F = -111.96, -112.49	H1 = 7.99 H2 = 7.50 H5 = 6.32 H6 = 7.64 F = -112.10, -112.12	H1 = 7.68 H5 = 7.30 H6 = 7.81 OH = 9.83 F = -115.2 ^c
 NP3^d	-	H2-CTC = 8.66 F-CTC = -112.47 H2-TTC = 8.24 F-TTC = -112.66	H5-CTT = 6.29 F-CTT = -112.62 H5-TTT = 6.31 F-TTT = -112.55	H1 = 7.70 H5 = 7.30 H6 = 7.84 OH = 9.90 F = -112.2 ^c
 NP4^c	F = -113.7	F = -110.1 -110.6	F = -109.5 -110.4	F = -113.6
 NP5^f	-	H1 = 7.74 H2 = 9.31 H5 = 6.50 H6 = 6.60	H1 = 8.16 H5 = 6.39	-
 NP6^f	-	H1 = 7.61 H2 = 9.22 H5 = 6.41 H6 = 6.47	H1 = 8.08 H5 = 6.26	-

1.1 Photochromism

<p>NP7^g</p>	-	H1-CTC = 8.09 H2-CTC = 9.09 H1-TTC = 7.65 H2-TTC = 9.52 H5-TTC = 6.52	H1-CTT = 8.54 H2-CTT = 7.04 H1-TTT = 7.97 H2-TTT = 7.47 H5-TTT = 6.32	-
<p>NP8^h</p>	H2 = 5.78 F = -113.1 -113.2	H2 = 8.88 H5 = 6.49 F = -110.0 -110.6	H1 = 7.31 H5 = 6.20 F = -109.6 -110.2	-
<p>NP9ⁱ</p>	H1 = 7.78 H2 = 6.00 H5 = 7.29 H6 = 7.64	H1 = 9.39 H2 = 9.26	H1 = 8.79 H2 = 7.17	-
<p>NP10^j</p>	H1 = 6.07 H2 = 6.72 H5 = 8.46	H1 = 7.89 H2 = 9.41 H5 = 7.68	H1 = 8.24	-

[a] Data from Ref.^[36], 1×10^{-2} M in CD_3CN , 228 K. [b] Data from Ref.^[17], 1×10^{-2} M in acetone- d_6 , 213 K. [c] Data from Ref.^[18], 1×10^{-2} M in acetone- d_6 , 213 K. [d] Data from Ref.^[49], 1×10^{-2} M in CD_3CN , 228 K. [e] Data from Ref.^[50], 1×10^{-2} M in toluene- d_8 , 243 K. [f] Data from Ref.^[51], 6×10^{-3} M- 1×10^{-2} M in toluene- d_8 , 228 K. [g] Data from Ref.^[52], 6×10^{-3} M- 1×10^{-2} M in toluene- d_8 , 213 K. [h] Data from Ref.^[53], 5×10^{-3} M in toluene- d_8 , 228 K. [i] Data from Ref.^[54], 5×10^{-3} M in toluene- d_8 , 293 K. [j] Data from Ref.^[55], 1×10^{-2} M in toluene- d_8 , 193-223 K.

1.1.3.3 Infrared Spectroscopy

IR spectroscopy is also a useful method to investigate the photochromic properties of naphthopyrans. The IR spectra changes of naphthopyran **N1** are presented in Figure 1.13. After UV irradiation, a new peak appeared at 1633 cm^{-1} , assigned to the ketone $\nu(\text{C}-(\text{C}=\text{O})-\text{C})$, confirming the formation of open forms. At the same time, both of two bands, $\nu(\text{Aryl-O})$ and $\nu(\text{O-Alkyl})$, decreased in intensity at 1247 and 1085 cm^{-1} , respectively.^[56] Therefore, the photochromic behavior of naphthopyrans can be explored.

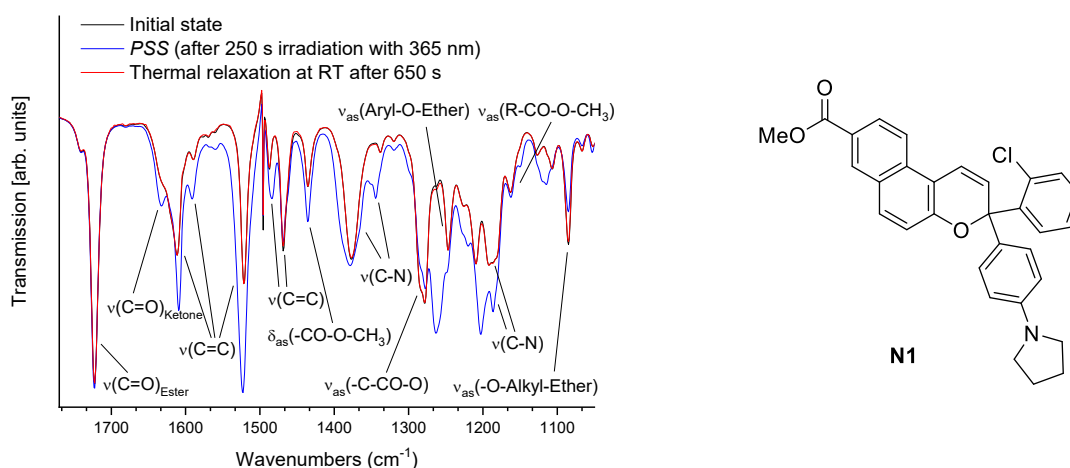


Figure 1.13 The IR spectra changes of naphthopyran **N1** (3.45×10^{-2} M in toluene at 293 K).^[56]

1.1.3.4 X-Ray Crystallography

The X-ray crystal structure of several 3*H*-naphthopyrans have been reported.^[57–59] From the data in Table 1.2, it is revealed that all the $\text{C}_3\text{-O}$ bonds ($1.440\text{--}1.462\text{ \AA}$) are longer than a typical C-O bond in a six-membered heterocycle ($1.41\text{--}1.43\text{ \AA}$).^[60] The $\text{C}_3\text{-O}$ bond length is affected by the substituents in the aryl rings. Moreover, the first X-ray crystal structure of open form was also reported (Figure 1.14). The bond lengths of both $\text{C}_1\text{-C}_{13\text{D}}$ and $\text{C}_2\text{-C}_3$ are 1.36 \AA . And $\text{C}_1\text{-C}_2$ bond length is 1.43 \AA , which is consistent with a quinoidal structure of an open isomer.^[54]

1.1 Photochromism

Table 1.2 Selected geometric parameters.

Naphthopyran	Ar ₁	Ar ₂	C ₃ -O (Å)	C ₄ -O (Å)	C-Ar ₁ (Å)	C-Ar ₂ (Å)	Ar ₁ -C-Ar ₂ (°)
NP1 ^[57]	Ph	Ph	1.458	1.372	1.530	1.527	110.5
NP11 ^[58]	2,6-diFC ₆ H ₃	Ph	1.440	1.369	1.539	1.544	108.1
NP12 ^[58]	2-FC ₆ H ₄	4-MeOC ₆ H ₄	1.464	1.380	1.525	1.527	113.1
NP13 ^[59]	2-MeOC ₆ H ₄	2-MeOC ₆ H ₄	1.462	1.373	-	-	93.3

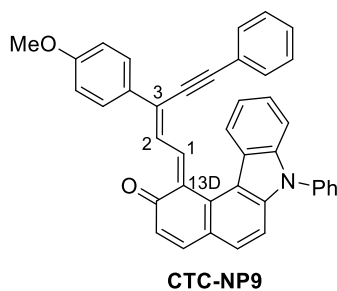


Figure 1.14 The structure of CTC form of naphthopyran **NP9**.

1.1.3.5 Mass Spectroscopy

During the fragmentation of 3,3-diaryl 3*H*-naphthopyrans the homolytic dissociation of either one of the aryl substituents was observed (Figure 1.15).^[61]

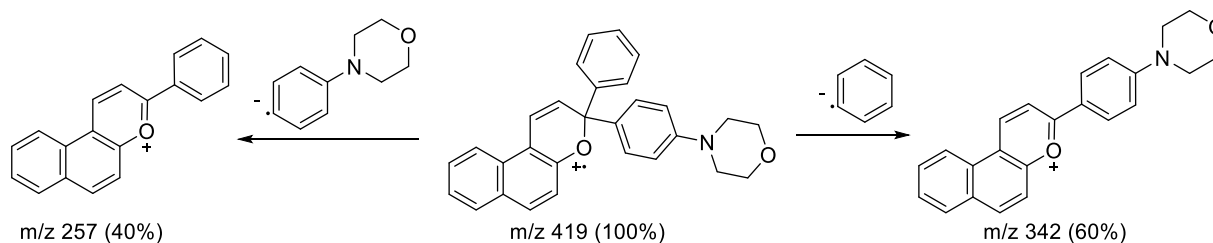


Figure 1.15 The fragmentation of 3*H*-naphthopyrans.

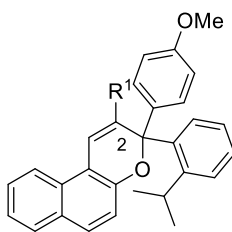
1.1.4 Photochromic Properties of 3*H*-Naphthopyrans Varied with Substituents

Different substituents will have a different influence on the photochromic performance of 3*H*-naphthopyrans, which depends on the geometric size, electronegativity, electropositivity of substituents and the substituted positions. The phenomena can be explained by the steric, electron inductive and electron resonance effects induced by the substituents.

1.1.4.1 2-Substituents

2-substituted 3*H*-naphthopyrans were firstly reported by the Rück-Braun group in 2009.^[62] In that article, the half-life of a 2-substituted benzopyran was reduced to 12 μ s. Afterwards, the Abe group measured the photochromic behavior of 2-Br-substituted 3*H*-naphthopyrans **NP15**.^[63] It was found that the half-life of **NP15** was reduced to 2.5 μ s from 34 min of **NP14** (the naphthopyran without 2-substituent) (Table 1.3). The sharp decrease of half-life is due to the large steric repulsion of the 2-substituent which destabilizes the open forms.

Table 1.3 Photochromic properties of 2-substituted 3*H*-naphthopyrans.^a



Naphthopyran	R ¹	λ_{\max}	$t_{1/2}$
NP14	H	465	34 min
NP15	Br	415	2.5 μ s

[a] Data from Ref.^[63], 8.5×10^{-5} M in toluene, 298 K.

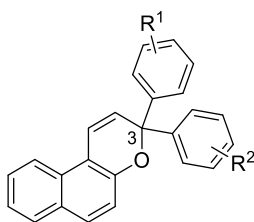
1.1.4.2 3-Substituents

The choice of substituents at 3-position phenyl rings can have a great influence on the photochromic performance of 3*H*-naphthopyrans and attract more and more attentions in the last

1.1 Photochromism

two decades. Heron and co-workers revealed that the electron-donating groups at *para*-position cause a bathochromic shift in the UV absorption spectra and promote the thermal relaxation rate. In contrast, electron-withdrawing groups at *para*-position bring a hypsochromic shift and retard the thermal bleaching speed (Table 1.4).^[58,64]

Table 1.4 Photochromic properties of 3*H*-naphthopyrans affected by substituents at 3-phenyl rings.^a



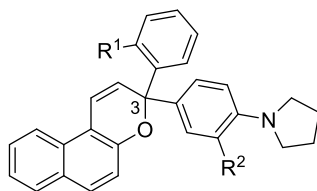
Naphthopyran	R ¹	R ²	λ_{\max} (nm)
NP1	H	H	430
NP16	H	<i>p</i> -MeO	458
NP17	<i>p</i> -NMe ₂	<i>p</i> -MeO	512
NP18	H	<i>p</i> -F	428
NP2	<i>p</i> -F	<i>p</i> -F	419

[a] Data from Ref.^[58,64] in toluene, 293 K.

For the effect of *ortho*- and *meta*-substituents, the size of the substituents is more important. As presented in Table 1.5, both electron withdrawing groups and electron-donating groups at *ortho*-position slow down the thermal back speed and the half-life increases as the size of substituents increases (**NP19-NP23**). However, the λ_{\max} is influenced by *ortho*-substituents barely.^[65] By contrast, *meta*-substituents have a major effect on the λ_{\max} . The *meta*-electron withdrawing groups cause a hypsochromic shift in the absorption spectra and reduce λ_{\max} as the size of substituents increases (**NP25-NP27**), because of decreasing conjugation between the pyrrolidine moieties and the whole structure. For the *meta*-electron donating groups, it depends on the comparison between geometric size and electron donating power, if geometric size contributes more, a hypsochromic

shift is observed (**NP28**); if electron donating power contributes more, it has to be a bathochromic shift (**NP29**). But all the *meta*-substituents have a negligible effect on the thermal back rate.^[66]

Table 1.5 The effect of *ortho*- and *meta*-substituents in 3-phenyl rings on photochromic properties of 3*H*-naphthopyrans.^a



Naphthopyran	R ¹	R ²	λ_{\max} (nm)	$t_{1/2}$ (s)
NP19	H	H	538	5
NP20	F	H	554	40
NP21	Cl	H	554	741
NP22	Br	H	554	1024
NP23	I	H	553	1167
NP24	OMe	H	555	351
NP25	H	F	529	4
NP26	H	Cl	513	4
NP27	H	Br	493	4
NP28	H	Me	517	3
NP29	H	OMe	557	5

[a] Data from Ref.^[65,66], 1×10^{-5} M in toluene, 293 K.

Except for phenyl rings, 3*H*-naphthopyrans with other substituents at 3-position have also been reported. Delbaere and co-workers investigated 3-thienyl-naphthopyrans (Figure 1.16).^[52] They

found that the ring opening rate decreases with an increasing number of thiophene rings and the concentration of open forms also reduces when the number of thiophene rings increase.

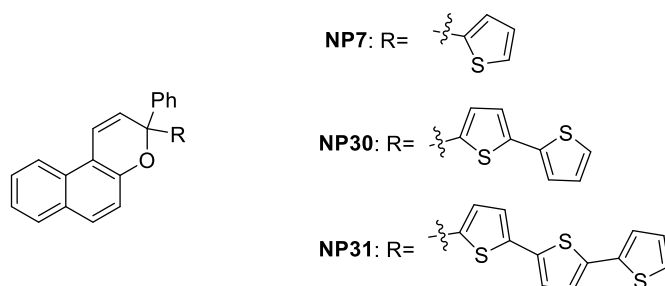


Figure 1.16 The structures of 3-thienyl-naphthopyrans.

In addition, CH- π bonds were adopted to the system.^[54] When an ethynyl group was added to the 3-carbon instead of a phenyl ring, the CH- π bond was observed between the phenyl ring of carbazole group and proton H2'' in the CTC form, and between the phenyl ring of the carbazole group and proton H2' in the CTT form, thereby stabilizing the open forms (Figure 1.17). Therefore, the ring opening reaction was achieved easily without UV light.

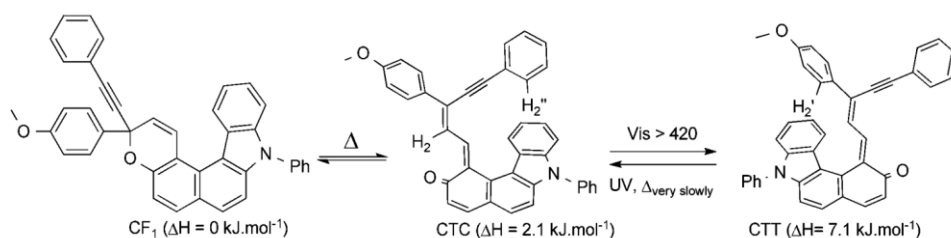


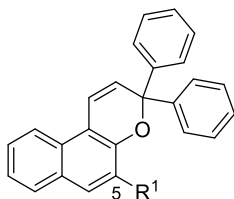
Figure 1.17 The photochromism of 3*H*-naphthopyrans with CH- π bonds.^[54] Copyright © 2012, American Chemical Society.

1.1.4.3 5-Substituents

In general, the 5-substituents have little effect on the λ_{max} of absorption spectra of 3*H*-naphthopyrans.^[67] But the thermal bleaching rate is decreased by 5-amino-substituents (NP32-NP35).^[68] Furthermore, when the π -conjugation group was introduced, the λ_{max} was induced as large bathochromic shift and the thermal bleaching rate was also accelerated^[38] (NP38) (Table 1.6).

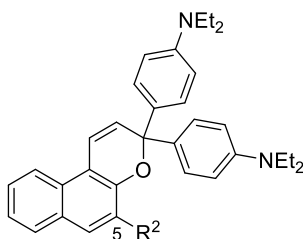
1 Introduction

Table 1.6 The effect of 5-substituents on photochromic properties of 3*H*-naphthopyrans.^a



Naphthopyran	R ¹	λ_{max} (nm)	k (s ⁻¹)
NP32	NH ₂	439	0.007
NP33		455	0.017
NP34		438	0.015
NP35		425	0.021
NP36^b	MeO	435	-

[a] Data from Ref.^[68], 5×10^{-5} M in toluene, 293 K. [b] Data from Ref.^[67], in aliphatic acrylic matrix.



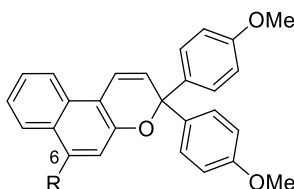
Naphthopyran	R ²	λ_{max} (nm)	$t_{1/2}$ (min)
NP37^c	H	580	6
NP38^c	CONHC ₆ H ₅	640	< 1

[c] Data from Ref.^[38]

1.1.4.4 6-Substituents

The 6-substituents have a large influence on the photochromic properties, especially the thermal relaxation rate. As it is demonstrated in Table 1.7, 6-electron donating substituents bring about a hypsochromic shift and retard the thermal bleaching speed^[64,69] (**NP39-NP41**). However, the effects of 6-electron withdrawing substituents are unknown.

Table 1.7 The effect of 6-substituents on photochromic properties of 3*H*-naphthopyrans.^a

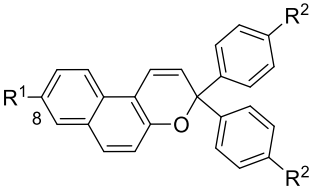


Naphthopyran	R	λ_{\max} (nm)	IODF ₁₀ %
NP13	H	475	45
NP39	OMe	456	10
NP40	Piperidino	452	11
NP41	Morpholino	452	13

[a] Data from Ref.^[64,69], in spectralite. IODF₁₀%: the percentage loss in initial optical density 10 s after removing the UV source (described in the literature^[69]).

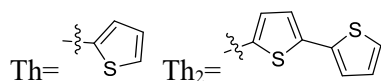
1.1.4.5 8-Substituents

As shown in Table 1.8, the 8-substituents can cause a bathochromic shift in the absorption spectra of 3*H*-naphthopyrans, including a π -conjugation group, thiophene^[45] (**NP42-NP43**), and electron donating substituents, methoxyl group^[69] (**NP46**). Moreover, the thermal bleaching rate is also accelerated by 8- π -conjugation substituents and it increases with the growth of the thiophene ring chain^[51] (**NP42-NP45**).

Table 1.8 The effect of 8-substituents on photochromic properties of 3*H*-naphthopyrans.^a


Naphthopyran	R ¹	R ²	λ_{max} (nm)	$k_{TC \rightarrow CF}$ (s ⁻¹)	$k_{TT \rightarrow TC}$ (s ⁻¹)
NP1	H	H	430 ^b	1.59×10^{-4}	-
NP42	Th	H	478 ^b	1.96×10^{-4}	5.19×10^{-6}
NP43	Th ₂	H	500 ^b	2.13×10^{-4}	9.90×10^{-6}
NP6	—≡—H	H	-	5.30×10^{-4}	9.76×10^{-6}
NP44	—≡—Th	H	-	3.69×10^{-4}	-
NP45	—≡—Th ₂	H	-	4.73×10^{-4}	-
NP13^c	H	OMe	475	-	-
NP46^c	OMe	OMe	502	-	-

[a] Data from Ref.^[51], 6×10^{-3} - 1×10^{-2} M in toluene-*d*₈, 243 K. [b] Data from Ref.^[45], 1×10^{-5} M in toluene, 280 K. [c] Data from Ref.^[69], in polyurethane.



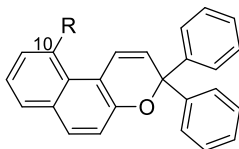
1.1.4.6 10-Substituents

The 10-substituents play a major role in the stability of open forms. Thus, the thermal bleaching rate will be impacted by different substituents. As presented in Table 1.9, half-life of **NP47** is sharply reduced, compared with the reference naphthopyran **NP1**, because of the destabilizing effect on the TC form by the large sterically demanding bromine substituent. However, the thermal bleaching rate is retarded by a 10-methoxyl group due to the C-H...O hydrogen bond, which

1.1 Photochromism

stabilizes the TC form. Correspondingly, the concentration of TT form is reduced, resulting from the promoted speed of the TT→TC process.^[43]

Table 1.9 The effect of 10-substituents on photochromic properties of 3*H*-naphthopyrans.^a



Naphthopyran	R	λ_{\max} (nm)	$t_{1/2}$ (s)	TT form/% ^b
NP1	H	425	6.9	16
NP47	Br	419	0.36	17
NP48	OMe	450	9.5	3

[a] Data from Ref.^[43], 5.5×10^{-5} M in toluene, 298 K. [b] data calculated from $A_2 / (A_1 + A_2)$ of equation 1 (for detail, see Chapter 1.1.3.1).

1.1.5 Applications of 3*H*-Naphthopyrans

Naphthopyrans are a kind of important organic photochromic materials for ophthalmic lenses, due to their efficient colorability, fast reversibility, good fatigue resistance and broad color range from purple to red.^[70,71] Besides, 3*H*-naphthopyrans can be applied as photochromic switches^[72], molecular electronic devices^[73], photoswitchable molecular receptors^[74], photoresponsive polymers^[75], photochromic thin films^[41,76], photoresponsive gels^[77,78], liquid crystalline materials^[79] and as molecular logic gates^[80].

1.2 *Meta*-C-H Functionalization of Benzene

Transition metal-catalyzed selective C–H functionalization is a versatile and powerful tool for the synthesis of complex organic compounds.^[81] Wherein *para*- and *ortho*-C-H functionalization can be achieved with classical Friedel-Crafts reaction easily in the presence of a donor group. Chelation-assisted *ortho*-C-H activation has also been developed very well during the past decades. Although an electron withdrawing group can direct the reaction forward to the *meta*-C-H functionalization product as the main product, usually a product mixture is observed. Consequently, selective *meta*-C-H functionalization remains a significant challenge.^[82,83] In the past few years, more and more attention has been attracted to this field and a few excellent designs have been published. Based on the mechanism, there are about six different types.

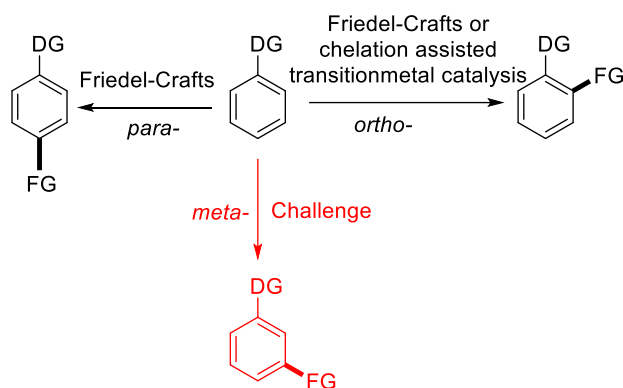


Figure 1.18 Functionalization of arenes.

- **Directed *meta*-C-H functionalization with nitrile-containing templates**

In 2012, Yu and co-workers described a proposal in which a series of newly designed templates containing a nitrile group was used as directing group to achieve *meta*-C-H functionalization of arenes.^[84] In later mechanism studies, a heterodimeric complex was regarded as the useful catalyst and concerted metalation–deprotonation (CMD) was the proposed procedure^[85] (Figure 1.19). Later, many other nitrile-containing templates for *meta*-C-H functionalization of arenes have also been designed.^[86–107]

1.2 *Meta*-C-H Functionalization of Benzene

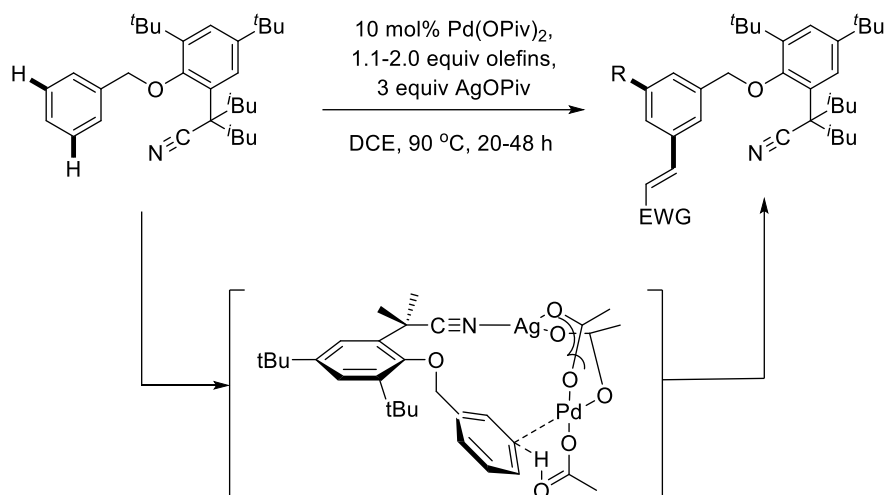


Figure 1.19 Pd-catalyzed *meta*-C-H functionalization using a nitrile end-on template.

- Copper-catalyzed *meta*-C-H arylation of arenes**

The second method was discovered by Phipps and Gaunt.^[83] They reported a Cu-catalyzed *meta*-C-H arylation of arenes with Ar₂IOTf under the catalysis of Cu(OTf)₂, and the amido group was used as a directing group. The proposed mechanism is through a dearomatizing “oxy-cupration” process (Figure 1.20).

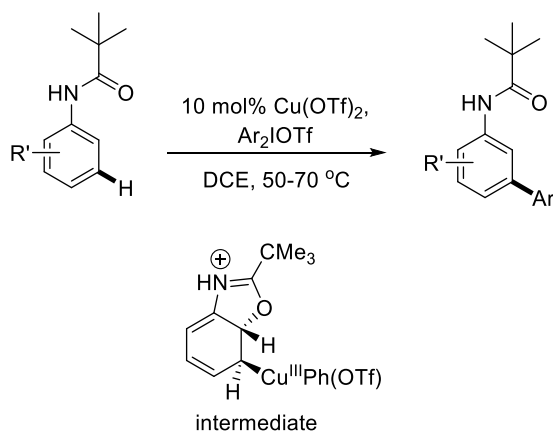


Figure 1.20 Cu-catalyzed *meta*-C-H functionalization.

- Traceless directing group**

In 2014, the Larrosa group reported the third method for achieving *meta*-C-H arylation of phenols via the *ortho*-directing effect of a temporarily introduced carboxyl group, thereby exploring a CO₂-based traceless directing group strategy^[108] (Figure 1.21).

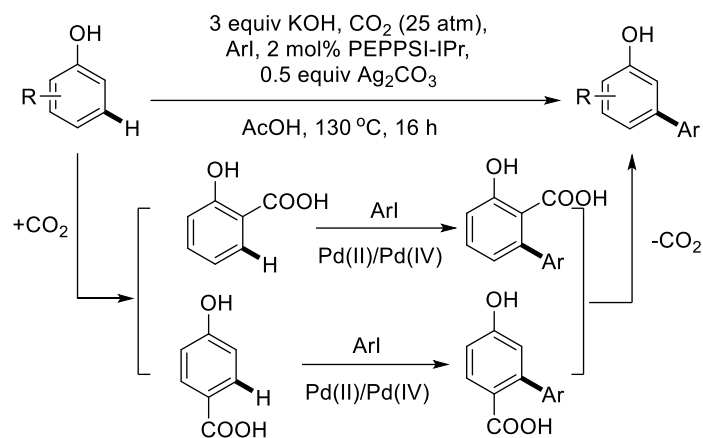


Figure 1.21 Using a traceless carboxyl directing group relay strategy to achieve *meta*-C–H arylation of phenols.

- **Metalation-directing *meta*-C–H functionalization**

The metalation-directing *meta*-C–H functionalization of arenes has also been reported. The Frost group described a Ru-catalyzed *meta*-sulfonylation of 2-phenylpyridines. The strong *ortho/para*-directing effect of the Ru(II) center by σ -activation led to electrophilic sulfonylation *para*- to the Ru–C aryl bond^[109] (Figure 1.22).

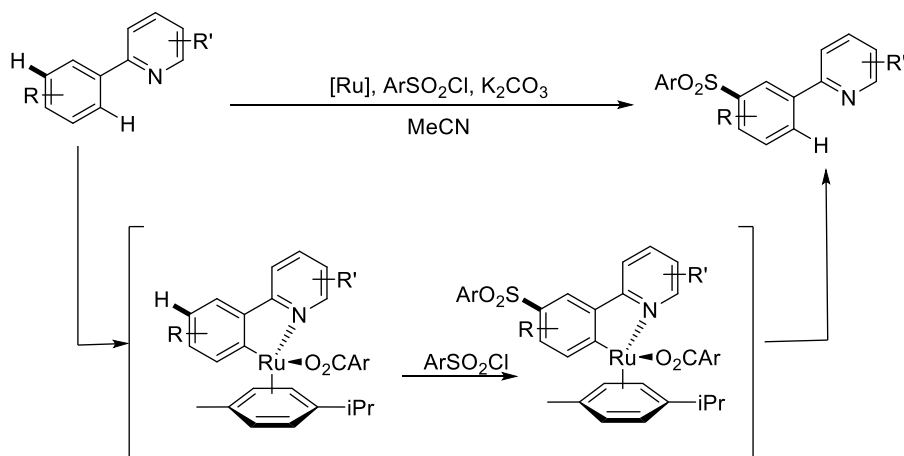


Figure 1.22 Ru-catalyzed *meta*-sulfonylation of 2-phenylpyridines.

- **Ion pair directed *meta*-C–H borylation**

The ion pair directing group was expected to achieve *meta*-C–H borylation by Phipps and co-workers.^[110] In the presence of a proper anionic sulfonate ligand, bis(pinacolato)diboron and an

1.2 *Meta*-C-H Functionalization of Benzene

iridium catalyst, a *meta*-C-H borylation product can be obtained effectively. But a small number of *para*-C-H borylation products also existed as byproducts (Figure 1.23).

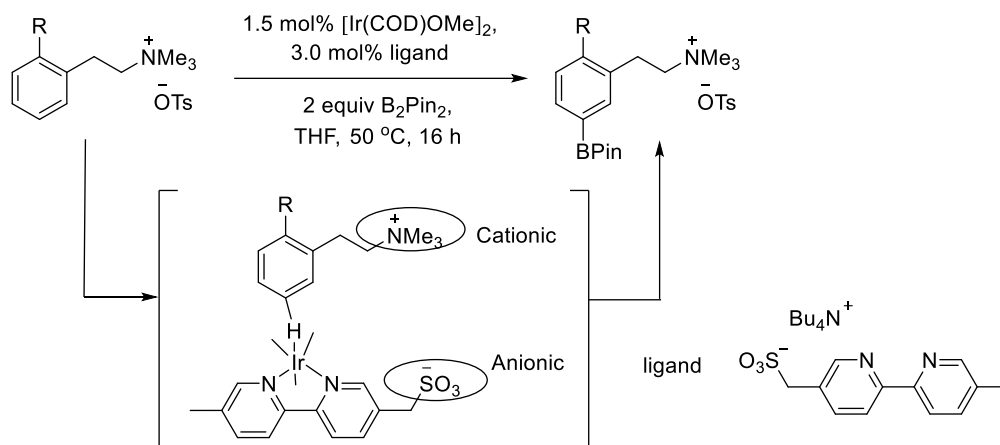


Figure 1.23 Ir-catalyzed ion pair directed *meta*-C-H borylation.

- Ligand controlled *meta*-C-H functionalization**

Nondirected selected *meta*-C-H activation is an excellent method, considering no need to introduce and remove the directing group. In 2018, the van Gemmeren group reported nondirected *meta*-C-H functionalization with steric and electronic control of regioselectivity. However, it is worth noting that *para*- and *ortho*-products were also observed in the reaction^[111] (Figure 1.24).

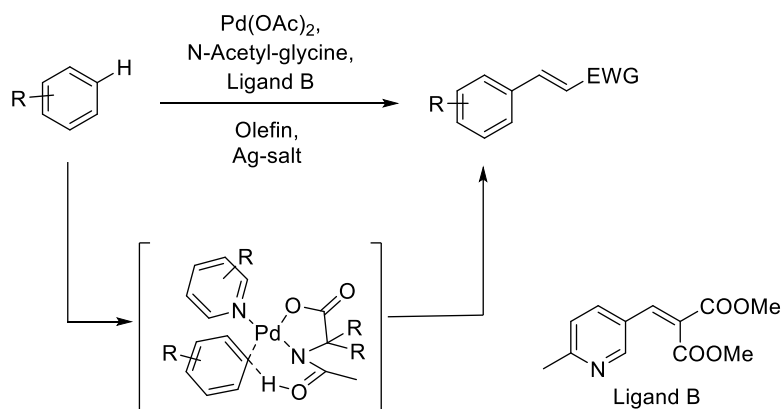


Figure 1.24 Nondirected *meta*-C-H functionalization.

1.3 Distant Selective-C-H Functionalization of Naphthalene

Naphthalene has a different geometric structure from benzene. For example, the bond lengths are not the same as that of benzene^[112] (Figure 1.25). For the chemistry properties, they are also different. As exhibited in Figure 1.26, the directing group gave the *ortho*-selective product for benzene, and the *meta*-selective product for naphthalene under the same conditions.^[113]

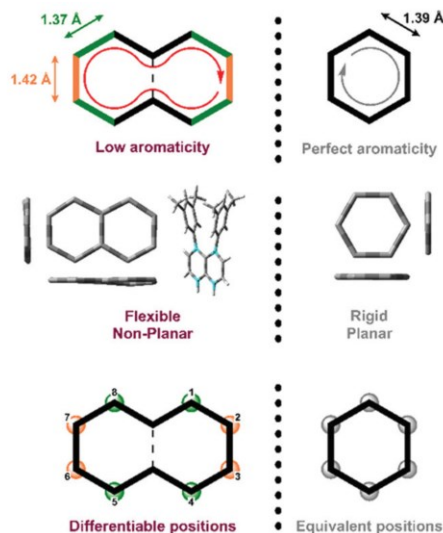


Figure 1.25 Different structure between naphthalene and benzene.^[112] Copyright © 2020, Thieme.

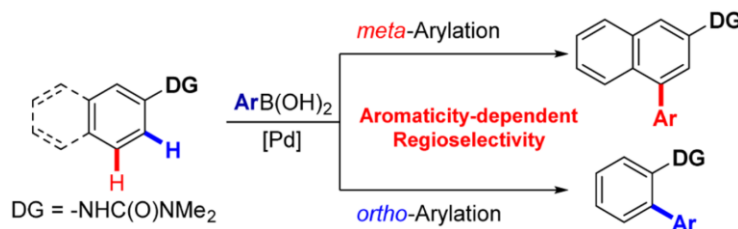


Figure 1.26 The difference between naphthalene and benzene during selective C-H functionalization.^[113] Copyright © 2015, American Chemical Society.

For the C-H activation of naphthalene, they can be divided into two types based on the position of the directing group: directing group at 1-position and directing group at 2-position (Figure 1.27). When the directing group is at 1-position, many work has been published dealing with selective C-H functionalization, and the challenge is selective C5-H, C6-H and C7-H bond activation.^[114]

1.3 Distant Selective-C-H Functionalization of Naphthalene

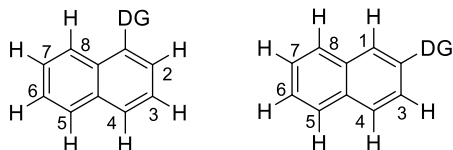


Figure 1.27 Two types of naphthalene.

According to my knowledge, selective C5-H functionalization has not been reported. The functionalization of C6-H was just described from two papers by Sakaki and Nakao group.^[115,116] C6-H bond was activated by the coordination between an aluminium compound and an amide directing group. Thus, selective C6-H alkylation was achieved with the help of a nickel catalyst (Figure 1.28).

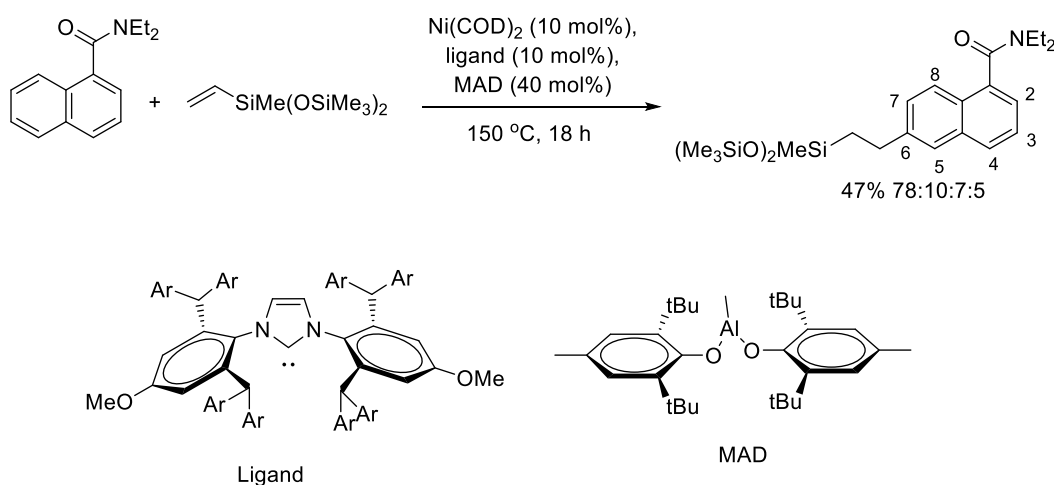


Figure 1.28 Selective C6-H functionalization.

Selective C7-H functionalization has not been achieved until very recently. In 2019, the Yang and You group reported the only example about selective C7-H functionalization of naphthalene.^[117] The palladium complex was oxidized by F^+ . The mechanistic pathway includes C8-H electrophilic activation, aryl migration and β -hydride elimination (Figure 1.29).

As for the second types of naphthalene, directing group at 2-position (Figure 1.27, right), 3-position functionalization is usually the same as for benzene.^[112] The study about C-H activation of the other positions is very few, only C4-H functionalization was reported by a few groups through *meta*-C-H functionalization.^[118–122] Interestingly, bis C-H functionalization, both the C8-H and C4-H functionalization were achieved by the Yu group.^[123] Pyridine was used as the template, in the presence of silver salt and palladium catalyst, a 4,8-disubstituted product was

obtained in 78% yield (Figure 1.30). However, selective mono-C8-H functionalization is still unknown.

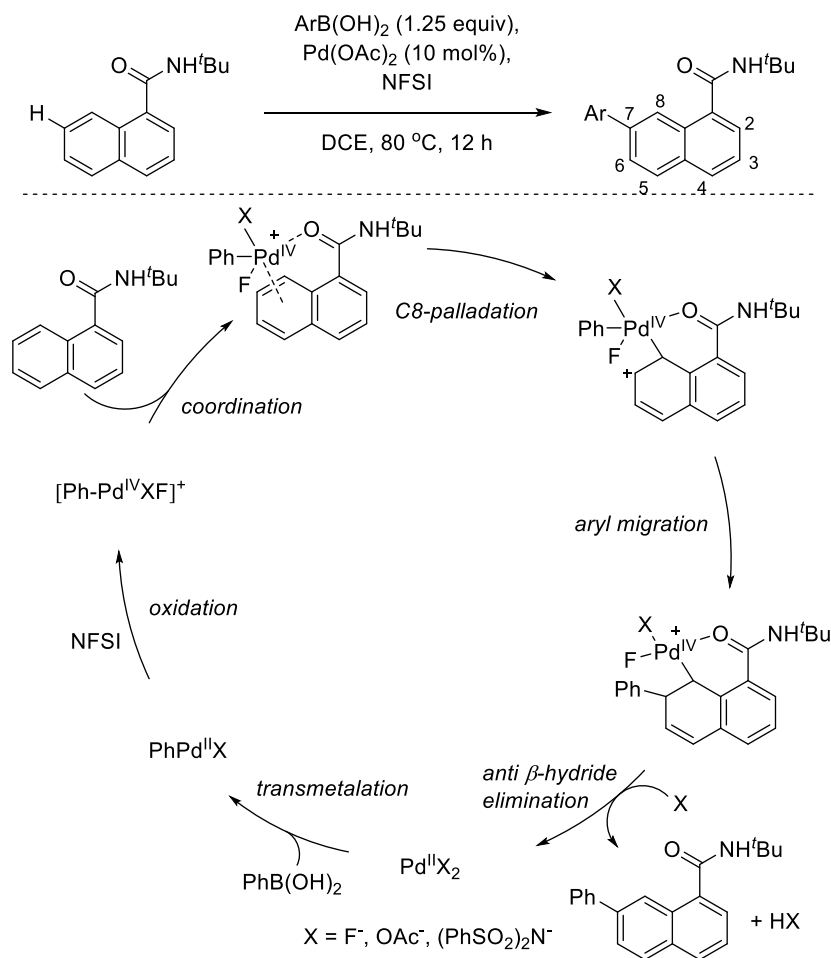


Figure 1.29 Selective C7-H functionalization.^[117]

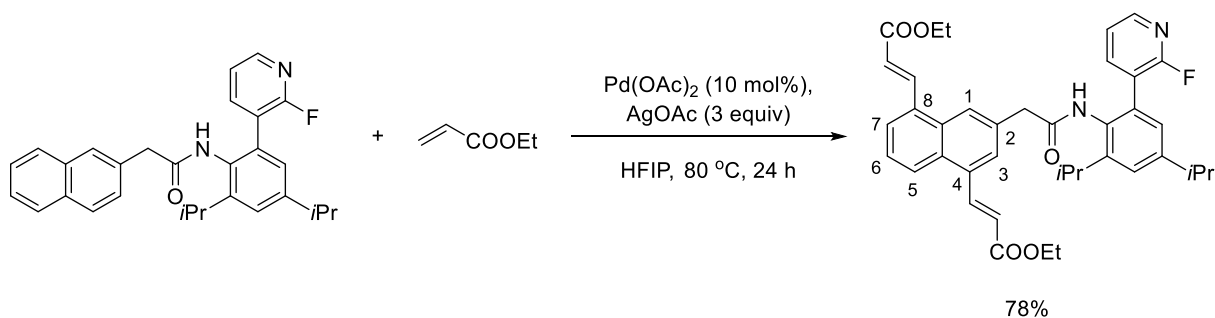


Figure 1.30 Bis C4-H and C8-H functionalization of naphthalene.

2. Aim and Strategy

From the introduction part, we can learn that 3*H*-naphthopyrans are a kind of important photochromic compounds and the substituents have a great effect on its photochromic properties. Consequently, it will promote the development of 3*H*-naphthopyrans to discover novel methods on introducing different substituents into different positions of 3*H*-naphthopyrans and to investigate the influence on photochromic properties by those substituted compounds.

Hence, the first part of my thesis is to find useful methods to introduce substituents into key positions of 3*H*-naphthopyrans. On the one hand, because we want to apply 3*H*-naphthopyrans on the silicon surfaces (Si (111)) in the future, 8-position, because of the longest distance from the pyran ring, is the perfect position for a linker. The 8-substituents will be kept. On the other hand, the positions we are interested in are 6- and 10-position, considering 6-position substituents have a major influence on the thermal bleaching rate and only very few compounds with a 6-donating group were reported, 3*H*-naphthopyrans with 6-electronic withdrawing substituent are still unknown. 10-position substituents affect the stabilities of the open forms. The introduction of a 6-electronic withdrawing group or larger steric 10-substituents is expected. Therefore, selective C-H functionalization is a favourable choice. So far, no example was reported about *meta*-C-H functionalization of naphthopyrans. Introducing 10-substituents will be interesting. Moreover, selective C6-H functionalization is a challenge, because selective C8-H functionalization of naphthalene is still unknown (Figure 2.1).

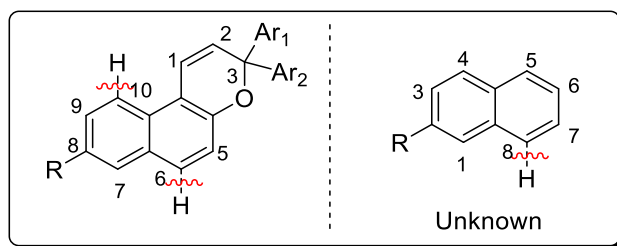


Figure 2.1 Expected selective C-H bond functionalization of naphthopyrans.

The second part of my thesis is devoted to explore the photochromic behavior of different substituted 3*H*-naphthopyrans. The investigated substituents include 2-, 6- and 8-substituents in this work. For 2-substituents, the effect of large steric substituents will be explored. For 6-substituents, the influence of an electron withdrawing group and conjugation will be investigated.

2 Aim and Strategy

For 8-substituents, ester, carboxylic acid, hydroxymethyl and ether methyl groups will be studied. In addition, the effect of 3-aryl substituents will also be investigated (Figure 2.2).

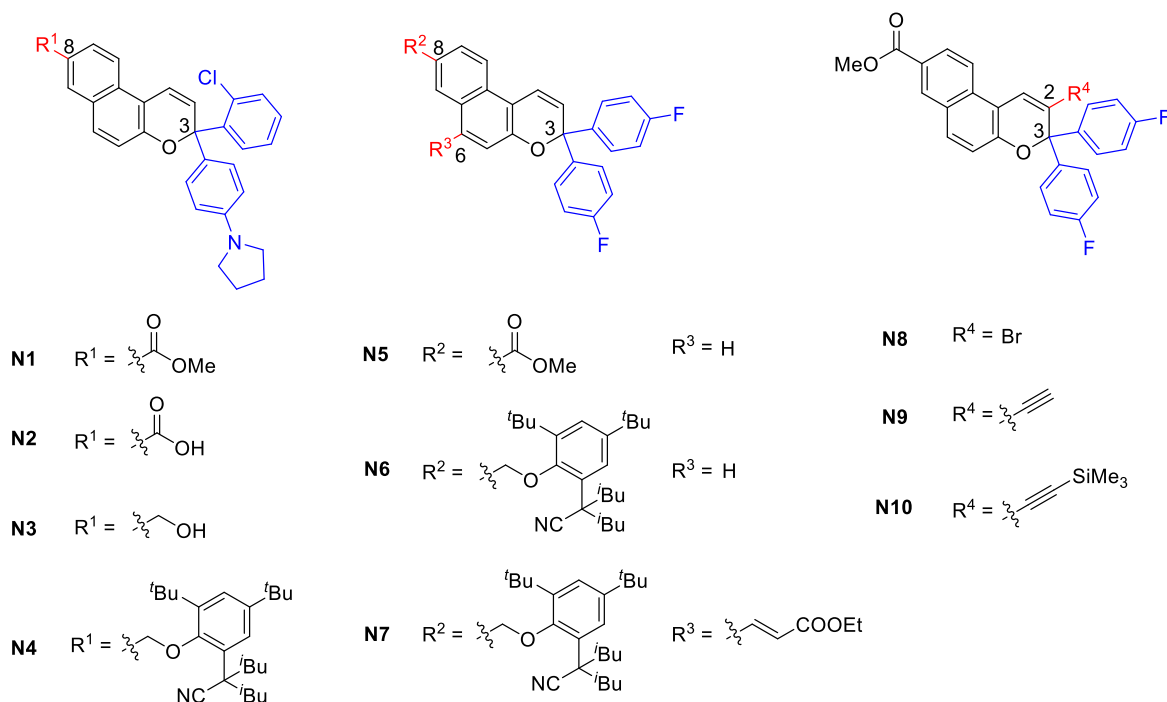


Figure 2.2 The 3H-naphthopyrans to be investigated.

The research method involves UV/Vis spectroscopy and *in-situ* NMR spectroscopy. The absorption spectra changes will be detected during irradiation with UV light, visible light and in the dark. The formation of different isomers will be observed with *in-situ* NMR spectroscopy during UV irradiation. Furthermore, kinetic studies will be adopted in both room temperature UV/Vis experiments and low temperature *in-situ* NMR measurements.

3. Synthesis of Remote Selective C-H Functionalization of Naphthopyrans

In this chapter, the directing group at 8-position was introduced and different synthetic methods were explored to achieve remote selective C-H bond functionalization of naphthopyrans.

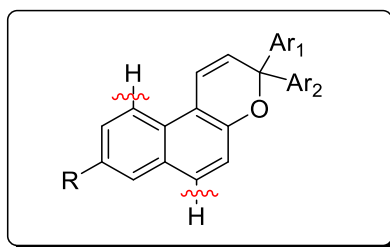


Figure 3.1 Remote selective C-H bond functionalization of naphthopyrans.

3.1 Method I: Directed Selective C-H Functionalization

In 2012, the Yu group reported palladium catalyzed *meta*-C-H activation of arene substrates.^[84] Encouraged by this interesting research, we designed our first synthesis method: palladium catalyzed directed *m*-C-H activation of naphthopyrans. And the target molecule is described in Figure 3.2.

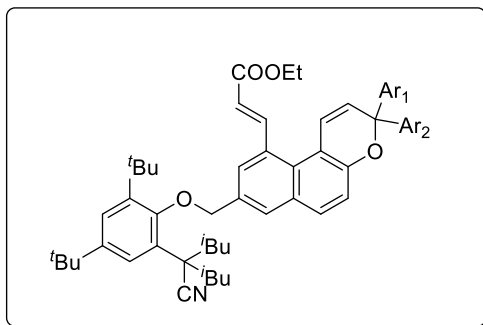


Figure 3.2 Target molecule of synthetic method I.

3.1.1 Route 1 of the Synthesis

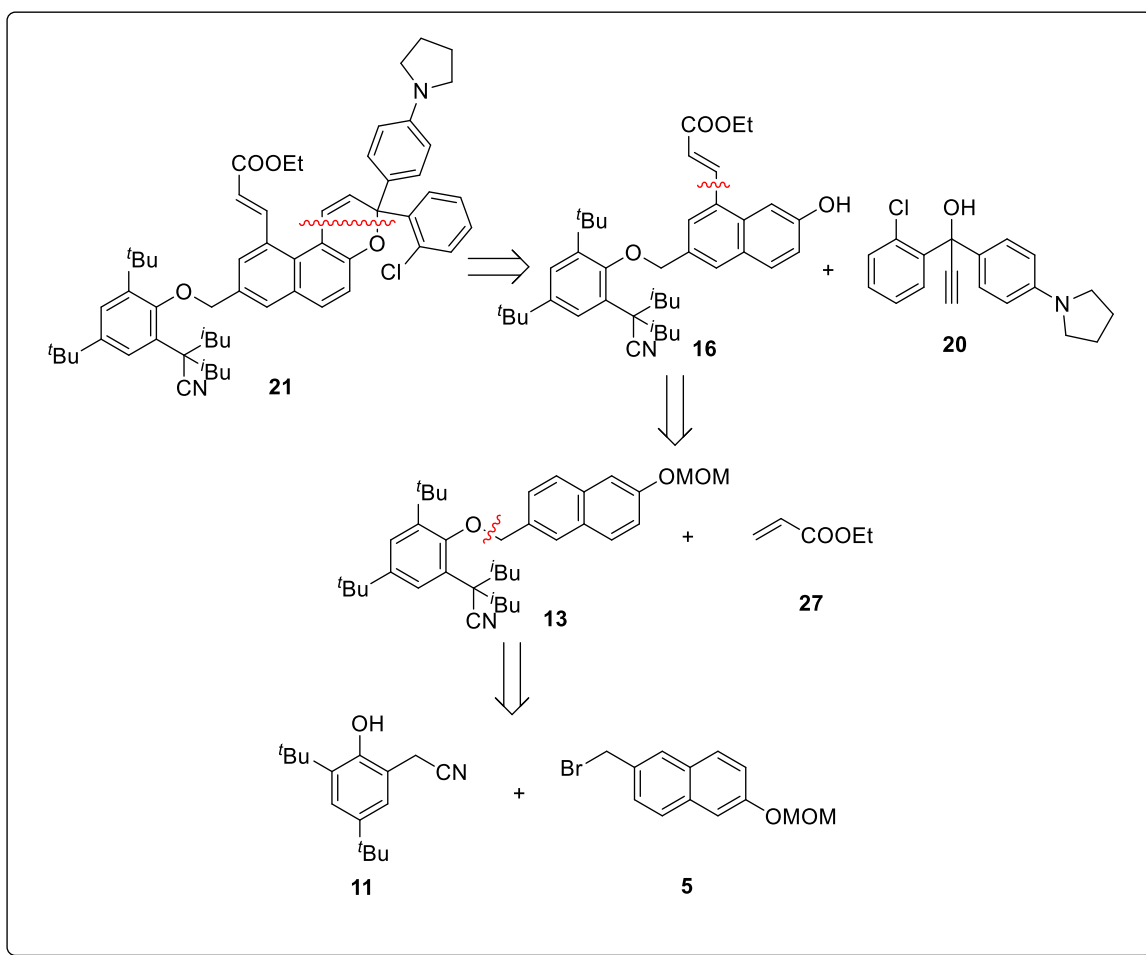
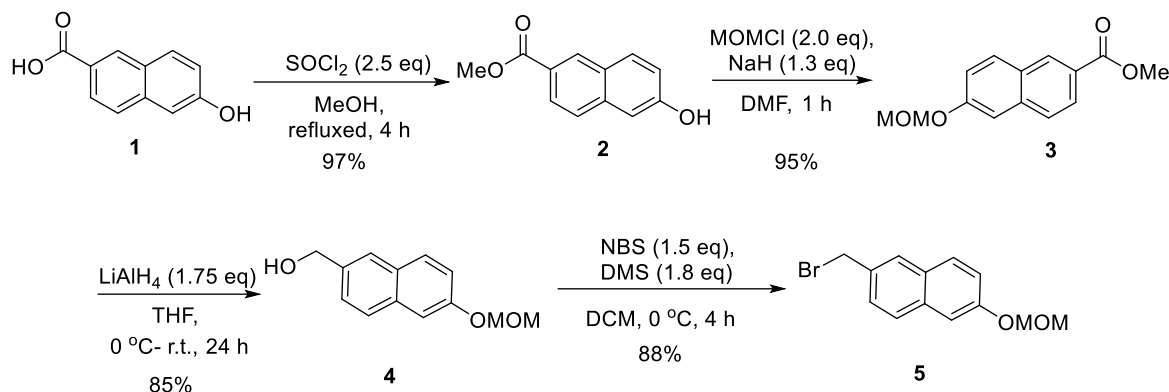


Figure 3.3 Proposed retrosynthetic route 1 about directed remote C-H functionalization of naphthopyrans.

The retrosynthetic route 1 for synthesizing the target compound is shown in Figure 3.3. The general strategy is described below: At first, the synthesis of target molecule naphthopyran **21** can be achieved from compound **16** and propargyl alcohol **20** under acid catalysis. Then naphthalene **16** can be obtained through *meta*-C-H activation of naphthalene **13**. In addition, compound **13** can be synthesized from compound **11** and naphthalene **5** through a nucleophilic substitution reaction. As for compound **11** and propargyl alcohol **20**, both of them were literature reported.^[65,84]

Synthesis of Compound 2-Bromomethyl-6-(methoxymethoxy)naphthalene (5)**Figure 3.4** Synthesis of naphthalene 5.

Our synthetic path started with the commercially available naphthol **1** (Figure 3.4). At first, an acid chloride was formed by reaction with thionyl chloride, after substitution with methanol via an addition-elimination mechanism, naphthol **2** was prepared in 97% yield.^[124] At second, considering the proton of the hydroxyl group will influence the next step C-H activation, the hydroxyl group in naphthol **2** needs to be protected. Sodium hydride was used for the removal of the proton from the hydroxyl group in naphthol **2**. Then the chloride of (chloromethyl) methyl ether (MOMCl) can be replaced with the intermediate naphtholate. Afterwards, the naphthalene **3** with the protecting group (MOM) was obtained in 95% yield.

For the synthesis of naphthalene **4**, classical LiAlH_4 was used as the reductant, and after 24 hours in THF, compound **3** was reduced to compound **4** and the latter isolated in 85% yield.^[125] As for the bromination of compound **4**, the commonly used PBr_3 was not suitable for this reaction. The possible reason is the produced phosphorous acid, which will induce the deprotection of the hydroxyl group. Then soft *N*-bromosuccinimide (NBS) is a favorable choice. After 10 min to a mixture of NBS and dimethyl sulfide (DMS), compound **4** was added and product **5** was obtained with a good yield of 88% after 4 h reaction time in DCM. Notably, because product **5** is sensitive to silica gel, only a short plug of silica gel was used for the purification of the crude product. The product **5** was also found to undergo easily decomposition under air and daylight in the fridge. Thus, storage under argon and shielding from light is necessary. The mechanism is depicted in Figure 3.5.

3.1 Method I: Directed Selective C-H Functionalization

The process can be divided into two parts. The first step is the formation of compound **31**. At first, DMS as a nucleophile attacked the bromine of NBS, resulting in formation of the succinimide anion **29**. After nucleophilic substitution and leaving of bromide, compound **31** was formed. The second step is the reaction between **31** and the starting material **4**. The sulfur atom of **31** was attacked by compound **4** and then compound **31** was converted into intermediate **32**, which owns a better leaving group compared to the initial hydroxyl group.^[126,127] Accordingly, bromine anion attacked **32** and product **5** was formed.

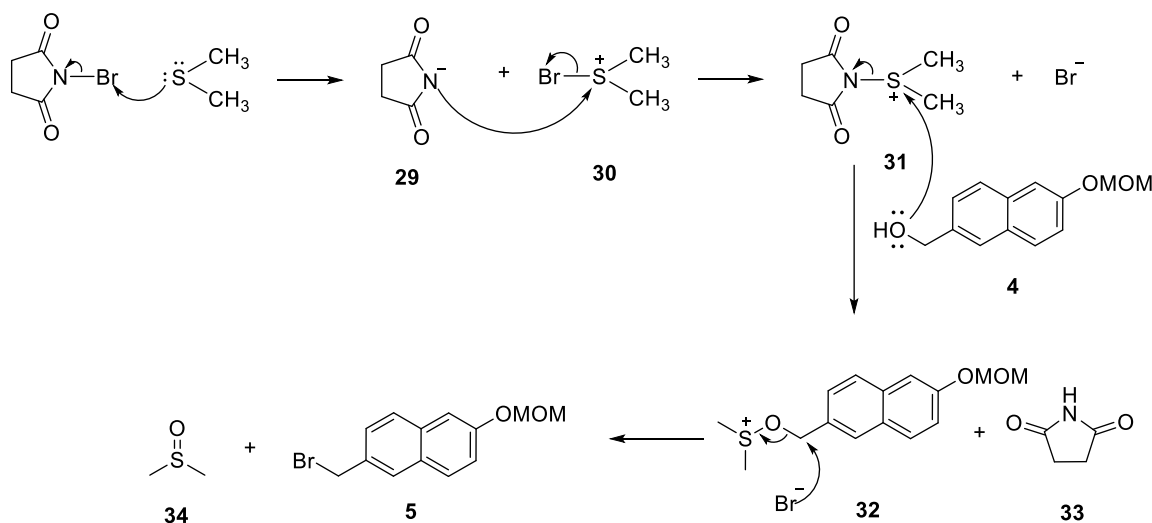


Figure 3.5 Mechanism of the bromination reaction.

Synthesis of 2-(3,5-Di-tert-butyl-2-hydroxyphenyl)acetonitrile (11)

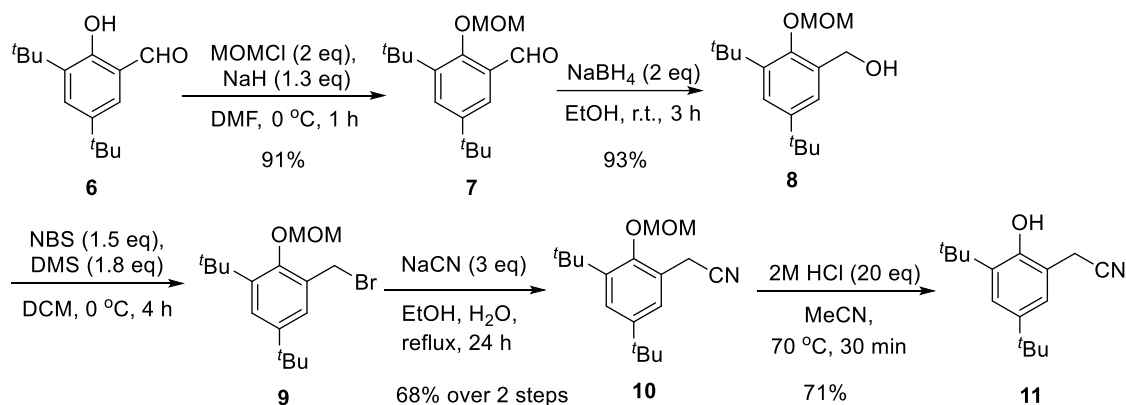


Figure 3.6 Synthesis of compound **11**.

3 Synthesis of Remote Selective C-H Functionalization of Naphthopyrans

The synthesis of compound **11** was reported in the literature before.^[84] Commercially available compound **6** was chosen as the starting material. Firstly, in the presence of NaH, MOMCl was used for protecting the hydroxyl group of compound **6**. Then compound **7** was reduced to compound **8** with a good yield of 93% by using NaBH₄ as the reductant. The third step is bromination of compound **8**, employing the same conditions as for the bromination reaction of compound **4**. After work up, the crude product **9** was directly used for the next step, considering it is sensitive to silica gel. In the presence of NaCN and H₂O, the nitrile group was introduced, and compound **10** was isolated in 68% yield over 2 steps. Significantly, NaCN is very toxic, so the reaction should be handled in a well-maintained fume hood and the operator should always have appropriate protection. The last step is deprotection of compound **10**. In the solvent of hydrochloric acid and acetonitrile, compound **10** can be converted into product **11** with a yield of 71% (Figure 3.6).

Synthesis of 2-(3,5-Di-tert-butyl-2-((6-(methoxymethoxy)naphthalen-2-yl)methoxy)phenyl)-2-isobutyl-4-methylpentanenitrile (13)

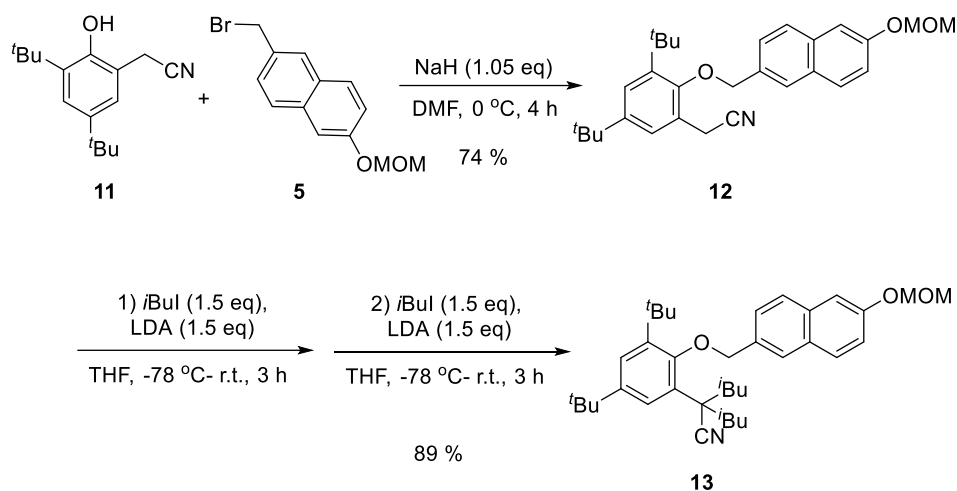


Figure 3.7 Synthesis of compound **13**.

With the directing group **11** and benzyl bromide **5** in hand, after deprotonation of compound **11** induced by NaH, we can afford substrate **12** by a simple nucleophilic substitution reaction in 74 % yield after 4 h in DMF. For the introduction of two isobutyl group, LDA was employed as the deprotonation reagent for the α -H of the nitrile group. Then the second *iso*-butyl group can be

3.1 Method I: Directed Selective C-H Functionalization

introduced into the α -position of the nitrile group. Afterwards, product **13** was obtained with a good yield of 89% (Figure 3.7).

C-H functionalization of naphthalene 13

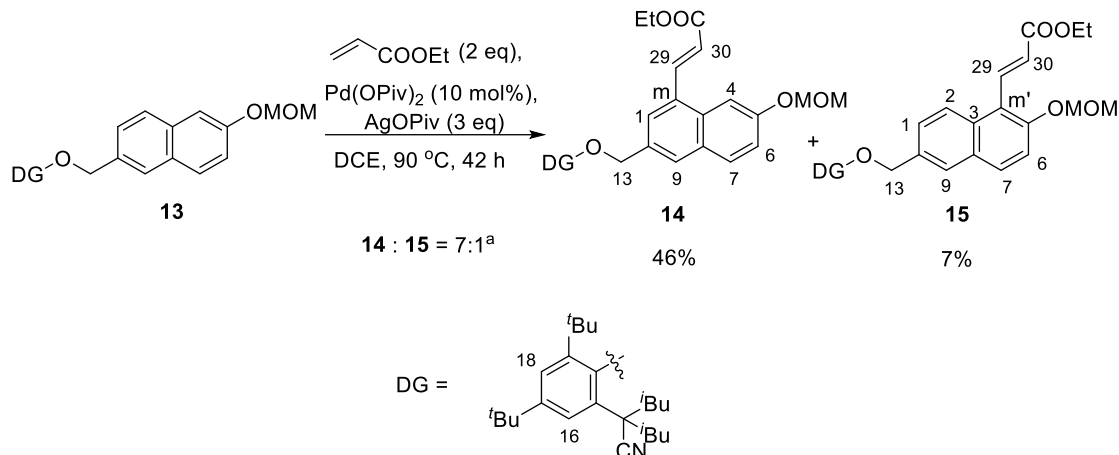


Figure 3.8 C-H functionalization of naphthalene **13** (a. the ratio was from ^1H NMR analysis of the unpurified reaction mixture using CH_2Br_2 as the internal standard).

The naphthalene **13** with directing group was prepared as the starting material of the C-H functionalization reaction. The other starting material is the commercially available ethyl acrylate. In the presence of Pd(OPiv)_2 and Ag(OPiv) , after 42 h reflux in DCE, product **14** was isolated with a yield of 46% as expected. Interestingly, product **15** was also detected and isolated in 7% yield. The ratio of the two products was $\text{14}:\text{15} = 7:1$ from ^1H NMR analysis of the unpurified reaction mixture (Figure 3.8). There are two reasons for the formation of **15**: 1) from spatial distance, m' -C is close to m -C, so that palladium can also activate the m' -C-H bond; 2) m' -position is a favorable position for classical Friedel-Crafts reaction. In addition, there were 16% of starting material **13** left, which can be recycled.

To characterize the structure of the products **14** and **15**, 2D NMR spectra were obtained, including ^{13}C DEPT NMR spectrum, ^1H - ^{13}C HMBC NMR spectrum, ^1H - ^{13}C HMQC NMR spectrum and ^1H - ^1H COSY NMR spectrum (see Chapter 8.2). At first, the chemical shifts of H-16, H-18, H-29 and H-30 were easily identified. For product **14**, the additional peaks in the aromatic area were as follows: a singlet at 7.86 ppm, a doublet at 7.75 ppm, a singlet at 7.70 ppm, a doublet at 7.60 ppm and a doublet of doublet at 7.23 ppm. One part of the ^1H - ^{13}C HMBC NMR spectrum and ^1H - ^1H COSY NMR spectrum of **14** is displayed in Figure 3.9. Correlations were observed between C-13

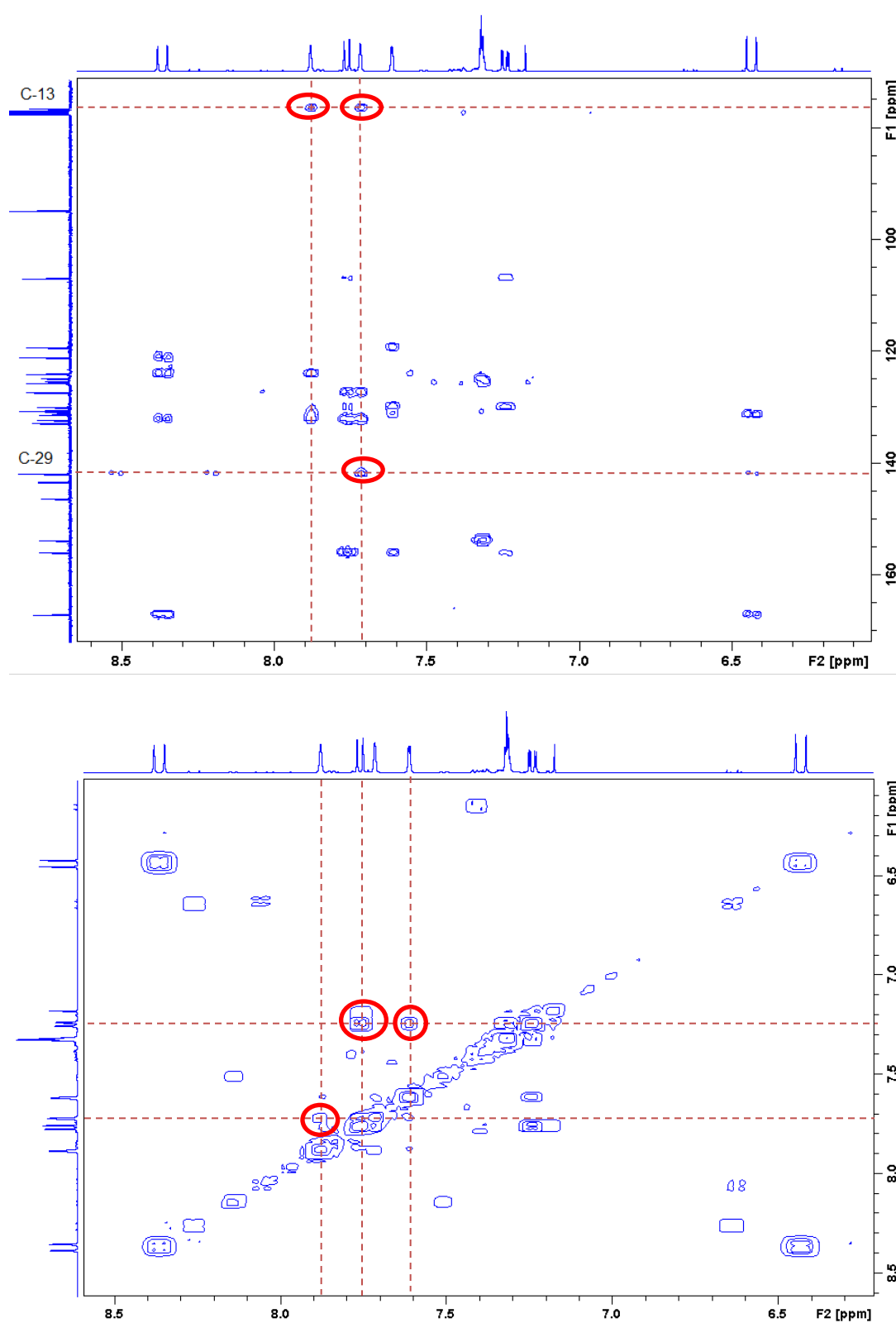


Figure 3.9 500 MHz ^1H - ^{13}C HMBC NMR spectrum (up) and ^1H - ^1H COSY NMR spectrum (down) of **14**.

3.1 Method I: Directed Selective C-H Functionalization

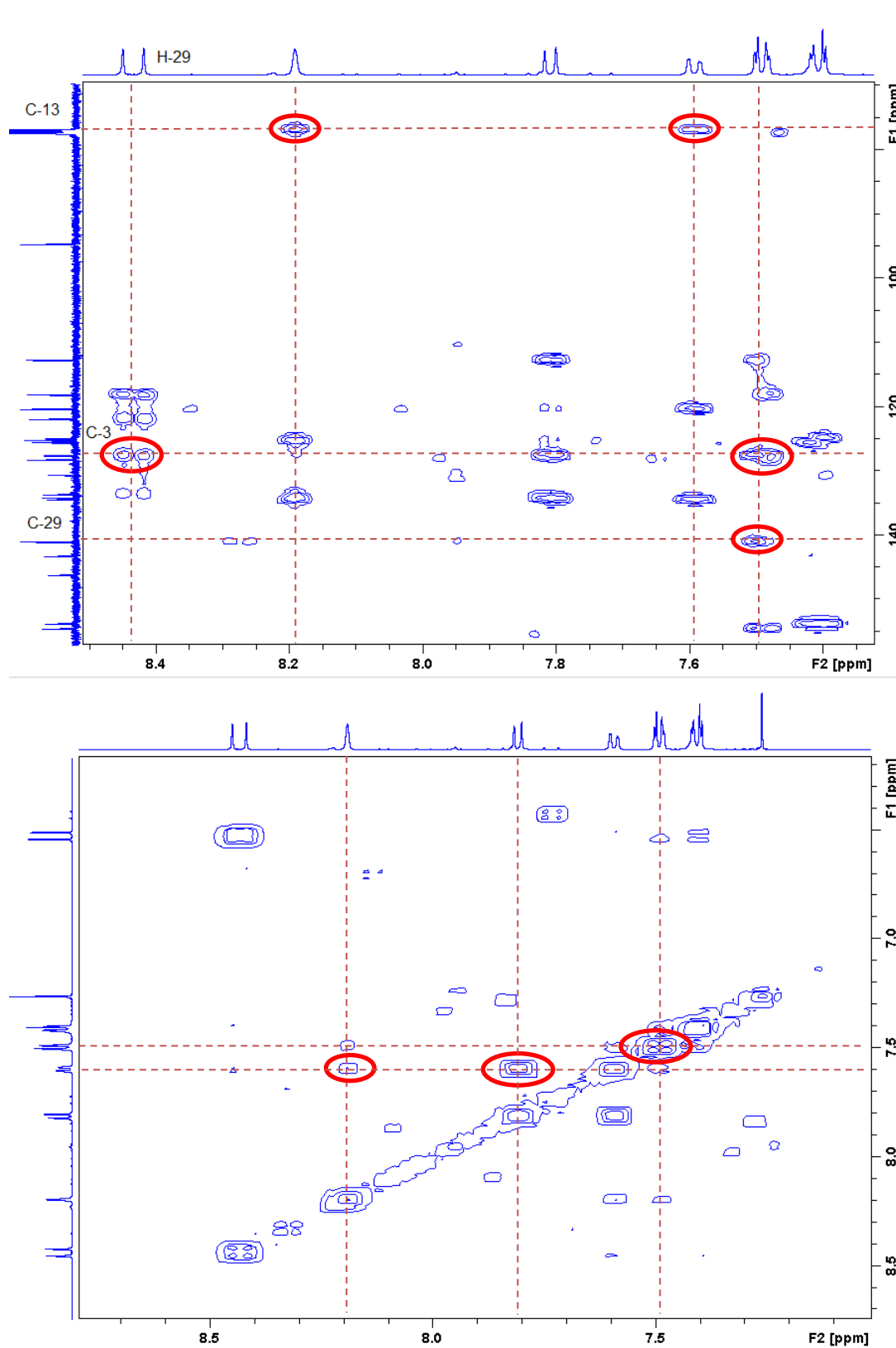


Figure 3.10 500 MHz ^1H - ^{13}C HMBC spectrum (up) and ^1H - ^1H COSY NMR spectrum (down) of **15**.

and two singlet peaks at 7.86 and 7.70 ppm, and a weak correlation was found between those two singlets. Accordingly, those two singlets were assigned to H-1 and H-9 and the acrylic ester substituent should be at *m*-position. When the correlation was observed between C-29 and the singlet at 7.70 ppm, the singlet at 7.70 ppm was assigned to H-1 and the other singlet was assigned to H-9. Correspondingly, H-4, H-6 and H-7 were identified, when doublet of doublet at 7.23 ppm was observed to be correlated with doublets at 7.75 and 7.60 ppm, respectively.

For product **15**, there were still four peaks to be identified in the aromatic area: one singlet at 8.19 ppm, one doublet at 7.81 ppm, one doublet of doublet at 7.59 ppm and one multiplet at 7.50-7.18 ppm. The ^1H - ^{13}C HMBC NMR spectrum in Figure 3.10 reveals that C-13 was correlated with the singlet at 8.19 ppm and the doublet of doublet at 7.59 ppm, respectively. Therefore, the singlet was assigned to H-9, and the doublet of doublet signal at 7.59 ppm was assigned to H-1. When a correlation was found between H-1 and doublet at 7.81 ppm in the ^1H - ^1H COSY NMR spectrum (Figure 3.10), the doublet at 7.81 ppm was assigned to H-2. Moreover, C-3 was noticed to be correlated with H-29, while no correlation was detected between C-8 and H-29. Thus, the acrylic ester substituent should be at *m'*-position. At last, the multiplet at 7.50-7.18 ppm was assigned to the mixture of H-6 and H-7.

The proposed mechanism for this reaction is presented in Figure 3.11, based on the literature.^[85,128] The useful catalyst is compound **35**, which was formed from $\text{Pd}(\text{OPiv})_2$ and $\text{Ag}(\text{OPiv})$. At first, the nitrile group of compound **13** coordinated with silver. Then the reaction was divided into two directions, which resulted in two different products: **14** and **15**. If the carbon at *m*-position coordinated with palladium, through a concerted metalation-deprotonation process, *meta*-C-H activation was achieved and intermediate **39** was obtained. Meanwhile, ethyl acrylate can coordinate with palladium. After alkene insertion, intermediate **42** was obtained. At last, product **14** was achieved through β -hydride elimination reaction, and catalyst **35** was reformed through the oxidation by $\text{Ag}(\text{OPiv})$. On the other hand, if the catalyst coordinated with the carbon at *m'*-position, product **15** can be obtained through similar processes.

3.1 Method I: Directed Selective C-H Functionalization

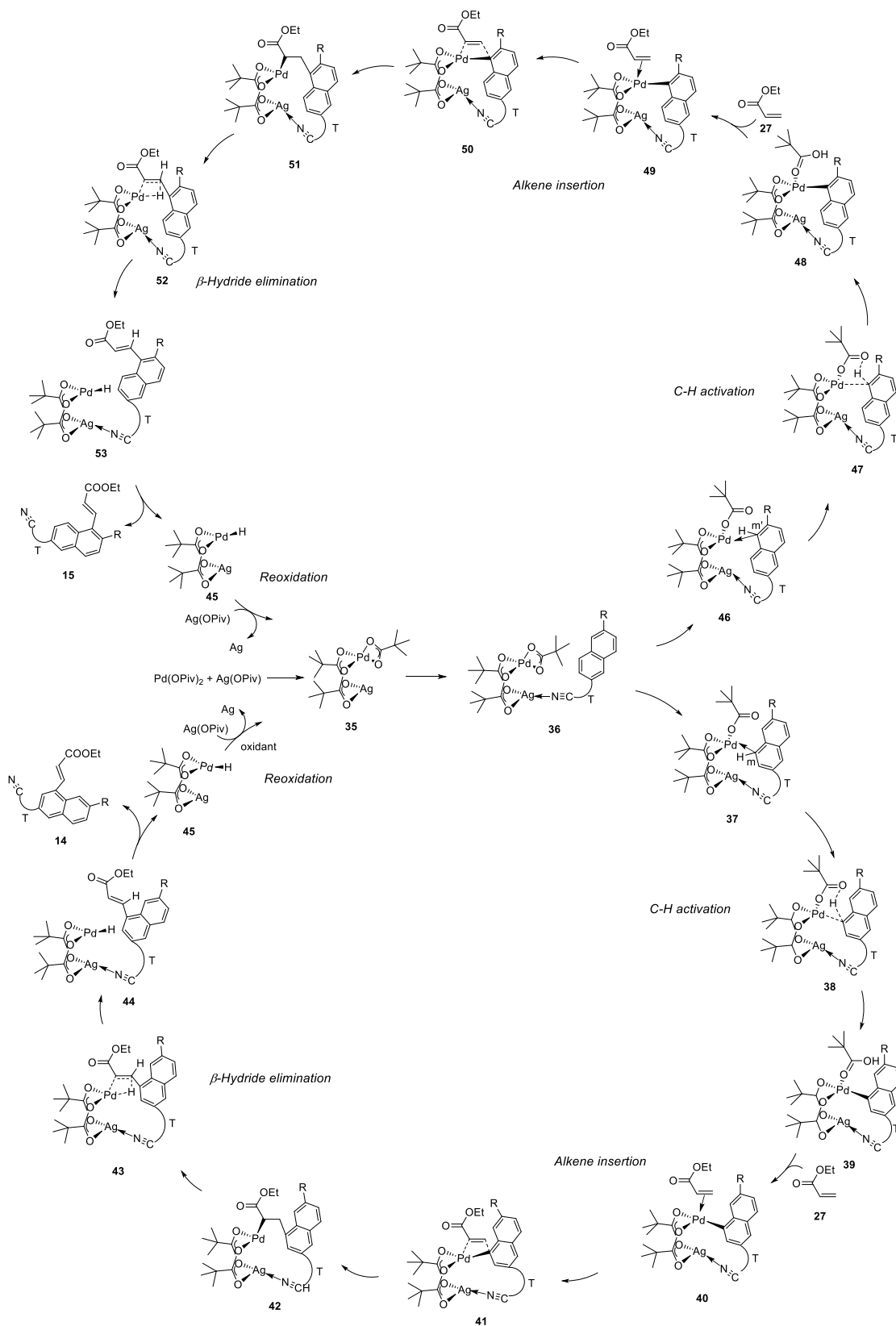


Figure 3.11 Proposed mechanism of C-H functionalization of naphthalene 13.

Synthesis of Ethyl (E)-3-(3-((2,4-di-tert-butyl-6-(4-cyano-2,6-dimethylheptan-4-yl)phenoxy)methyl)-7-hydroxynaphthalen-1-yl)acrylate (16)

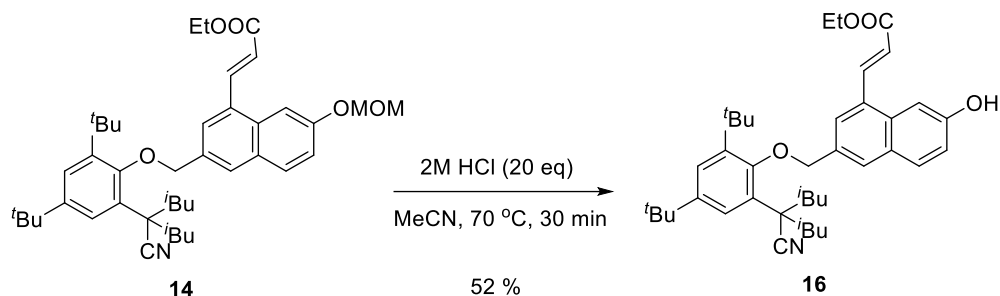


Figure 3.12 Synthesis of compound **16**.

The m-C-H activation product **14** was employed for the final synthesis of a naphthopyran. After 30 min in the solvent of hydrochloric acid and acetonitrile, the key building block **16** was isolated with a yield of 52% (Figure 3.12).

Synthesis of 1-(2-Chlorophenyl)-1-(4-(pyrrolidin-1-yl)phenyl)prop-2-yn-1-ol (20)

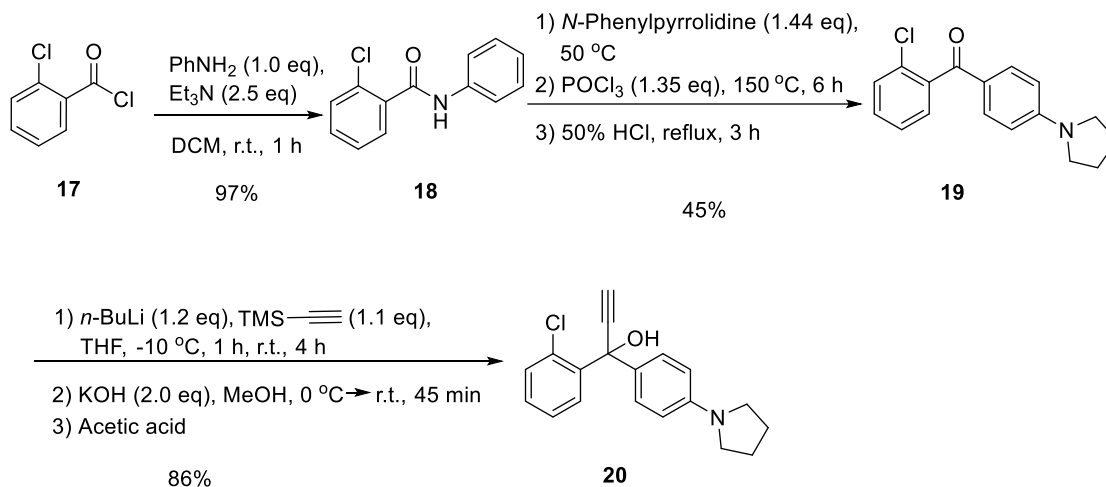


Figure 3.13 Synthesis of compound **20**.

3.1 Method I: Directed Selective C-H Functionalization

Synthesis of compound **20** started with the commercially available compound **17** (Figure 3.13). At first, compound **17** was activated by triethylamine. Then aniline nucleophilic attacked the activated acid chloride **17**. After formation of triethylamine hydrochloride, product **18** was obtained in 97% yield.^[129]

The conversion from compound **18** to **20** was achieved according to the reported literature.^[65] The synthesis of compound **18** from **19** went through a Vilsmeier-Haack reaction. The mechanism is demonstrated in Figure 3.14. The reaction was carried out in two steps. The first step was the formation of the Vilsmeier reagent: iminium salt **57**. The second step was the reaction between *N*-phenylpyrrolidine and iminium salt **57** to afford compound **19**. At first, POCl₃ was attacked by the oxygen of **18'** to afford intermediate **54**. After the leaving of the chlorine anion, intermediate **55** was generated. Then the carbon of **55** was nucleophilic attacked by the chlorine anion. After leaving of the phosphorus salt, iminium salt **57** was formed. Afterwards intermediate **58** was obtained through an electrophilic aromatic substitution reaction between *N*-phenylpyrrolidine and iminium salt **57**. After elimination of hydrogen chloride, intermediate **59** was obtained. At last, product **19** was isolated in a yield of 45% by hydrolysis through aqueous workup.

For the preparation of compound **20**, firstly, lithium (trimethylsilyl)acetylide was prepared *in-situ* during the reaction between trimethylsilylacetylene and *n*-butyllithium solution. Then the solution of starting material **19** in THF was added. By the addition of potassium hydroxide in methanol, the trimethylsilyl group was removed and the product propargyl alcohol **20** was obtained in 86% yield.

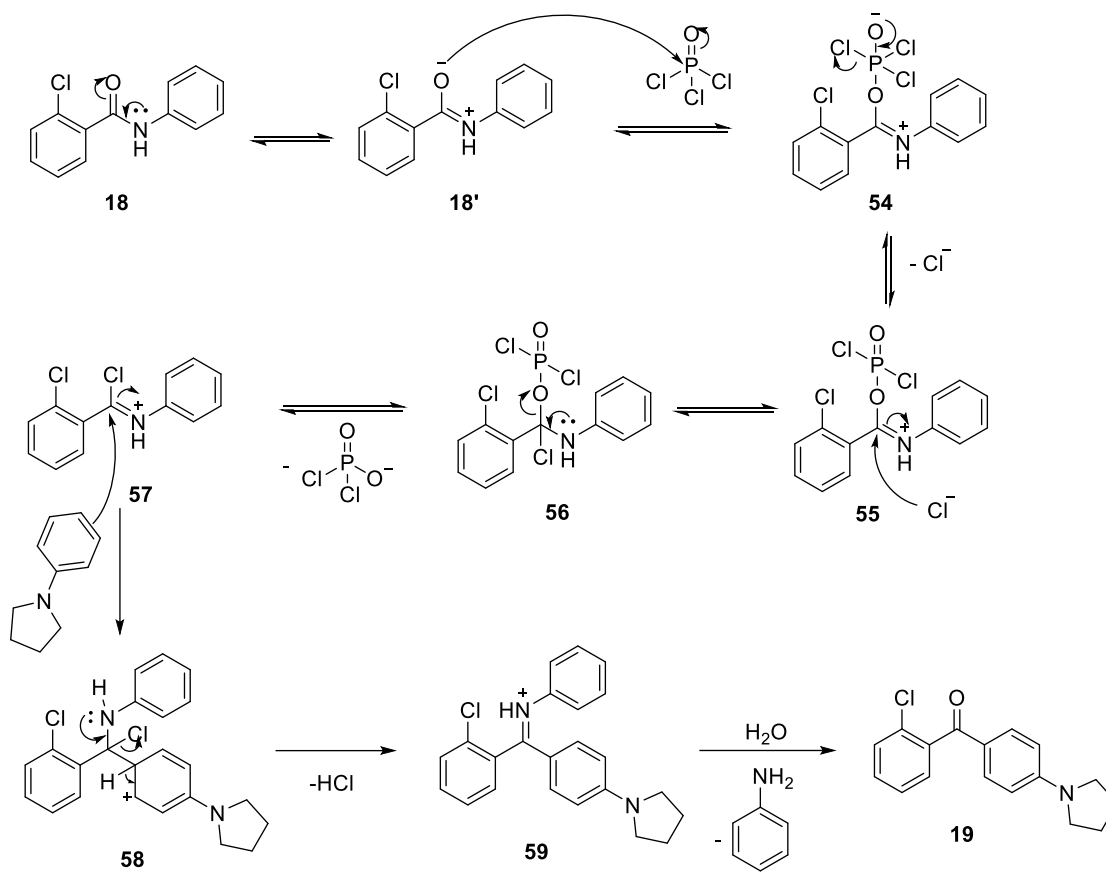


Figure 3.14 Mechanism of the Vilsmeier-Haack reaction.

Synthesis of naphthopyran **21**

With the building block **16** and propargyl alcohol **20** in hand, the preparation of naphthopyran **21** was investigated with the method reported by Gabbutt et al.^[65] (Figure 3.15). Unfortunately, naphthopyran **21** was not detected, after 1.5 h stirring with acidic aluminium oxide in toluene. Approximately 85% of starting material **16** was left. In addition, byproduct **22** was isolated in 40% yield, which was generated through a Meyer–Schuster rearrangement.^[31,130]

The mechanism is described in Figure 3.16. In the beginning, compound **20** was protonated by the acid catalyst. After leaving of one molecule water, intermediate **61** was formed. Then water nucleophilic attacked the allene group of **61**, and intermediate **62** was generated. After deprotonation, intermediate **63** was obtained. At last, byproduct **22** was formed through keto-enol tautomerism.

3.1 Method I: Directed Selective C-H Functionalization

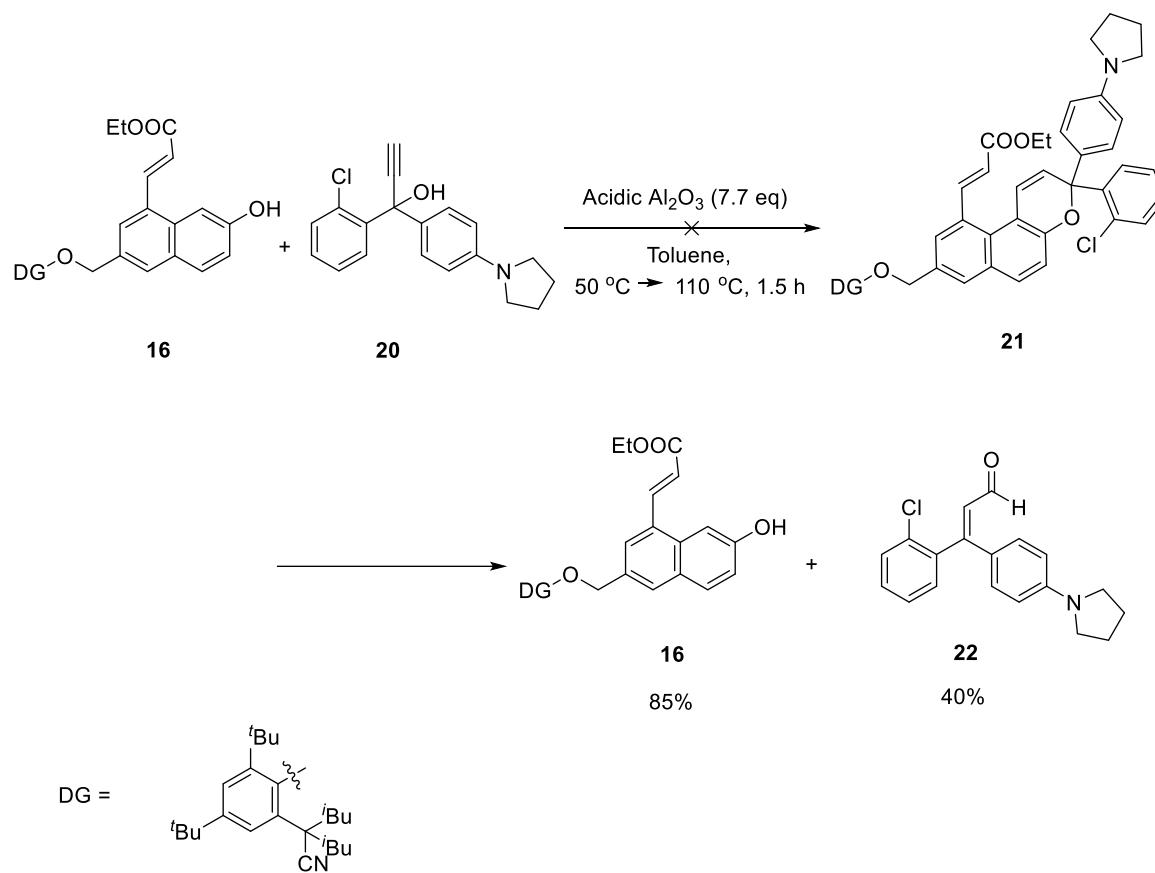


Figure 3.15 Synthesis of naphthopyran **21**.

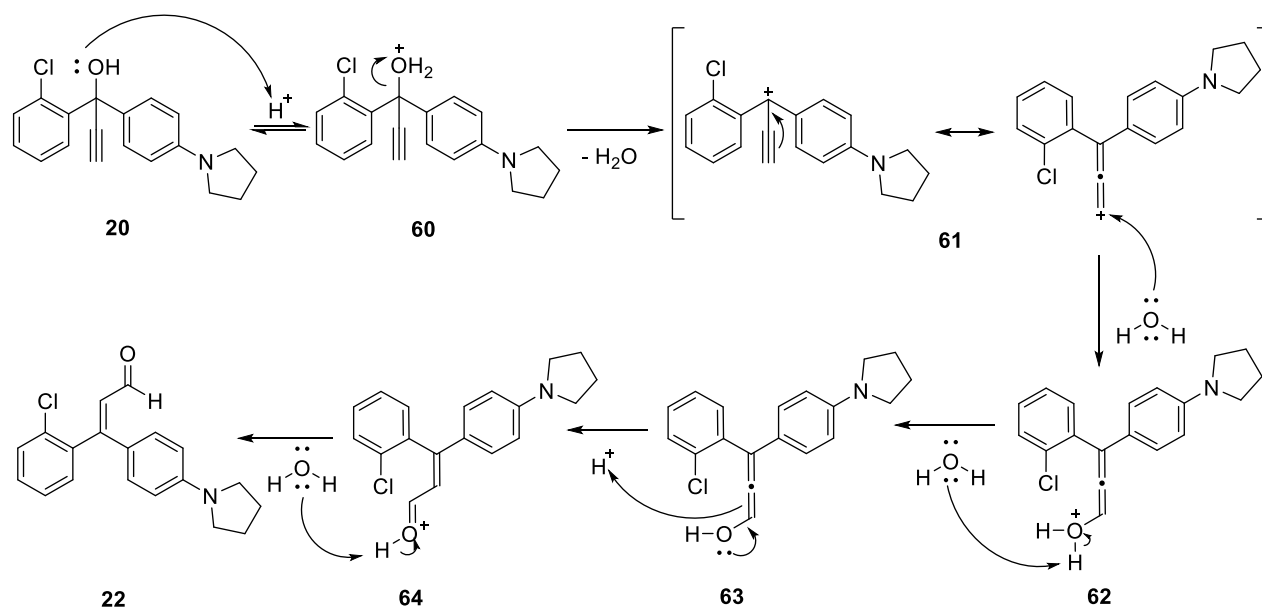


Figure 3.16 Mechanism of Meyer-Schuster rearrangement.

3.1.2 Route 2 of the Synthesis

Considering it is difficult to synthesize naphthopyrans using *m*-C-H functionalization of the naphthalene **16** from route 1, route 2 was proposed in Figure 3.17. In this way, the naphthopyrans with directing group, **N4** and **N6**, were prepared firstly. Then remote C-H functionalization of the naphthopyran can be investigated. Naphthopyrans **N4** and **N6** can be obtained through acid-catalyzed etherification of naphthol **23**, followed by Claisen rearrangement, enolization, 1,5-hydrogen-shift and electrocyclization with propargyl alcohols **20** and **25**, respectively. Naphthol **23** can be prepared through deprotection of compound **13** and the protected precursor **13** can be generated from compound **11** and **5**.

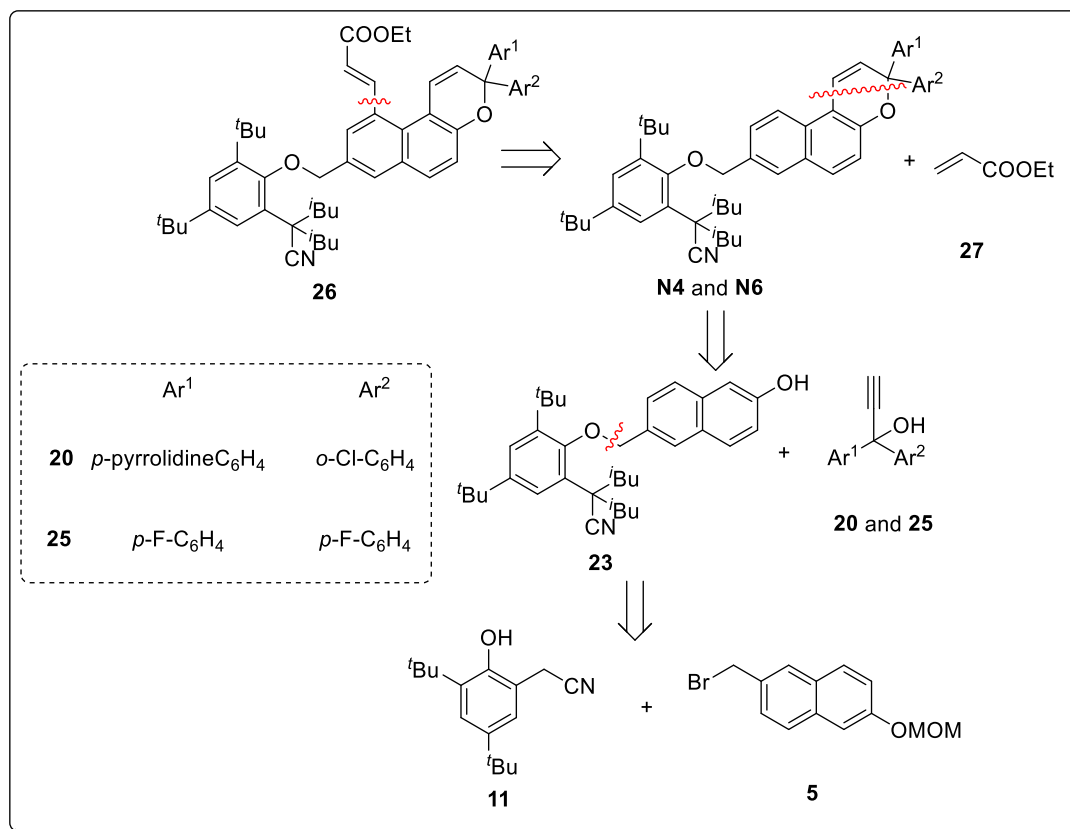
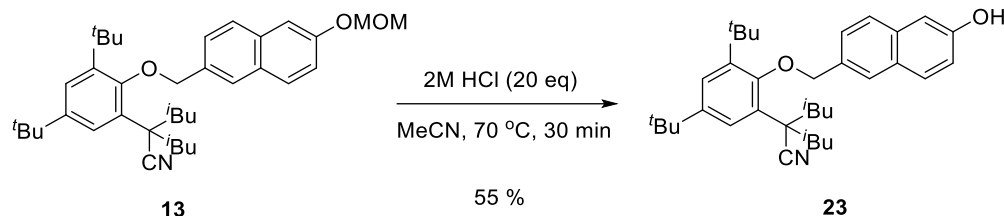
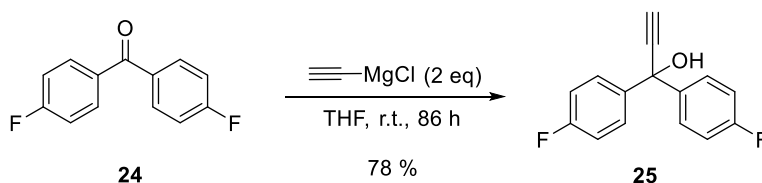


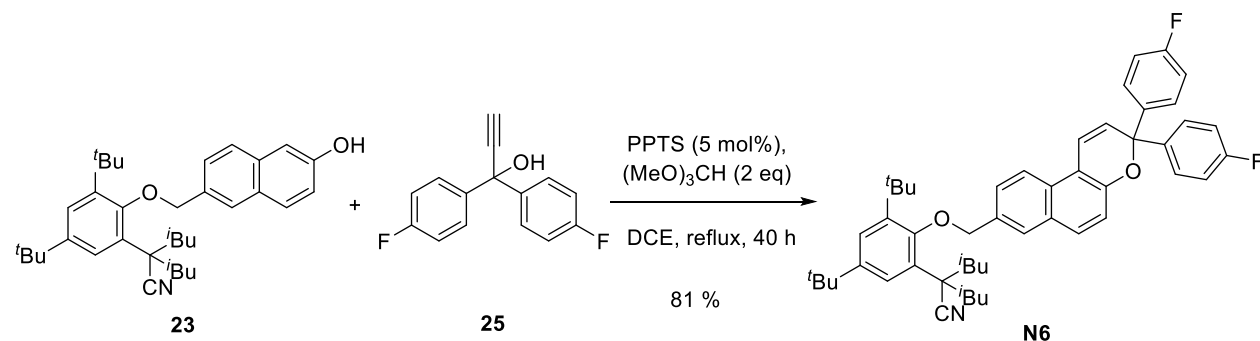
Figure 3.17 Proposed retrosynthetic route 2 about directed remote C-H functionalization of naphthopyrans **N4** and **N6**.

Synthesis of 2-(3,5-Di-tert-butyl-2-((6-hydroxynaphthalen-2-yl)methoxy)phenyl)-2-isobutyl-4-methylpentanenitrile (23)**Figure 3.18** Synthesis of naphthol **23**.

The synthesis route 2 started from compound **13**, which was synthesized in route 1 (Chapter 3.1.1). In the solution of 2M hydrochloric acid in acetonitrile, after 30 min stirring at 70 °C and aqueous workup, the protection group MOM was removed and product **23** was isolated in 55% yield (Figure 3.18).

Synthesis of 1,1-Bis(4-fluorophenyl)prop-2-yn-1-ol (25)**Figure 3.19** Synthesis of propargyl alcohol **25**.

Propargyl alcohol **25** was synthesized from commercially available compound **24** based on the known literature.^[58] After 86 h stirring in THF, product **25** was isolated in a good yield of 78% through a Grignard reaction with ethynylmagnesium chloride (Figure 3.19).

Synthesis of naphthopyrans N4 and N6**Figure 3.20** Synthesis of naphthopyran **N6**.

3 Synthesis of Remote Selective C-H Functionalization of Naphthopyrans

For the synthesis of naphthopyran **N6**, compounds **23** and **25** were employed as starting materials and PPTS was used as the catalyst.^[131] After 40 h refluxing in DCE solution in the presence of (MeO)₃CH, **N6** was afforded in 81% yield (Figure 3.20).

The mechanism is presented in Figure 3.21. At first, in the presence of the acid catalyst, one molecule of water was removed and intermediate **66** was formed. Then **66** was nucleophilic attacked by compound **23** and intermediate **67** was obtained. By a Claisen rearrangement, intermediate **67** was converted to intermediate **68**. Subsequently, intermediate **69** was obtained via keto-enol tautomerism and aromatization. After [1, 5]-H-Shift, intermediate **70** was formed. At last, product **N6** was prepared through an electrocyclic ring closure reaction.

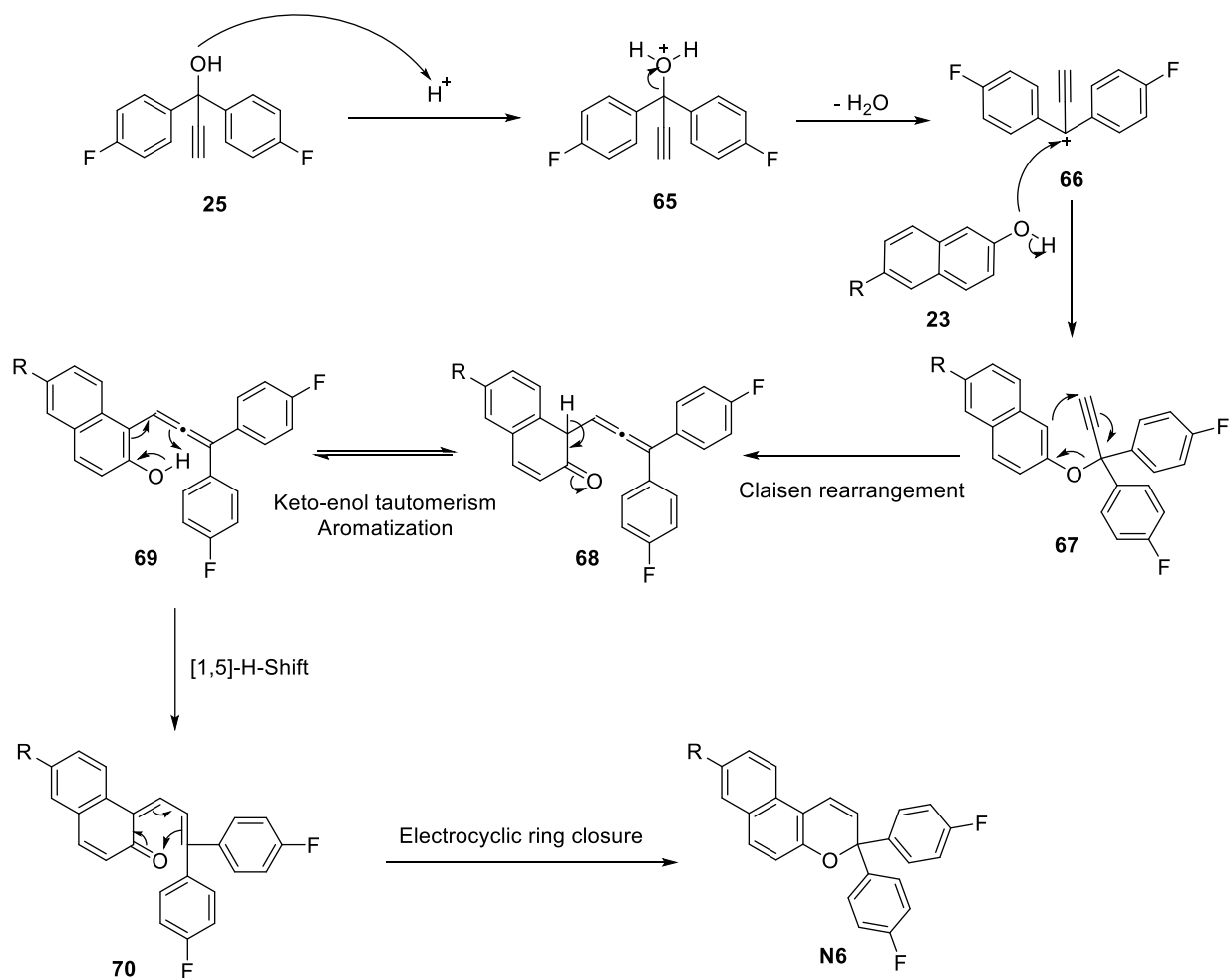


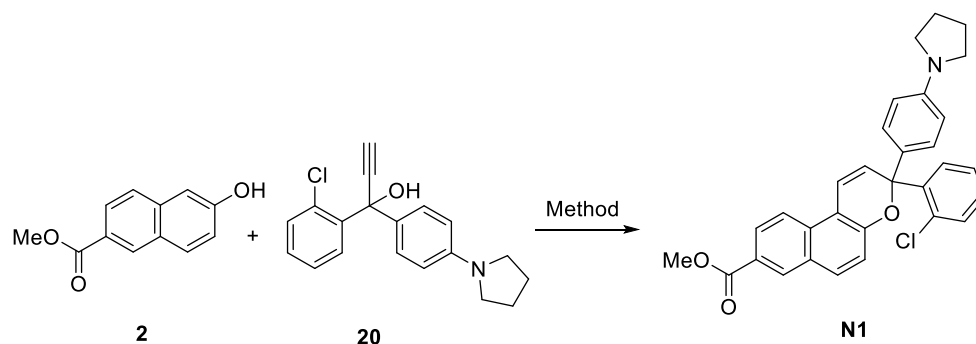
Figure 3.21 Mechanism of the synthesis of naphthopyran **N6**.

3.1 Method I: Directed Selective C-H Functionalization

From the investigation of the synthesis methods of naphthopyran **N1** (Table 3.1), it was revealed that method A was not suitable compared with method B. Presumably because naphthopyran **N1** is unstable at high temperature, considering the reaction temperature is more than 110 °C for method A while 84 °C for method B.

Considering naphthopyran **N4** has a similar structure with **N1**, method B was employed for the synthesis of naphthopyran **N4**. Compounds **23** and **20** were starting materials and acidic aluminium oxide was chosen as the catalyst.^[65] After 1.5 h reflux in toluene, naphthopyran **N4** was obtained in 55% yield (Figure 3.22). The mechanism is similar to the mechanism of the synthesis of naphthopyran **N6**.

Table 3.1 Optimization of the synthetic methods.^a



Entry	Method	Reaction time	Yield
1	A	27 h	23 %
2	B	26 h	46 %

[a] 0.5 mmol scale. Method A: PPTS (5 mol%), (MeO)₃CH (2 equiv), DCE, reflux; Method B: acidic Al₂O₃ (7.7 equiv), toluene, reflux. Data from PhD Thesis of Diana Liebmann in the Rück-Braun group.

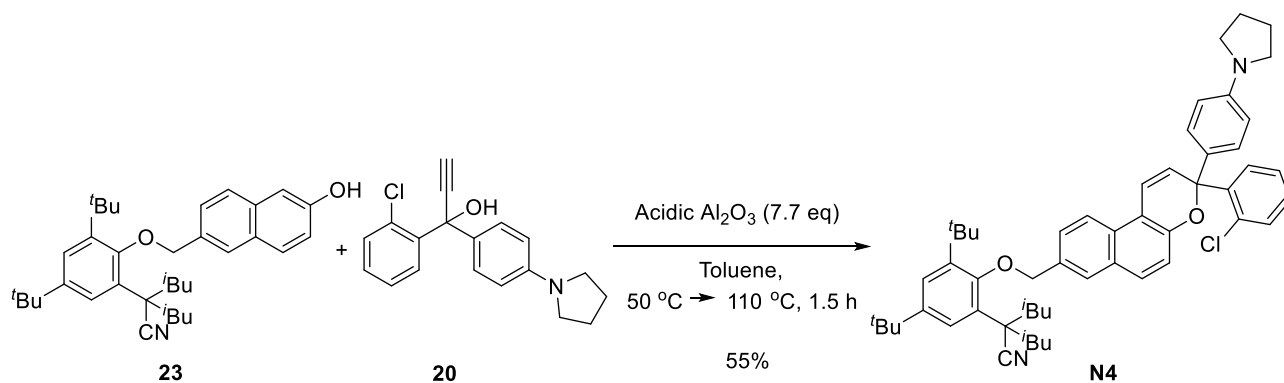


Figure 3.22 Synthesis of naphthopyran **N4**.

Remote C-H functionalization of naphthopyran **N6**

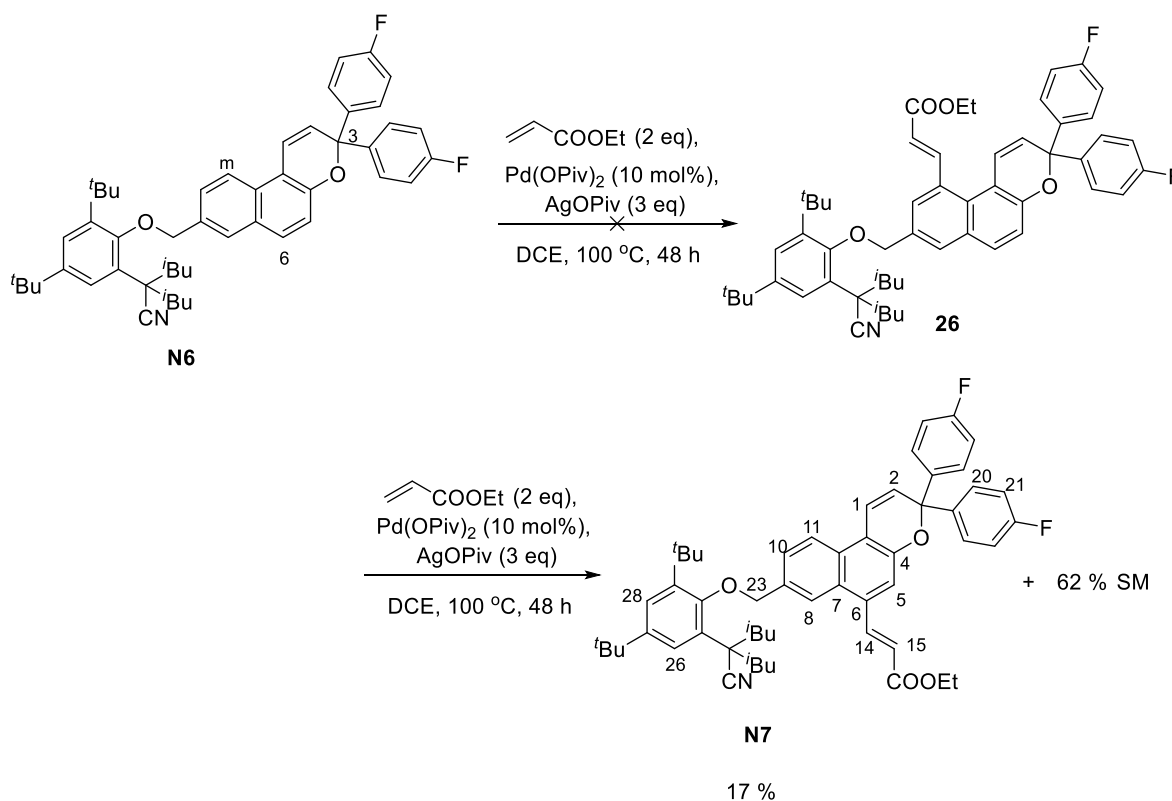


Figure 3.23 C-H functionalization of naphthopyran **N6**.

With the prepared naphthopyran **N6** with the directing group in hand, the reaction of remote C-H functionalization of **N6**, catalyzed by $\text{Pd}(\text{OPiv})_2$, in the presence of $\text{Ag}(\text{OPiv})$, by refluxing in DCE solution with acrylic acid ethyl ester for 48 h was investigated. Surprisingly, the *m*-C-H activation product **26** was not detected. However, the 6-position C-H activation product **N7** was isolated by chromatography in 17% yield (Figure 3.23).

3.1 Method I: Directed Selective C-H Functionalization

To characterize the structure of **N7**, 2D ^{13}C DEPT NMR spectrum, ^1H - ^{13}C HMBC NMR spectrum, ^1H - ^{13}C HMQC NMR spectrum and ^1H - ^1H COSY NMR spectrum were acquired (see Chapter 8.2). Accordingly, it is easy to identify the chemical shifts of H-1, H-2, H-14, H-15, H-20, H-21, H-26 and H-28. A singlet at 8.16 ppm, a doublet at 8.05 ppm, a doublet of doublet at 7.68 ppm and a singlet at 7.46 ppm were still unidentified in the aromatic area. Based on the ^1H - ^{13}C HMBC NMR spectrum (Figure 3.24), it was observed that C-23 was correlated with the singlet at 8.16 ppm and the doublet of doublet at 7.68 ppm, respectively. In the ^1H - ^1H COSY NMR spectrum (Figure 3.24), there existed correlations between the doublet of doublet at 7.68 ppm and the doublet at 8.05 ppm, and a weak correlation between the doublet of doublet at 7.68 ppm and the singlet at 8.16 ppm. As a result, the singlet at 8.16 ppm was assigned to H-8, the doublet at 8.05 ppm was assigned to H-11, and the doublet of doublet at 7.68 ppm was assigned to H-10. At last, H-14 was observed to correlate with C-7, while there was no correlation between C-4 and H-14. Hence, the acrylic ester substituent should be at 6-position and the singlet at 7.46 ppm was assigned to H-5.

Remote C-H functionalization of naphthopyran **N4** was also investigated under the same conditions. Unfortunately, there was no desired C-H functionalization product observed from the reaction, and only damaged **N4** was found. To investigate the effect of directing group, naphthopyran **28** was prepared according to the literature^[131]. After 48 h reflux under the same conditions, almost 100% of starting materials were left observed from ^1H NMR spectroscopy (Figure 3.25, for ^1H NMR spectrum, see Chapter 8.1, Figure 8.2). The results indicated that the reaction is obviously accelerated by the coordination of the nitrile group to the catalyst and the directing group can affect the reactivity and selectivity of the C-H functionalization reaction.

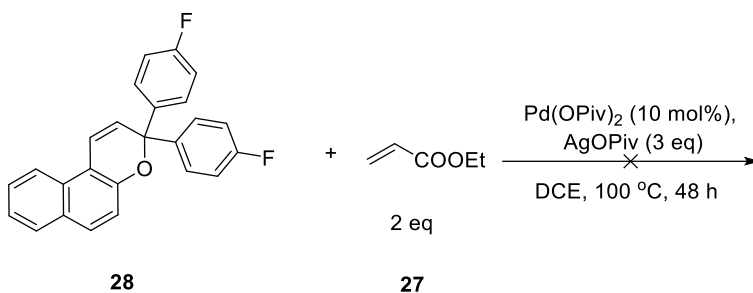


Figure 3.25 C-H functionalization of naphthopyran **28** without directing group.

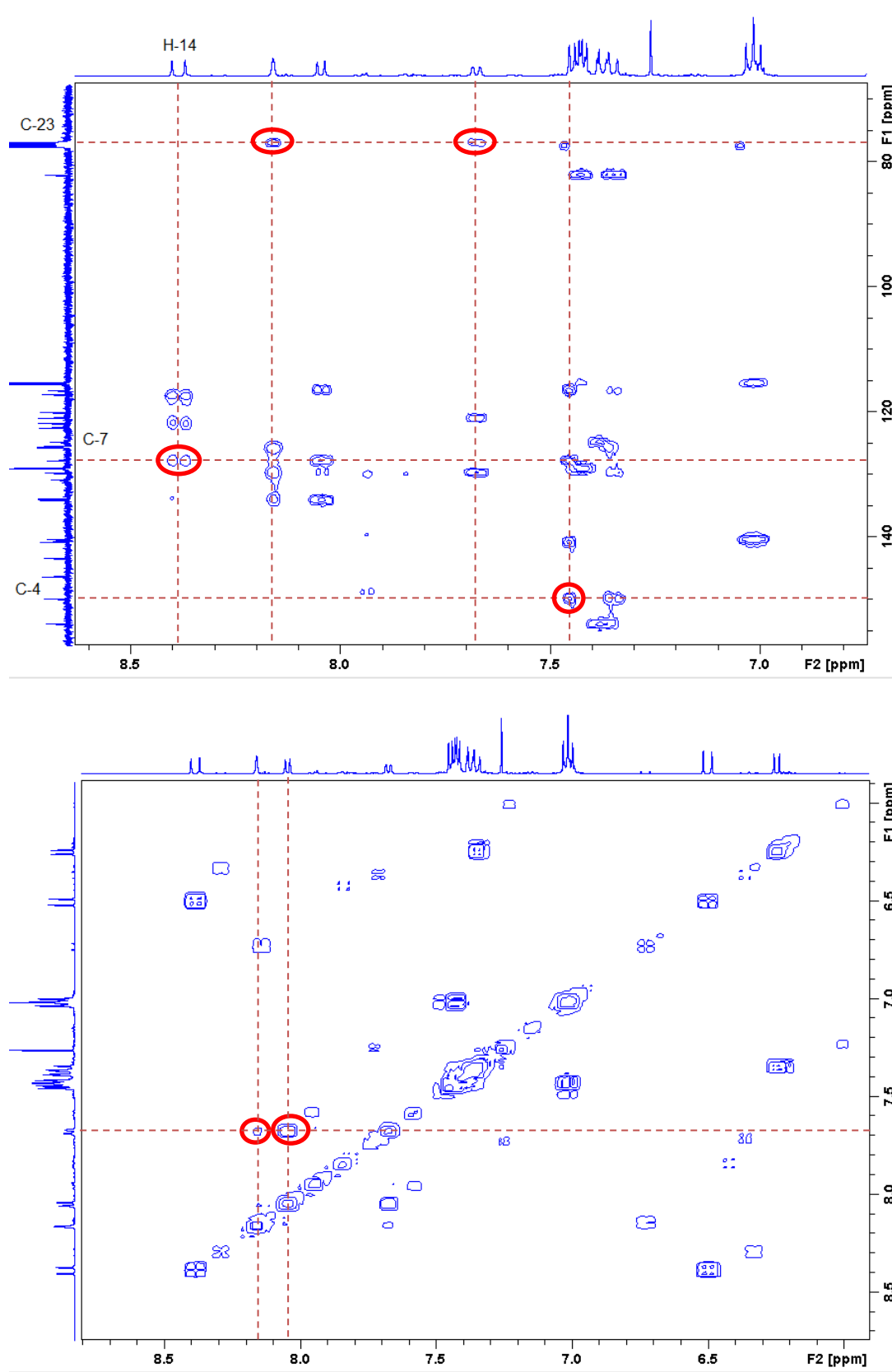


Figure 3.24 500 MHz ^1H - ^{13}C HMBC (up) and ^1H - ^1H COSY NMR spectrum (down) of N7.

3.2 Method II: Nondirected *Meta*-C-H Functionalization

Nondirected selected C-H activation is an attractive method, because building complex directing groups is not necessary in this way. Correspondingly, we do not need to remove them afterwards. In 2018, the van Gemmeren group reported their good results about dual ligand-enabled nondirected C-H olefination of benzene compounds,^[111] which gave us an inspiration to investigate a method to achieve *meta*-C-H functionalization of naphthopyrans.

The proposed synthetic route is shown in Figure 3.26. Considering the intricate structure of naphthopyran **72**, achieving C-H olefination of naphthalene **3** firstly is a favorable choice. Then after deprotection, naphthol **71** can be obtained. Under acidic catalysis and reaction with propargyl alcohol, the final C-H functionalization and the formation of naphthopyran **72** can be achieved, based on the research experience of the Rück-Braun group.

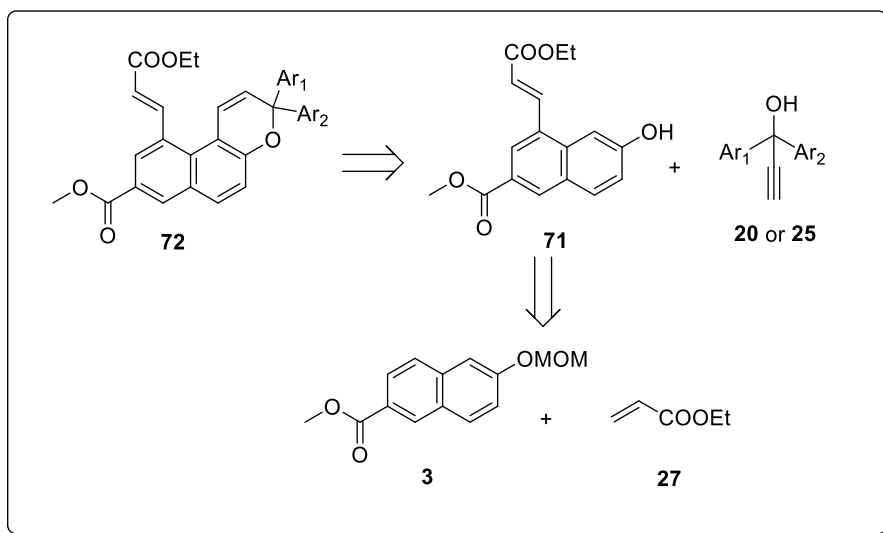
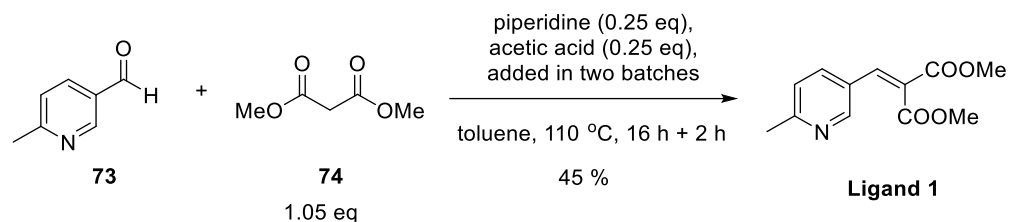
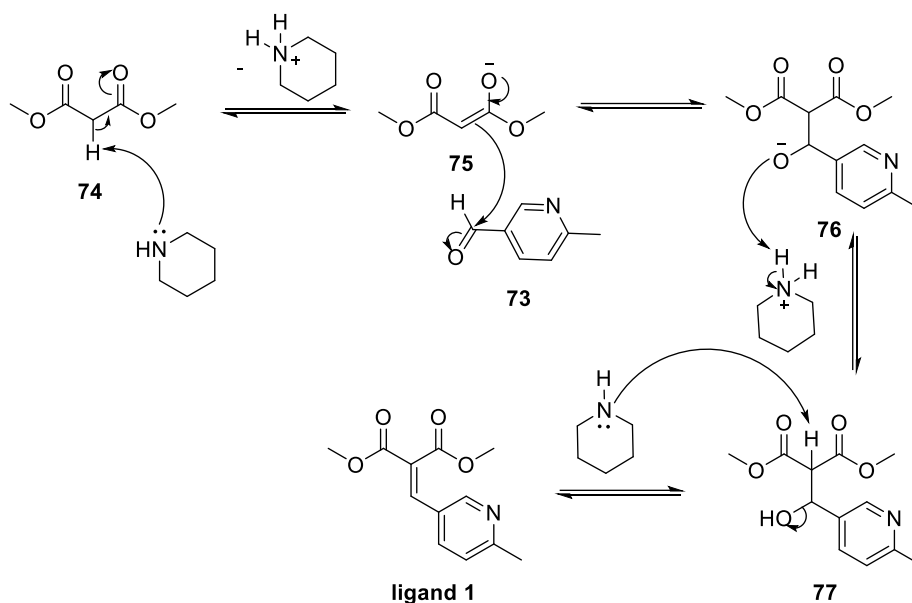


Figure 3.26 Proposed retrosynthetic route about nondirected *m*-C-H functionalization of naphthalene.

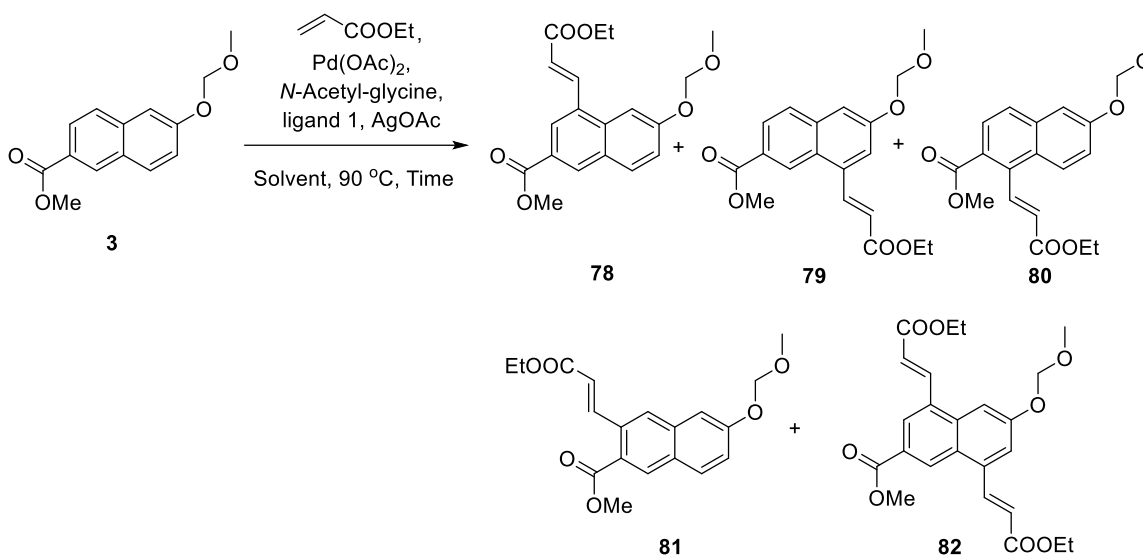
Synthesis of Ligand 1**Figure 3.27** Synthesis of **ligand 1**.

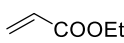
Our synthetic path started with the synthesis of **ligand 1**. In the presence of piperidine and acetic acid, **ligand 1** was obtained from aldehyde **73** and dimethyl malonate **74** with a yield of 45%,^[111] through a Knoevenagel condensation (Figure 3.27). The mechanism is described in Figure 3.28. Firstly, compound **74** was deprotonated by the piperidine. Intermediate **75** attacked aldehyde **73**. After protonation, **77** was formed. Finally, **ligand 1** was obtained after the elimination of one molecule water.

**Figure 3.28** The mechanism of the Knoevenagel condensation.

3.2 Method II: Nondirected *Meta*-C-H Functionalization

Table 3.2 Control experiments.^a



Entry		Solvent	Time	Conversion	Product ratio ^b
1	3 equiv	HFIP	24 h	84 %	25:30:32:8:5
2	1 equiv	HFIP	24 h	63 %	60:14:9:11:6
3	3 equiv	HFIP	14 h	43 %	54:14:6:14:12
4	3 equiv	DCE	14 h	40 %	48:22:10:4:16

[a] 0.2 mmol scale. Pd(OAc)₂ (10 mol%), *N*-Acetyl-glycine (30 mol%), ligand 2 (20 mol%), AgOAc (0.6 mmol), solvent (2 mL), 90 °C. Yields were determined by ¹H NMR analysis using CH₂Br₂ as the internal standard (for spectrum, see Chapter 8.1, Figure 8.1). [b] Ratios were identified by the hydrogen signals of alkene substituents.

The starting material **3** was prepared according to method I (Chapter 3.1.1) and **ligand 1** was also prepared. As for ethyl acrylate **27**, Pd(OAc)₂, AgOAc and *N*-acetyl-glycine, they are all commercially available. Hence the experiments of nondirected C-H activation of naphthalene **3** were investigated under the conditions of Table 3.2. After 24 h reflux, about five different products were identified, which could not be separated from each other by column chromatography. According to the information from the literature,^[111] the C-H activation prefers to happen in the

ortho- and *meta*-position of the electron-withdrawing substituent and the *meta*-position of the electron rich substituent. Thus, five possible structures are presented in Table 3.2. We tried to control the ratio by reducing the reaction time, decreasing the amount of ethyl acrylate **27** and changing the solvent. However, unfortunately, isolation of pure products was not achieved. What we isolated was always the mixture. Therefore, we cannot continue with this method anymore. This nondirected *meta*-C-H activation seems to be suitable for benzene compounds but not for naphthalene compounds. Hence effective methods for nondirected *meta*-C-H activation of naphthalene should be investigated in the future.

3.3 Discussion

3.3.1 The Selection for C-H Functionalization of Naphthopyran N6

Remote C-H functionalization of naphthalene **27** resulted in *m*- and *m'*-selected products, while 6-selected product **N7** was obtained from remote C-H functionalization of naphthopyran **N6** (Figure 3.29). Reviewing the mechanism of remote C-H functionalization of naphthalene in Figure 3.11, intermediates **38** and **47** are the key intermediates in the process of C-H activation. According to the computation from the literature,^[85] the directing group coordinated with catalyst favored to activate *meta*-C-H bonds for normal benzene compound. For naphthalene **13**, the *m'*-C-H is adjacent to *m*-C-H, thus *m'*-C-H functionalization product **15** was formed. However, in the *m*-C-H (10-position) activation process of naphthopyran **N6**, there exist large steric restrictions in the structure of the intermediate **83**. Consequently, 6-selected C-H functionalization product **N7** was formed since the intermediate **84** is favorable (Figure 3.30).

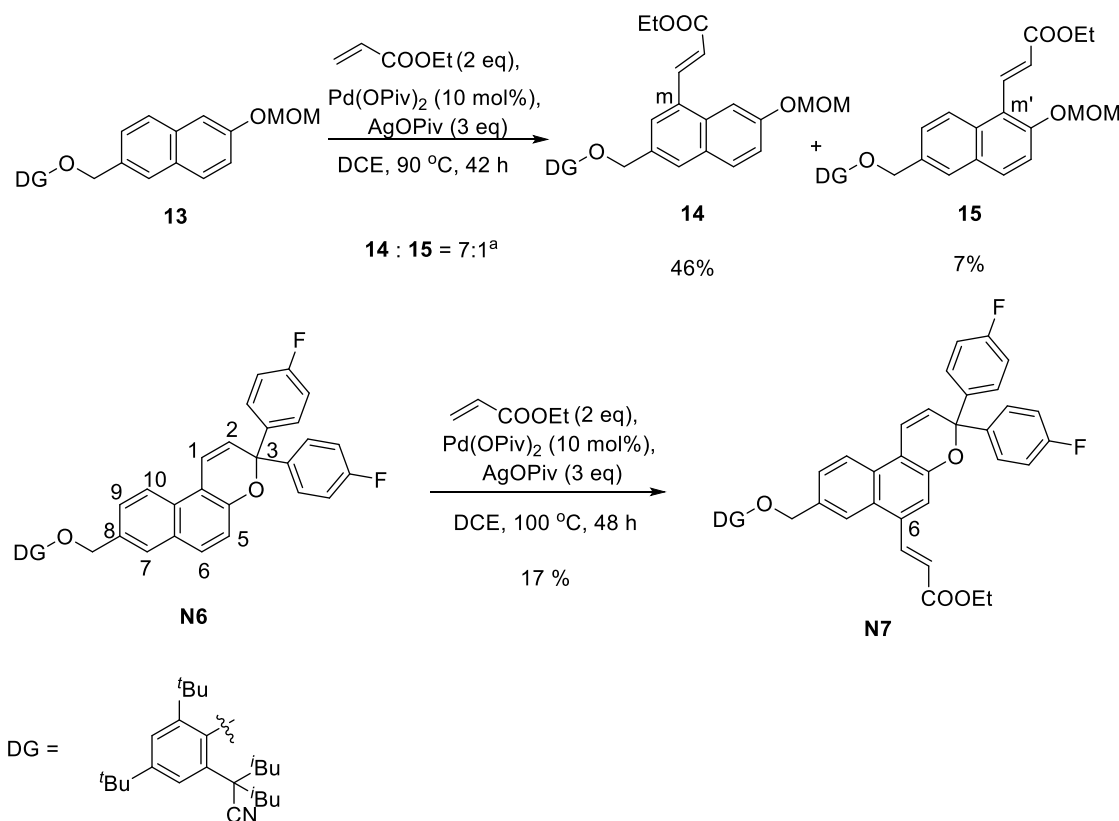


Figure 3.29 C-H functionalization of naphthalene **13** and naphthopyran **N6**.

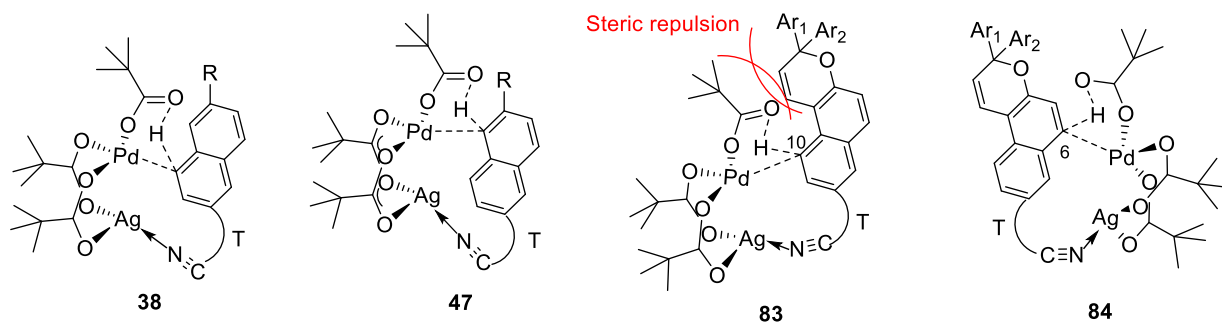


Figure 3.30 The intermediates of the C-H activation processes of naphthalene **27** and naphthopyran **N6**.

3.3.2 The Failure for Formation of Naphthopyran **21** in Route 1 of Method I

The last step of route 1, the conversion from compound **16** to naphthopyran **21**, was not achieved. But byproduct **22** was isolated in 40% yield. In order to investigate the reason, a related mechanism is shown in Figure 3.31, indicating that the former two steps were the same for the formation of the two products. If intermediate **61** is nucleophilic attacked by naphthol **16**, intermediate **85** will be formed. The reaction will follow Route A. After Claisen rearrangement, keto-enol tautomerism, [1, 5]-H-shift and electrocyclic ring closure reaction, product **21** will be obtained. On the contrary, if the allene form of intermediate **61** is nucleophilic attacked by the water molecule, the reaction will follow Route B. Then byproduct **22** will be generated through Meyer–Schuster rearrangement. Therefore, Route A and Route B are two competing reactions. Interestingly, under the same conditions, naphthopyran **N4** was prepared successfully, while naphthopyran **21** was not. The only difference between the starting materials of the two reactions is the *meta*-substituent group of compound **16**. Thus, naphthopyran **21** was not generated from compound **16** and **20**, presumably resulting from the *meta*-substituent group, which hindered the formation of intermediate **85**. The reaction went along route B and byproduct **22** was generated.

3.3 Discussion

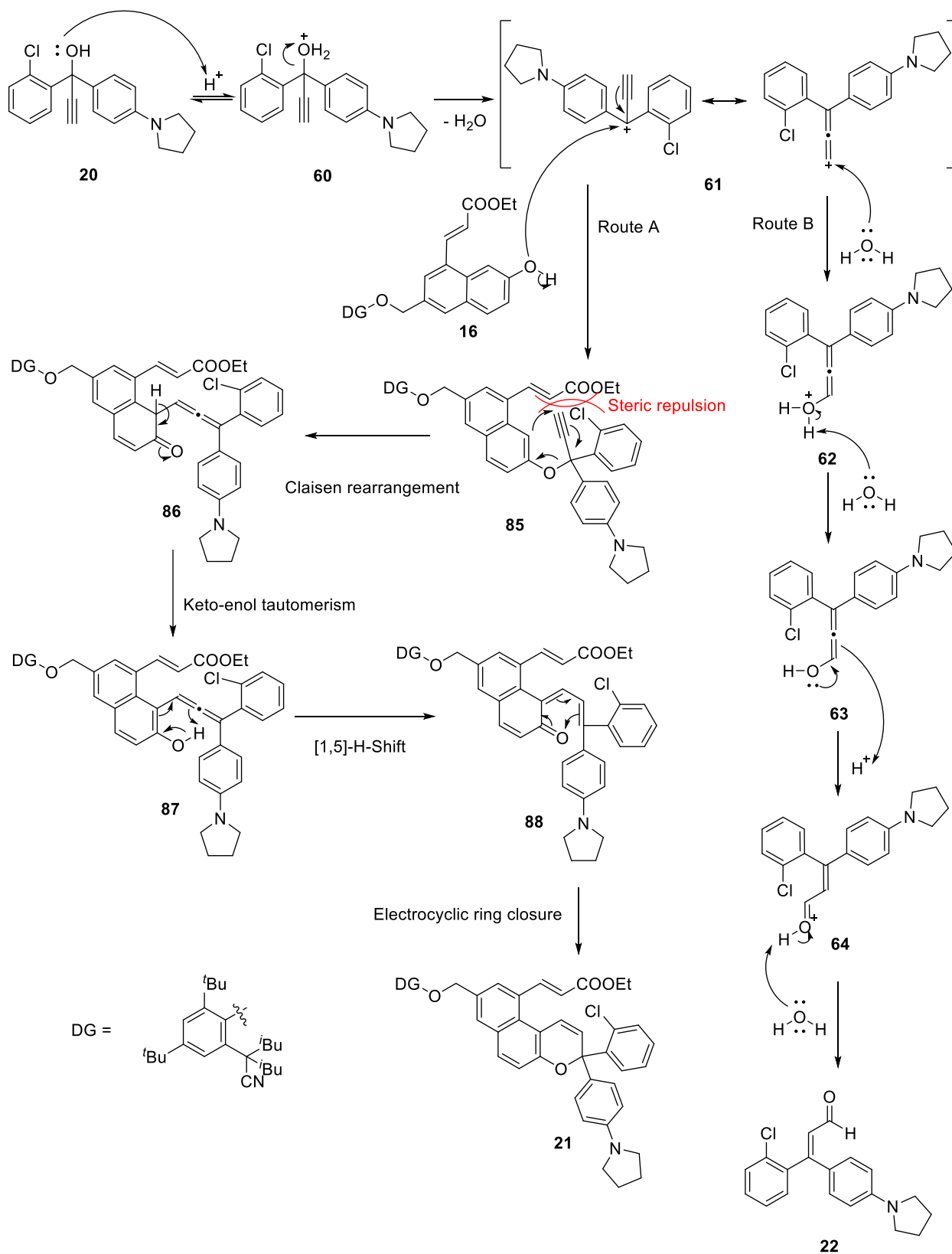
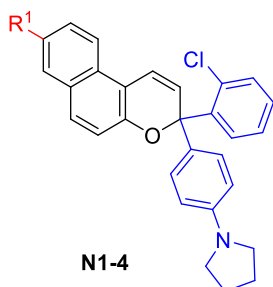


Figure 3.31 Mechanism for the synthesis of naphthopyran **21** and byproduct **22**.

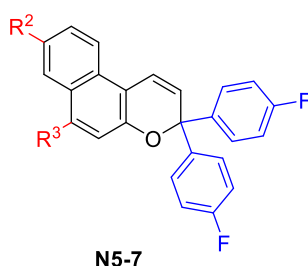
4. UV/Vis Spectroscopy

The photochromic properties of 7 different naphthopyrans were investigated, and all the data are from the experiments of an *Avantes* AvaSpec Dual-channel Fibre Optic Spectrometer (for details, see Chapter 7.2) in this chapter. All the seven compounds are divided into 2 types: two states system and three states system (Figure 4.1). Those naphthopyrans without residual color left after thermal back reaction are considered as “two states system” (initial state- PSS (UV)). Otherwise, they are regarded as “three states system” (initial state-PSS(UV)-PSS(dark)).

Two states system:



Three states system:



Super fast system:

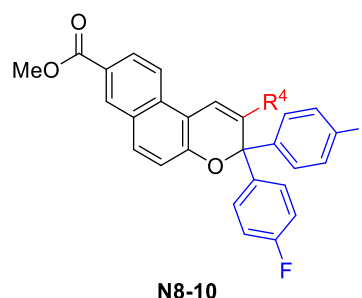


Figure 4.1 Structures of different kinds of naphthopyrans.

4.1 UV/Vis Studies of Two States System: Naphthopyrans N1, N2, N3 and N4

4.1.1 UV Irradiation

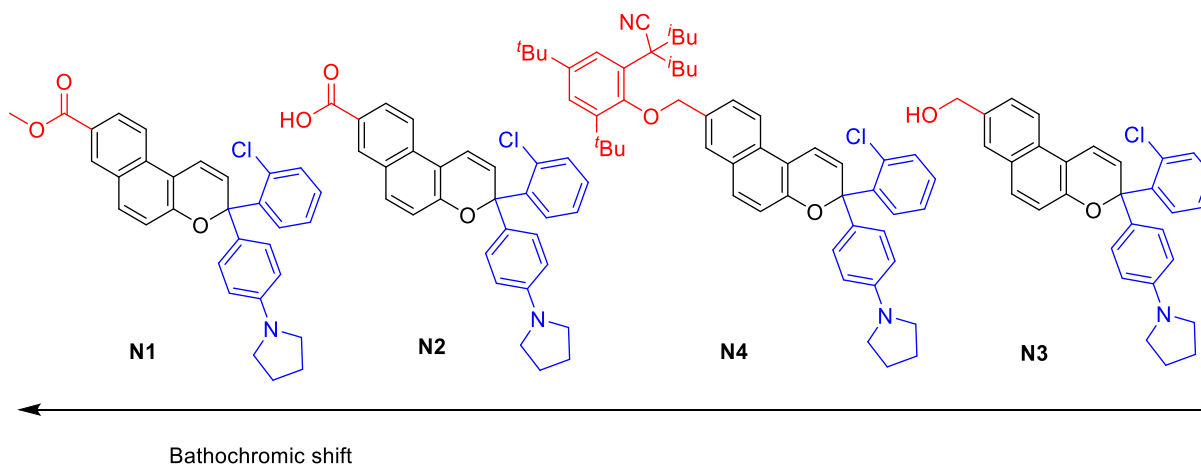


Figure 4.2 Structures of naphthopyrans N1, N2, N3 and N4.

4.1 UV/Vis Studies of Two States System: Naphthopyrans **N1**, **N2**, **N3** and **N4**

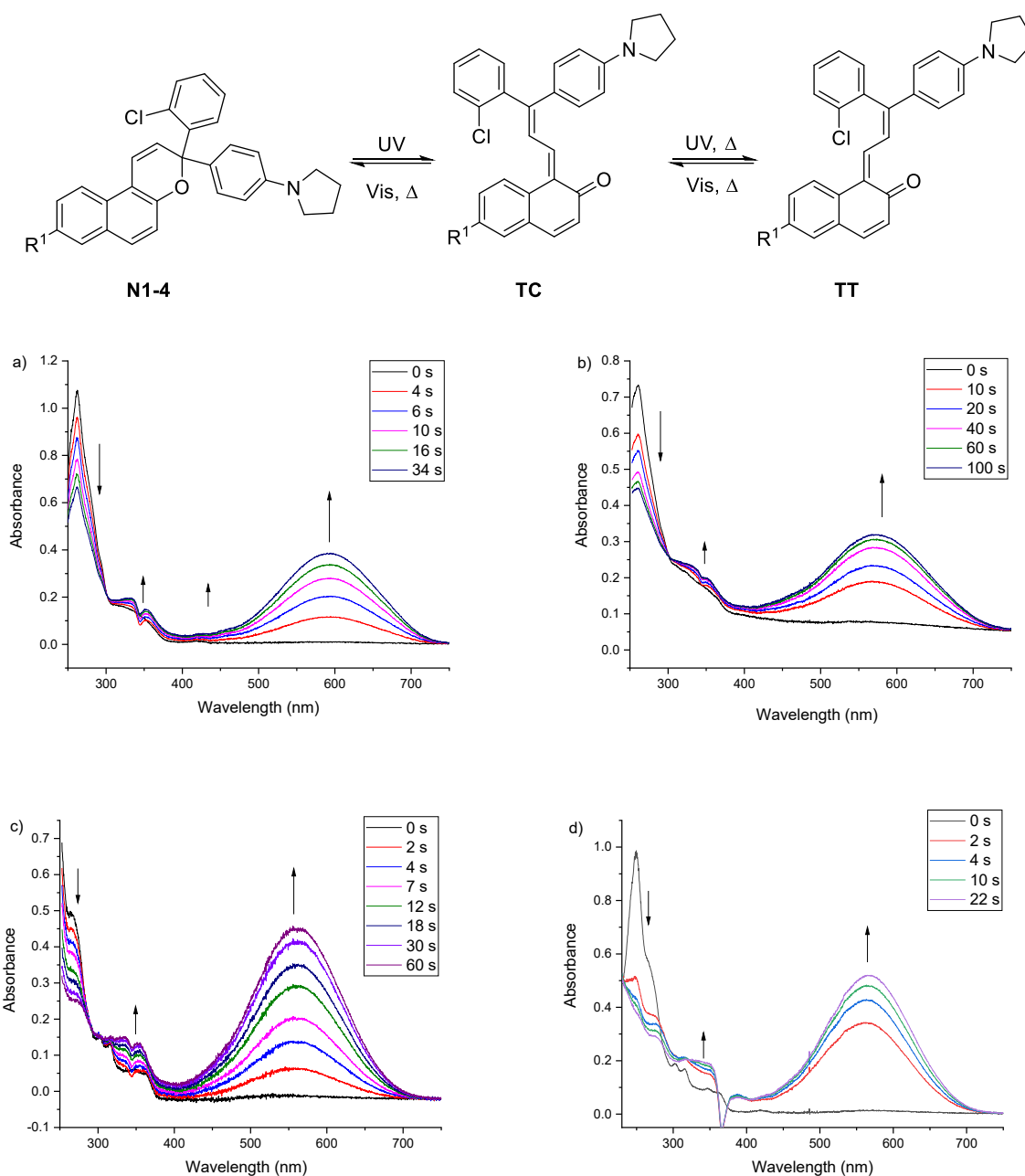


Figure 4.3 Absorption spectra changes of a) **N1**, b) **N2**, c) **N3** and d) **N4** upon UV irradiation (**N1**, **N2** and **N3**: 340 nm, 12 mW/cm², **N4**: 365 nm, 110 mW/cm², 1.5×10^{-5} M in acetonitrile, 293 K).

The structures of the naphthopyrans **N1**, **N2**, **N3** and **N4** are exhibited in Figure 4.2. From the initial UV absorption spectra of 4 compounds (Figure 4.3), it was found that two strong absorptions were centered at 261 nm and 260 nm in the spectra of naphthopyran **N1** and **N2**, respectively, while two strong absorptions around 250 nm were detected in the spectra of **N3** and **N4**. Compared

with the spectra of **N3** and **N4**, the spectra of **N1** and **N2** have a bathochromic shift by 10 nm, which is a consequence of the extended π conjugation of carboxylic acid ester group at 8-position.

Upon UV irradiation, four new visible absorption bands which are centered around 561-592 nm for **N1**, **N2**, **N3** and **N4** emerged, which are corresponding to the ring-open forms: TC and TT, and the absorption peaks at 250-260 nm were reduced. After less than 2 min, all these 4 compounds can reach a photostationary state (PSS). It was noted that the absorption spectra of open forms of **N1** and **N2** also have a bathochromic shift with respect to that of **N3** and **N4**. The λ_{max} of open forms of naphthopyrans bearing 8-substituent follows the order: Ester > Carboxylic acid > Ether methyl > Hydroxymethyl. As it is depicted in Table 4.1, t_{pss} is the time needed to arrive at the PSS. Naphthopyran **N1** is the fastest compound to arrive at the PSS. Moreover, the speed of the ring opening reaction was affected by the light intensity. If irradiated with 340 nm, 12 mW/cm² light, it took 30 seconds to arrive at the PSS for compound **N1**, while 15 seconds were needed under 365 nm, 110 mW/cm² light irradiation.

Table 4.1 Absorption properties of **N1**, **N2**, **N3** and **N4** in the procedure of UV irradiation.^a

Naphthopyran	λ_{max} [nm] (Closed form)	λ_{max} [nm] (Open forms)	λ_{iso} [nm]	t_{pss} [s]
N1	261, 318	592	301	30, 15 ^b
N2	260, 315	571	301	106
N3	249, 265, 302, 317, 347, 363	561	289	43
N4^b	250, 261, 300, 315, 347, 362	567	288	24

[a] 1.5×10^{-5} M in acetonitrile, 293 K, UV light: 340 nm, 12 mW/cm². [b] UV light: 365 nm, 110 mW/cm².

4.1.2 Thermal Back Reaction

As displayed in Figure 4.4, once UV light was switched off, all the open forms of naphthopyran **N1**, **N2**, **N3** and **N4** can return to the closed forms thermally. The absorbance changes at λ_{max} of open forms were monitored in Figure 4.5 and 4.6. For **N1**, **N2**, **N3** and **N4**, a different position of λ_{max} was not observed. Therefore, the λ_{max} of the TC and TT forms can not be distinguished.

4.1 UV/Vis Studies of Two States System: Naphthopyrans **N1**, **N2**, **N3** and **N4**

Notably, there was no residual color left. For compound **N1**, after more than 5 times UV/dark cycles, residual color was detected, which was not observed due to the TT form, but because of the decomposition of the naphthopyran. The decrease in absorbance of **N1** at PSS of different cycles correlates with the increase in remaining absorbance (residual color). However, the naphthopyran **N3** has a different behavior and no residual color was observed. Additional cycles were not investigated for **N2** and **N4** because of the slow thermal back rates.

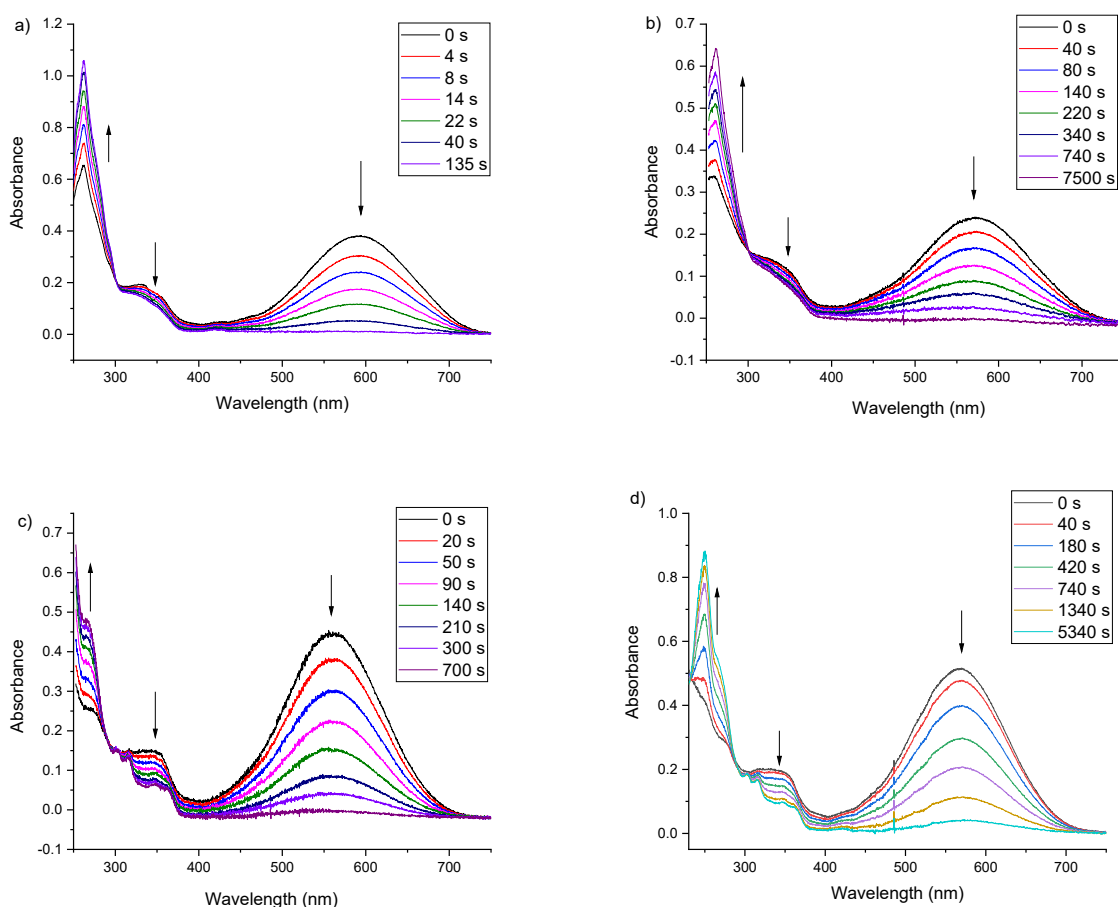


Figure 4.4 Absorption spectra changes of a) **N1**, b) **N2**, c) **N3** and d) **N4** during thermal relaxation ($c = 1.5 \times 10^{-5}$ M in acetonitrile, 293 K).

In general, there exist two processes: $TC \rightarrow CF$ and $TT \rightarrow TC$, and the latter one is slower. A common way of describing the bleaching of the colored forms is by introduction of $t_{1/2}$ and $t_{3/4}$ values, which are defined as the time taken from absorbance to reduce by $\frac{1}{2}$ and $\frac{3}{4}$ of the initial absorbance, respectively. The thermal bleaching kinetics were calculated from time-resolved

absorption spectra, by fitting the experimental data to the biexponential decay (**Equation 1**) (Fitting information see Chapter 7.2).^[37,42,132]

$$A(t) = A_1 e^{-k_1 t} + A_2 e^{-k_2 t} + A_{th} \quad (1)$$

Where $A(t)$ is the absorbance at the λ_{max} , A_1 and A_2 are contributions to the initial absorbance A_0 , k_1 and k_2 are rate constants of fast and slow components, respectively. A_{th} is the residual absorbance when time approaches infinity. Spectrokinetic data are presented in Table 4.2.

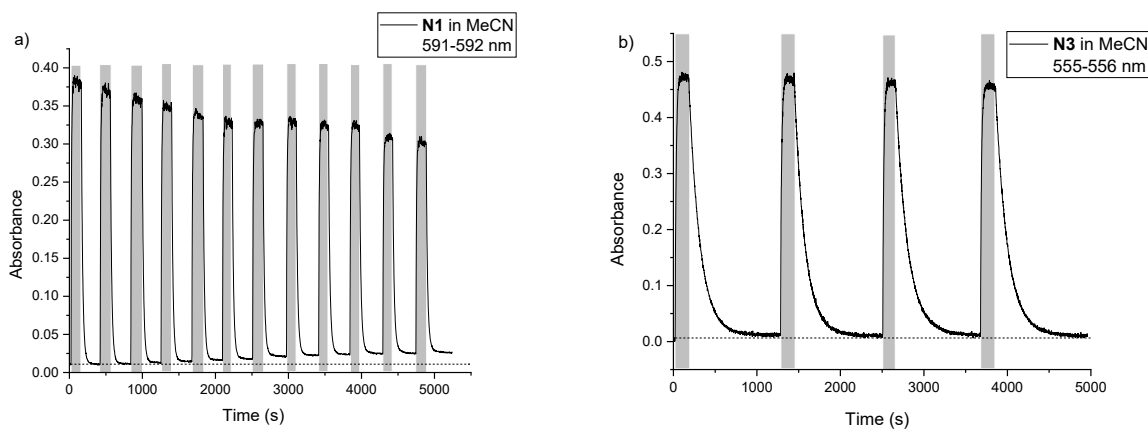


Figure 4.5 Coloration/decoloration cycles for a) naphthopyran **N1** (monitoring wavelength is between 591 and 592 nm) and b) naphthopyran **N3** (monitoring wavelength is between 555 and 556 nm) in MeCN ($c = 1.5 \times 10^{-5}$ M) at 293 K. The grey regions: UV light: 340 nm, 12 mW/cm². Non-marked regions present the periods when the sample was in the dark.

The data of Table 4.2 indicate that $t_{1/2}$ and $t_{3/4}$ of naphthopyran **N1** are 12 and 25 s, respectively, which are quite smaller than that of **N3** ($t_{1/2} = 91$ s, $t_{3/4} = 187$ s). Compared with **N3**, the k_2 of **N4** ($k_2 = 1.33 \times 10^{-3} \text{ s}^{-1}$) is only a sixth of that of **N3** ($k_2 = 7.62 \times 10^{-3} \text{ s}^{-1}$), although the k_1 of **N4** ($k_1 = 9.89 \times 10^{-3} \text{ s}^{-1}$) is larger than that of **N3** ($k_1 = 7.62 \times 10^{-3} \text{ s}^{-1}$), naphthopyran **N4** still has the slowest thermal back reaction ($t_{1/2} = 518$ s, $t_{3/4} = 1140$ s). Both k_1 and k_2 of **N1** are very large: the k_1 of **N1** ($k_1 = 9.09 \times 10^{-2} \text{ s}^{-1}$) is approximately 12 times as fast as that of **N3** ($k_1 = 7.62 \times 10^{-3} \text{ s}^{-1}$), and 9 times as fast as that of **N4** ($k_1 = 9.89 \times 10^{-3} \text{ s}^{-1}$). The k_2 of **N1** ($k_2 = 4.71 \times 10^{-2} \text{ s}^{-1}$) is about 6 times as fast as that of **N3** ($k_2 = 7.62 \times 10^{-3} \text{ s}^{-1}$), and 35 times as fast as that of **N4** ($k_2 = 1.33 \times 10^{-3} \text{ s}^{-1}$). Accordingly, the thermal back speed of naphthopyran **N1** is the fastest. Unexpectedly, both k_1 and k_2 of **N2** ($k_1 = 5.72 \times 10^{-3} \text{ s}^{-1}$, $k_2 = 3.5 \times 10^{-4} \text{ s}^{-1}$) are smaller than that of **N3**. The possible reason is the presence of a dimer structure of the acid substituted naphthopyran **N3**,^[133] and the photochromic properties are

4.1 UV/Vis Studies of Two States System: Naphthopyrans **N1**, **N2**, **N3** and **N4**

impacted by that. When **N3** was investigated in different solvents, its photochromic properties changed a lot (For details, see Chapter 4.1.4). For an overview of photochromic properties of two states system naphthopyrans, the k_1 and k_2 of naphthopyrans bearing an 8-substituent follows the order: Hydroxymethyl < Ether methyl < Ester.

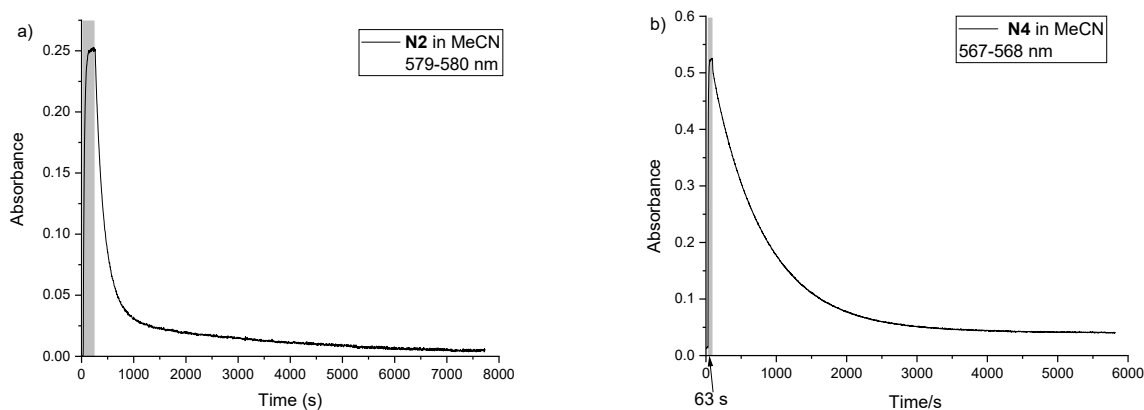


Figure 4.6 Absorbance changes monitored at λ_{\max} for a) naphthopyran **N2** (monitoring wavelength is between 579 and 580 nm) and b) naphthopyran **N4** (monitoring wavelength is between 567 and 568 nm) in MeCN ($c = 1.5 \times 10^{-5}$ M) at 293 K. The grey regions: UV light irradiation (**N2**: 340 nm, 12 mW/cm²; **N4**: 365 nm, 110 mW/cm², irradiation for 63 s). Non-marked regions present the periods when the sample was in the dark.

Table 4.2 Photochromic properties in the procedure of thermal back reaction. A_1 , A_2 , A_{th} , k_1 and k_2 are the fitting parameters from **Equation 1**; $t_{1/2}$, $t_{3/4}$ and A_0 were obtained from experimental data.^a

	$t_{1/2}$ (s)	$t_{3/4}$ (s)	A_0	k_1 (10^{-3} s^{-1})	k_2 (10^{-3} s^{-1})	A_1	A_2	A_{th}
N1	12	25	0.3807	90.9	47.1	0.118	0.256	0.012
N2	140	340	0.2513	5.72	0.35	0.210	0.032	0.002
N3	91	187	0.4653	7.62 (7.62076)	7.62 (7.62049)	1.329	0.525	0.012
N4	518	1140	0.5243	9.89	1.33	0.014	0.453	0.041

[a] 1.5×10^{-5} M in acetonitrile, 293 K.

4.1.3 Visible Light Irradiation

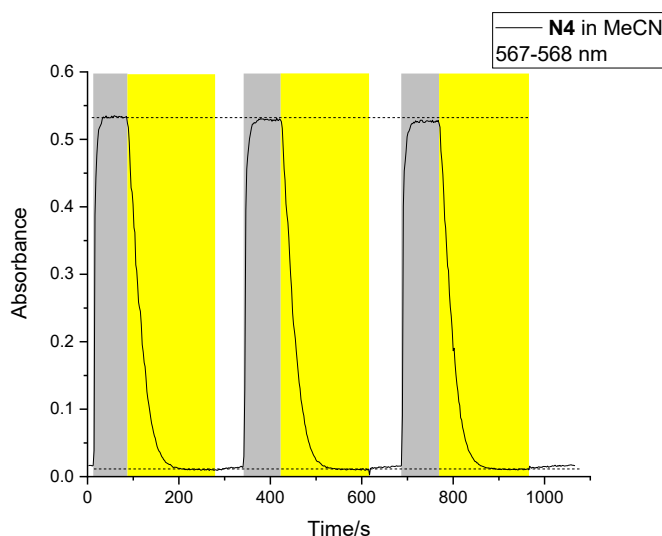


Figure 4.7 Coloration/decoloration cycles for naphthopyran **N4** (monitoring wavelength is between 567 and 568 nm) in MeCN ($c = 1.5 \times 10^{-5}$ M) at 293 K. The grey regions: UV light irradiation (365 nm, 110 mW/cm²). The yellow regions: visible light irradiation (565 nm, 84 mW/cm²). Non-marked regions present the periods when the sample was in the dark.

Table 4.3 Photochromic properties in the procedure of visible light irradiation. A_1 , A_2 , A_{th} , k_1 and k_2 are the fitting parameters from **Equation 1**; $t_{1/2}$, $t_{3/4}$ and A_0 were obtained from experimental data.^a

	$t_{1/2}$ (s)	$t_{3/4}$ (s)	A_0	k_1 (10^{-3} s^{-1})	k_2 (10^{-3} s^{-1})	A_1	A_2	A_{th}
N4	25	43	0.5243	34.9 (34.9372)	34.9 (34.9369)	0.266	0.282	-0.0003

[a] Visible light: 565 nm, 84 mW/cm², 1.5×10^{-5} M in acetonitrile, 293 K.

To promote the decoloration process of naphthopyran **N4**, visible light irradiation was applied (Figure 4.7). When naphthopyran **N4** arrived at the PSS for about 80 s under UV irradiation, UV light irradiation was switched off, and 565 nm light irradiation was switched on at the same time until naphthopyran **N4** arrived at the PSS under 565 nm light irradiation, which is also the same with the initial state. Then the sample was in the dark and no obvious change in absorbance was observed. The visible light decoloration behavior was investigated by fitting it to the biexponential decay (**Equation 1**) (Fitting information see Chapter 7.2). Upon irradiation with 565 nm light, the k_1 of **N4** ($34.9 \times 10^{-3} \text{ s}^{-1}$) was accelerated to 3.5 times faster than that in the thermal back process and k_2 was increased 25-fold, to $34.9 \times 10^{-3} \text{ s}^{-1}$. Correspondingly, the $t_{1/2}$ and $t_{3/4}$ of naphthopyran

4.1 UV/Vis Studies of Two States System: Naphthopyrans **N1**, **N2**, **N3** and **N4**

N4 were promoted to 25 and 43 s, respectively (Table 4.3). After three circles of UV irradiation/visible light irradiation, there was no residual color or decomposition observed.

4.1.4 Solvent Effect on the Photochromic Properties

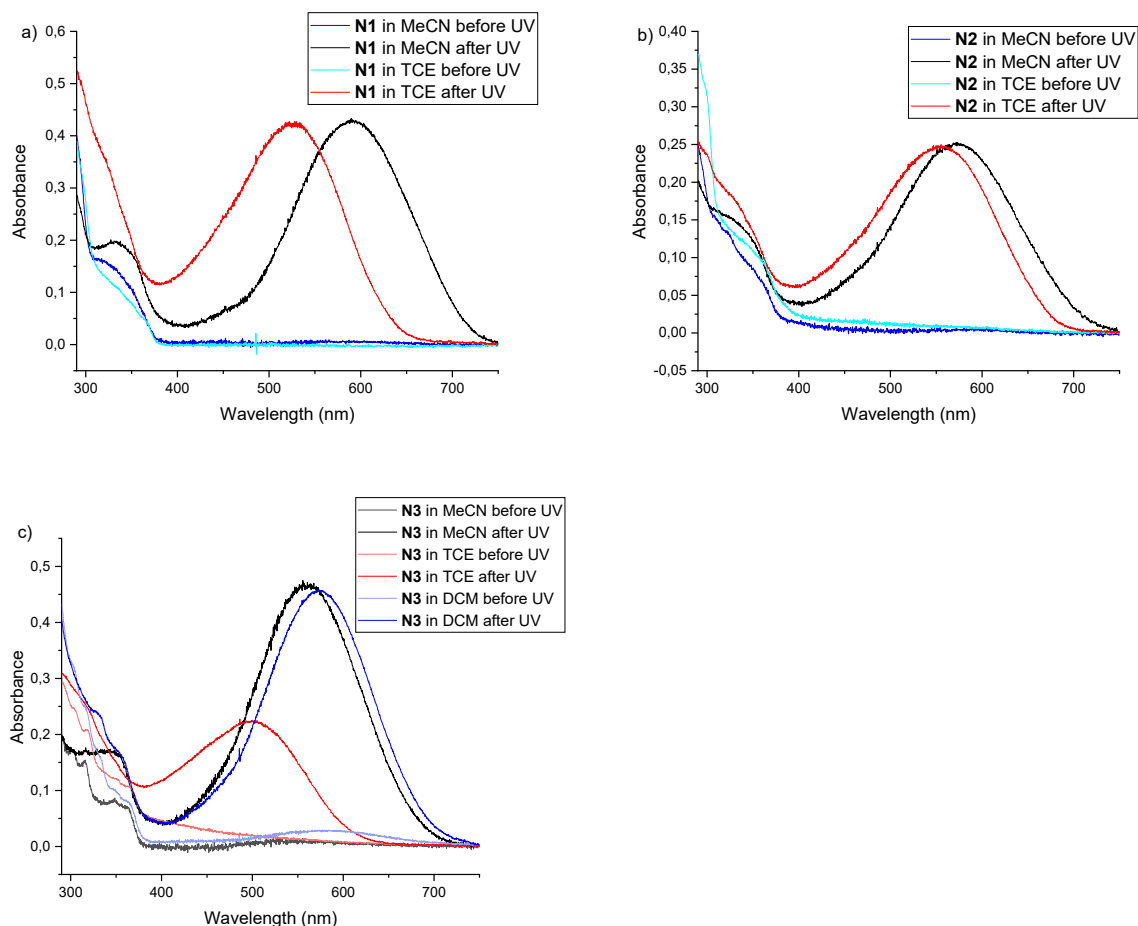


Figure 4.8 Absorption spectra of a) **N1**, b) **N2** and c) **N3** in the initial state and after UV irradiation in different solvents (UV light: 340 nm, 12 mW/cm², $c = 1.5 \times 10^{-5}$ M, 293 K).

To investigate the solvent effect on the photochromic properties of naphthopyrans, nonpolar solvents, tetrachloroethylene (TCE) and dichloromethane (DCM), were also applied to the UV/Vis experiments. As exhibited in Figure 4.8, all the absorption spectra of **N1**, **N2** and **N3** in TCE have a blue shift with respect to that in acetonitrile. By contrast, the absorption spectrum of **N3** just has a small bathochromic shift (12 nm) in DCM compared with that in acetonitrile. In respect of the ring opening speed, **N1** arrived at the PSS quicker than **N3**, which is consistent with the behavior in MeCN. In contrast, **N2** was improved to the fastest naphthopyran to arrive PSS in TCE from

the slowest naphthopyran to arrive PSS in MeCN, because of the effects on the formation of an acid dimer by the different solvents.^[133] Besides that, the other naphthopyrans, both **N1** and **N3**, arrived at the PSS slower in TCE than that in MeCN (Table 4.2 and 4.4).

Table 4.4 Absorption properties of **N1**, **N2** and **N3** in the procedure of UV irradiation in TCE. ^a

Naphthopyran	λ_{\max} [nm] (Closed form)	λ_{\max} [nm] (Open forms)	λ_{iso} [nm]	t_{pss} [s]
N1	324	526	302	168
N2	323	553	306	80
N3	318, 352, 366	498	- ^b	214
N3 ^c	273, 296, 321, 351, 364	573	296	100

[a] 1.5×10^{-5} M in TCE, 293 K, UV light: 340 nm, 12 mW/cm². [b] $\lambda_{\text{iso}} < 290$ nm cannot be detected, because the UV cut-off of TCE is 290 nm. [c] 1.5×10^{-5} M in DCM.

Table 4.5 Photochromic properties of **N1**, **N2** and **N3** in the procedure of thermal back reaction. A_1 , A_2 , A_{th} , k_1 and k_2 are the fitting parameters from **Equation 1**; $t_{1/2}$, $t_{3/4}$ and A_0 were obtained from experimental data. ^a

	$t_{1/2}$ (s)	$t_{3/4}$ (s)	A_0	k_1 (10^{-3} s^{-1})	k_2 (10^{-3} s^{-1})	A_1	A_2	A_{th}
N1	347	700	0.4004	3.75	1.96	0.012	0.381	0.005
N2	101	219	0.2465	42.7	6.16	0.019	0.205	0.019
N3	1365	2192	0.2216	0.535	0.064	0.177	0.043	0.002
N3 ^b	129	269	0.4706	99	5.19	0.017	0.422	0.033

[a] 1.5×10^{-5} M in TCE at 293 K. [b] 1.5×10^{-5} M in DCM.

4.1 UV/Vis Studies of Two States System: Naphthopyrans **N1**, **N2**, **N3** and **N4**

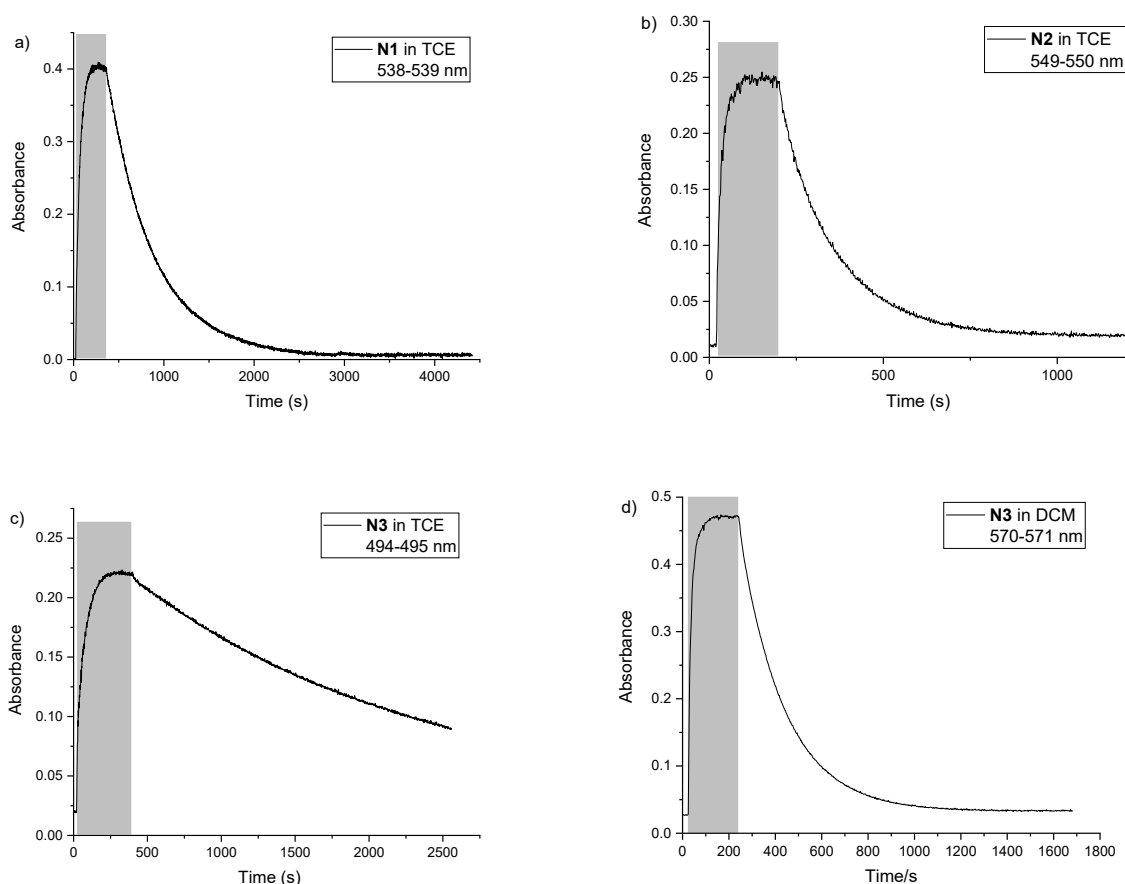


Figure 4.9 Absorbance changes monitored at λ_{\max} for a) naphthopyran **N1** (monitoring wavelength is between 538 and 539 nm) in tetrachloroethylene, b) naphthopyran **N2** (monitoring wavelength is between 549 and 550 nm) in tetrachloroethylene, c) naphthopyran **N3** (monitoring wavelength is between 494 and 495 nm) in tetrachloroethylene and naphthopyran **N3** (monitoring wavelength is between 570 and 571 nm) in DCM ($c = 1.5 \times 10^{-5}$ M) at 293 K. The grey regions: UV light irradiation (340 nm, 12 mW/cm²). Non-marked regions present the periods when the sample was in the dark.

The thermal relaxation kinetics were calculated from time-resolved absorbance changes at λ_{\max} , by fitting the experimental data to the biexponential decay (**Equation 1**) (Figure 4.9) (Fitting information see Chapter 7.2). For the thermal back relaxation period, it was noted that the thermal back speed of both **N1** ($k_1 = 3.75 \times 10^{-3} \text{ s}^{-1}$, $k_2 = 1.96 \times 10^{-3} \text{ s}^{-1}$) and **N3** ($k_1 = 5.35 \times 10^{-4} \text{ s}^{-1}$, $k_2 = 6.4 \times 10^{-5} \text{ s}^{-1}$) in TCE were retarded compared to that in acetonitrile. While both k_1 ($4.27 \times 10^{-2} \text{ s}^{-1}$) and k_2 ($6.16 \times 10^{-3} \text{ s}^{-1}$) of **N2** were larger than that in acetonitrile, which can be explained by the different effects on the formation of an acid dimer by different solvents,^[133] while the photochromic properties of **N2** varied with the dimer concentration. Last but not least, compared with the $t_{1/2}$ (1365 s) and $t_{3/4}$ (2192 s) of naphthopyran with 8-hydroxymethyl substituent, **N3**, those

of **N1** ($t_{1/2} = 347$ s, $t_{3/4} = 700$ s) were smaller (Table 4.5). Consequently, the $t_{1/2}$ and $t_{3/4}$ of naphthopyrans bearing 8-substituent follow the order: Ester < Hydroxymethyl, which has the same trend as in acetonitrile. Regarding the photochromic behavior of **N3** in DCM, k_1 was promoted to $9.9 \times 10^{-2} \text{ s}^{-1}$, while k_2 ($5.19 \times 10^{-3} \text{ s}^{-1}$) was almost the same as that in acetonitrile. Notably, there exist decomposition in the coloration/decoloration cycles of **N2** in TCE and **N3** in DCM (Figure 4.10). The decrease in absorbance of **N2** in TCE and **N3** in DCM at PSS of different cycles correlates with the increase in remaining absorbance (residual color).

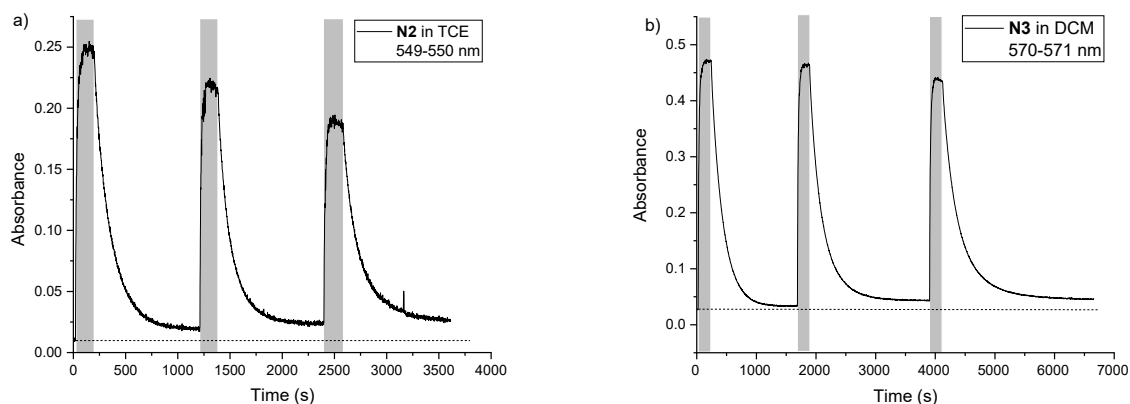


Figure 4.10 Coloration/decoloration cycles for a) naphthopyran **N2** (monitoring wavelength is between 549 and 550 nm) in TCE and b) naphthopyran **N3** (monitoring wavelength is between 570 and 571 nm) in DCM ($c = 1.5 \times 10^{-5}$ M) at 293 K. The grey regions: UV light: 340 nm, 12 mW/cm². Non-marked regions present the periods when the sample was in the dark.

In conclusion, a positive solvatochromism was observed for **N1**, **N2** and **N3**, resulting from a hypsochromic shift with decreasing solvent polarity (for the polarity of solvent, see Chapter 8.3, Table 8.1). Besides that, the thermal back rates were reduced in nonpolar solvent (Tables 4.2 and 4.5), which is in agreement with the other reports about substituted 3*H*-naphthopyrans.^[47]

4.2 UV/Vis Studies of Three States System: Naphthopyrans **N5** and **N6**

4.2.1 UV Irradiation

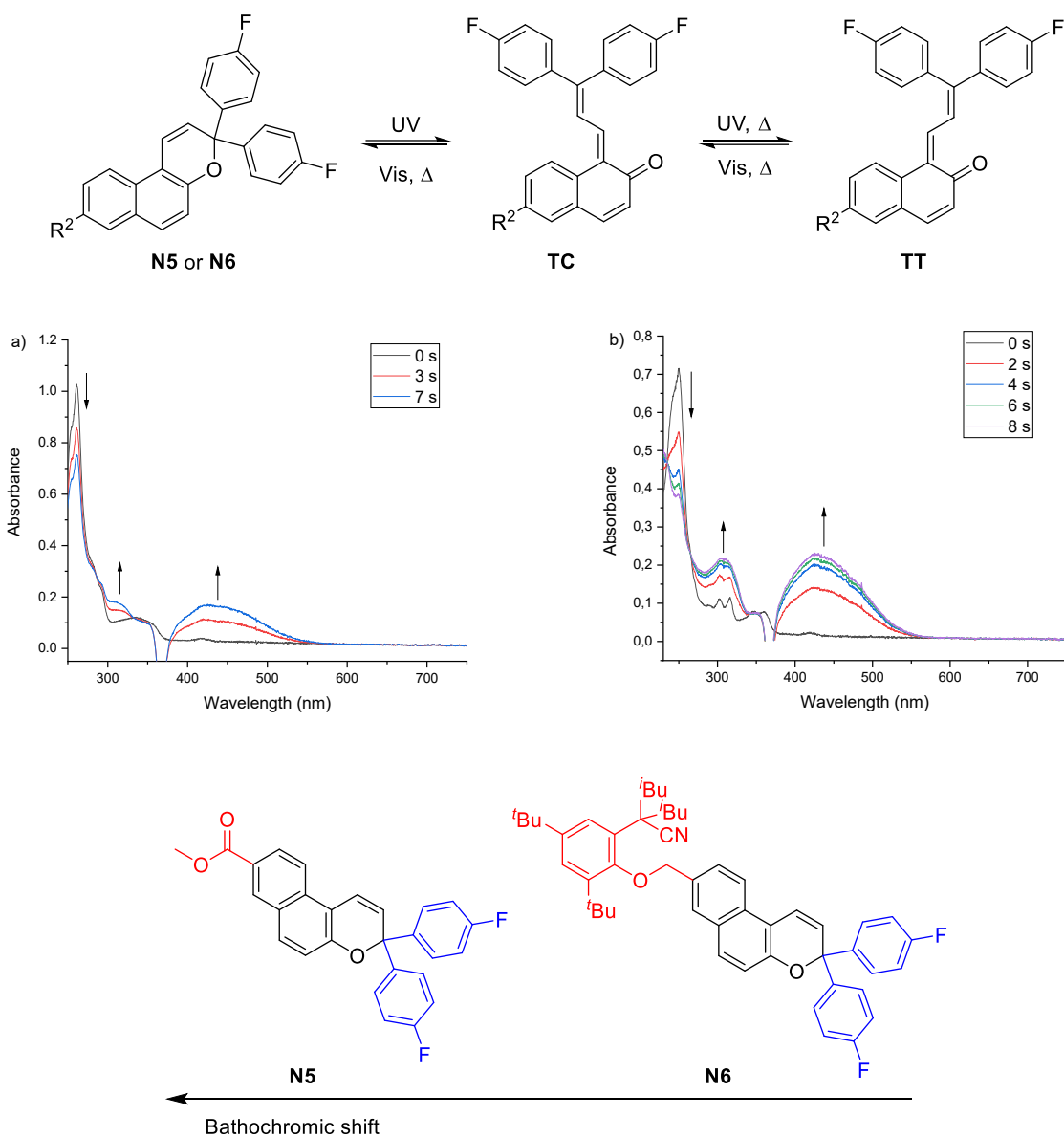


Figure 4.11 Structures of **N5** and **N6** (below) and absorption spectra changes of a) **N5** and b) **N6** upon UV irradiation (UV light: 365 nm, 110 mW/cm², 1.5×10⁻⁵ M in acetonitrile, 293 K).

The structures and absorption spectra of **N5** and **N6** are displayed in Figure 4.11. Before UV irradiation, the spectra of **N5** and **N6** have a strong absorption at 261 and 250 nm, respectively. Upon UV irradiation, a new absorption centered at 427-429 nm emerged corresponding to the ring-

open forms: TC and TT forms, and the absorption peaks around 250 and 261 nm were reduced. According to the data of Table 4.6, it is noted that the spectra of both closed forms and open forms of naphthopyran **N5** have a bathochromic shift with respect to that of **N6**, which is due to the extended π conjugation of the carboxylic acid ester group in naphthopyran **N5** as mentioned in chapter 4.1.1.

Table 4.6 Absorption properties of **N5** and **N6** in the procedure of UV irradiation.^a

Naphthopyran	λ_{\max} [nm] (Closed form)	λ_{\max} [nm] (Open forms)	t_{pss} [s]
N5	261, 338	429	7
N6	250, 302, 316, 345, 360	427	8

[a] 1.5×10^{-5} M in acetonitrile, 293 K, UV light: 365 nm, 110 mW/cm².

4.2.2 Thermal Back Reaction

As it is demonstrated in Figure 4.12, once UV light was switched off, the absorption around 427 nm of **N5** and **N6** reduced quickly until about 0.04 of absorbance left. After a few minutes in the dark, no obvious change in the residual color was observed, and for that the long lifetime of the TT forms are responsible. The time-resolved absorbance at λ_{\max} was monitored in Figure 4.13. In the procedure of thermal relaxation, $t_{1/2}$ and $t_{3/4}$ values were also measured for **N5** and **N6**.

Upon UV light was switched off, two processes were observed in the system: TC→CF and TT→TC→CF. But the speed of the process TT→TC was by far slower than the speed of the TC→CF process. The TT form was almost not reduced during the short thermal relaxation time. Thus, the absorbance curves during thermal bleaching were fitted to the first order decay (**Equation 2**)^[45,46] (Fitting information see Chapter 7.2).

$$A_t = A_1 e^{-kt} + A_{th} \quad (2)$$

Where $A_{(t)}$ is the absorbance at the λ_{\max} , A_1 is the contributions to the initial absorbance A_0 , k is rate constant of fast component ($k_{TC \rightarrow CF, \text{ thermal}}$), and A_{th} is the residual absorbance at the termination of testing time. Spectrokinetic data are exhibited in Table 4.7.

4.2 UV/Vis Studies of Three States System: Naphthopyrans **N5** and **N6**

The $k_{TC \rightarrow CF, thermal}$ of **N5** (0.634 s^{-1}) was approximately 4.5 times as fast as that of **N6** (0.141 s^{-1}). That is why the $t_{1/2}$ (1.6 s) and $t_{3/4}$ (3.4 s) of **N5** were smaller than those of **N6** ($t_{1/2} = 4.8 \text{ s}$, $t_{3/4} = 9.7 \text{ s}$). Thus, the $t_{1/2}$ and $t_{3/4}$ of naphthopyrans bearing an 8-substituent were increased in the order: Ester < Ether methyl. Correspondingly, the thermal back speed was increased in the inverse order.

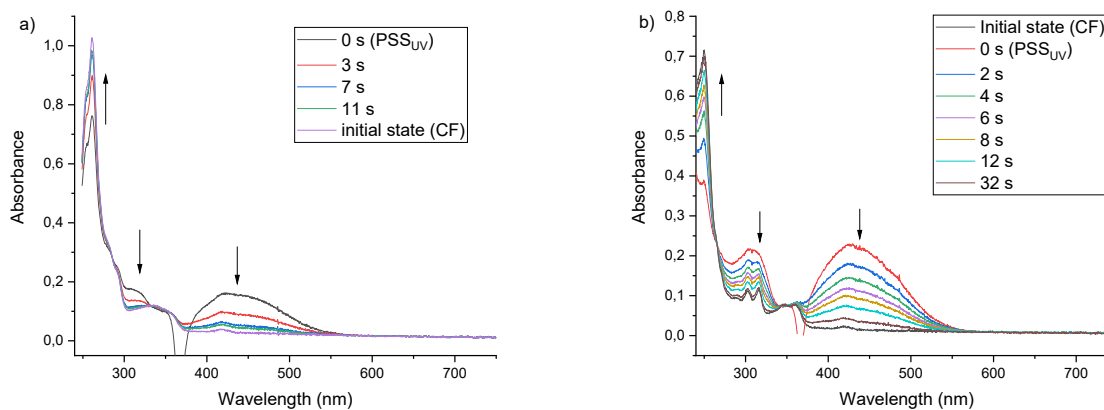


Figure 4.12 Absorption spectra changes of a) **N5** and b) **N6** during thermal relaxation started from PSS (UV) ($1.5 \times 10^{-5} \text{ M}$ in acetonitrile, 293 K).

Table 4.7 Photochromic properties of **N5** and **N6** in the procedure of thermal back reaction. A_{th} and k are the fitting parameters from **Equation 2**; $t_{1/2}$, $t_{3/4}$ and A_0 were obtained from experimental data.^a

	$t_{1/2} \text{ (s)}$	$t_{3/4} \text{ (s)}$	A_0	$k \text{ (s}^{-1}\text{)}$	A_{th}
N5	1.6	3.4	0.164	0.634	0.038
N6	4.8	9.7	0.231	0.141	0.041

[a] $1.5 \times 10^{-5} \text{ M}$ in acetonitrile, 293 K.

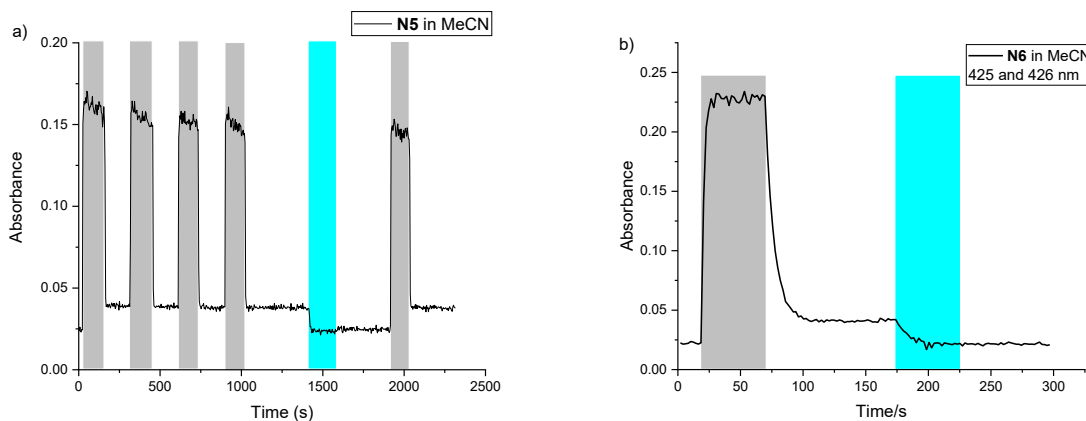


Figure 4.13 Coloration/decoloration cycles for a) naphthopyran **N5** (monitoring wavelength is between 427 and 428 nm) and b) naphthopyran **N6** (monitoring wavelength is between 425 and 426 nm) in acetonitrile ($c = 1.5 \times 10^{-5}$ M) at 293 K. The grey regions: UV light irradiation (365 nm, 110 mW/cm²). Non-marked regions present the periods when the sample was in the dark. The blue regions: visible light irradiation (420 nm, 73 mW/cm²).

However, the spectra of **N5** and **N6** can return to the initial state, when the thermal relaxation time was long enough. If the sample of **N5** was put in the dark for an additional hour (1 h) after the fast total thermal relaxation of the TC form, the slow thermal relaxation of the TT form was observed (Figure 4.14). Therefore, $k_{TT \rightarrow TC, thermal}$ of **N5** was obtained by fitting the absorbance curve into monoexponential decay (Fitting information see Chapter 7.2). From the experimental data, it was revealed that the half life of the TT form is 1150 s, 720 times as long as that of the TC form. The thermal relaxation speed of the TC form is about 900 times as fast as that of the TT form ($6.8 \times 10^{-4} \text{ s}^{-1}$) (Table 4.8). Accordingly, two different monoexponential decays were observed during the whole thermal relaxation period.

Table 4.8 Photochromic properties of **N5** in the procedure of thermal back reaction. A_{th} and $k_{TT \rightarrow TC, thermal}$ are the fitting parameters from **Equation 2**; $t_{1/2, TT}$ and A_0 were obtained from experimental data.^a

	$t_{1/2, TT} \text{ (s)}$	$k_{TT \rightarrow TC, thermal} \text{ (s}^{-1}\text{)}$	A_{th}
N5	1150	6.8×10^{-4}	0.028

[a] 1.5×10^{-5} M in acetonitrile, 293 K.

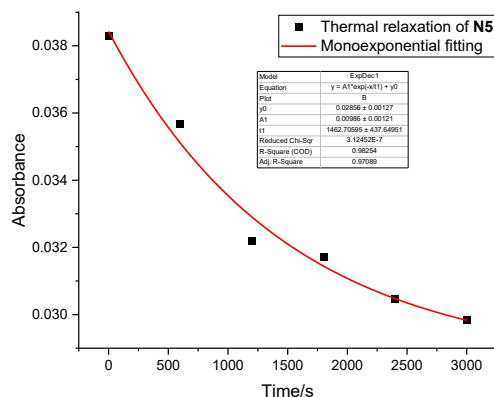


Figure 4.14 The time-resolved absorbance of **N5** at λ_{\max} during long time thermal relaxation (black dots) and monoexponential decay fitting (red line) in MeCN ($c = 1.5 \times 10^{-5}$ M) at 293 K.

4.2.3 Visible Light Irradiation

After several minutes' thermal relaxation, there still existed residual color in the absorption spectra of **N5** and **N6**, which disappeared rapidly under the irradiation with visible light. Upon irradiation with 420 nm light, the spectra of both **N5** and **N6** returned to the initial state (Figure 4.15), resulting from the faster speed of the procedure $TT \rightarrow TC \rightarrow CF$. There were only two isomers, TT and CF, in the system of **N5** and **N6** after several minutes' thermal back reaction. Upon the visible light irradiation was switched on, the Vis-process, $TT \rightarrow TC \rightarrow CF$ existed in the system. Wherein the Vis-process $TT \rightarrow TC$ was the rate determining step because of the faster speed of the Vis-process $TC \rightarrow CF$. Accordingly, the visible light bleaching kinetics were investigated from the time-resolved absorbance curve (Figure 4.13), by fitting the experimental data to the monoexponential decay (**Equation 2**) (Fitting information see Chapter 7.2). Spectrokinetic data are demonstrated in Table 4.9.

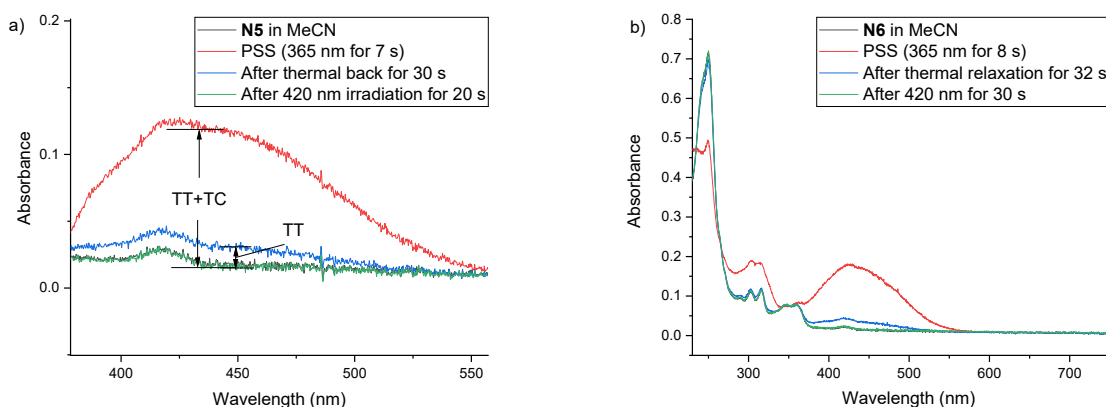


Figure 4.15 The comparison of absorption spectra of a) **N5** and b) **N6**: initial (black), after UV irradiation (red, 365 nm, 110 mW/cm²), after thermal relaxation (blue) and after visible light irradiation (green, 420 nm, 73 mW/cm²) (1.5×10^{-5} M in acetonitrile, 293 K).

Table 4.9 Photochromic properties of **N5** and **N6** in the procedure of visible light irradiation. A_{th} and $k_{TT \rightarrow TC, VIS}$ are the fitting parameters from **Equation 2**.^a

	$k_{TT \rightarrow TC, VIS} (s^{-1})$	A_{th}
N5	0.150	0.023
N6	0.106	0.022

[a] Visible light: 420 nm, 73 mW/cm², 1.5×10^{-5} M in acetonitrile, 293 K.

Upon irradiation with 420 nm light, the $k_{TT \rightarrow TC, VIS}$ of **N5** and **N6**, the speed of Vis-process from TT to TC, were increased to 0.150 and 0.106 s⁻¹, respectively. Consequently, total decoloration was achieved in 30 seconds. Compared to the visible light bleaching speed of **N6**, $k_{TT \rightarrow TC, VIS}$ of **N5** is still faster. The trend of the visible light promoted back reaction is consistent with the procedure of thermal back reaction.

4.3 UV/Vis Studies of C-H Functionalization Product N7

4.3.1 UV Irradiation

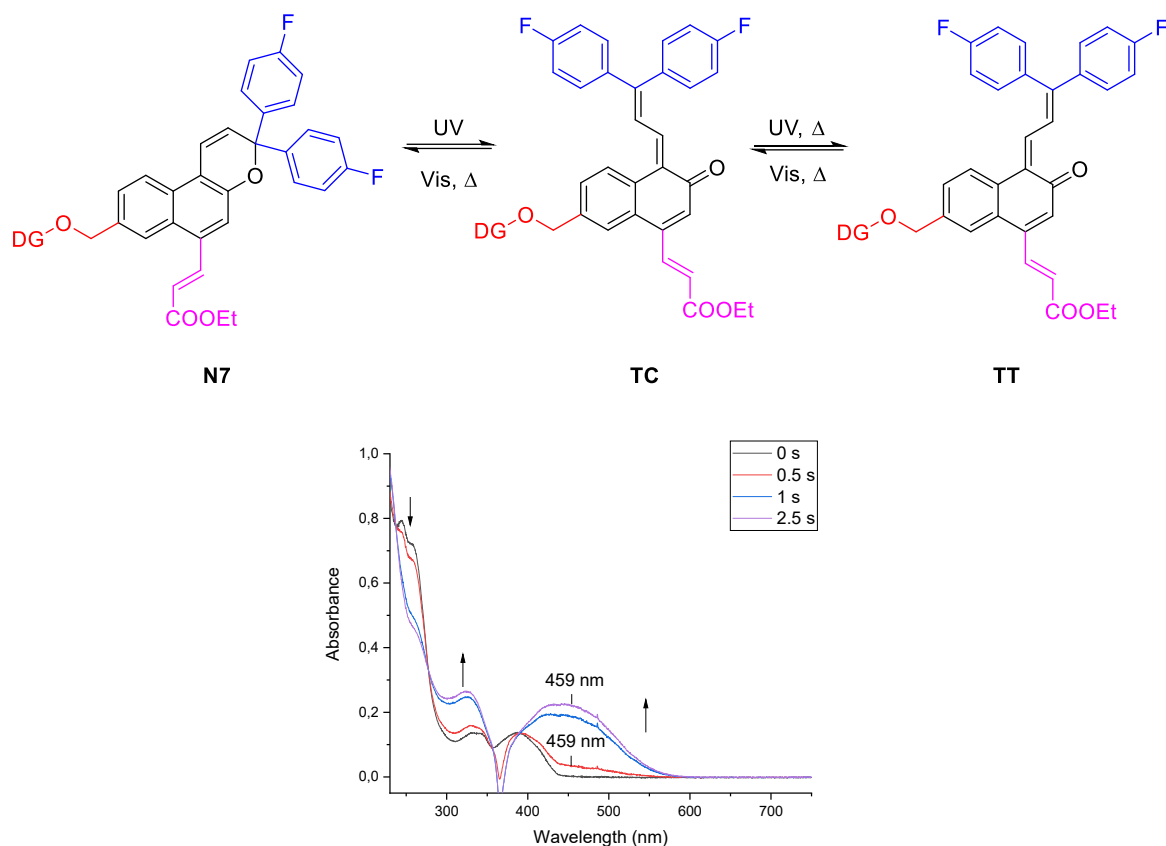


Figure 4.16 Structure (up) and absorption spectra changes (down) of **N7** after UV irradiation (365 nm, 110 mW/cm²) in acetonitrile ($c = 1.5 \times 10^{-5}$ M) at 293 K.

The absorption spectra of **N7** is shown in Figure 4.16. Before UV irradiation, an absorption peak at 388 nm was observed in the spectra of **N7**. Compared with **N6**, the bathochromic shift in the absorption spectra of **N7** is due to the extended π conjugation of the acrylic ester substituent in the 6-position of the naphthopyran.

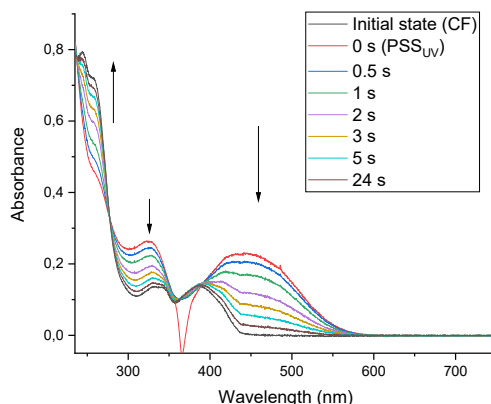
Upon continuous irradiation with 365 nm UV light at 293 K, a new visible absorption band centered at 459 nm emerged in the spectra of **N7**. After just 2.5 seconds, **N7** can reach a PSS (Table 4.10). Accordingly, the introduction of the acrylic ester substituent at 6-position brings about a bathochromic shift in the spectra of both closed and open forms and an increase in the speed of the ring opening reaction.

Table 4.10 Absorption properties of **N6** and **N7** in the procedure of UV irradiation.^a

Naphthopyran	λ_{\max} [nm] (Closed form)	λ_{\max} [nm] (Open forms)	t_{pss} [s]
N6	250, 302, 316, 345, 360	427	8
N7	244, 255, 331, 340, 388	459	2.5

[a] 1.5×10^{-5} M in acetonitrile, 293 K, UV light: 365 nm, 110 mW/cm².

4.3.2 Thermal Back Reaction


Figure 4.17 Absorption spectra changes of **N7** during thermal relaxation in acetonitrile started from PSS (UV) ($c = 1.5 \times 10^{-5}$ M) at 293 K.

Once the solution of naphthopyran **N7** was in the dark, the absorbance around 459 nm reduced quickly until 0.03 in the absorbance (Figure 4.17), for which the long lifetime of the TT form is responsible. Therefore, totally returning back to the initial spectrum was expected, if the thermal relaxation was long enough. The absorbance changes at λ_{\max} were monitored over time in Figure 4.18. The thermal bleaching kinetics were fitted to the first order decay (**Equation 2**) (Fitting information see Chapter 7.2). As it is exhibited in Table 4.11, the $k_{TC \rightarrow CF, thermal}$ of **N7** was 0.401 s^{-1} , approximately 3 times as large as that of **N6**. Correspondingly, the $t_{1/2}$ (1.8 s) and $t_{3/4}$ (3.5 s) of **N7** were smaller. Moreover, the absorbance of **N7** was the same as that of **N6** in the PSS under UV irradiation, but less residual colour was observed from the spectra of **N7**.

4.3 UV/Vis Studies of C-H Functionalization Product N7

Table 4.11 Photochromic properties of **N6** and **N7** in the procedure of thermal back reaction. A_{th} and $k_{TC \rightarrow CF, thermal}$ are the fitting parameters from **Equation 2**; $t_{1/2}$, $t_{3/4}$ and A_0 were obtained from experimental data.^a

	$t_{1/2}$ (s)	$t_{3/4}$ (s)	A_0	$k_{TC \rightarrow CF, thermal}$ (s ⁻¹)	A_{th}
N6	4.8	9.1	0.2310	0.141	0.041
N7	1.8	3.5	0.2310	0.401	0.030

[a] 1.5×10^{-5} M in acetonitrile, 293 K.

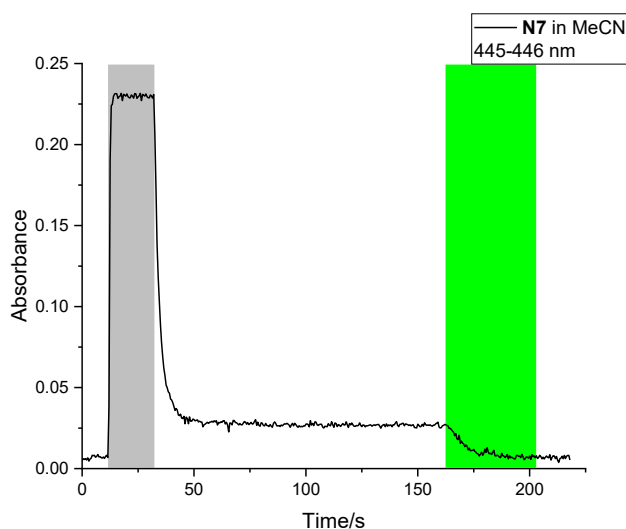


Figure 4.18 Absorbance changes monitored at λ_{max} for naphthopyran **N7** (monitoring wavelength is between 445 and 446 nm) in acetonitrile ($c = 1.5 \times 10^{-5}$ M) at 293 K. The grey regions: UV light irradiation (started at 12 s and the PSS was reached after 2.5 s of UV irradiation. 365 nm, 110 mW/cm²). Non-marked regions present the periods when the sample was in the dark. The green regions: visible light irradiation (505 nm, 70 mW/cm²).

4.3.3 Visible Light Irradiation

After several minutes in the dark, no obvious change in the residual color of **N7** was observed. Upon irradiation with 505 nm light, the spectra returned to the initial state in 25 seconds (Figure 4.19). The visible light bleaching kinetics were investigated from time-resolved absorption spectra (Figure 4.18), by fitting the experimental data to the monoexponential decay (**Equation 2**) (Fitting information see Chapter 7.2). Spectrokinetic data are depicted in Table 4.12.

Under 505 nm light irradiation, the $k_{TT \rightarrow TC, VIS}$ of **N7** was 0.149 s^{-1} , which is 1.5 times as large as that of **N6** in the Vis-process. Notably, the residual colour of **N7** did not disappear under 420 nm light irradiation. For details, you can see the *in-situ* NMR analysis for naphthopyran **N7** (Chapter 5.3).

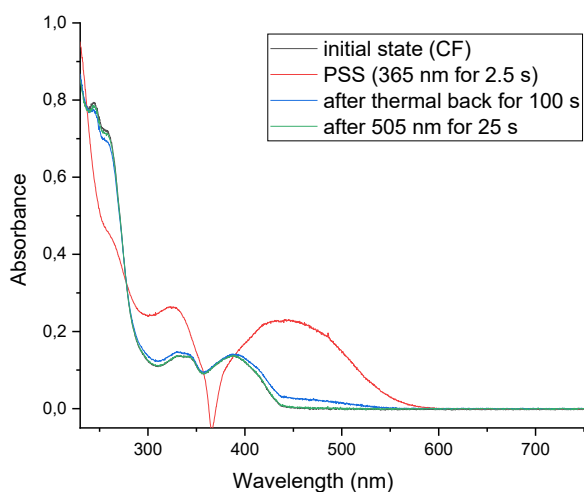
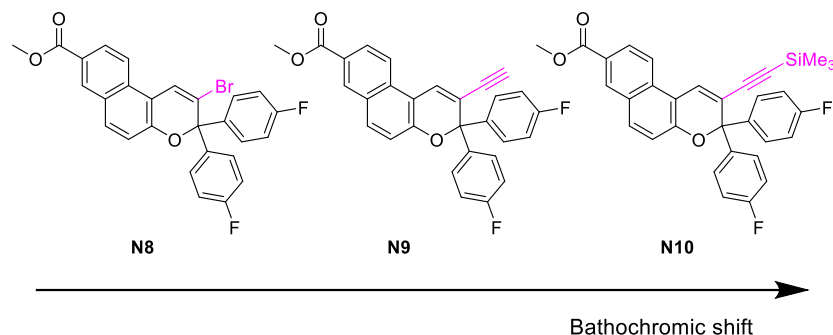


Figure 4.19 The comparison of absorption spectra of **N7** in acetonitrile ($c = 1.5 \times 10^{-5} \text{ M}$) at 293 K: initial (black), after UV irradiation (red, 365 nm, 110 mW/cm^2), after thermal relaxation (blue) and after visible light irradiation (green, 505 nm, 70 mW/cm^2) (derived from Figure 4.18).

Table 4.12 Photochromic properties of **N6** and **N7** in the procedure of visible light irradiation. A_{th} and $k_{TT \rightarrow TC, VIS}$ are the fitting parameters from **Equation 2**.^a

	$k_{TT \rightarrow TC, VIS} (\text{s}^{-1})$	A_{th}
N6 ^b	0.106	0.021
N7 ^c	0.149	0.008

[a] $1.5 \times 10^{-5} \text{ M}$ in acetonitrile, 293 K. [b] Visible light: 420 nm, 73 mW/cm^2 . [c] Visible light: 505 nm, 70 mW/cm^2 .

4.4 UV/Vis Studies of Naphthopyrans **N8**, **N9** and **N10****Figure 4.20** Structures of naphthopyrans **N8**, **N9** and **N10**.**Table 4.13** Absorption properties of **N8**, **N9**, and **N10**.^a

Naphthopyran	N8	N9	N10
λ_{max} [nm]	265, 328	267, 365	272, 369

[a] 1.5×10^{-5} M in acetonitrile, 293 K.

The structures and absorption spectra of **N8**, **N9** and **N10** are described in Figure 4.20 and Figure 4.21, respectively. From the initial state, it was illustrated that the extended π conjugation with the alkyne substituent at 2-position lead to a bathochromic shift in the spectra of **N9** with respect to the absorption spectra of **N8**. The TMS substituent, which has an electron donating effect, resulted in a further bathochromic shift in the spectra of **N10** (Table 4.13).

However, there were no new peaks observed in the spectra of **N8**, **N9** and **N10** after several minutes of irradiation with UV light. The possible reason is the large steric substituent at 2-position destabilizing the TC and TT forms (Figure 4.22). Therefore, the switching between closed and open forms is too fast to be detected under our experimental apparatus and conditions in hand. In fact, the synthesis of **N8** and **N10** were reported by the Rück-Braun group before^[62] and later the photochromic properties of a similar structural naphthopyran **2-Br-NP** was reported by the Abe group (Figure 4.22 below).^[63] The half life of the open forms of **2-Br-NP** is 2.5 ms. While the machine we used for the experiments in hand has a shortest time limitation with 100 ms to record

a single spectrum (for details, see Chapter 7.2). Accordingly, the photochromic properties of **N8**, **N9** and **N10** were and are not available for the moment.

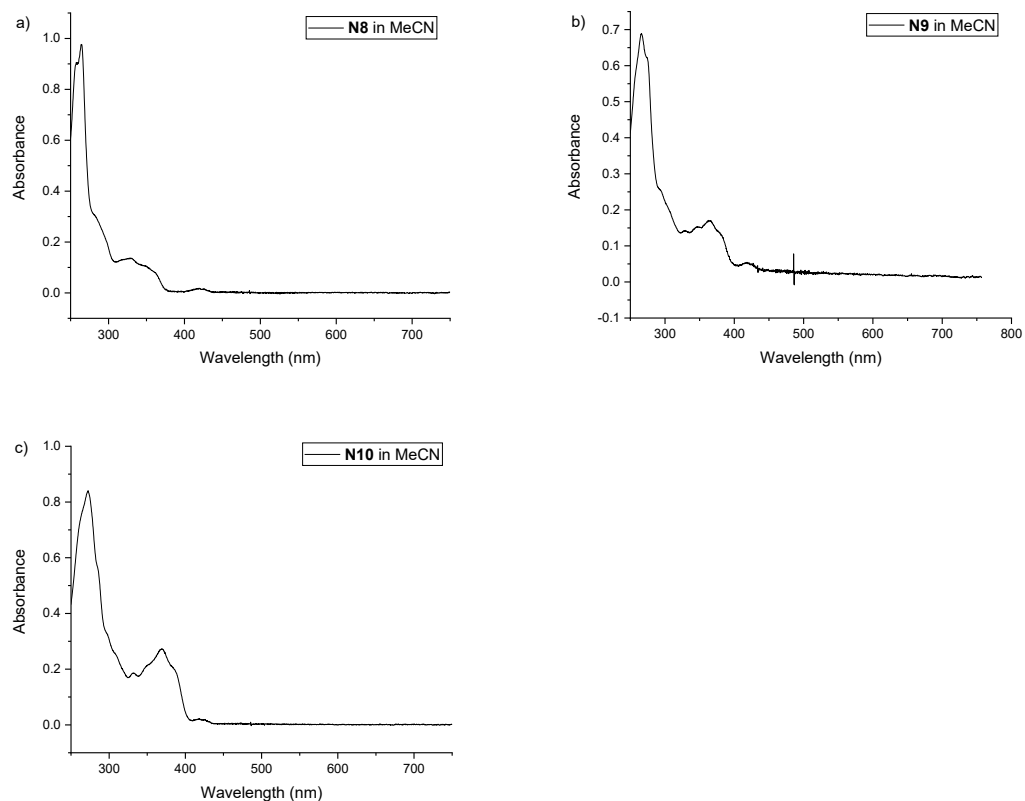


Figure 4.21 Absorption spectra of a) **N8**, b) **N9** and c) **N10** in acetonitrile ($c = 1.5 \times 10^{-5}$ M) at 293 K.

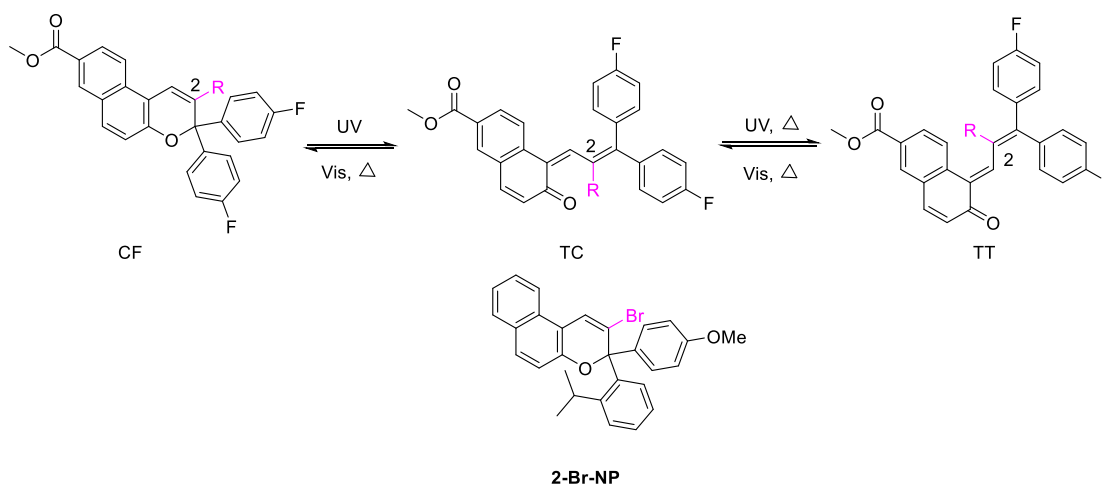


Figure 4.22 Photochromic equilibrium for **N8**, **N9** and **N10** (up) and the structure of naphthopyran **2-Br-NP** (down).

4.5 Discussion

4.5.1 The Effect of 8-Substituent on the Photochromic Properties of Naphthopyrans

From the former information of the Chapters 4.1 and 4.2, it was revealed that, no matter in two states system or three states system, the ester group at 8-position of naphthopyrans plays an important role in the photochromic properties: bathochromic shift for both open and closed forms, decrease in the time of arriving at the PSS and the acceleration in the rate of thermal relaxation. The bathochromic shift in the absorption spectra was observed, because of the extended π conjugation with the ester group. For the reduction in the time of arriving at the PSS, in general, the $\pi \rightarrow \pi^*$ transitions are concerned with the photochromic behavior of naphthopyrans. Thus, the extended π conjugation can promote the photochromic behavior. In addition, the increase in the rate of thermal relaxation can be explained by the resonance electron-withdrawing effect of the ester group. As depicted in Figure 4.23 below, there originally exist electron-poor centers at 3, 7 and 9 position. Meanwhile, the ester group at 8 position can withdraw the electrons from 3, 7 and 9 position thereby destabilizing the open forms. Consequently, the speed of thermal relaxation is accelerated.

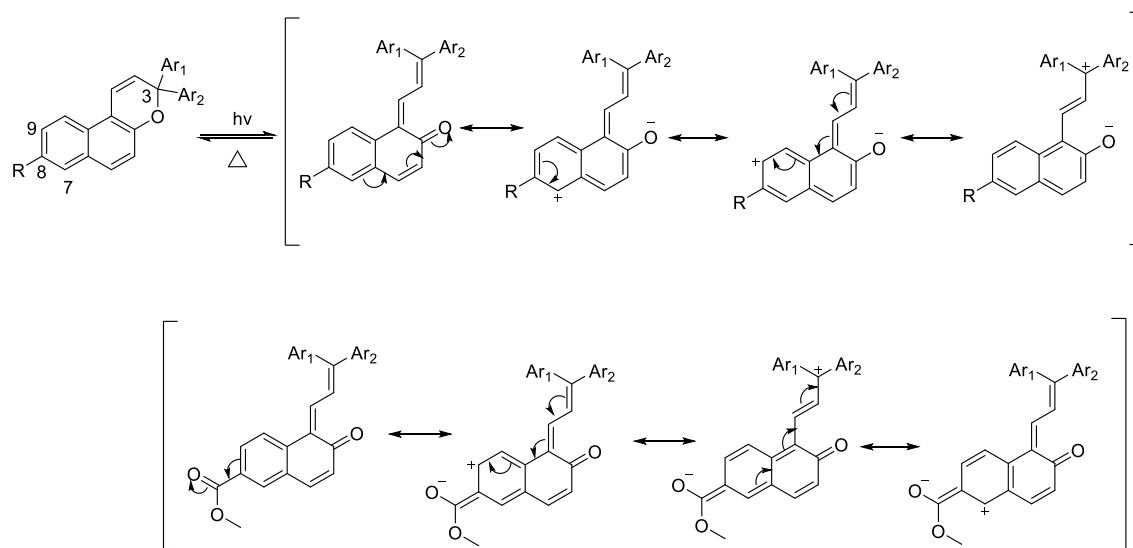


Figure 4.23 The resonance electron-withdrawing effect of the ester group at 8-position.

4.5.2 Comparison between Two States System and Three States System

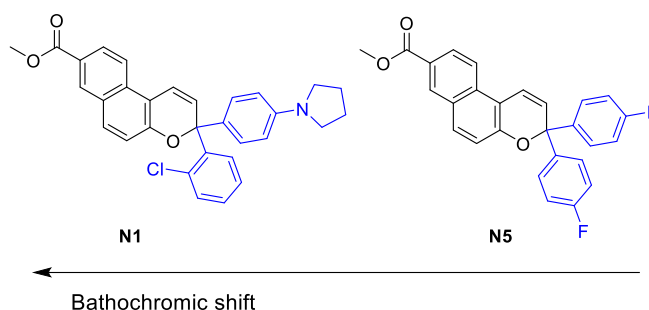


Figure 4.24 The structures of **N1** and **N5**.

Naphthopyran **N1** and **N5** are chosen as the examples to investigate the difference between two states system and three states system (Figure 4.24). For the absorption spectra of the closed form, compounds have the same λ_{\max} at 261 nm. However, upon irradiation with UV light, the electron donating pyrrolidine ring on the aryl ring at 3-position can be conjugated with the whole open form structure, correspondingly inducing a bathochromic shift in λ_{\max} of 163 nm.

In the period of thermal relaxation, the $k_{TC \rightarrow CF, thermal}$ of **N1** is about one seventh as fast as that of **N5**. This phenomena is resulting from the *ortho*-chlorine group of the 3-aryl-substituent, which hinders the re-formation of the CC form, but the CC form is necessary for the ring-closure reaction (Figure 4.25).^[65] The influence can also be found from the crystal structure of naphthopyrans with similar *ortho*-substituents.^[59] Interestingly, the $k_{TT \rightarrow TC, thermal}$ of **N1** is increased, and is 70fold faster than that of **N5**, which is attributed to the *para*-pyrrolidine substituent. As a result, for **N1**, the ratio of k_1/k_2 is approximately 2, while it is about 930 for **N5** (Table 4.14). Accordingly, the thermal relaxation of **N1** follows a biexponential decay, while the thermal relaxation of **N5** follows a fast monoexponential decay (TC \rightarrow CF) and another slow monoexponential decay (TT \rightarrow TC \rightarrow CF). Moreover, the latter step is faster under irradiation with visible light. And that is why we can see three states in the time resolved UV/Vis spectra of **N5**.

4.5 Discussion

Table 4.14 Photochromic properties of **N1** and **N5** in the procedure of thermal back isomerization.^a

	λ_{\max} [nm] (Closed)	λ_{\max} [nm] (Open)	$t_{1/2}$ (s)	$t_{3/4}$ (s)	A_0	k_1 (10^{-3} s^{-1})	k_2 (10^{-3} s^{-1})
N1	261, 318	592	12	25	0.3807	90.9 ^b	47.1 ^b
N5	261, 338	429	1.6	3.4	0.164	634 ^c	0.68 ^c

[a] 1.5×10^{-5} M in acetonitrile, 293 K. λ_{\max} , $t_{1/2}$, $t_{3/4}$ and A_0 are obtained from experimental data. [b] k_1 and k_2 are the fitting parameters from **Equation 1** and data from Figure 4.5-a and Table 4.2. [c] k_1 and k_2 are the fitting parameters from **Equation 2**. k_1 ($k_{TC \rightarrow CF, \text{ thermal}}$) from Figure 4.13 and Table 4.7, k_2 ($k_{TT \rightarrow TC, \text{ thermal}}$) from Figure 4.14 and Table 4.8.

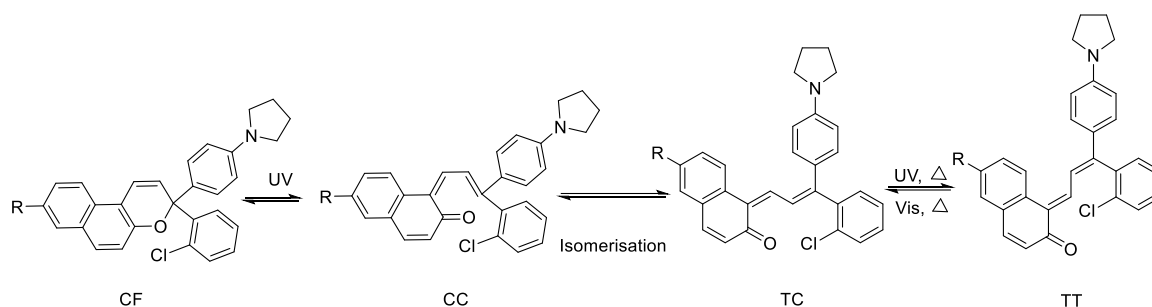


Figure 4.25 Photochromic equilibrium for naphthopyran **N1**.

4.5.3 The Effect of 6-Substituent on Photochromic Properties of Naphthopyran

From the information of Chapter 4.3, it was found that the introduction of an acrylic ester substituent at 6-position, through a remote C-H activation, had a great influence on the photochromic properties of the naphthopyran. Except for the bathochromic shift in the absorption spectra, the thermal relaxation speed and visible light bleaching speed were accelerated. In order to investigate the reason, the resonance structures of **N7** are shown in Figure 4.26. Because of the inductive electron-withdrawing effect of the ester group, the TC form of compound **N7** is less stable than that of the naphthopyran without the acrylic ester substituent at 6-position. Hence the ring-closure reaction was promoted.

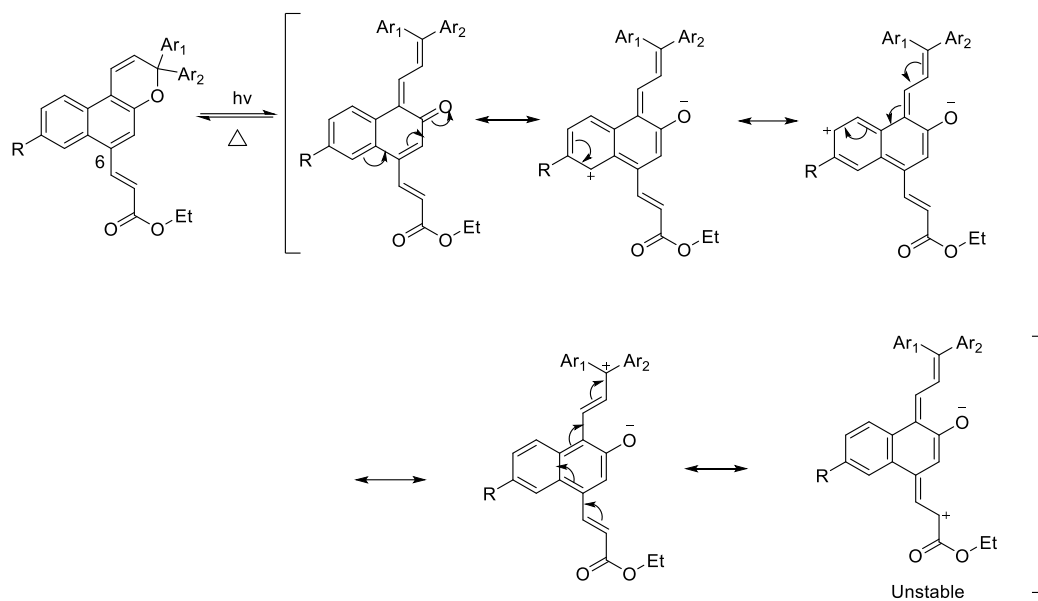


Figure 4.26 The resonance structures of naphthopyran N7.

5. *In-situ* NMR Analysis

Low temperature *in-situ* NMR experiments allow us to investigate how many species are formed during the UV irradiation, thermal relaxation and visible light irradiation processes. We also can evaluate the change between the different forms directly so that the transformation processes among different forms will be clear.

5.1 *In-situ* ^1H NMR Analysis of Two States System: Naphthopyran N1, N3 and N4

5.1.1 Structural Identification of Different Isomers of N1

The ^1H *in-situ* NMR spectra of naphthopyran **N1** is displayed in Figure 5.1. Upon irradiation with UV light, a new signal at 9.02 ppm appeared, which belonged to the H at 2-position of the TC form according to the literature.^[49,51,55,134] The low field is due to the deshielding induced by the C=O group.^[36] At the same time, the signals of H-17 and H-19 of the TC form appeared at 3.32 and 3.82 ppm, respectively. The signal of H-16 of the TC form appeared at 6.54 ppm. Thus, the conversion from CF to TC was detected. After 6 min UV irradiation, another signal was observed at 8.15 ppm, which was assigned to the 1-position proton of the TT form.^[48] Meanwhile, the H-5 of the TT form appeared at 6.29 ppm. Thereby the transformation from TC to TT was detected. After 35 min irradiation, the system arrived at the PSS. The ratio of different forms was obtained as CF : TC : TT = 18:71:11. Moreover, based on the ^1H - ^1H COSY NMR experiment measured at PSS under UV irradiation (Figure 5.2), the signals of other protons of the TC form were also identified (Table 5.1).

5.1 *In-situ* ^1H NMR Analysis of Two States System: **N1**, **N3** and **N4**

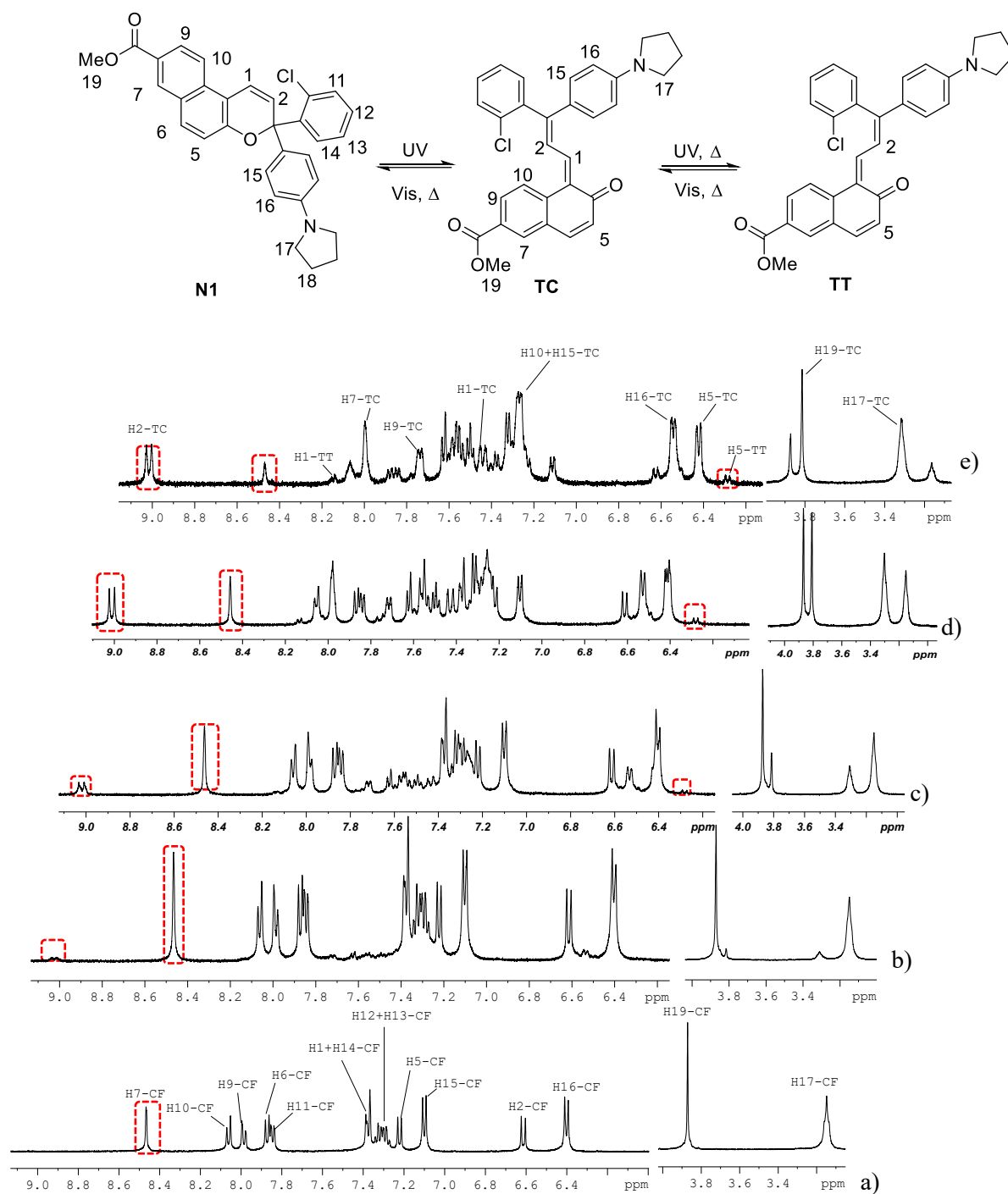


Figure 5.1 500 MHz ^1H NMR spectra of **N1** a) before UV irradiation, b) after 1 min of UV irradiation, c) after 6 min of UV irradiation, d) after 20 min of UV irradiation and e) after 65 min of UV irradiation at the PSS in CD_3CN ($c = 1 \times 10^{-2}$ M) at 238 K. (UV light: 365 nm, 0.45 mW/cm², 500 MHz Bruker NMR spectrometer)

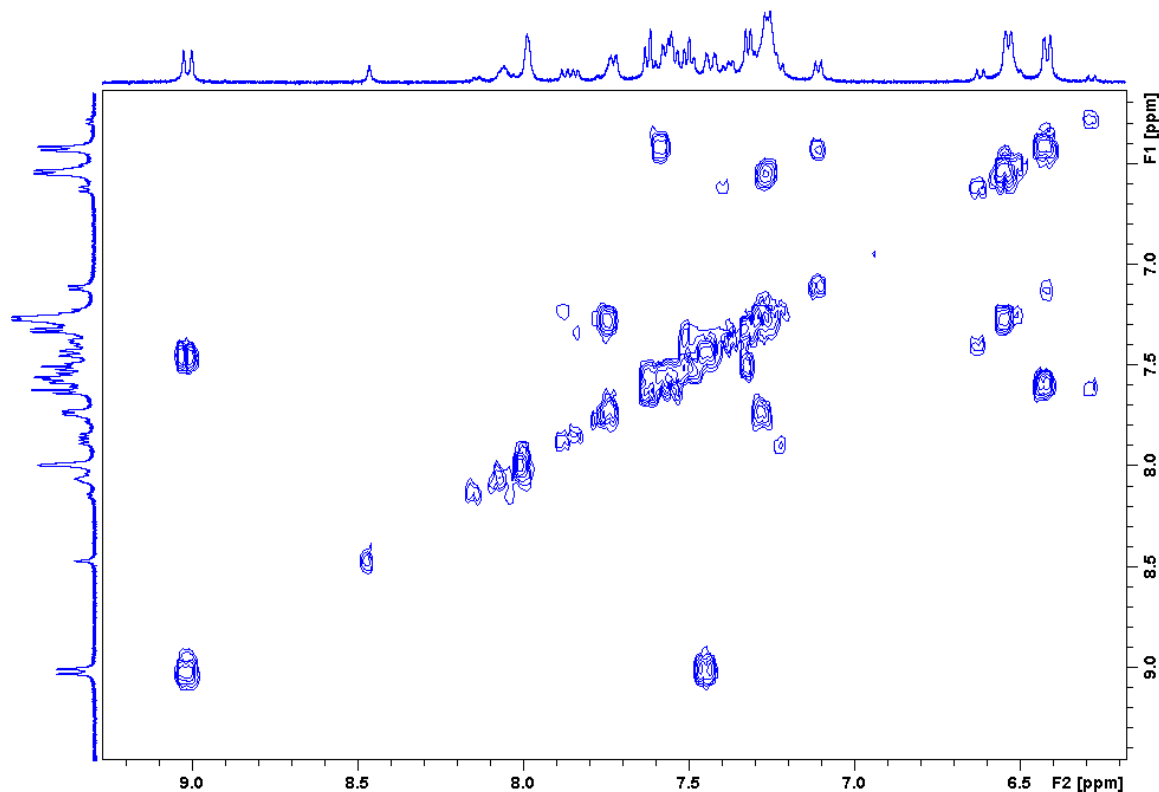


Figure 5.2 500 MHz ^1H - ^1H COSY NMR spectrum of **N1** at the PSS in CD_3CN ($c = 1 \times 10^{-2}$ M) at 238 K. (UV light: 365 nm, 0.45 mW/cm^2 , 500 MHz Bruker NMR spectrometer)

Table 5.1 ^1H NMR chemical shifts (in ppm) of different isomers of **N1** obtained from *in-situ* NMR experiments.^a

	H1	H2	H5	H7	H9	H10	H15	H16	H17	H19
CF	7.38	6.61	7.22	8.47	7.99	8.06	7.10	6.40	3.15	3.87
TC	7.44	9.02	6.42	8.00	7.74	7.27	7.27	6.54	3.32	3.82
TT	8.15		6.29							

[a] 1×10^{-2} M in CD_3CN at 238 K. UV light: 365 nm, 0.45 mW/cm^2 .

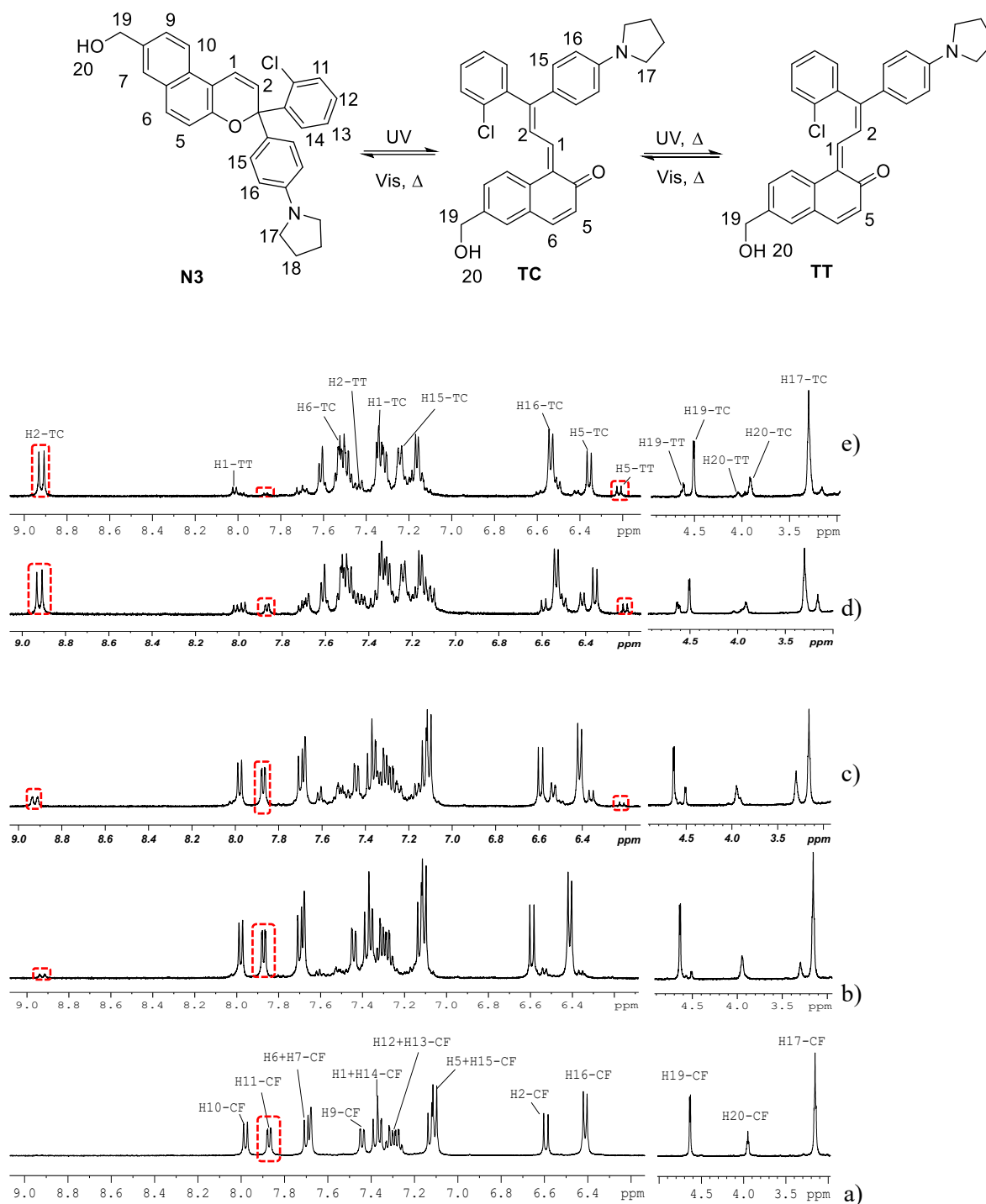
5.1.2 Structural Identification of Different Isomers of **N3**

Figure 5.3 500 MHz ^1H NMR spectra of **N3** a) before UV irradiation, b) after 1 min of UV irradiation, c) after 6 min of UV irradiation, d) after 40 min of UV irradiation and e) after 115 min of UV irradiation at the PSS in CD_3CN ($c = 1 \times 10^{-2}$ M) at 238 K. (UV light: 365 nm, 0.45 mW/cm^2 , 500 MHz Bruker NMR spectrometer)

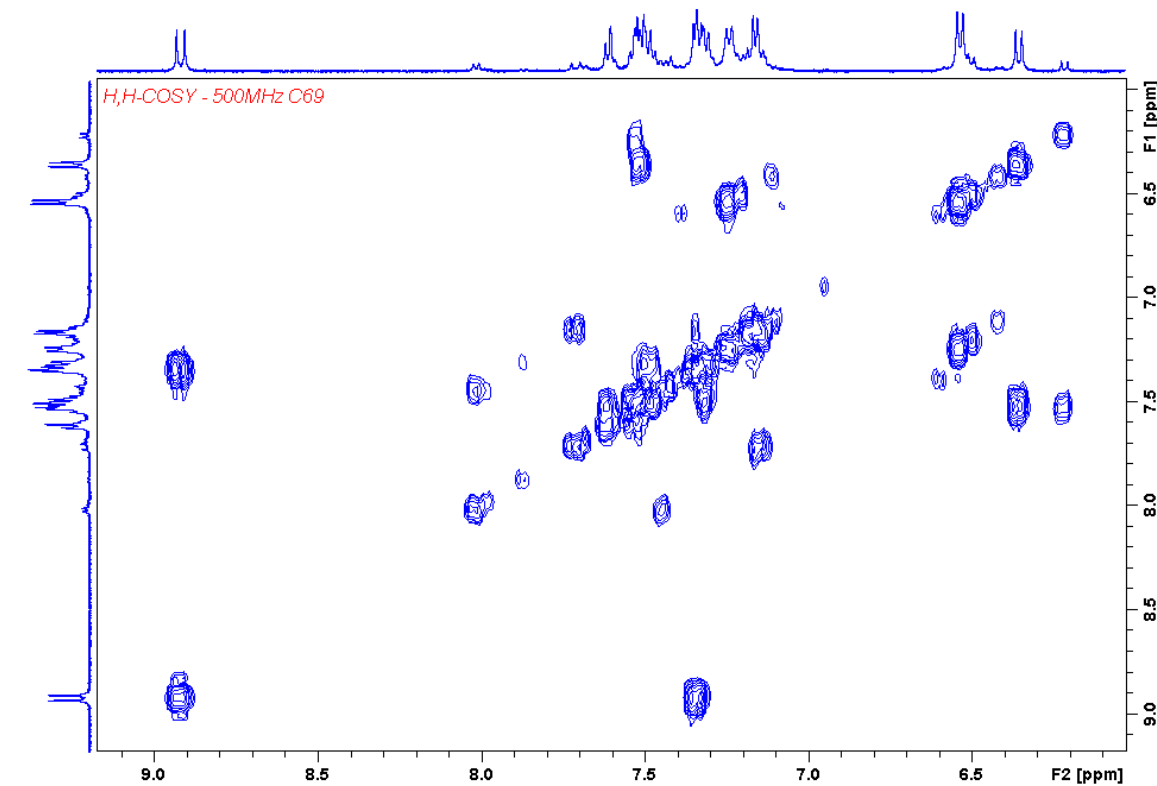


Figure 5.4 500 MHz ^1H - ^1H COSY NMR spectrum of **N3** at the PSS in CD_3CN ($c = 1 \times 10^{-2}$ M) at 238 K. (UV light: 365 nm, $0.45 \text{ mW}/\text{cm}^2$, 500 MHz Bruker NMR spectrometer)

Table 5.2 ^1H NMR chemical shifts (in ppm) of different isomers of **N3** obtained from *in-situ* NMR experiments.^a

	H1	H2	H5	H6	H11	H15	H16	H17	H19	H20
CF	7.38	6.59	7.13	7.70	7.87	7.11	6.41	3.16	4.64	3.95
TC	7.35	8.92	6.36	7.52	-	7.24	6.54	3.30	4.51	3.91
TT	8.02	7.44	6.22		-				4.61	4.04

[a] 1×10^{-2} M in CD_3CN at 238 K. UV light: 365 nm, $0.45 \text{ mW}/\text{cm}^2$.

As exhibited in Figure 5.3 (a), the signals of all the protons of **N3** have been identified in the spectrum. Upon irradiation with UV light, the TC form was converted from closed form (CF). A new signal assigned to the H-2 of the TC form appeared at 8.92 ppm. At the same time, the signals of H-5 and H-16 of the TC form appeared at 6.36 and 6.54 ppm, respectively. The signals of H-17 and H-19 of the TC form were detected at 3.30 and 4.51 ppm, respectively. After 6 min UV irradiation, the signals of the TT form were also observed. The signal at 6.22 ppm was assigned to the 5-position proton of the TT form. The signal at 8.02 ppm was assigned to the 1-position proton of TT form. Thus, the transformation from TC to TT was detected. After 115 min irradiation with UV light, the signals of the CF form were almost disappeared, and the system arrived at the PSS. The ratio of the different forms is CF : TC : TT = 5:80:15. In addition, the signals of other protons of TC and TT forms (Table 5.2) can be identified from the ^1H - ^1H COSY NMR experiment measured at the PSS under UV irradiation (Figure 5.4).

5.1.3 Structural Identification of Different Isomers of **N4**

The *in-situ* ^1H NMR spectra of **N4** is shown in Figure 5.5. The signals of all the protons of **N4** have been identified in the spectrum of Figure 5.5 (a). Upon UV irradiation, three new doublet signals appeared at 8.95, 6.36 and 3.31 ppm. The former one signal belonged to H-2 of the TC form. The latter two signals were assigned to H-5 and H-17 of the TC form, respectively. After 6 min UV irradiation, the signals of the TT form were observed due to conversion from the TC form to the TT form. The signal which appeared at 8.11 ppm was assigned to the 1-position proton (H-1) of the TT form. And the signal at 6.24 ppm belonged to the 5-position proton (H-5) of the TT form. After 35 min UV irradiation, the system of **N4** arrived at the PSS, and the ratio of different forms is CF : TC : TT = 13:73:14. In addition, H-21 and H-22 of the TC form were identified at 1.27 and 1.32 ppm, respectively (Table 5.3).

5.1 *In-situ* ¹H NMR Analysis of Two States System: **N1**, **N3** and **N4**

Table 5.3 ¹H NMR chemical shifts (in ppm) of different isomers of **N4** obtained from *in-situ* NMR experiments.^a

	H1	H2	H5	H10	H16	H17	H21	H22
CF	-	6.65	7.18	8.07	6.45	3.20	1.32	1.38
TC	-	8.95	6.36	-	6.55	3.31	1.27	1.32
TT	8.11	-	6.24	-	6.50	3.28	-	-

[a] 1×10⁻² M in CD₃CN at 238 K. UV light: 365 nm, 3.86 mW/cm².

5.1.4 Kinetic Analysis of **N1**, **N3** and **N4** during Different Processes

When we followed the H-7 (8.47 ppm) of CF, H-2 (9.02 ppm) of TC and H-5 (6.29 ppm) of TT under UV irradiation and in the dark, the evolution of different isomers of **N1** was obtained in Figure 5.6 (a). The evolution of different isomers of **N3** was achieved in Figure 5.6 (b) by following the H-11 (7.87 ppm) of CF, H-2 (8.92 ppm) of TC and H-5 (6.22 ppm) of TT. As exhibited in the Figure 5.6, upon irradiation with UV light, the TC form was converted from the CF form, meanwhile, the TT form was converted from the TC form. When the sample was in the dark, the TC form can be converted from the TT form slowly, and the CF form were converted from the TC form quickly. The kinetics of CF→TC, TC→TT, TC→CF and TT→TC were fitted to the first order reaction (**Equation 3**).

$$c_t = A_1 e^{-kt} + c_{th} \quad (3)$$

c_t is the concentration of CF, TC or TT, k is the rate constant. Spectrokinetic data are demonstrated in Table 5.4.

Under UV irradiation, the speed of **N1** in the process CF→TC (k_3) and TC→TT (k_4) were $9.98 \times 10^{-4} \text{ s}^{-1}$ and $8.36 \times 10^{-4} \text{ s}^{-1}$, respectively, which were similar with that of **N3** ($k_3 = 1.04 \times 10^{-3} \text{ s}^{-1}$, $k_4 = 1.04 \times 10^{-3} \text{ s}^{-1}$). For the thermal back period, k_5 of **N1** ($5.02 \times 10^{-4} \text{ s}^{-1}$) was approximately 50 times as fast as that of **N3** ($9.69 \times 10^{-6} \text{ s}^{-1}$). In the process of TT→TC, k_6 of **N1** ($2 \times 10^{-4} \text{ s}^{-1}$) was about 33-fold faster than that of **N3** ($6.09 \times 10^{-6} \text{ s}^{-1}$). Accordingly, the trend was

consistent with the result of room temperature UV/Vis experiments (see Chapter 4.1): the thermal relaxation speed was accelerated by the ester group at 8-position of the naphthopyran. Furthermore, the ratio of k_5/k_6 ($k_5/k_6 = 2.5$) of **N1** was revealed to have a similar relationship with k_1/k_2 ($k_1/k_2 = 2$) of **N1** in the room temperature UV/Vis experiments. Compared to the ratio of k_1/k_2 ($k_1/k_2 = 1$) of **N3** in the room temperature UV/Vis experiments, the ratio of k_5/k_6 ($k_5/k_6 = 1.5$) of **N3** was also similar.

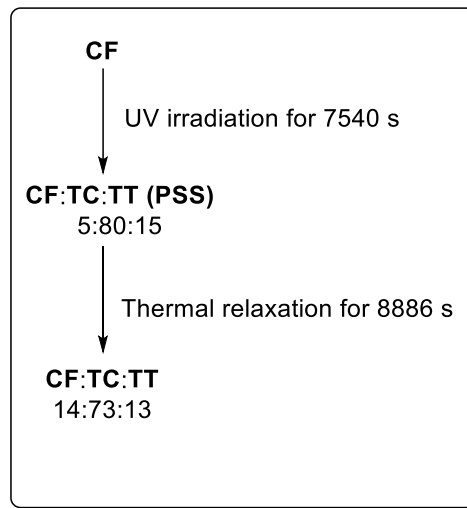
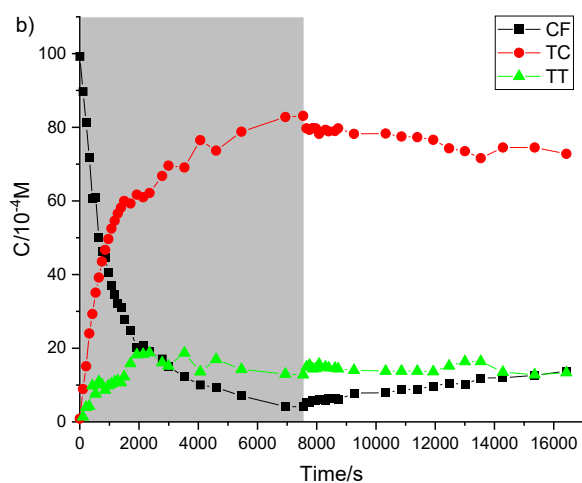
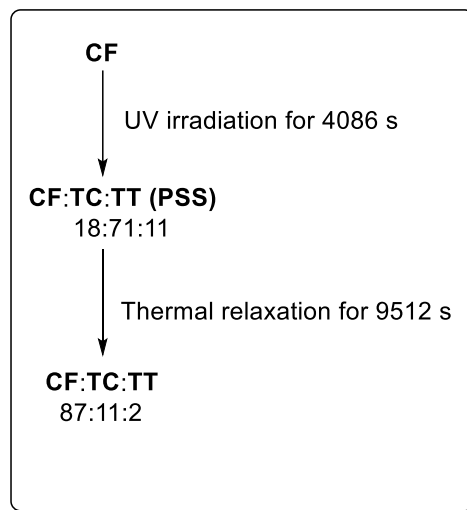
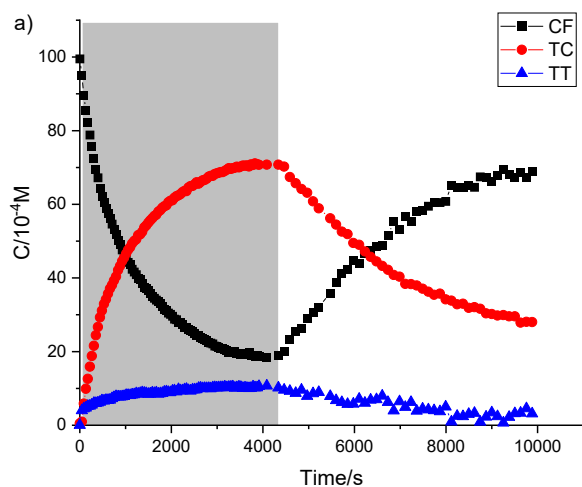
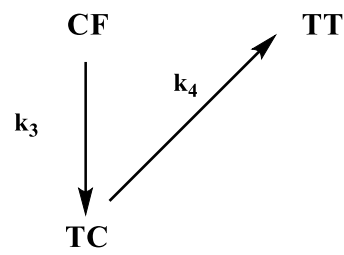
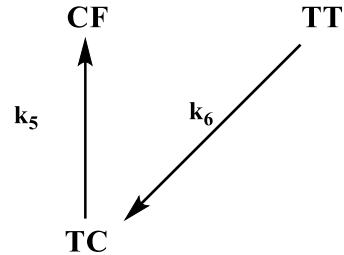


Figure 5.6 Evolution of CF, TC and TT of a) **N1** and b) **N3** in CD_3CN ($c = 1 \times 10^{-2} \text{ M}$) at 238 K. The grey region signals the periods when the sample was irradiated with UV light (365 nm, 0.45 mW/cm^2); non-marked region presents the periods when the sample was in the dark.

5.1 *In-situ* ^1H NMR Analysis of Two States System: **N1**, **N3** and **N4**

Table 5.4 Rate constants of **N1** and **N3** from *in-situ* NMR.^a

	Irradiation with 365 nm light			In the dark	
					
	k_3 (s ⁻¹)	k_4 (s ⁻¹)	k_5 (s ⁻¹)	k_6 (s ⁻¹)	Ratio
N1	9.98×10^{-4}	8.36×10^{-4}	5.02×10^{-4}	2.00×10^{-4}	CF : TC : TT = 18:71:11
N3	1.04×10^{-3}	1.04×10^{-3}	9.69×10^{-6}	6.09×10^{-6}	CF : TC : TT = 5:80:15

[a] 1×10^{-2} M in CD_3CN at 238 K. UV light: 365 nm, 0.45 mW/cm².

The evolution of different isomers of **N4** upon UV irradiation was acquired in Figure 5.7, if the H-10 (8.07 ppm) of CF, H-2 (8.95 ppm) of TC and H-1 (8.11 ppm) of TT were followed. The kinetics of different processes were fitted to the first order reaction (**Equation 3**). Upon UV irradiation, the TC form was converted from the CF form with a rate constant of $1.65 \times 10^{-3} \text{ s}^{-1}$. At the same time, the TT form was converted from the TC form with a rate constant of $1.48 \times 10^{-3} \text{ s}^{-1}$. Compared with **N1** and **N3**, the ring opening reaction of **N4** was faster due to the higher power of the UV light (3.86 mW/cm^2). Considering the slow thermal back reaction from the data of room temperature UV/Vis experiments (see Chapter 4.1), visible light irradiation was applied for promotion of the TT→TC process. Once the system arrived the PSS, UV light was switched off, and visible light was switched on. The k_5 and k_6 of **N4** were promoted to $1.37 \times 10^{-4} \text{ s}^{-1}$ and $1.16 \times 10^{-4} \text{ s}^{-1}$, respectively, approximately 14 and 19 times faster than that of **N3**, while the thermal back speed of **N4** was similar with that of **N3** in the room temperature UV/Vis experiments. In addition, the ratio of k_5/k_6 ($k_5/k_6 = 1.2$) of **N4** was similar with k_1/k_2 ($k_1/k_2 = 1$) of **N4** under irradiation with visible light in the room temperature UV/Vis experiments.

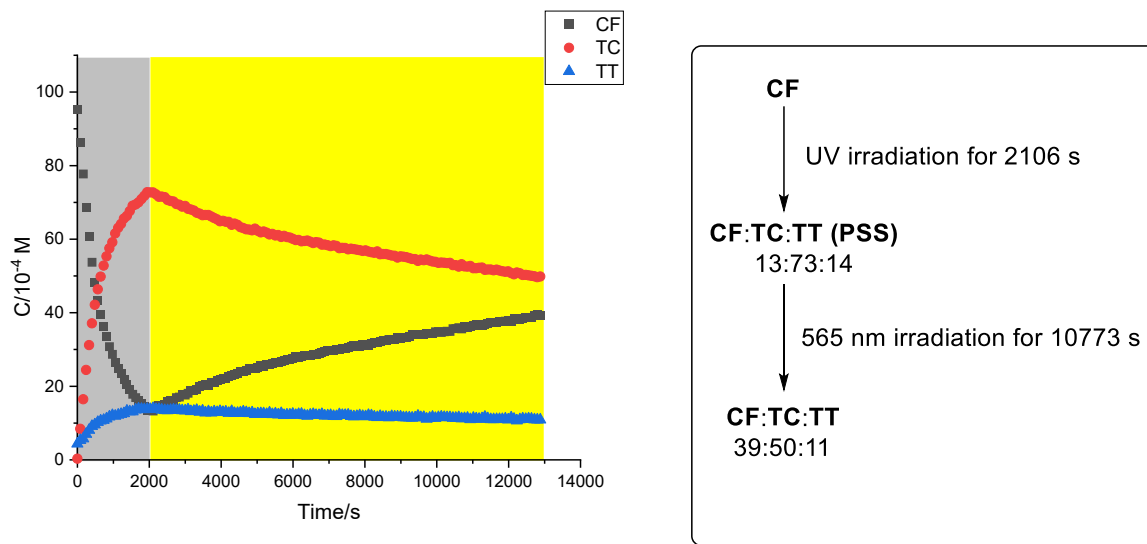


Figure 5.7 Evolution of CF, TC and TT of **N4** in CD_3CN ($c = 1 \times 10^{-2} \text{ M}$) at 238 K. The grey region signals the periods when the sample was irradiated with UV light (365 nm, 3.86 mW/cm²); the yellow region signals the periods when the sample was irradiated with visible light (565 nm, 3.20 mW/cm²).

Table 5.5 Rate constants of **N4** from *in-situ* NMR.^a

	Irradiation with 365 nm light		Irradiation with 565 nm light		
	$\begin{array}{c} \text{CF} \\ \downarrow k_3 \\ \text{TC} \end{array} \quad \begin{array}{c} \nearrow k_4 \\ \text{TT} \end{array}$		$\begin{array}{c} \text{CF} \\ \uparrow k_5 \\ \text{TC} \end{array} \quad \begin{array}{c} \nwarrow k_6 \\ \text{TT} \end{array}$		
	$k_3 (\text{s}^{-1})$	$k_4 (\text{s}^{-1})$	$k_5 (\text{s}^{-1})$	$k_6 (\text{s}^{-1})$	Ratio
N4	1.65×10^{-3}	1.48×10^{-3}	1.37×10^{-4}	1.16×10^{-4}	CF : TC : TT = 13:73:14

[a] $1 \times 10^{-2} \text{ M}$ in CD_3CN at 238 K. UV light: 365 nm, 3.86 mW/cm². Visible light: 565 nm, 3.20 mW/cm².

5.2 *In-situ* ^{19}F NMR analysis of Three States System: Naphthopyran **N5** and **N6**

The ^{19}F NMR spectra have less peaks than the ^1H NMR spectra to be investigated and the ^{19}F nucleus is also easily observable, because of its 100% natural abundance, $\frac{1}{2}$ spin and similarly high sensitivity with ^1H nucleus.^[36] Since the relation between ^{19}F NMR spectra and ^1H NMR spectra have been investigated by the literatures^[18,36,48,49] the *in-situ* ^1H NMR spectra are not necessary for the exploration of naphthopyrans **N5**, **N6** and **N7** any more. The *in-situ* ^{19}F NMR spectra of **N5** are depicted in Figure 5.8. The signals of fluorine of different isomers are easily identified. Before UV irradiation, the signal of **N5** was located at -115.84 ppm. Upon UV irradiation, two new signals were observed at -112.42 ppm and -113.13 ppm, respectively, which were assigned to the TC form. After 3 min UV irradiation, the signals of the TT form appeared at -112.64 and -112.75 ppm, respectively. Particularly, the signal of an allenyl-naphthol compound (AP) was detected at -116.21 ppm, signals which were also observed from other naphthopyrans.^[17,18,36,48,135,136] After 32 min of UV irradiation, the system of **N5** arrived at the PSS with a ratio of CF : TC : TT : AP = 10:60:8:22. Similar performance was also observed in the evolution of naphthopyran **N6**. After about 30 min irradiation with UV light, an equilibrium was established in the system of **N6** with a ratio of CF : TC : TT : AP = 15:72:5:8. The chemical shifts of different isomers of **N5** and **N6** are presented in Table 5.6.

Table 5.6 ^{19}F NMR chemical shifts (in ppm) of different isomers of **N5** and **N6** obtained from *in-situ* NMR experiments.^a

	N5				N6			
	CF	TC	TT	AP	CF	TC	TT	AP
F	-115.84	-112.42 -113.13	-112.64 -112.75	-116.21	-116.06	-113.00 -113.54	-113.15	-116.28

[a] 1×10^{-2} M in CD_3CN at 238 K. UV light: 365 nm, 3.86 mW/cm².

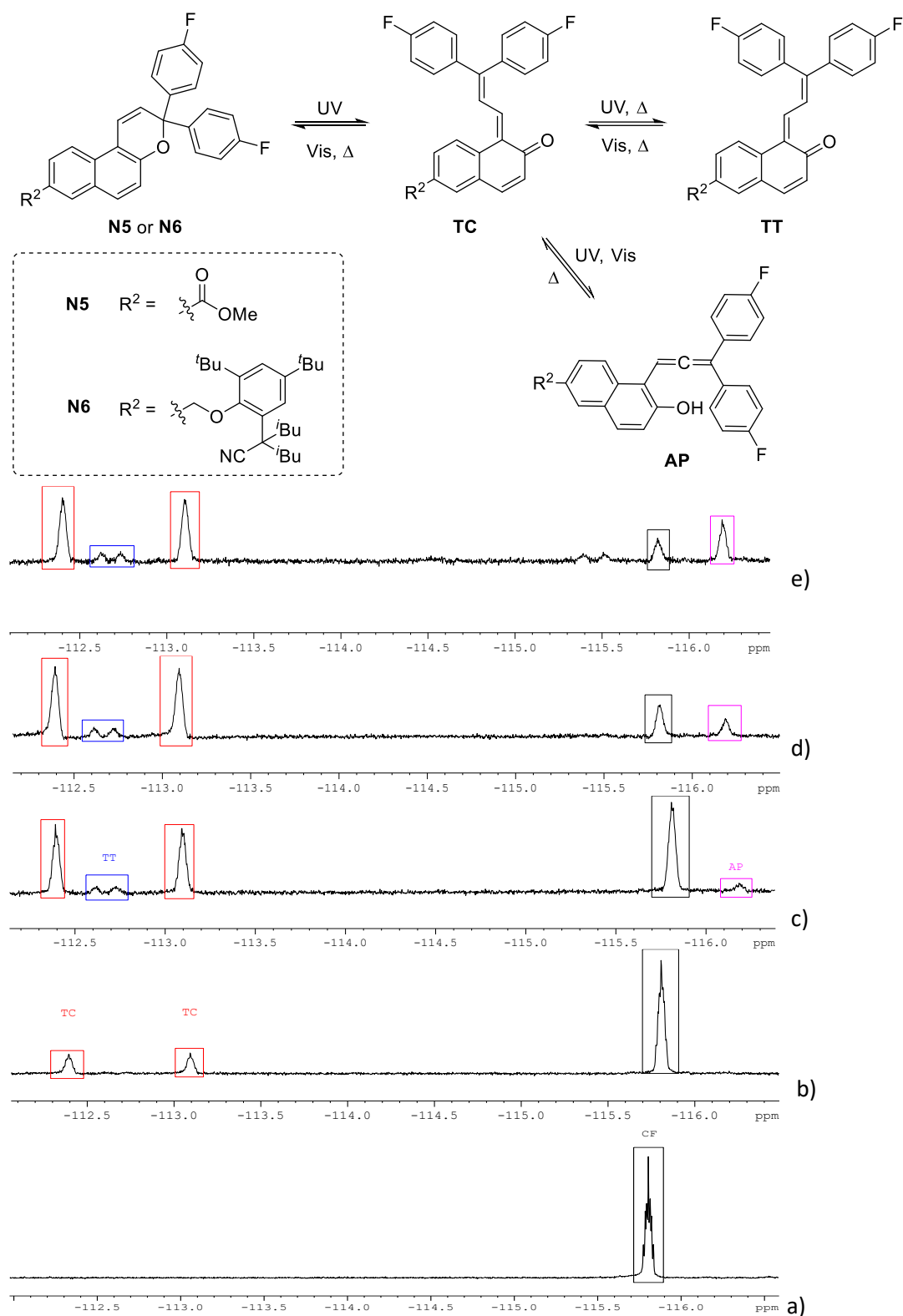


Figure 5.8 470 MHz ^{19}F NMR spectra of **N5** a) before UV irradiation, b) after 1 min of UV irradiation, c) after 3 min of UV irradiation, d) after 10 min of UV irradiation and e) after 32 min of UV irradiation at the PSS in CD_3CN ($c = 1 \times 10^{-2}$ M) at 238 K. (365 nm, 3.86 mW/cm², 500 MHz Bruker NMR spectrometer)

5.2 *In-situ* ^{19}F NMR Analysis of Three States System: Naphthopyrans **N5** and **N6**

When the fluorine signals of CF, TC, TT and AP were followed, the evolution of different isomers of **N5** were obtained in Figure 5.9 (a). The kinetics of all the transformation processes between any two related isomers were fitted to the first order reaction (**Equation 3**) (Table 5.8). Upon UV irradiation, the CF form was converted into the TC form with a rate constant of $k_3 = 5.38 \times 10^{-3} \text{ s}^{-1}$, meanwhile, TT and AP forms were converted from the TC form with rate constants of $k_4 = 3.78 \times 10^{-3} \text{ s}^{-1}$ and $k_7 = 4.92 \times 10^{-4} \text{ s}^{-1}$, respectively. At the same time, byproduct was observed at -115.5 ppm after 32 min UV irradiation (Figure 5.8, e). When the sample was in the dark, the CF form was increased, TC and AP forms started to be decreased, because of the two following processes: $\text{TC} \rightarrow \text{CF}$ ($k_8 = 9.59 \times 10^{-4} \text{ s}^{-1}$) and $\text{AP} \rightarrow \text{TC}$ ($k_{10} = 8.00 \times 10^{-4} \text{ s}^{-1}$). Surprisingly, TT form was increased when the sample was in the dark, which differed from room temperature UV/Vis experiments. Similar phenomenon was observed for chromene and they think it is resulting from the process $\text{TC} \rightarrow \text{TT}$,^[136] although the process $\text{AP} \rightarrow \text{TT}$ is also a possible reason. The rate constant of process $\text{TC} \rightarrow \text{TT}$ in the dark is $k_9 = 1.54 \times 10^{-4} \text{ s}^{-1}$. It is worth noting that, if the UV light was switched on again, the TT form was converted into the TC form until arriving at the same ratio as obtained under UV irradiation in the beginning. In addition, after 396 s UV irradiation, the CF form content was decreased to ($9 \times 10^{-4} \text{ M}$) and did not change any more, while the content of the TC form was increased to ($6.2 \times 10^{-3} \text{ M}$) for the first 396 s UV irradiation and reduced to ($5.5 \times 10^{-3} \text{ M}$) until the PSS was reached in the following 924 s of UV irradiation. At the same time, AP content was increasing until the PSS was reached in the whole 1320 s UV irradiation process. That is an evidence that the AP form was converted from the TC form.

The evolution of different isomers of **N6** is presented in Figure 5.9 (b). Upon UV irradiation, both processes $\text{CF} \rightarrow \text{TC}$ and $\text{TC} \rightarrow \text{TT}$ were detected with rate constants of $k_3 = 2.81 \times 10^{-3} \text{ s}^{-1}$ and $k_4 = 1.55 \times 10^{-3} \text{ s}^{-1}$, respectively, which are slower than the processes observed for **N5**. But the transformation from TC to AP ($k_7 = 2.35 \times 10^{-3} \text{ s}^{-1}$) is faster than the process of **N5**. When the UV light was switched off, the TC form of **N6** was converted into the CF form with a slower speed ($k_8 = 3.25 \times 10^{-4} \text{ s}^{-1}$) than that of **N5**, which has a same trend as in the room temperature UV/Vis experiments for **N5** and **N6**. However, there is no clear change for the TT form during the whole thermal back period, which is different from naphthopyran **N5**. The process: $\text{AP} \rightarrow \text{TC}$ ($k_{10} = 8.00 \times 10^{-4} \text{ s}^{-1}$) is faster than that of **N5**. After about 2 h in the dark, no AP form was detected, and a new equilibrium was established in the system of **N6** with a ratio of CF : TC : TT = 87:6:7. Upon irradiation with 420 nm light, the TC content was increased firstly, and then was reduced due to

the concurrent three processes: $TC \rightarrow CF$, $TT \rightarrow TC$ and $TC \rightarrow AP$. The AP form appeared again, and all the TT form disappeared. A new equilibrium was observed with a ratio of $CF : TC : AP = 92:3:5$. When visible light was switched off, TC was converted from all the AP form. A new thermal equilibrium was reached between CF and TC ($CF : TC = 94:6$).

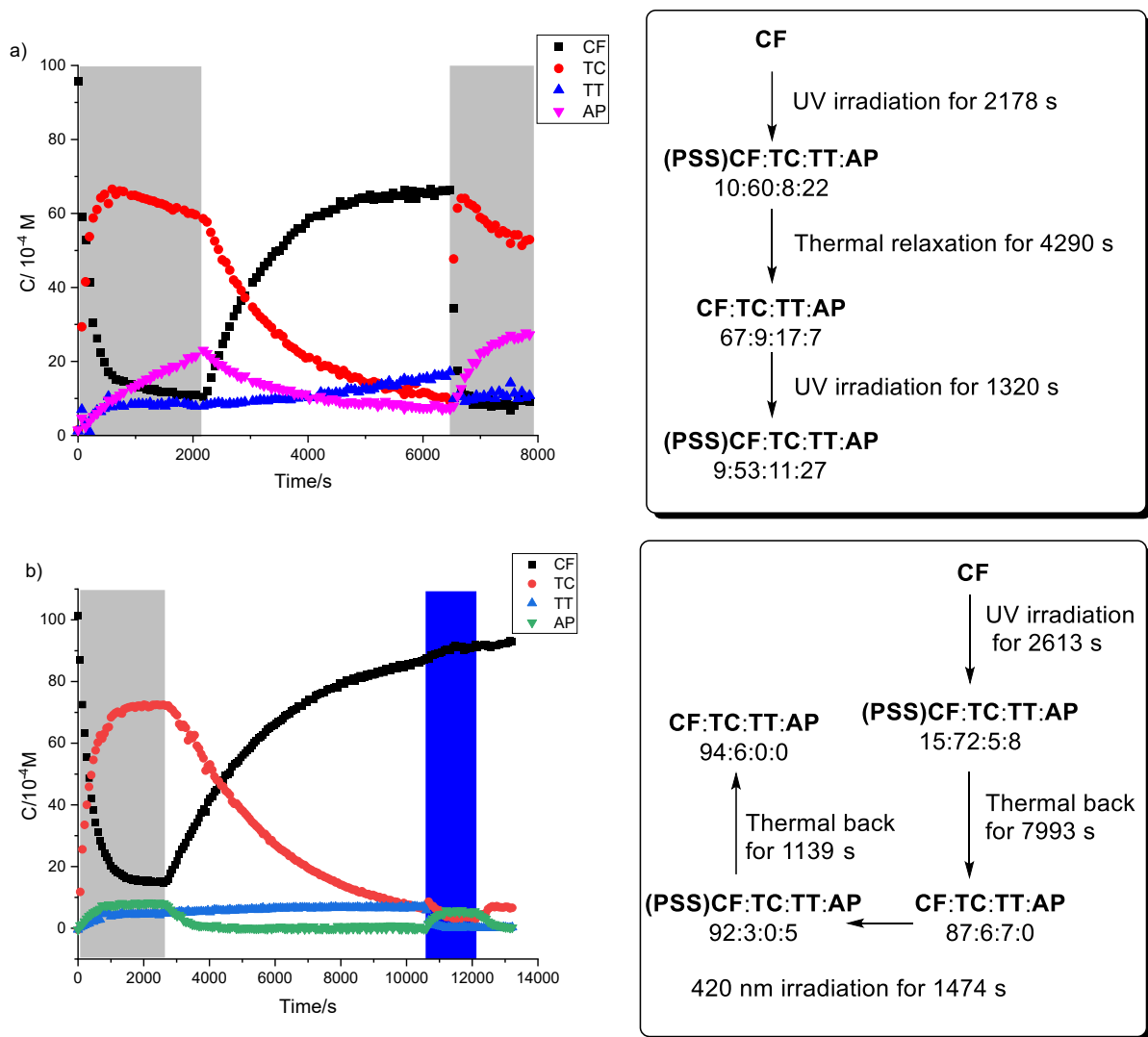


Figure 5.9 Evolution of CF, TC, TT and AP of a) **N5** and b) **N6** in CD_3CN ($c = 1 \times 10^{-2}$ M) at 238 K. The grey regions: UV light irradiation (365 nm, 3.86 mW/cm²); the blue region: visible light irradiation (420 nm, 8.10 mW/cm²); non-marked regions: the sample was in the dark.

5.2 *In-situ* ^{19}F NMR Analysis of Three States System: Naphthopyrans **N5** and **N6**

Table 5.7 The ratios among different isomers of **N5** and **N6** in the PSS under UV irradiation.^a

Naphthopyran	Ratio
N5	CF : TC : TT : AP = 10:60:8:22
N6	CF : TC : TT : AP = 15:72:5:8

[a] 1×10^{-2} M in CD_3CN at 238 K. UV light: 365 nm, 3.86 mW/cm²

Table 5.8 Rate constants of **N5** and **N6** from *in-situ* NMR.^a

a. Irradiated with 365 nm light.

b. In the dark.

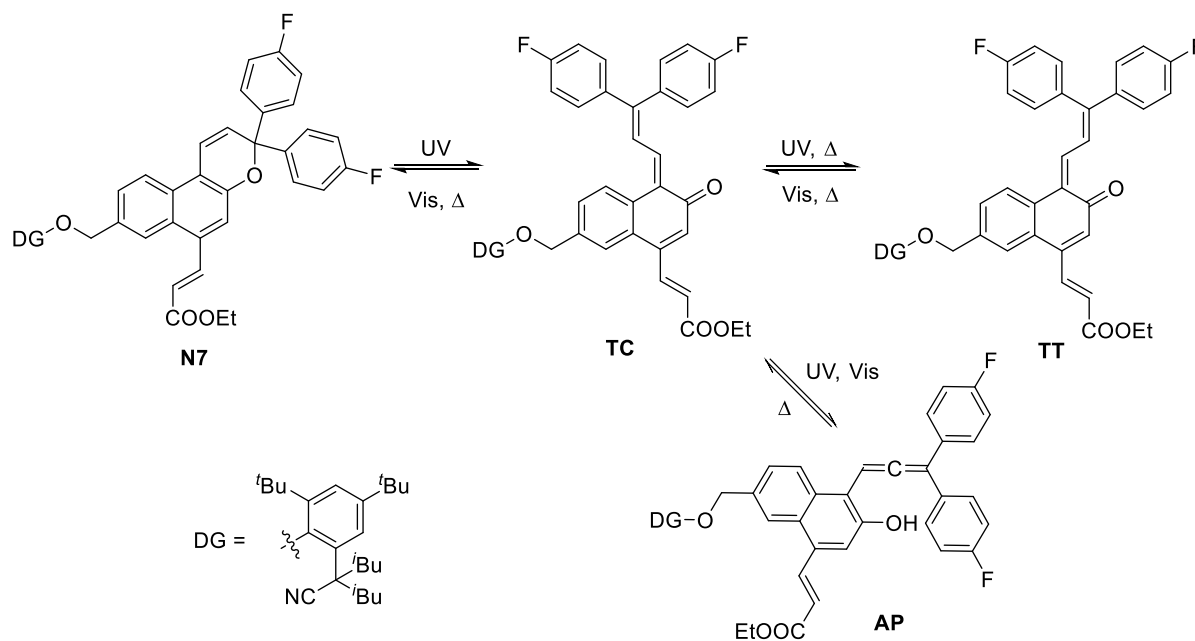
c. Irradiated with visible light.

	k_3 (10^{-3} s^{-1})	k_4 (10^{-3} s^{-1})	k_7 (10^{-3} s^{-1})	k_8 (10^{-3} s^{-1})	k_9 (10^{-3} s^{-1})	k_{10} (10^{-3} s^{-1})	k_{11} (10^{-3} s^{-1})	k_{12} (10^{-3} s^{-1})	k_{13} (10^{-3} s^{-1})
N5	5.38	3.78	0.492	0.959	0.154	0.800	- ^c	- ^c	- ^c
N6^b	2.81	1.55	2.35	0.325	-	1.82	1.89	6.37	4.32

[a] 1×10^{-2} M in CD_3CN at 238 K. UV light: 365 nm, 3.86 mW/cm² [b] Visible light: 420 nm, 8.10 mW/cm². [c] For compound **N5**, irradiation with visible light was not investigated.

5.3 Investigation of Visible Light Wavelength Influence on PSS_{vis} of N7 by *In-situ* ¹⁹F NMR analysis

Table 5.9 ¹⁹F NMR chemical shifts (in ppm) of different isomers of **N7** obtained from *in-situ* NMR experiments.^a



N7				
	CF	TC	TT	AP
F	-115.84	-112.81 -113.38	-113.00	-116.09

[a] 1×10^{-2} M in CD₃CN at 238 K. UV light: 365 nm, 3.86 mW/cm².

The chemical shifts of different isomers of **N7** are reported in Table 5.9 (for NMR spectra, see Chapter 8.4). If we followed the F signals of CF, TC, TT and AP, the evolution of different forms of **N7** was achieved as presented in Figure 5.10. Upon UV irradiation, the CF content was decreased, the content of the other three forms: TC, TT and AP, were increased. After about 24 min irradiation, the system arrived at the PSS with a ratio of CF : TC : TT : AP = 32:53:13:2. When the sample was in the dark, two processes, TC→CF and AP→TC were detected and the TT form did not change, which is the same as compound **N6** and different from compound **N5**. After 45

5.3 Investigation of Visible Light Wavelength Influence on PSS_{Vis} of N7 by *In-situ* ¹⁹F NMR analysis

min in the dark, one equilibrium was found with a ratio of CF : TC : TT = 80:6:14. However, when the sample was irradiated with 420 nm light, the TT form were converted to the CF form until the content of (9×10^{-4} M), and the process CF→TC was observed, which is different from the compound N6. After 2 min irradiation with 420 nm light, a ratio of CF : TC : TT : AP = 53:34:9:4 was established. Furthermore, the total disappearance of TT form were not observed under the irradiation with 455 nm, too. The process CF→TC was also detected (Figure 5.10 blue and Table 5.10). This phenomenon is resulting from the absorption band at 375-450 nm of the closed form of N7. Therefore, the cleavage of the C-O bond can be induced by the irradiation with both 420 nm and 455 nm light. Finally, after 6 min 505 nm irradiation, all the TT form was converted to the TC form, and the TC form was converted to the CF form with an equilibrium of CF : TC : AP = 92:4:4, established under the irradiation with 505 nm light.

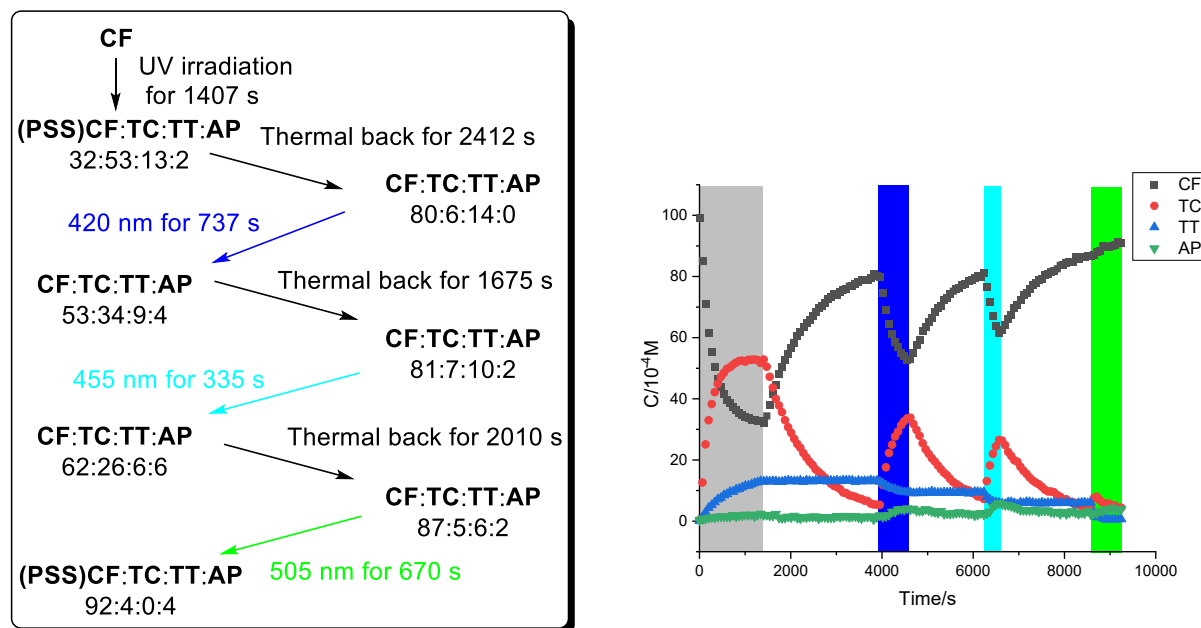


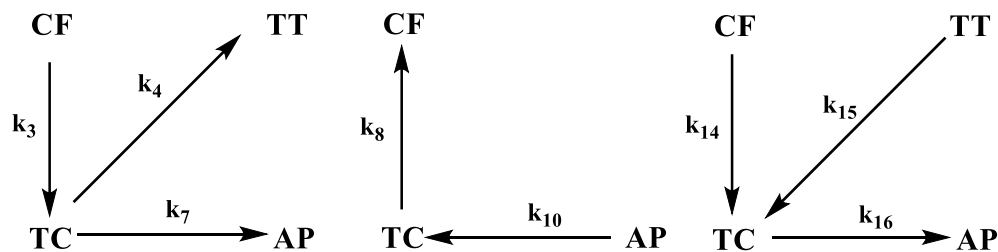
Figure 5.10 Evolution of CF, TC, TT and AP of N7 in CD₃CN ($c = 1 \times 10^{-2}$ M) at 238 K. The grey regions: UV light irradiation (365 nm, 3.86 mW/cm²); the blue region: visible light irradiation (420 nm, 8.10 mW/cm²); the light blue region: visible light irradiation (455 nm, 4.30 mW/cm²); the green region: visible light irradiation (505 nm, 2.37 mW/cm²); non-marked regions: the sample was in the dark.

The kinetics of all the transformation processes between any two related isomers of **N7** can be fitted to the first order reaction (**Equation 3**) (Table 5.10). By comparison of the photochromic behavior between **N6** and **N7** (Table 5.8 and Table 5.10), it was revealed that k_3 of **N7** ($3.93 \times 10^{-3} \text{ s}^{-1}$) is faster than that of **N6** ($2.81 \times 10^{-3} \text{ s}^{-1}$), that is why naphthopyran **N7** can arrive at the PSS quicker. This trend is also in agreement with the photochromic performance in the UV/Vis experiments. The speeds of process TC \rightarrow TT are almost the same for **N6** and **N7**: $1.56 \times 10^{-3} \text{ s}^{-1}$. But AP of **N6** can be converted from TC faster than that of **N7**. In the thermal relaxation period, the speed from TC to CF of **N7** ($k_8 = 1.10 \times 10^{-3} \text{ s}^{-1}$) is approximately 3 time as fast as that of **N6** ($k_8 = 3.25 \times 10^{-2} \text{ s}^{-1}$), which is in accordance with the data from room temperature UV/Vis experiments. In the visible light irradiation period, under 505 nm irradiation, the reconversion speed of k_{20} ($2.11 \times 10^{-3} \text{ s}^{-1}$) and k_{21} ($12.97 \times 10^{-3} \text{ s}^{-1}$) are faster than k_{11} and k_{12} of **N6**, which has the same trend as in the room temperature UV/Vis experiments. At last, in the procedure of different visible light irradiation of **N7**, it was indicated that the longer the wavelength of visible light, the faster is transformation from TT to TC. The rate constants are: 420 nm: $2.80 \times 10^{-3} \text{ s}^{-1}$, 455 nm: $7.92 \times 10^{-3} \text{ s}^{-1}$ and 505 nm: $12.97 \times 10^{-3} \text{ s}^{-1}$.

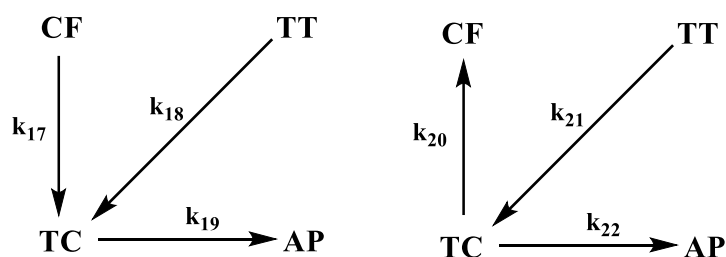
5.3 Investigation of Visible Light Wavelength Influence on PSS_{vis} of N7 by *In-situ* ¹⁹F NMR analysis

Table 5.10 Rate constants and the ratio in the PSS under UV irradiation of N7 from *in-situ* NMR.^a

a. Irradiated with 365 nm light. b. In the dark. c. Irradiated with 420 nm light.



d. Irradiated with 455 nm light. e. Irradiated with 505 nm light.



k_3 (10^{-3} s^{-1})	k_4 (10^{-3} s^{-1})	k_7 (10^{-3} s^{-1})	k_8 (10^{-3} s^{-1})	k_{10} (10^{-3} s^{-1})	k_{14} (10^{-3} s^{-1})	k_{15} (10^{-3} s^{-1})	k_{16} (10^{-3} s^{-1})	k_{17} (10^{-3} s^{-1})
3.93	1.56	1.92	1.10	2.02	3.29	2.80	3.50	2.31
k_{18} (10^{-3} s^{-1})	k_{19} (10^{-3} s^{-1})	k_{20} (10^{-3} s^{-1})	k_{21} (10^{-3} s^{-1})	k_{22} (10^{-3} s^{-1})	Ratio			
7.92	2.00	2.11	12.97	4.47	CF : TC : TT : AP = 32:53:13:2			

[a] $1 \times 10^{-2} \text{ M}$ in CD_3CN at 238 K. UV light: 365 nm, 3.86 mW/cm². Visible light: 420 nm, 8.10 mW/cm²; 455 nm, 4.30 mW/cm²; 505 nm, 2.37 mW/cm².

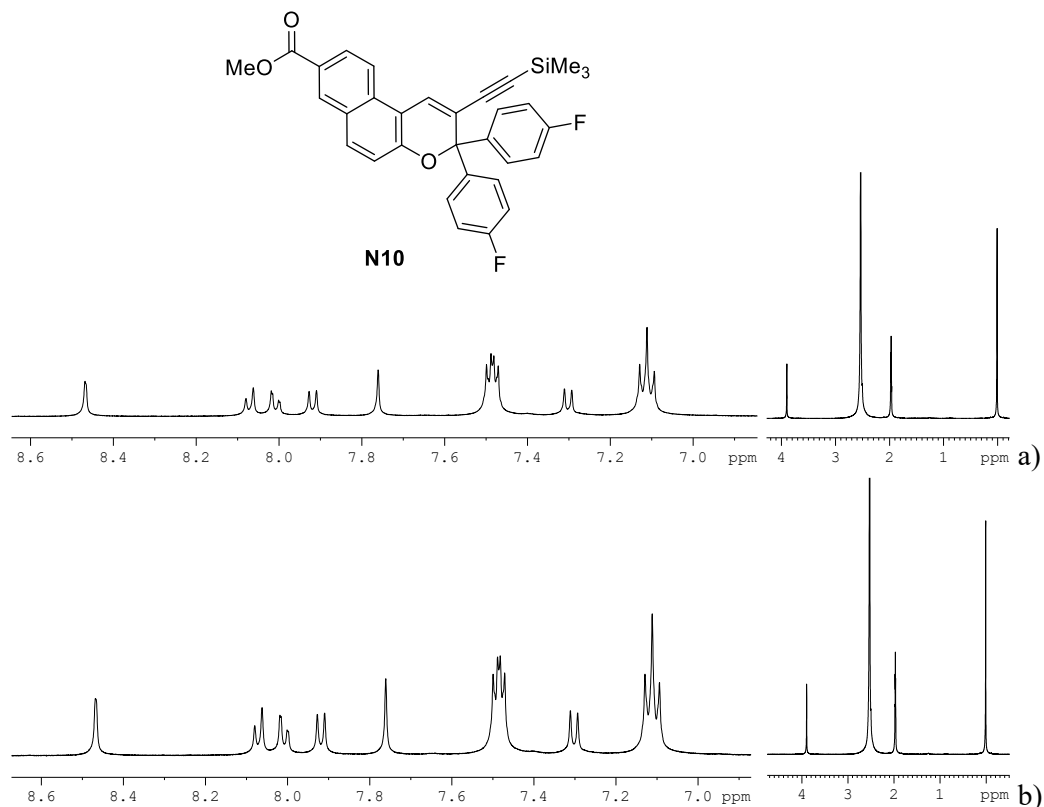
5.4 *In-situ* ^1H NMR analysis of Naphthopyrans **N8**, **N9** and **N10**

Figure 5.11 500 MHz ^1H NMR spectra of **N10** a) before UV irradiation and b) after 20 min of UV irradiation in CD_3CN ($c = 1 \times 10^{-2}$ M) at 238 K. (UV light: 365 nm, 3.86 mW/cm^2 , 500 MHz Bruker NMR spectrometer)

Because of the extremely fast thermal relaxation speed of naphthopyran **N8**, **N9** and **N10**, normal room temperature UV/Vis experiments are not effective in the detection of the open forms (Chapter 4.4). Therefore, **N8**, **N9** and **N10** were monitored by low temperature *in-situ* NMR experiments. As shown in Figure 5.11, after 20 min UV irradiation at 238 K, no new signal was detected in the spectra of **N10**. And the same phenomena were also observed in the spectra of **N8** and **N9**. Then lower temperature experiments at 213 K were performed for **N8** and **N9** (Figure 5.12). Unfortunately, new signals were still not observed in toluene- d_8 solution at 213 K, and 213 K is the lowest temperature for long time *in-situ* NMR measurements in the Institute. Hence the photochromic data of **N8**, **N9** and **N10** are not available at present.

5.4 *In-situ* ^1H NMR Analysis of Naphthopyrans **N8**, **N9** and **N10**

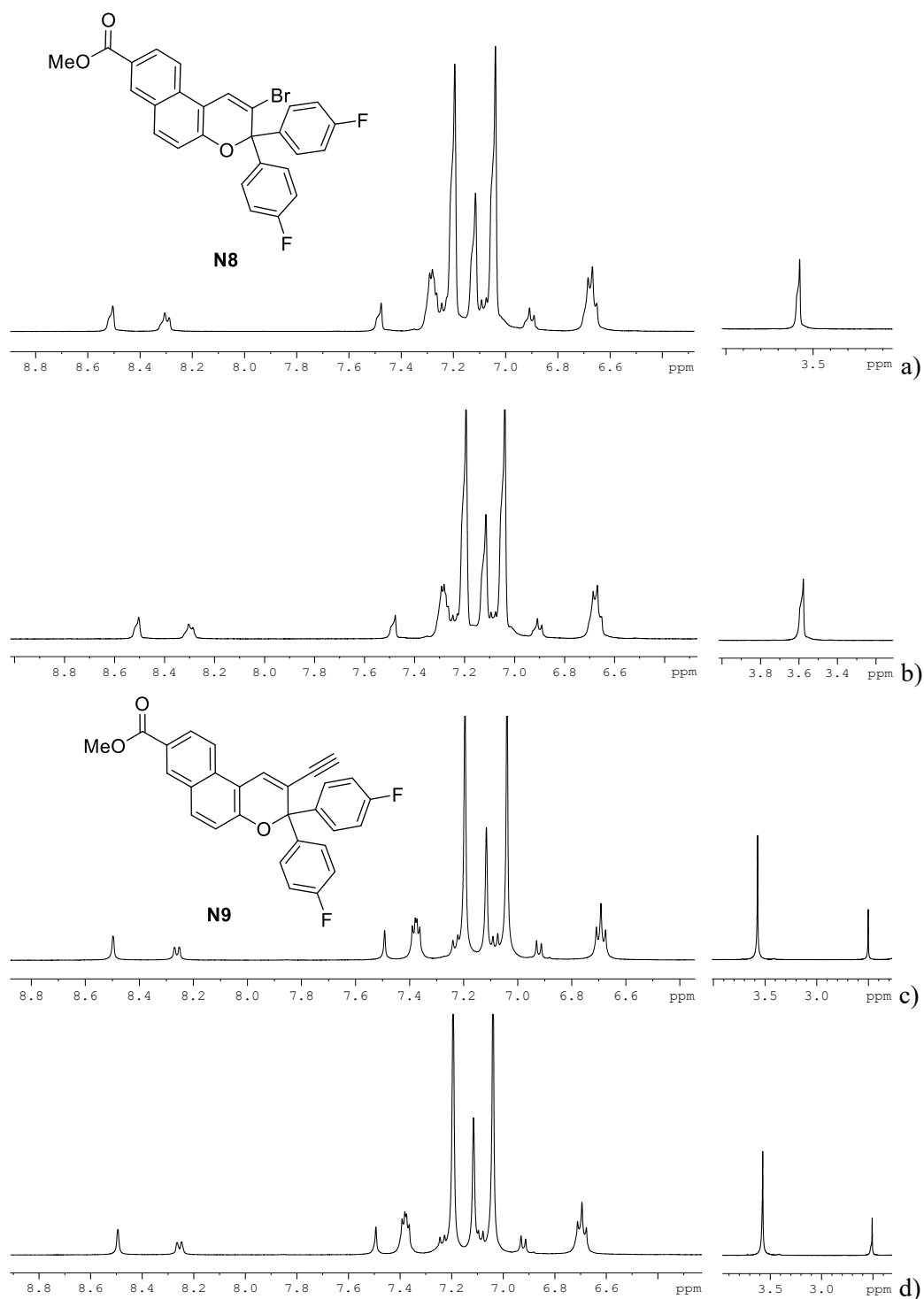


Figure 5.12 500 MHz ^1H NMR spectra of a) **N8** before UV irradiation, b) **N8** after 20 min of UV irradiation, c) **N9** before UV irradiation and d) **N9** after 20 min of UV irradiation in $\text{toluene-}d_8$ ($c = 1 \times 10^{-2}$ M) at 213 K. (UV light: 365 nm, 3.86 mW/cm², Bruker NMR spectrometer)

5.5 Discussion

5.5.1 The Different Performance between Two States System and Three States System during the Low Temperature *in-situ* NMR Measurements

Comparing the photochromic behaviors of two states system with three states system naphthopyrans, **N1** (Table 5.4) and **N5** (Table 5.7), in the low temperature *in-situ* NMR experiments, it was found that TT→TC process was observed in the two states system **N1** during the thermal relaxation. In contrast, TC→TT process was observed in the three states system **N5** during the low temperature thermal relaxation. In order to explain the phenomenon, the proposed energy diagram is illustrated in Figure 5.14, in which the AP form is not involved, because the AP form was not detected in the two states system. Presumably, the activation energy (ΔG_5) between TT form and transition state 3 is too large to reach in the three states system at 238K. Meanwhile, the energy barrier between TC form and transition state 3 is low enough to climb. As a result, only the TC→TT process was observed. However, when the temperature rose to 293 K, the TT form had enough energy to climb to the transition state 3. Thus, all the processes TC→TT, TT→TC and TC→CF existed in the system. Due to the decreasing TC form, the TT→TC process was observed. Therefore, the rate constant ($k_{\text{TT} \rightarrow \text{TC, thermal}}$) of the TT→TC process was detected during thermal relaxation in the room temperature UV/Vis experiments (Table 4.12). Nevertheless, $k_{\text{TC} \rightarrow \text{CF, thermal}}$ of **N5** is far larger than $k_{\text{TT} \rightarrow \text{TC, thermal}}$ of **N5**, because ΔG_5 is larger than ΔG_3 .

As for the two states system **N1**, in the period of thermal relaxation, the low energy barrier (ΔG_6) between TT form and transition state 3 make it possible for process TT→TC at both 293 K and 238 K. In addition, as mentioned in Chapter 4.5.2, the *ortho*-chlorine group of aryl is a hindrance to the re-formation of CC form (Figure 5.13).^[65] So the energy barrier (ΔG_2) between TC form and transition state 2 is higher than that of three states system **N5** (ΔG_1). That is why the rate constant of process TC→CF (k_1) of **N5** is larger than that of **N1** at 293 K, and k_8 of **N5** is also larger than k_5 of **N1** at 238 K. Meanwhile, it was revealed that the difference between ΔG_4 and ΔG_6 is not as much as the difference between ΔG_5 and ΔG_3 , which can explain why the ratio of k_1/k_2 of **N5** is much bigger than that of **N1**. Correspondingly, under UV irradiation, the rate constant of process CF→TC (k_3) of **N5** is larger than that of **N1** due to the smaller ΔG_1 compared with ΔG_2 .

5.5 Discussion

Furthermore, the rate constant of process $\text{TC} \rightarrow \text{TT}$ (k_4) of **N5** is larger than that of **N1**, because ΔG_3 is smaller than ΔG_4 .

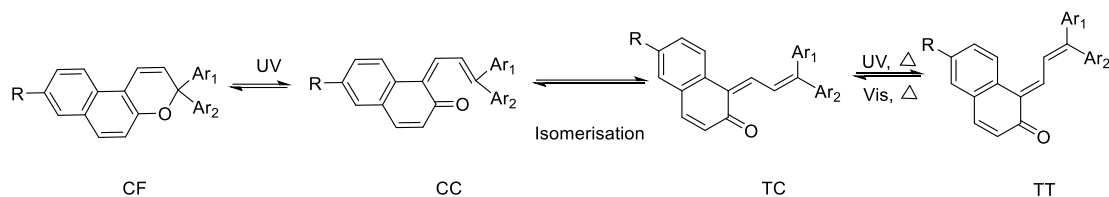


Figure 5.13 Photochromic equilibrium for naphthopyran.

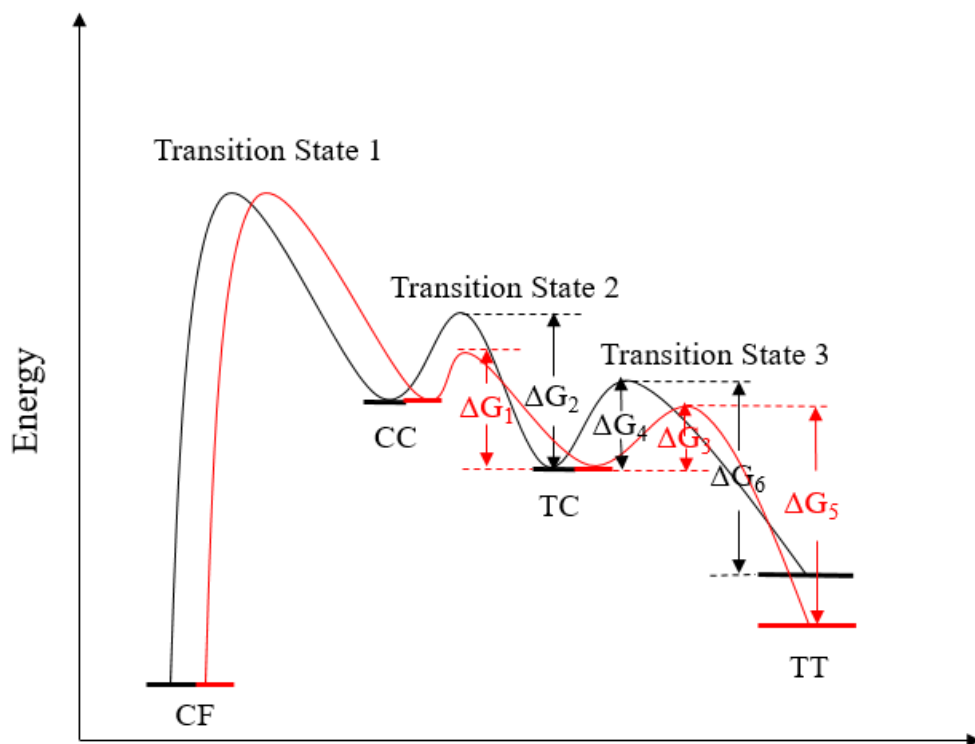


Figure 5.14 The proposed energy diagram of two states system (black line) and three states system (red line) (the energy barriers are not accurate, further need to be modified by the calculation).

5.5.2 The Effect of 6-Substituent on Photochromic Properties of Naphthopyran during the Visible Light Irradiation in Low Temperature *in-situ* NMR Measurements

During low temperature *in-situ* NMR measurements, naphthopyran **N7** had a different photochromic behavior during visible light irradiation, compared with the unsubstituted naphthopyran **N6** (Figures 5.9-b and 5.10). Under irradiation with 420 nm light, the TT form of **N7** was not converted into the CF form totally in the presence of the process CF→TC, although TT→TC was observed. The increasing TC form prevent the complete conversion of the TT form because of the process TC→TT (Figure 5.10 and Table 5.10). On the contrary, the process TC→CF was detected in the system of **N6** under 420 nm irradiation. In order to explain this phenomenon, the UV spectra of **N6** and **N7** should be considered (Figure 5.15). There was no absorption detected in the area ≥ 370 nm for the closed form of **N6**. However, an absorption band between 370 and 450 nm was detected in the UV spectrum of **N7**. Accordingly, the 420 nm light can induce the ring-open reaction for **N7**, but not for **N6**. As for the bathochromic shift in the spectrum of **N7**, it is resulted from the presence of the 6-acrylic ester group, which extends π conjugation within the whole structure.

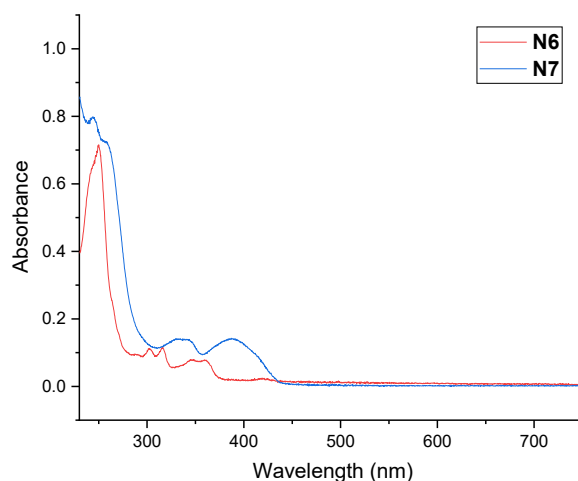


Figure 5.15 Absorption spectra of **N6** and **N7** before UV irradiation in acetonitrile (1.5×10^{-5} M) at 293 K.

6. Summary and Outlook

In this work, the synthesis of remote selective C-H functionalization of naphthopyrans was achieved. The photochromic properties of different substituted 3*H*-naphthopyrans were investigated by UV/Vis spectroscopy and *in-situ* NMR measurements. Different transformations between isomers, including allenyl-naphthol (AP) formation, were discussed in detail.

6.1 The Synthesis of Naphthopyrans by Selective C-H Functionalization

In this part, two methods were applied for the *m*-C-H functionalization of naphthopyrans. The first method was directed selective C-H functionalization of naphthopyrans, and a nitrile containing directing group was used. For this method, two different routes were investigated: 1) selective C-H functionalization of naphthalene **13** was achieved firstly and two different products, *m*-selective product **14** and *m'*-selective product **15**, were obtained with a ratio of **14:15** = 7:1 (Figure 6.1). However, the desired naphthopyran **21** was not detected during the naphthopyran synthesis due to the unstable intermediate **85**, while byproduct **22** was obtained in 40% yield. Therefore, route 2 was explored as follows: 2) the naphthopyran with the directing group, **N6**, was synthesized firstly. Then directed C-H functionalization of **N6** was achieved successfully. Interestingly, only the 6-selective product **N7** was observed (Figure 6.2).

The second method was nondirected C-H functionalization of naphthopyrans. The route was exploring nondirected C-H functionalization of naphthalene **3** firstly, before trying to synthesize the corresponding naphthopyran. Unfortunately, 5 different products were detected, which cannot be distinguished and separated from each other. Although this method works well for benzene compounds under the control of steric or electronic effects,^[111] there are too many active positions in a naphthalene structure. Thus, new methods concerning nondirected C-H functionalization of naphthalenes should be developed in the future.

6.1 The Synthesis of Selective C-H Functionalization of Naphthopyrans

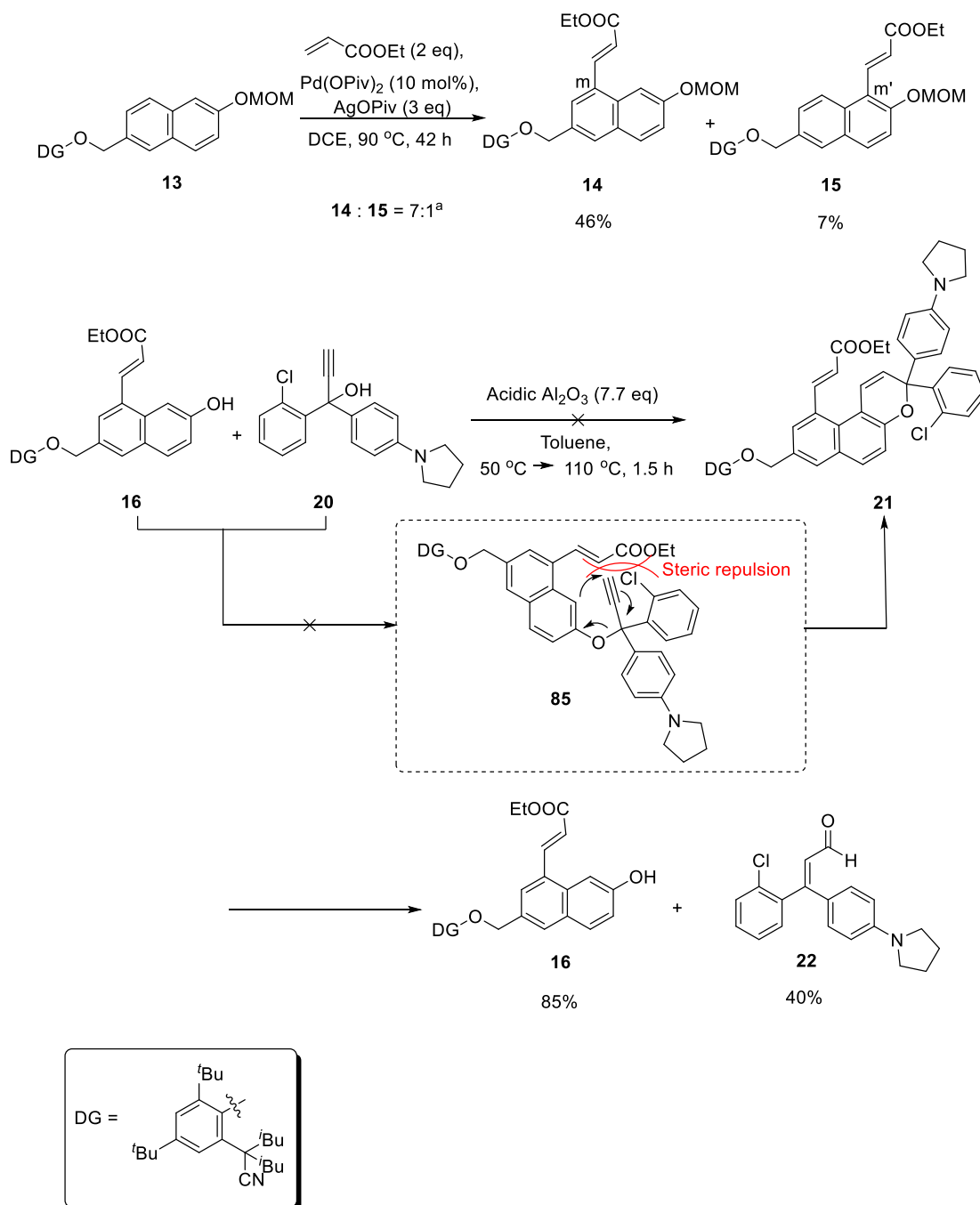


Figure 6.1 The route 1 of directed *m*-C-H functionalization of naphthopyrans.

6 Summary and Outlook

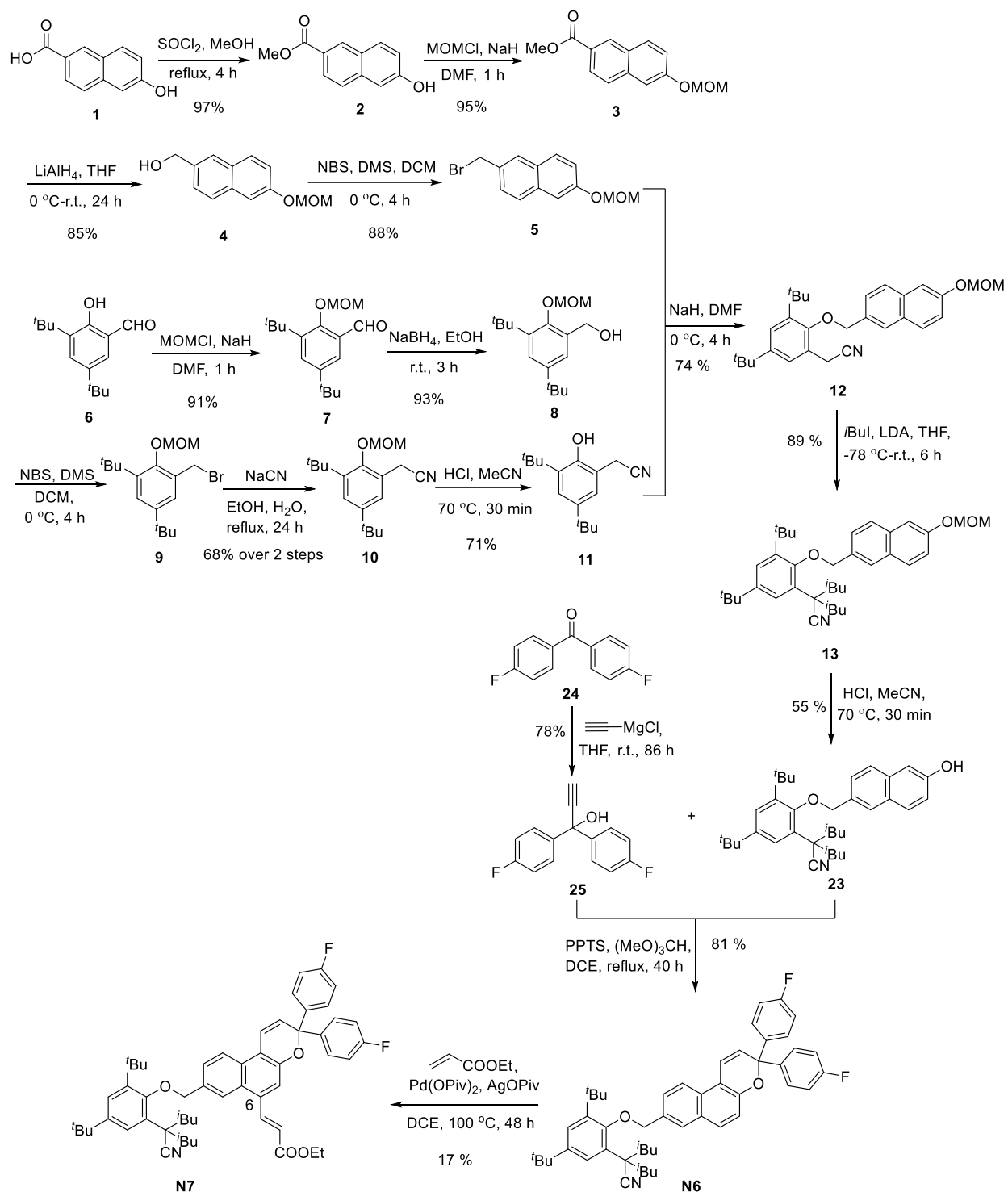


Figure 6.2 The route 2 of directed *m*-C-H functionalization of naphthopyrans.

6.2 The Photochromic Properties of 3H-Naphthopyrans

In this work, the photochromic behavior of 10 different 3H-naphthopyrans were explored with room temperature UV/Vis spectroscopy and low temperature *in-situ* NMR experiments (Figure 6.3), wherein the effects of substituents at 4 different positions on photochromic properties were discussed: 8-substituent, 6-substituent, 2-substituent and the different aryl-substituents attached to C3-atom.

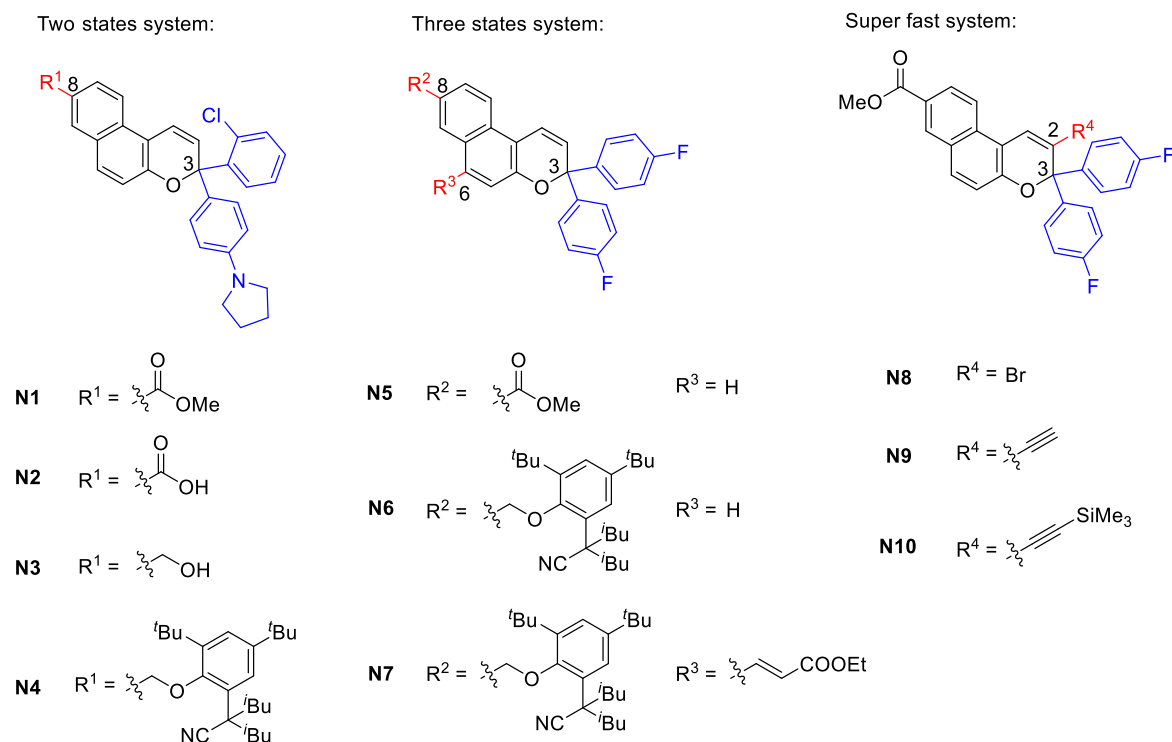


Figure 6.3 The structures of naphthopyrans investigated in this work.

For the effects of 8-substituents on photochromic properties of naphthopyrans, four different substituents, ester, carboxylic acid, hydroxymethyl and ether methyl were investigated in this work. In both two states system and three states system, naphthopyrans with an 8-ester substituent always had a bathochromic shift in the UV/Vis absorption spectra. During thermal relaxation, the thermal back speed (both of the processes TC→CF and TT→TC) of naphthopyrans with 8-ester substituent were faster (Figure 6.4). However, in the procedure of UV irradiation, the ring-open speed (CF→TC) of the 8-ester naphthopyran was faster among three states system with 3-C₆H₄F substituent (Table 6.1) while slower among two states system (Table 6.2). As for the 8-ether methyl and 8-hydroxymethyl substituents, they made similar impact on the photochromic behavior of

naphthopyrans, and both of them had longer half-life open forms in comparison to the 8-ester naphthopyran. Moreover, the photochromic behavior of the naphthopyran with 8-carboxylic acid substituent (**N2**) was influenced by the formation of acid dimers, which was solvent dependent.

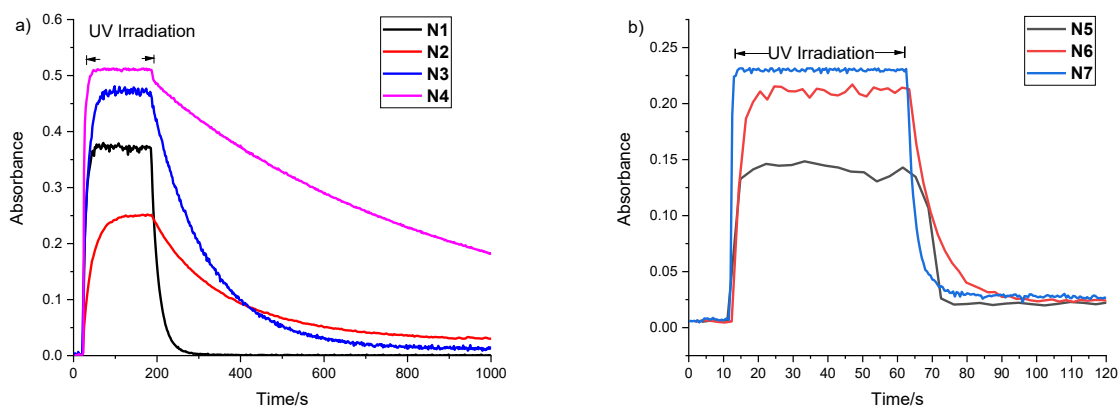
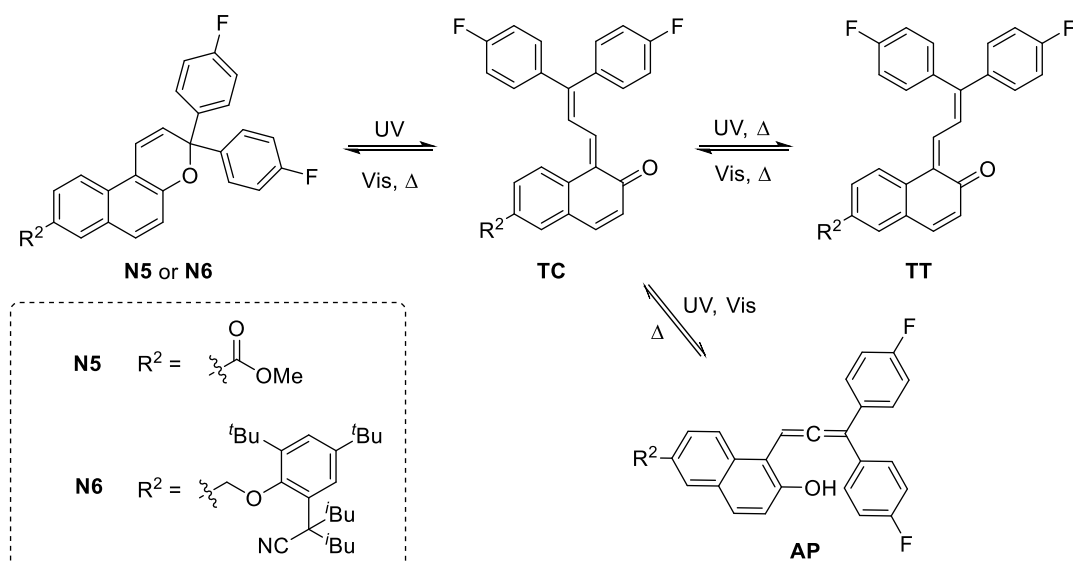
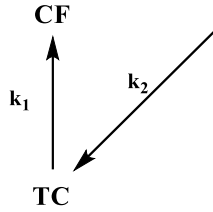
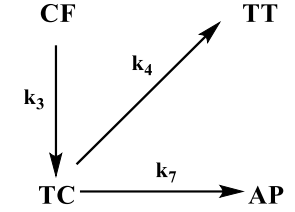
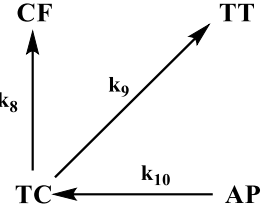


Figure 6.4 Comparison of time resolved absorbance at λ_{\max} of a) naphthopyran **N1**, **N2**, **N3** and **N4** and b) naphthopyran **N5**, **N6** and **N7** (UV light: 340 nm, 12 mW/cm² for **N1**, **N2** and **N3**; 365 nm, 110 mW/cm² for **N4**, **N5**, **N6** and **N7**. 1.5×10^{-5} M in acetonitrile at 293 K).

Table 6.1 Comparison of photochromic properties of naphthopyrans **N5** and **N6**.

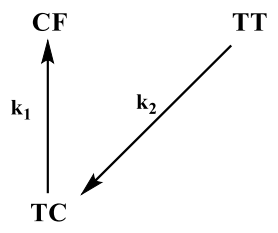
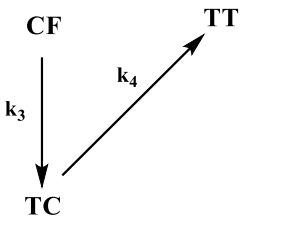
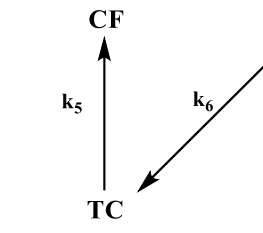


6.2 The Photochromic Properties of 3*H*-Naphthopyrans

UV/Vis spectroscopy 293 K	Irradiated with 365 nm light (238 K <i>in-situ</i> NMR)		In the dark (238 K <i>in-situ</i> NMR)			
					k_1^a	k_2^b
	k_3^c	k_4^c	k_7^c	k_8^c	k_{10}^c	
Trend	N5 > N6	N5 > N6	N5 > N6	N5 > N6	N5 < N6	N5 > N6

[a] In the dark, 1.5×10^{-5} M in acetonitrile, 293 K. [b] Irradiated with 420 nm light, 73 mW/cm², 1.5×10^{-5} M in acetonitrile, 293 K. [c] 1×10^{-2} M in CD₃CN at 238 K. UV light: 365 nm, 3.86 mW/cm².

Table 6.2 Comparison of photochromic properties of naphthopyrans **N1**, **N3** and **N4**.

In the dark (293 K UV/Vis spectroscopy)	Irradiation with 365 nm light (238 K <i>in-situ</i> NMR)		In the dark (238 K <i>in-situ</i> NMR)
			
	Trend		
λ_{\max}^a	N1 > N4 > N3		
k_1^a	N1 > N4 > N3		
k_2^a	N1 > N3 > N4		
k_3^b	N1 < N3 < N4		
k_4^b	N1 < N3 < N4		
k_5^b	N1 > N3		
k_6^b	N1 > N3		

[a] 1.5×10^{-5} M in acetonitrile, 293 K. [b] UV light: 365 nm, 0.45 mW/cm² for **N1** and **N3**, 3.86 mW/cm² for **N4**, 1×10^{-2} M in CD₃CN, 238 K.

The 6-acrylic ester substituent on naphthopyran **N7** was introduced by C-H functionalization. From the UV absorption spectra (Figure 6.5), the 6-acrylic ester induced a bathochromic shift. For the ring-open speed (CF \rightarrow TC) under UV irradiation and the ring closure speed (TC \rightarrow CF and TT \rightarrow TC) in the dark, the 6-acrylic ester brought an acceleration (Table 6.3). Particularly, regarding visible light irradiation, the ring opening reaction was observed for the naphthopyran with the 6-acrylic ester substituent (**N7**) under irradiation with 420 nm light, while ring closure reaction was found for **N6** with this wavelength, the naphthopyran without 6-substituent.

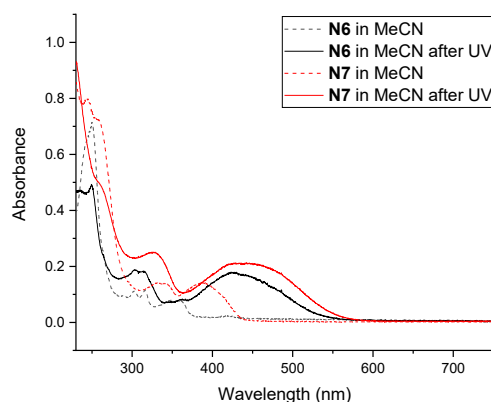


Figure 6.5 Comparison of UV absorption spectra of naphthopyrans **N6** and **N7** (UV light: 365 nm, 110 mW/cm². 1.5×10^{-5} M in acetonitrile at 293 K).

Table 6.3 Comparison of photochromic properties of naphthopyrans **N6** and **N7**.

	UV/Vis spectroscopy 293 K		Irradiated with 365 nm light (238 K <i>in-situ</i> NMR)		In the dark (238 K <i>in-situ</i> NMR)		
	CF	TT	CF	TT	CF		
	k_1	k_2	k_3	k_4	k_8	k_{10}	
	TC		TC	AP	TC	AP	
	k_1^a	k_2^b	k_3^c	k_4^c	k_7^c	k_8^c	k_{10}^c
Trend	N7 > N6	N7 > N6	N7 > N6	N7 = N6	N7 < N6	N7 > N6	N7 > N6

[a] In the dark, 1.5×10^{-5} M in acetonitrile, 293 K. [b] Irradiated with 420 nm light, 73 mW/cm² for **N6**, 505 nm light, 70 mW/cm² for **N7**, 1.5×10^{-5} M in acetonitrile, 293 K.

[c] 1×10^{-2} M in CD₃CN at 238 K. UV light: 365 nm, 3.86 mW/cm².

6.2 The Photochromic Properties of 3*H*-Naphthopyrans

Two different kinds of substituents were explored for the aryl substituents attached to the C3-atom, resulting in two different systems: two states system and three states system (Figure 6.3, blue part). On the one hand, in the UV absorption spectra, *para*-pyrrolidine of two states system (**N1**) brought a bathochromic shift for the ring-open forms (Table 6.4). During the thermal relaxation, the combination of *ortho*-chlorine and *para*-pyrrolidine substituent accelerated the speed of TT→TC (k_2) while decreased the speed of TC→CF (k_1). Thus, the difference between k_1 and k_2 of **N5** was far larger than that of **N1**, leading to two stage monoexponential decay for three states system (**N5-7**) while one biexponential decay for two states system (**N1-4**). At the same time, the speed of TT→TC of three states system was faster under irradiation with visible light, although it can thermal back to initial state after long enough time in the dark. On the other hand, in the low temperature *in-situ* NMR measurements, TT→TC was detected for two states system during thermal relaxation. By contrast, TC→TT was observed for **N5**, which was also different from room temperature UV/Vis experiments. In addition, the ratios between rates of thermal back reaction of two states system (**N1** and **N3**) are similar at different temperature (293 K UV/Vis experiments and 238 K *in-situ* NMR measurements), and the ratios between rates of visible light irradiation of two states system (**N4**) are similar at different temperature, too (Table 6.5).

Table 6.4 Photochromic properties of **N1** and **N5** in the procedure of thermal back reaction.^a

	λ_{\max} [nm] (Closed)	λ_{\max} [nm] (Open)	$t_{1/2}$ (s)	$t_{3/4}$ (s)	A_0	k_1 (10^{-3} s^{-1})	k_2 (10^{-3} s^{-1})
N1	261, 318	592	12	25	0.3807	90.9 ^b	47.1 ^b
N5	261, 338	429	1.6	3.4	0.164	634 ^c	0.68 ^c

[a] 1.5×10^{-5} M in acetonitrile, 293 K. λ_{\max} , $t_{1/2}$, $t_{3/4}$ and A_0 are obtained from experimental data. [b] k_1 and k_2 are the fitting parameters from **Equation 1** and data from Figure 4.5-a and Table 4.2 (Chapter 4). [c] k_1 and k_2 are the fitting parameters from **Equation 2**. k_1 ($k_{TC \rightarrow CF, \text{thermal}}$) from Figure 4.13 and Table 4.7, k_2 ($k_{TT \rightarrow TC, \text{thermal}}$) from Figure 4.14 and Table 4.8 (Chapter 4).

Table 6.5 Comparison of ratios between rates of naphthopyrans **N1**, **N3** and **N4**.

	In the dark (293 K UV/Vis spectroscopy)	In the dark (238 K <i>in-situ</i> NMR)	Irradiation with 565 nm light (293 K UV/Vis spectroscopy)	Irradiation with 565 nm light (238 K <i>in-situ</i> NMR)
	Ratio			
	N1	N3	N4	
k_1 / k_2^a	2	1	-	
k_5 / k_6^b	2.5	1.5	-	
$k_{TC \rightarrow CF, \text{Vis, 293K}} / k_{TT \rightarrow TC, \text{Vis, 293K}}^c$	-	-	1	
$k_{TC \rightarrow CF, \text{Vis, 238K}} / k_{TT \rightarrow TC, \text{Vis, 238K}}^d$	-	-	1.2	

[a] 1.5×10^{-5} M in acetonitrile, 293 K. [b] 1×10^{-2} M in CD_3CN at 238 K. [c] 1.5×10^{-5} M in acetonitrile, 293 K, 565 nm light, 84 mW/cm². [d] 1×10^{-2} M in CD_3CN at 238 K, 565 nm light, 3.2 mW/cm².

At last, 2-position substituents on **N8**, **N9** and **N10** destabilized the open forms of naphthopyrans. Therefore, the thermal relaxation is too fast to be observed. Even in the low temperature *in-situ* NMR measurements, the presence of switching was still not detected.

In addition, the photochromic behavior of naphthopyrans was influenced by solvents. When TCE was employed as the solvent, a blue shift was found in the UV absorption spectra and thermal back speeds were reduced, resulting from the interaction of open forms and intermediates and tetrachloroethylene molecule. However, the thermal back speed of **N2** was faster in TCE, because of the formation of acid dimers, which is solvent dependent.^[133] Furthermore, a small bathochromic shift was observed in the UV absorption spectrum of **N3** in DCM and the rate of thermal relaxation was accelerated, compared with that in acetonitrile.

6.3 Outlook

Remote 6-selective C-H functionalization of naphthopyrans was achieved. Long term this method and related methods can be used for introducing different 6-position substituents in naphthopyrans. Besides, considering the yield is not so good and more than 60% of starting material was left, further improvement is still possible.

On the other hand, with different 3*H*-naphthopyrans and their photochromic properties in hand, these naphthopyrans can be applied for the development of photoswitchable monolayers on a Si(111) surface according to the research experience of the Rück-Braun group.^[7,8,137] **N1**, **N4**, **N5**, **N6** and **N7** are potential compounds and candidates for monolayer designs. If we need two states system, **N1** and **N4** are fast and slow thermal relaxation naphthopyrans, respectively. If three states system are preferable, **N5** and **N6** are fast and slow thermal relaxation naphthopyrans, respectively. If different visible light control is expected, **N7** is a favourable choice (Figure 6.6).

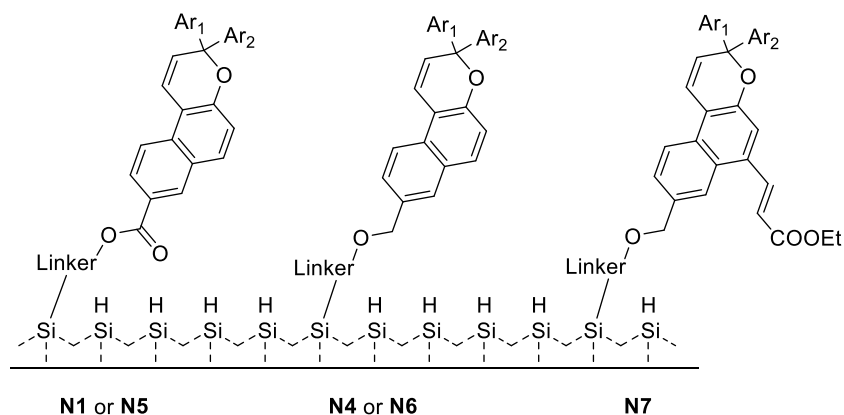


Figure 6.6 Future application of photoswitchable monolayers on a Si (111) surface.

7. Experimental Section

7.1 Synthesis

7.1.1 General Information

All starting materials and reagents were purchased from Sigma-Aldrich, Alfa Aesar, Acros, TCI and abcr of the highest available purity and were used without further purification. Solvents were dried prior to use according to standard procedures.^[1] The reactions were monitored by analytical thin-layer chromatography (TLC, silica gel, Merck 60 F₂₅₄ plates) and visualized by UV light, potassium permanganate or Seebach reagent (phosphomolybdic acid/Ce(IV)(SO₄)₂) stain.

Chromatography

Flash-column chromatography was performed using silica gel (MP silica, 32-63 μ m, 60 Å, MP Biomedicals Germany GmbH).

Melting points

Melting points were measured with a Büchi M-560 melting point apparatus using open capillary tubes and remain uncorrected.

NMR spectroscopy

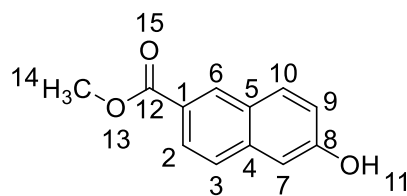
¹H, ¹³C NMR spectra were recorded on a Bruker Avance II 400 MHz spectrometer or a Bruker Avance III 500 MHz spectrometer at room temperature, unless otherwise stated. Chemical shifts were reported in parts per million (ppm) and were referenced to the residual solvent signals as the internal standard (CDCl₃: δ = 7.26 ppm for ¹H NMR and δ = 77.16 ppm for ¹³C NMR; DMSO-*d*₆: δ = 2.50 ppm for ¹H NMR and δ = 39.52 ppm for ¹³C NMR; Acetonitrile-*d*₃: δ = 1.94 ppm for ¹H NMR and δ = 118.26 ppm for ¹³C NMR). Data were reported as follows: chemical shift, multiplicity (s = singlet, d = doublet, t = triplet, q = quartet, m = multiplet), coupling constants (Hz), and integration.

IR spectroscopy

Infrared spectra were recorded as ATR (attenuated total reflectance) on a Nicolet FTIR 750 spectrometer and are reported as wavenumbers in cm^{-1} .

Mass spectrometry

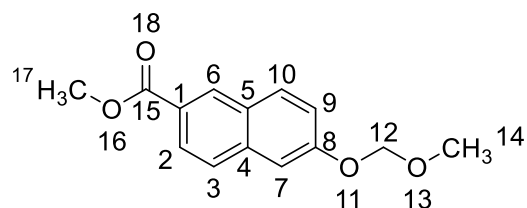
High-resolution mass spectra were measured with a Finnigan MAT 95S or Thermo Fisher Scientific LTQ Orbitrap XL apparatus.

7.1.2 Procedure**Methyl-6-hydroxy-2-naphtoate (2)**^[124]

To a solution of 6-hydroxy-2-naphtoic-acid **1** (1.935 g, 10.0 mmol, 1.00 eq.) in MeOH (10 mL), SOCl_2 (1.85 mL, 25.0 mmol, 2.50 eq.) was added dropwise. The reaction was refluxed for 3 h at 75 °C. MeOH was removed and the reaction

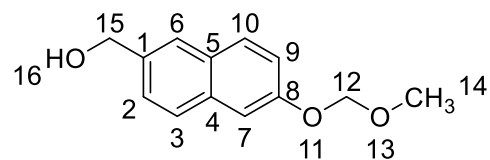
mixture was diluted in EA (50 mL). It was washed by saturated NaHCO_3 (3×25 mL) and dried over NaSO_4 . The solvent was removed under reduced pressure and purification by column chromatography (pentane/EA = 5:1) to give product **2** (1.965 g, 9.7 mmol, 97%) as a white solid.

R_f = 0.72 (pentane/ EA, 1:1); **Mp**: 171.3-172.6 °C; **¹H-NMR** (400 MHz, $\text{DMSO}-d_6$): δ 10.18 (s, 1H, H-11(OH)), 8.49 (s, 1H, H-6), 7.97 (d, $^3J = 8.8$ Hz, 1H, H-10), 7.86 (dd, $^3J = 8.6$ Hz, $^4J = 1.7$ Hz, 1H, H-2), 7.77 (d, $^3J = 8.6$ Hz, 1H, H-3), 7.19-7.15 (m, 2H, H-9, H-7), 3.88 (s, 3H, H-14); **¹³C-NMR** (126 MHz, $\text{DMSO}-d_6$): δ 166.5 (C-12), 157.8 (C-8), 137.2 (C-4), 131.3 (C-10), 130.6 (C-6), 126.7 (C-5), 126.5 (C-3), 125.2 (C-2), 123.8 (C-1), 119.8 (C-9), 108.8 (C-7), 52.1 (C-14); **IR** (ATR): $\tilde{\nu}$ (cm^{-1}) = 3389, 2953, 1679, 1433, 1203, 1098, 917, 812, 756; **HRMS (APCI)** calculated for $\text{C}_{12}\text{H}_{11}\text{O}_3^+$ $[\text{M}+\text{H}]^+$, m/z : 203.0703; found: 203.0708.

Methyl-6-(methoxymethoxy)-2-naphthoate (3)

One clean 2-neck round bottom flask was dried carefully under a nitrogen atmosphere. Dry DMF (10 mL) and NaH (60% in mineral oil, 260 mg, 6.5 mmol, 1.30 eq.) was added. Then ester **2** (1.019 g, 5.0 mmol, 1.00 eq.) was added portion wise at -5 °C. After the bubbling had subsided, MOMCl (0.8 mL, 10.0 mmol, 2.00 eq.) was added dropwise to the reaction mixture. After stirring for 1 h at room temperature, the reaction was completed as checked by TLC. The mixture was cooled again to 0 °C and distilled water was added. The mixture was extracted with Ethyl acetate (3 × 25 mL) and the organic layers were combined and washed with distilled water (3 × 15 mL) and brine (15 mL), and then dried over Na₂SO₄. The solvent was removed under reduced pressure and purification by column chromatography (pentane/EA = 15:1) yielded product **3** (1.256 g, 4.5 mmol, 90%) as a white solid.

R_f = 0.72 (pentane/ ethyl acetate, 2:1); **Mp**: 78.3-79.2 °C; **¹H-NMR** (400 MHz, CDCl₃): δ 8.54 (s, 1H, H-6), 8.02 (dd, ³J = 8.8 Hz, ⁴J = 1.7 Hz, 1H, H-2), 7.87 (d, ³J = 9.0 Hz, 1H, H-10), 7.76 (d, ³J = 8.5 Hz, 1H, H-3), 7.41 (d, ⁴J = 2.3 Hz, 1H, H-7), 7.27 (dd, ³J = 8.8 Hz, ⁴J = 2.4 Hz, 1H, H-9), 5.32 (s, 2H, H-12), 3.97 (s, 3H, H-17), 3.53 (s, 3H, H-14); **¹³C-NMR** (126 MHz, CDCl₃): δ 167.5 (C-15), 157.1 (C-8), 137.1 (C-4), 131.1 (C-10), 131.0 (C-6), 128.5 (C-5), 127.3 (C-3), 126.0 (C-2), 125.8 (C-1), 119.9 (C-9), 109.8 (C-7), 94.6 (C-12), 56.4 (C-14), 52.2 (C-17); **IR** (ATR): $\tilde{\nu}$ (cm⁻¹) = 3003, 2953, 2907, 2850, 2828, 1708, 1626, 1600, 1478, 1428, 1416, 1383, 1339, 1286, 1248, 1198, 1148, 1125, 1097, 1076, 997, 911, 859, 841, 825, 812, 782, 766, 751, 723, 651, 621, 548, 527, 476; **HRMS (APCI)** calculated for C₁₄H₁₅O₄⁺ [M+H]⁺, m/z: 247.0965; found: 247.0962.

(6-(Methoxymethoxy)naphthalene-2-yl)methanol (4)^[125]

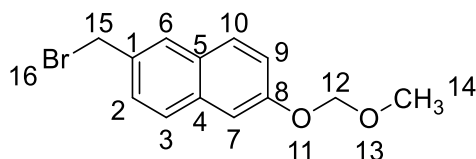
One clean 2-neck round bottom flask was dried carefully under a nitrogen atmosphere. Compound **3** (492 mg, 2.0 mmol, 1.00 eq.) and 10 mL dry THF were added. The mixture was cooled down to 0°C. To the cooled solution, LiAlH₄ (140 mg, 3.5 mmol, 1.75 eq.) was added portionwise. The reaction was stirred for 24 h until complete consumption of the starting

7.1 Synthesis

material and quenched with cold water slowly. Then the mixture was filtered over Celite® and the filtrate was extracted with EA (3 × 15 mL) and washed with brine (15 mL). The organic layer was dried over Na₂SO₄. The solvent was removed under reduced pressure and purification by column chromatography (pentane/EA = 8:1) gave product **4** (370 mg, 1.7 mmol, 85%) as a white-yellow solid.

R_f = 0.31 (pentane/ ethyl acetate, 2:1); **Mp**: 55.3-56.1 °C; **¹H-NMR** (400 MHz, CDCl₃): δ 7.76-7.73 (m, 3H, H-10, H-3, H-6), 7.44 (dd, ³J = 8.4 Hz, ⁴J = 1.5 Hz, 1H, H-2), 7.39 (d, ⁴J = 2.5 Hz, 1H, H-7), 7.22 (dd, ³J = 8.8 Hz, ⁴J = 2.5 Hz, 1H, H-9), 5.29 (s, 2H, H-12), 4.81 (s, 2H, H-15), 3.53 (s, 3H, H-14); **¹³C-NMR** (126 MHz, CDCl₃): δ 155.28 (C-8), 136.64 (C-1), 134.10 (C-4), 129.53 (C-10), 129.49 (C-5), 127.63 (C-3), 125.96 (C-2), 125.55 (C-6), 119.38 (C-9), 110.06 (C-7), 94.69 (C-12), 65.63 (C-15), 56.24 (C-14); **IR** (ATR): $\tilde{\nu}$ (cm⁻¹) = 3290, 2993, 2909, 2833, 1630, 1604, 1480, 1150, 1025, 991, 862, 755; **HRMS (ESI)** calculated for C₁₃H₁₃O₂⁺ [M-OH]⁺, m/z: 201.0910; found: 201.0911.

2-Bromomethyl-6-(methoxymethoxy)naphthalene (**5**)



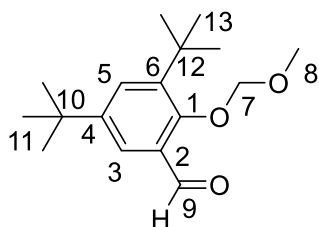
One clean 2-neck round bottom flask was dried carefully under a nitrogen atmosphere. Dimethyl sulfide (DMS, 215 μL, 2.93 mmol, 1.80 eq.) was added to a suspension of N-bromosuccinimide (NBS, 440 mg, 2.45 mmol, 1.5 eq.)

in dry DCM (2.5 mL) at 0 °C and stirred for 10 min. The reaction mixture was cooled to -20 °C and alcohol **4** (355 mg, 1.63 mmol, 1 eq.) in dry DCM (2.5 mL) was added dropwise. The mixture was further stirred at 0 °C for additional 4 h. The reaction mixture was poured into cold water (10 mL) and extracted with DCM (3 × 15 mL). The organic layer was washed with brine (15 mL) and dried over Na₂SO₄. The solvent was removed under reduced pressure. Then crude product **5** was purified by quick filtration through a short plug of silica gel, product **5** (403 mg, 1.42 mmol, 88%) was isolated as a yellow solid.

R_f = 0.89 (pentane/ ethyl acetate, 4:1); **Mp**: 71.3-71.8 °C; **¹H-NMR** (400 MHz, CDCl₃): δ 7.76 (s, 1H, H-6), 7.75-7.72 (m, 2H, H-10, H-3), 7.47 (dd, ³J = 8.4 Hz, ⁴J = 2.0 Hz, 1H, H-2), 7.39 (d, ⁴J = 2.5 Hz, 1H, H-7), 7.23 (dd, ³J = 9 Hz, ⁴J = 2.5 Hz, 1H, H-9), 5.30 (s, 2H, H-12), 4.66 (s, 2H,

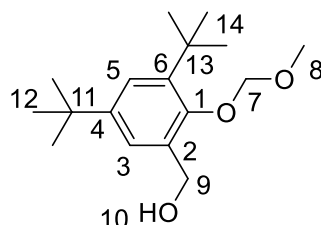
H-15), 3.53 (s, 3H, H-14); $^{13}\text{C-NMR}$ (126 MHz, CDCl_3): δ 155.81 (C-8), 134.35 (C-1), 133.39 (C-4), 129.63 (C-3), 129.27 (C-5), 128.04 (C-6), 127.84 (C-10), 127.47 (C-2), 119.68 (C-9), 110.07 (C-7), 94.65 (C-12), 56.26 (C-14), 34.47 (C-15); **IR** (ATR): $\tilde{\nu}$ (cm^{-1}) = 3321, 2924, 2850, 2828, 1993, 1729, 1627, 1602, 1502, 1476, 1439, 1379, 1342, 1297, 1260, 1209, 1147, 1121, 1076, 985, 937, 921, 901, 861, 823, 755, 687, 668, 588; **HRMS** (APCI) calculated for $\text{C}_{13}\text{H}_{13}\text{O}_2^+ [\text{M-Br}]^+$, m/z : 201.0910; found: 201.0912.

3,5-Di-*tert*-butyl-2-(methoxymethoxy)benzaldehyde (**7**)^[84]



One clean 2-neck round bottom flask was dried carefully under a nitrogen atmosphere. Dry DMF (7 mL) and NaH (60% in mineral oil, 0.33 g, 13.0 mmol, 1.30 eq.) was added. Then aldehyde **6** (2.35 g, 10.0 mmol, 1.00 eq.) were added portionwise at $-5\text{ }^\circ\text{C}$. After the bubbling had subsided, MOMCl (1.60 mL, 20.0 mmol, 2.00 eq.) was added dropwise to the reaction mixture. After stirring for 1 h at room temperature, the reaction was completed as checked by TLC. The mixture was cooled to $0\text{ }^\circ\text{C}$ again and distilled water was added. Then the mixture was extracted with ethyl acetate ($3 \times 25\text{ mL}$) and the organic layers was combined and washed with distilled water ($3 \times 15\text{ mL}$) and brine (15 mL), and then dried over Na_2SO_4 . The solvent was removed under reduced pressure and purification by column chromatography (pentane/EA = 100:1) yielded product **7** (2.54 g, 9.14 mmol, 91%) as colorless oil.

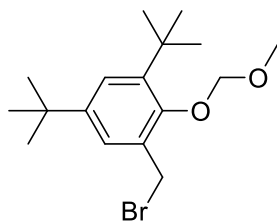
R_f = 0.91 (pentane/ ethyl acetate, 5:1); $^1\text{H-NMR}$ (400 MHz, CDCl_3): δ 10.22 (s, 1H, H-9), 7.72 (d, 4J = 2.6 Hz, 1H, H-3), 7.64 (d, 4J = 2.6 Hz, 1H, H-5), 5.02 (s, 2H, H-7), 3.63 (s, 3H, H-8), 1.46 (s, 9H, H-13), 1.32 (s, 9H, H-11); $^{13}\text{C-NMR}$ (126 MHz, CDCl_3): δ 191.7 (C-9), 158.0 (C-1), 146.7 (C-4), 142.9 (C-6), 130.6 (C-2), 130.2 (C-3), 123.7 (C-5), 102.3 (C-7), 57.6 (C-8), 35.2 (C-12), 34.7 (C-10), 31.3 (C-13), 30.9 (C-11); **IR** (ATR): $\tilde{\nu}$ (cm^{-1}) = 2956, 2906, 2870, 1685, 1597, 1576, 1477, 1438, 1385, 1362, 1298, 1266, 1235, 1159, 1116, 1072, 956, 929, 894, 816, 744, 675, 649; **HRMS** (APCI) calculated for $\text{C}_{17}\text{H}_{27}\text{O}_3^+ [\text{M}+\text{H}]^+$, m/z : 279.1955; found: 279.1959.

(3,5-Di-tert-butyl-2-(methoxymethoxy)phenyl)methanol (8**)**^[84]

To a cooled solution of aldehyde **7** (2.54 g, 9.14 mmol, 1.00 eq.) in EtOH (30 mL), NaBH₄ (0.69 g, 18.3 mmol, 2 eq.) was added portionwise at 0 °C. The reaction was warmed to room temperature and stirred for 3 h. Then EtOH was removed, and 30 mL of water was added at 0 °C to quench the reaction. The reaction mixture was extracted with

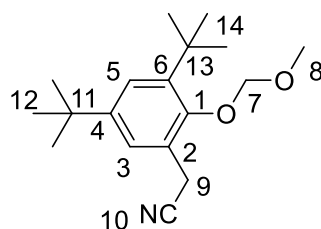
EA (30 mL) three times. The combined organic layers were washed with brine (25 mL) and dried over Na₂SO₄. The solvent was removed and purification by column chromatography (pentane/EA = 20:1) yielded product **8** (2.39 g, 8.51 mmol, 93%) as a colorless oil.

R_f = 0.52 (pentane/ ethyl acetate, 5:1); **Mp**: 39 °C; **¹H-NMR** (400 MHz, CDCl₃): δ 7.34 (d, ⁴J = 2.5 Hz, 1H, H-3), 7.28 (d, ⁴J = 2.5 Hz, 1H, H-5), 4.99 (s, 2H, H-7), 4.59 (s, 2H, H-9), 3.69 (s, 3H, H-8), 1.39 (s, 9H, H-14), 1.31 (s, 9H, H-12); **¹³C-NMR** (126 MHz, CDCl₃): δ 153.9 (C-1), 146.8 (C-4), 142.2 (C-6), 134.3 (C-2), 126.3 (C-3), 124.5 (C-5), 100.4 (C-7), 62.0 (C-9), 57.1 (C-8), 35.2 (C-13), 34.5 (C-11), 31.5 (C-12), 31.2 (C-14); **IR** (ATR): $\tilde{\nu}$ (cm⁻¹) = 3391, 2953, 2902, 2868, 1603, 1477, 1438, 1392, 1362, 1301, 1273, 1229, 1197, 1160, 1123, 1063, 1008, 965, 933, 881, 818, 652, 552, 495; **HRMS (APCI)** calculated for C₁₇H₂₇O₂⁺ [M-OH]⁺, m/z: 263.2006; found: 263.2009.

1-(Bromomethyl)-3,5-di-tert-butyl-2-(methoxymethoxy)benzene (9**)**^[84]

One clean 2-neck round bottom flask was dried carefully under a nitrogen atmosphere. Dimethyl sulfide (DMS, 1.12 mL, 15.3 mmol, 1.80 eq.) was added to a suspension of N-bromosuccinimide (NBS, 2.27 g, 12.8 mmol, 1.5 eq.) in dry DCM (6 mL) at 0 °C and stirred for 10 min. The reaction mixture was cooled to -20 °C and alcohol **8** (2.39 g, 8.51 mmol, 1 eq.) in

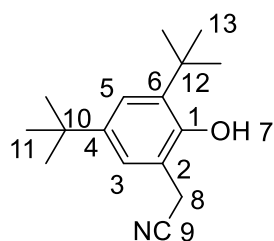
dry DCM (6 mL) was added dropwise. The mixture was further stirred at 0 °C for 4 h. The reaction mixture was poured into cold water (10 mL) and extracted with DCM (3 × 15 mL). The organic layer was washed with brine (10 mL) and dried over Na₂SO₄. The solvent was removed under reduced pressure. Then the crude product was purified by quick filtration through a short plug of silica gel to yield crude product **9** as a yellow solid.

2-(3,5-Di-*tert*-butyl-2-(methoxymethoxy)phenyl)acetonitrile (10)^[84]

Crude bromide **9** was then dissolved in EtOH (15 mL) and a solution of NaCN (1.03 g, 21.0 mmol, 3.0 eq.) in 3 mL of water was added to it. (CAUTION: NaCN is an extremely toxic chemical and should be handled in a well maintained fume hood. The operator should have appropriate protection at all times.) The reaction was refluxed

overnight. The solvent was removed under reduced pressure and 80 mL of EA was added. The organic layer was washed with water (5×40 mL), brine (40 mL) and dried over Na₂SO₄. The solvent was removed under reduced pressure and purification by column chromatography (pentane/EA = 100:1) yielded product **10** (1.68 g, 5.80 mmol, 68% over 2 steps) as an orange crystalline solid.

R_f = 0.44 (pentane/ ethyl acetate, 20:1); **Mp**: 48 °C; **¹H-NMR** (500 MHz, CDCl₃): δ 7.34 (d, ⁴J = 2.3 Hz, 1H, H-3), 7.30 (d, ⁴J = 2.3 Hz, 1H, H-5), 4.96 (s, 2H, H-7), 3.93 (s, 2H, H-9), 3.64 (s, 3H, H-8), 1.39 (s, 9H, H-14), 1.31 (s, 9H, H-12); **¹³C-NMR** (126 MHz, CDCl₃): δ 153.2 (C-1), 147.1 (C-4), 142.8 (C-6), 125.0 (C-5), 124.6 (C-2), 123.8 (C-3), 118.9 (C-10), 101.0 (C-7), 57.2 (C-8), 35.3 (C-13), 34.6 (C-11), 31.4 (C-12), 31.2 (C-14), 20.3 (C-9); **IR** (ATR): $\tilde{\nu}$ (cm⁻¹) = 2961, 2951, 2906, 2873, 2828, 2246 (CN), 1785, 1602, 1476, 1460, 1441, 1411, 1402, 1393, 1361, 1315, 1273, 1232, 1197, 1159, 1120, 1073, 945, 931, 898, 892, 878, 819, 794, 776, 725, 666, 652, 623, 616, 570; **HRMS (APCI)** calculated for C₁₈H₂₈NO₂⁺ [M+H]⁺, m/z: 290.2115; found: 290.2111.

2-(3,5-Di-*tert*-butyl-2-hydroxyphenyl)acetonitrile (11)^[84]

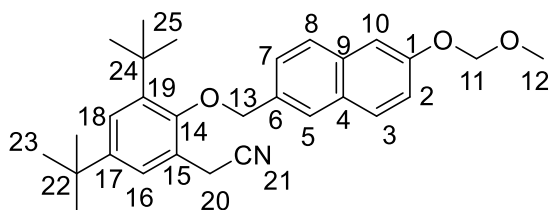
MOM-protected phenol **10** (1.68 g, 5.80 mmol, 1 eq.) was taken up in MeCN (150 mL). Aqueous HCl (2 M, 60 mL, 20 eq.) was added to the flask and the reaction mixture was warmed to 70 °C for 30 min. The solvent was removed under reduced pressure and water (25 mL) was added. The mixture was then extracted with DCM (3×25 mL). The organic layer was

washed with brine (15 mL) and dried over Na₂SO₄. The solvent was removed under reduced pressure and purification by column chromatography (pentane/EA = 40:1) yielded fairly pure

phenol **11**. The product was further purified by re-crystallization from hot pentane/cyclohexane yielded pure phenol **11** (1.01 g, 4.10 mmol, 71%) as white-yellow crystals.

R_f = 0.35 (pentane/ ethyl acetate, 10:1); **Mp**: 110 °C; **¹H-NMR** (500 MHz, CDCl₃): δ 7.27 (d, 4J = 2.4 Hz, 1H, H-3), 7.21 (d, 4J = 2.4 Hz, 1H, H-5), 4.97 (s, 1H, H-7), 3.71 (s, 2H, H-8), 1.45 (s, 9H, H-13), 1.30 (s, 9H, H-11); **¹³C-NMR** (126 MHz, CDCl₃): δ 149.6 (C-1), 143.6 (C-4), 134.7 (C-6), 124.5 (C-3), 123.8 (C-2), 118.3 (C-9), 34.4 (C-10), 34.1 (C-12), 31.5 (C-11), 30.4 (C-13), 19.3 (C-8); **IR** (ATR): $\tilde{\nu}$ (cm⁻¹) = 3297, 2957, 2906, 2867, 2268 (CN), 1481, 1446, 1412, 1391, 1361, 1344, 1312, 1276, 1225, 1205, 1165, 1122, 925, 906, 892, 874, 824, 797, 762, 723, 675, 650, 566; **HRMS** (APCI) calculated for C₁₆H₂₄NO⁺ [M+H]⁺, m/z: 246.1852; found: 246.1858.

2-(3,5-Di-tert-butyl-2-((6-(methoxymethoxy)naphthalen-2-yl)methoxy)phenyl)acetonitrile (**12**)



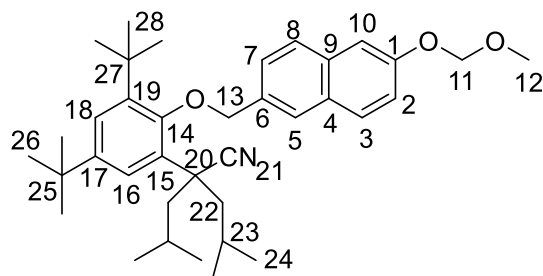
One clean 2-neck round bottom flask was dried carefully under a nitrogen atmosphere. To a cooled solution of phenol **11** (492 mg, 2.0 mmol) in DMF (2 mL), NaH (60% in mineral oil, 84 mg, 2.1 mmol, 1.05 eq.) was added portion wise at 0 °C. After the

bubbling had subsided, benzyl bromide **5** (562 mg, 2.0 mmol, 1.00 eq.) was added portion wise to the reaction mixture. After 4 h of stirring, 5 mL distilled water was added. The mixture was extracted with Ethyl acetate (3 × 15 mL) and the organic layers were washed with distilled water (3 × 10 mL) and brine (10 mL), and then dried over Na₂SO₄. The solvent was removed under reduced pressure and purification by column chromatography yielded the benzyl ether product **12** (660 mg, 1.48 mmol, 74%) as a white-yellow solid.

R_f = 0.60 (pentane/ ethyl acetate, 10:1); **Mp**: 124.5-125 °C; **¹H-NMR** (500 MHz, CDCl₃): δ 7.90 (s, 1H, H-5), 7.82 (d, 3J = 8.9 Hz, 1H, H-3), 7.81 (d, 3J = 8.4 Hz, 1H, H-8), 7.53 (dd, 3J = 8.4 Hz, 4J = 1.7 Hz, 1H, H-7), 7.44 (d, 4J = 2.5 Hz, 1H, H-10), 7.40 (d, 4J = 2.4 Hz, 1H, H-16), 7.35 (d, 4J = 2.4 Hz, 1H, H-18), 7.27 (dd, 3J = 8.9 Hz, 4J = 2.5 Hz, 1H, H-2), 5.32 (s, 2H, H-11), 5.02 (s, 2H, H-13), 3.77 (s, 2H, H-20), 3.55 (s, 3H, H-12), 1.46 (s, 9H, H-25), 1.35 (s, 9H, H-23); **¹³C-NMR** (126 MHz, CDCl₃): δ 155.5 (C-1), 153.8 (C-14), 147.2 (C-17), 143.0 (C-19), 134.2 (C-9), 132.8

(C-6), 129.7 (C-3), 129.5 (C-4), 127.7 (C-8), 125.4 (C-5), 125.3 (C-18), 125.2 (C-7), 125.1 (C-16), 123.9 (C-15), 119.6 (C-2), 118.8 (C-21), 110.1 (C-10), 94.7 (C-11), 75.8 (C-13), 56.3 (C-12), 35.8 (C-24), 34.8 (C-22), 31.6 (C-23), 31.5 (C-25), 19.4 (C-20); **IR** (ATR): $\tilde{\nu}$ (cm⁻¹) = 2962, 2899, 2360, 2252, 1631, 1603, 1477, 1441, 1375, 1225, 1151, 1078, 986, 923, 890, 854, 821; **HRMS** (APCI) calculated for C₂₉H₃₆NO₃⁺ [M+H]⁺, m/z: 446.2690; found: 446.2688.

2-(3,5-Di-tert-butyl-2-((6-(methoxymethoxy)naphthalen-2-yl)methoxy)phenyl)-2-isobutyl-4-methylpentanenitrile (13)



One clean 2-neck round bottom flask was dried carefully under a nitrogen atmosphere. THF (3 mL) and lithium diisopropylamide (LDA) (2.0 M in THF, 2.22 mmol, 1.50 eq.) were added. The mixture was cooled to -78 °C. Then a solution of benzyl ether **12** (660 mg, 1.48 mmol, 1.00 eq.) from the previous step

dissolved in THF (2 mL) was added dropwise at -78 °C. After stirring for 30 min, 1-iodo-2-methylpropane (0.25 mL, 2.22 mmol, 1.50 equiv.) was added dropwise to the reaction mixture and stirring for 30 min was continued at -78 °C. The reaction was then warmed up to room temperature and stirring was continued for 2 h. Then saturated aqueous NH₄Cl was added dropwise (3 mL) and THF was removed in vacuo. Afterwards, EA (15 mL) was added and the organic layer was washed with water (2 × 8 mL), followed by brine (8 mL), and then dried over Na₂SO₄. Subsequently, the solvent was removed, and the crude product was dried under high vacuum. The sequence was repeated again using the crude mixture. The product was further purified by column chromatography and yielded the α-cyano dialkylated product **13** (737 mg, 1.32 mmol, 89%) as a white-yellow solid.

R_f = 0.58 (pentane/ ethyl acetate, 20:1); **Mp**: 155.3-156.7 °C; **¹H-NMR** (500 MHz, CDCl₃): δ 7.88 (s, 1H, H-5), 7.81-7.77 (m, 2H, H-3, H-8), 7.50 (dd, ³J = 8.5 Hz, ⁴J = 1.3 Hz, 1H, H-7), 7.45 (d, ⁴J = 2.4 Hz, 1H, H-18), 7.42 (d, ⁴J = 2.3 Hz, 1H, H-10), 7.35 (d, ⁴J = 2.4 Hz, 1H, H-16), 7.25 (dd, ³J = 8.9 Hz, ⁴J = 2.3 Hz, 1H, H-2), 5.31 (s, 2H, H-11), 5.05 (s, 2H, H-13), 3.54 (s, 3H, H-12), 2.21-2.19 (m, 2H, H-22), 1.85-1.81 (m, 2H, H-22), 1.76-1.69 (m, 2H, H-23), 1.43 (s, 9H, H-28), 1.35 (s, 9H, H-26), 1.02 (d, ³J = 6.6 Hz, 6H, H-24), 0.75 (d, ³J = 6.6 Hz, 6H, H-24); **¹³C-NMR** (126 MHz, CDCl₃): δ 155.2 (C-1), 153.9 (C-14), 146.2 (C-17), 143.4 (C-19), 134.0 (C-9), 133.3 (C-6),

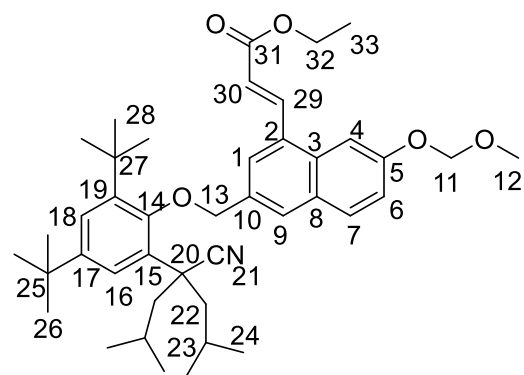
130.6 (C-15), 129.7 (C-3), 129.5 (C-4), 127.4 (C-8), 125.7 (C-16), 125.4 (C-21), 125.2 (C-18), 124.8 (C-7), 124.7 (C-5), 119.4 (C-2), 110.2 (C-10), 94.8 (C-11), 76.8 (C-13), 56.2 (C-12), 50.1 (C-22), 46.2 (C-20), 36.3 (C-27), 34.8 (C-25), 32.3 (C-28), 31.6 (C-26), 26.2 (C-23), 24.0 (C-24), 23.6 (C-24); **IR** (ATR): $\tilde{\nu}$ (cm⁻¹) = 2954, 2869, 2361, 2229, 1636, 1607, 1507, 1467, 1439, 1388, 1363, 1333, 1260, 1218, 1170, 1147, 1118, 1078, 1001, 923, 910, 884, 864, 810, 732, 648, 476, 459, 419; **HRMS** (APCI) calculated for C₃₇H₅₂NO₃⁺ [M+H]⁺, m/z: 558.3942; found: 558.3937.

Silver pivalate^[138]

Pivalic acid (2.527 g, 24.5 mmol, 0.98 eq) was added to 25 mL H₂O. Then NaOH (960 mg, 24 mmol, 0.96 eq) was added to this solution. After stirring for 15 min at room temperature, a solution of AgNO₃ (4.247 g, 25 mmol, 1.0 eq) in 40 mL H₂O was added dropwise. After stirring for 15 min at room temperature, the mixture was filtered and a white solid was collected, which was washed by H₂O (3 × 25 mL), MeOH (3 × 25 mL) and hexane (3 × 25 mL), respectively. After being dried under vacuum, silver pivalate was afforded as a white solid with a yield of 80 % (4.180 g, 20 mmol).

¹H-NMR (400 MHz, DMSO-*d*₆): δ 1.10 (s, 9H).

Ethyl (E)-3-(3-((2,4-di-tert-butyl-6-(4-cyano-2,6-dimethylheptan-4-yl)phenoxy)methyl)-7-(methoxymethoxy)naphthalen-1-yl)acrylate (14)



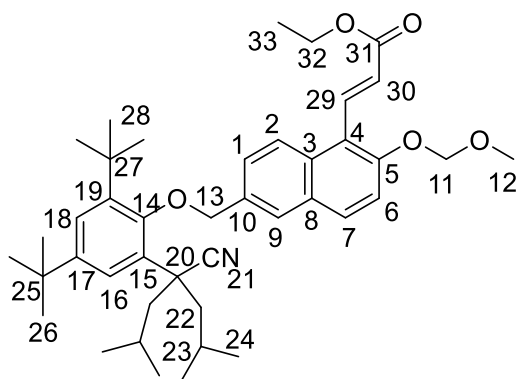
A 10 mL sealed tube (with a Teflon cap, ACS Glass incorporated) was flame dried and compound **13** (55.8 mg, 0.10 mmol, 1.0 equiv.), Pd(OPiv)₂ (3.4 mg, 0.010 mmol, 10 mol%), AgOPiv (62.7 mg, 0.30 mmol, 3.0 equiv.) and ethyl acrylate (22 μ L, 0.20 mmol, 2.0 equiv.) were added, before DCE (1.0 mL) was used to wash down the solids on the sides of the tube wall.

The tube was then capped and submerged into a preheated 90 °C oil bath. The oil bath was covered with aluminum foil to stabilize the oil bath temperature and to shield the reaction from light. After one day of stirring, the tube was shaken manually to dislodge the silver salt off the sides of the wall. The reaction was stirred for a total of

42 h and then cooled down to room temperature. The reaction mixture was filtered through a pad of Celite and washed with EA (3×3 mL). The solvent was removed under reduced pressure and purified by column chromatography (pentane/EA, 100/1) to yield product **14** (30 mg, 0.046 mmol, 46%) as a yellow oil.

R_f = 0.25 (pentane/ ethyl acetate, 20:1); $^1\text{H-NMR}$ (500 MHz, CDCl_3): δ 8.45 (d, 3J = 15.7 Hz, 1H, H-29), 7.96 (s, 1H, H-9), 7.85 (d, 3J = 9.0 Hz, 1H, H-7), 7.80 (s, 1H, H-1), 7.70 (d, 3J = 2.3 Hz, 1H, H-4), 7.41-7.39 (m, 2H, H-16, H-18), 7.33 (dd, 3J = 9.0 Hz, 4J = 2.3 Hz, 1H, H-6), 6.52 (d, 3J = 15.7 Hz, 1H, H-30), 5.34 (s, 2H, H-11), 5.07 (s, 2H, H-13), 4.32 (q, 3J = 7.1 Hz, 2H, H-32), 3.54 (s, 3H, H-12), 2.17-2.15 (m, 2H, H-22), 1.89-1.85 (m, 2H, H-22), 1.77-1.72 (m, 2H, H-23), 1.43 (s, 9H, H-28), 1.37 (t, 3J = 7.1 Hz, 3H, H-33), 1.35 (s, 9H, H-26), 1.03 (d, 3J = 6.6 Hz, 6H, H-24), 0.75 (d, 3J = 6.6 Hz, 6H, H-24); $^{13}\text{C-NMR}$ (126 MHz, CDCl_3): δ 167.0 (C-31), 155.9 (C-5), 153.7 (C-14), 146.3 (C-17), 143.3 (C-19), 141.8 (C-29), 132.8 (C-10), 132.1 (C-3), 131.2 (C-2), 130.8 (C-15), 130.5 (C-7), 129.9 (C-8), 127.3 (C-9), 125.6 (C-18), 125.3 (C-21), 124.8 (C-16), 123.9 (C-1), 121.0 (C-30), 119.2 (C-6), 106.9 (C-4), 94.8 (C-11), 76.5 (C-13), 60.7 (C-32), 56.3 (C-12), 50.5 (C-22), 45.5 (C-20), 36.3 (C-27), 34.7 (C-25), 32.2 (C-28), 31.5 (C-26), 26.1 (C-23), 24.0 (C-24), 23.6 (C-24), 14.5 (C-33); **IR** (ATR): $\tilde{\nu}$ (cm^{-1}) = 2955, 2870, 2232, 1712, 1627, 1606, 1505, 1466, 1439, 1393, 1364, 1308, 1255, 1219, 1173, 1153, 1123, 1080, 1049, 1005, 976, 924, 865, 826, 809, 734, 652, 588, 557, 518; **HRMS (APCI)** calculated for $\text{C}_{42}\text{H}_{58}\text{NO}_5^+$ $[\text{M}+\text{H}]^+$, m/z : 656.4310; found: 656.4301.

Ethyl (*E*)-3-(6-((2,4-di-tert-butyl-6-(4-cyano-2,6-dimethylheptan-4-yl)phenoxy)methyl)-2-(methoxymethoxy)naphthalen-1-yl)acrylate (15**)**



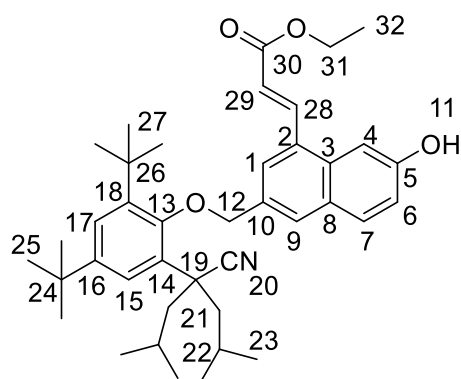
A 10 mL sealed tube (with a Teflon cap) was flame dried and compound **13** (55.8 mg, 0.10 mmol, 1.0 equiv.), $\text{Pd}(\text{OPiv})_2$ (3.4 mg, 0.010 mmol, 10 mol%), AgOPiv (62.7 mg, 0.30 mmol, 3.0 equiv.), ethyl acrylate (22 μL , 0.20 mmol, 2.0 equiv.) were added. DCE (1.0 mL) was used to wash down the solids on the sides of the tube wall. The tube was then capped and submerged into a preheated 90 $^\circ\text{C}$ oil bath. The oil bath

7.1 Synthesis

was covered with aluminum foil to stabilize the oil bath temperature and to shield the reaction from light. After one day of stirring, the tube was shaken manually to dislodge the silver salt off the sides of the wall. The reaction was stirred for a total of 42 h and then cooled down to room temperature. The reaction mixture was filtered through a pad of Celite and washed with EA (3 × 3 mL). The solvent was removed under reduced pressure and purified by column chromatography (pentane/EA, 100/1) to yield product **15** (5 mg, 0.007 mmol, 7%) as a yellow oil.

R_f = 0.30 (pentane/ ethyl acetate, 20:1); $^1\text{H-NMR}$ (500 MHz, CDCl_3): δ 8.43 (d, 3J = 15.8 Hz, 1H, H-29), 8.19 (s, 1H, H-9), 7.81 (d, 3J = 8.5 Hz, 1H, H-2), 7.59 (dd, 3J = 8.5 Hz, 4J = 1.3 Hz, 1H, H-1), 7.50-7.48 (m, 2H, H-6, H-7), 7.42-7.40 (m, 2H, H-16, H-18), 6.52 (d, 3J = 15.8 Hz, 1H, H-30), 5.31 (s, 2H, H-11), 5.09 (s, 2H, H-13), 4.29 (q, 3J = 7.1 Hz, 2H, H-32), 3.53 (s, 3H, H-12), 2.18-2.16 (m, 2H, H-22), 1.84-1.80 (m, 2H, H-22), 1.75-1.67 (m, 2H, H-23), 1.44 (s, 9H, H-28), 1.36-1.33 (m, 12H, H-26, H-33), 1.01 (d, 3J = 6.6 Hz, 6H, H-24), 0.74 (d, 3J = 6.6 Hz, 6H, H-24); $^{13}\text{C-NMR}$ (126 MHz, CDCl_3): δ 166.7 (C-31), 154.6 (C-5), 153.8 (C-14), 146.3 (C-17), 143.4 (C-19), 141.1 (C-29), 134.5 (C-10), 134.3 (C-8), 133.7 (C-4), 130.7 (C-21), 128.3 (C-2), 127.7 (C-3), 125.6 (C-16), 125.5 (C-15), 125.3 (C-1), 125.1 (C-18), 122.0 (C-30), 120.4 (C-9), 118.2 (C-6), 112.8 (C-7), 94.8 (C-11), 76.9 (C-13), 60.8 (C-32), 56.3 (C-12), 50.4 (C-22), 45.9 (C-20), 36.4 (C-27), 34.8 (C-25), 32.3 (C-28), 31.6 (C-26), 26.2 (C-23), 24.1 (C-24), 23.6 (C-24), 14.5 (C-33); **IR** (ATR): $\tilde{\nu}$ (cm^{-1}) = 2959, 2236, 1715, 1637, 1604, 1467, 1439, 1387, 1363, 1219, 1150, 1122, 1079, 1019, 975, 923, 862, 805, 647, 520; **HRMS (APCI)** calculated for $\text{C}_{42}\text{H}_{58}\text{NO}_5^+$ $[\text{M}+\text{H}]^+$, m/z : 656.4310; found: 656.4303.

Ethyl (*E*)-3-((2,4-di-*tert*-butyl-6-(4-cyano-2,6-dimethylheptan-4-yl)phenoxy)methyl)-7-hydroxynaphthalen-1-yl)acrylate (**16**)

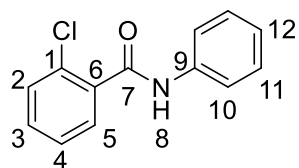


MOM-protected compound **14** (90 mg, 0.137 mmol, 1 eq.) was taken up in MeCN (4 mL). Aqueous HCl (2 M, 1.4 mL, 20 eq.) was added to the flask and the reaction was warmed to 70 °C for 30 min. The solvent was removed under reduced pressure and water (5 mL) was added. The water layer was then extracted with DCM (3×10 mL). The combined organic layers were washed with brine (10 mL) and dried over

Na₂SO₄. The solvent was removed under reduced pressure and purification by column chromatography (pentane/EA = 20:1) yielded a fairly pure product. The product was further purified by re-crystallization from hot pentane/cyclohexane to yield pure **16** (43 mg, 0.07 mmol, 52%) as yellow oil.

R_f = 0.27 (pentane/ ethyl acetate, 6:1); **¹H-NMR** (500 MHz, CDCl₃): δ 8.36 (d, 3J = 16 Hz, 1H, H-28), 7.93 (s, 1H, H-9), 7.74 (s, 1H, H-1), 7.69 (d, 3J = 9 Hz, 1H, H-7), 7.40 (d, 3J = 2 Hz, 1H, H-17), 7.35 (d, 3J = 2 Hz, 1H, H-4), 7.33 (d, 3J = 2 Hz, 1H, H-15), 7.05 (dd, 3J = 9 Hz, 4J = 2 Hz, 1H, H-6), 6.48 (d, 3J = 16 Hz, 1H, H-29), 5.08 (s, 2H, H-12), 4.31 (q, 3J = 7 Hz, 2H, H-31), 2.15-2.13 (m, 2H, H-21), 1.92-1.88 (m, 2H, H-21), 1.77-1.74 (m, 2H, H-22), 1.42 (s, 9H, H-27), 1.37 (t, 3J = 7 Hz, 3H, H-32), 1.34 (s, 9H, H-25), 1.05 (d, 3J = 7 Hz, 1H, H-23), 0.76 (d, 3J = 7 Hz, 1H, H-23); **¹³C-NMR** (126 MHz, CDCl₃): δ 167.6 (C-30), 155.1 (C-5), 153.8 (C-13), 146.3 (C-16), 143.4 (C-18), 142.3 (C-28), 132.4 (C-10), 131.7 (C-3), 130.9 (C-14), 130.5 (C-7), 130.2 (C-2), 129.0 (C-8), 127.4 (C-9), 125.4 (C-17), 125.2 (C-20), 124.3 (C-15), 123.6 (C-1), 120.0 (C-29), 118.6 (C-6), 105.6 (C-4), 76.7 (C-12), 60.8 (C-31), 51.0 (C-21), 44.8 (C-19), 36.2 (C-26), 34.7 (C-24), 32.0 (C-27), 31.5 (C-25), 26.1 (C-22), 24.0 (C-23), 23.7 (C-23), 14.5 (C-32); **IR** (ATR): $\tilde{\nu}$ (cm⁻¹) = 2953, 2925, 2868, 2236, 1712, 1606, 1508, 1467, 1365, 1219, 1173, 1120, 1031, 862, 831, 808, 798, 789, 754; **HRMS (APCI)** calculated for C₄₀H₅₃NNaO₄⁺ [M+Na]⁺, m/z: 634.3867; found: 634.3864.

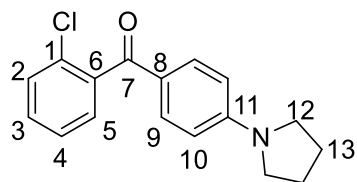
2-Chloro-N-phenylbenzamide (**18**)^[129]



The compound **17** (875 mg, 5.0 mmol, 1.0 eq.) was dissolved in anhydrous DCM (10 ml), and added dropwise to a mixture of aniline (0.46 mL, 5.0 mmol, 1.0 eq.) and Et₃N (1.75 mL, 12.5 mmol, 2.5 eq.) in DCM (10 ml). The resulting suspension was stirred for another 1 h. The mixture was diluted with water, and the organic layer separated. The water layer was then extracted with DCM (3×25 mL). The organic layer was washed with 1 M HCl (15 mL), 2 M NaOH (15 mL) and brine (15 mL) successively, and then dried over Na₂SO₄. The solvent was removed under reduced pressure and purification by column chromatography (pentane/EA = 15:1) yielded amide **18** (1.125 g, 4.85 mmol, 97%) as a colorless solid.

R_f = 0.53 (pentane/ ethyl acetate, 5:1); **Mp**: 118 °C; **$^1\text{H-NMR}$** (400 MHz, CDCl_3): δ 7.93 (br s, 1H, H-8), 7.74 (dd, 4J = 2.0 Hz, 3J = 7.3 Hz, 1H, H-5), 7.65-7.63 (2H, H-10), 7.46-7.34 (m, 5H, H-2, H-3, H-4, H-11), 7.19-7.15 (m, 1H, H-12); **$^{13}\text{C-NMR}$** (101 MHz, CDCl_3): δ 164.6 (C-7), 137.7 (C-9), 135.3 (C-6), 131.8 (C-2), 130.7 (C-1), 130.51 (C-3), 130.47 (C-5), 129.3 (C-11), 127.4 (C-4), 125.0 (C-12), 120.3 (C-10); **IR** (ATR): $\tilde{\nu}$ (cm^{-1}) = 3238, 3190, 3137, 3072, 3042, 2982, 2929, 2864, 2320, 2052, 1824, 1650, 1640, 1622, 1598, 1590, 1544, 1488, 1472, 1443, 1431, 1328, 1284, 1275, 1264, 1175, 1158, 1138, 1124, 1079, 1050, 1032, 1001, 988, 968, 953, 910, 894, 838, 830, 817, 793, 779, 759, 752, 724, 717, 691, 652, 628, 615, 588, 568, 559, 547, 532, 522, 506, 490, 484, 475, 463, 451, 446, 442, 428, 423, 419, 414, 410, 405; **HRMS (ESI)** calculated for $\text{C}_{13}\text{H}_{11}\text{ClNO}^+$ $[\text{M}+\text{H}]^+$, m/z : 232.0524; found: 232.0518.

(2-Chlorophenyl)(4-(pyrrolidin-1-yl)phenyl)methanone (19)^[65]

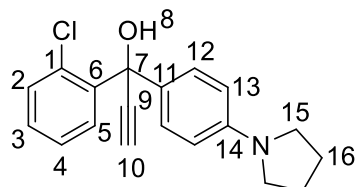


Under nitrogen atmosphere, a solution of benzamide **18** (1.125 g, 4.85 mmol, 1.00 eq.) in N-phenylpyrrolidine (1.02 mL, 7.08 mmol, 1.46 eq.) was added in a 50 ml two-necked flask with a reflux condenser and stirred at 50 °C for 45 min. Phosphorus oxychloride (0.59 mL, 6.50 mmol, 1.34 eq.) was added dropwise to the mixture at 50 °C over a period of 50 min. The reaction mixture was then stirred at 150 °C for 5 h and then at room temperature for 16 h. After the TLC control (ethyl acetate / pentane 1:10, R_f = 0.63) indicated complete conversion, the reaction mixture was mixed with 50% HCl (aq) (5.2 mL) and stirred at 110 °C for 3 h. After further TLC control (ethyl acetate / pentane 1:10, R_f = 0.31) indicated complete conversion, water (35 mL) and NaOH (aq) solution (2 M, 6.5 mL) were added. The aqueous layer was then extracted with DCM (3 × 15 mL). The combined organic layers were washed with NaOH (aq) solution (0.2 M, 15 mL), HCl (aq) solution (0.2 M, 15 mL) and water (2 × 15 mL), dried over Na_2SO_4 and the solvent was removed under reduced pressure. The brown crude product was purified by column chromatography (ethyl acetate / pentane 1:10 to 1: 5) and yielded **19** (627 mg, 2.19 mmol, 45%) as a yellow solid.

R_f = 0.31 (pentane/ ethyl acetate, 10:1); **Mp**: 118 °C; **$^1\text{H-NMR}$** (400 MHz, CDCl_3): δ 7.72-7.68 (m, 2H, H-9), 7.44-7.42 (m, 1H, H-4), 7.39-7.30 (m, 3H, H-2, H-3, H-5), 6.52 (d, 3J = 9.0 Hz, 2H,

H-10), 3.39-3.36 (m, 4H, H-12), 2.05-2.02 (m, 4H, H-13); ^{13}C -NMR (101 MHz, CDCl_3): δ 193.2 (C-7), 151.6 (C-11), 140.1 (C-6), 132.9 (C-9), 131.2 (C-1), 130.3 (C-2), 129.9 (C-3), 128.9 (C-5), 126.6 (C-4), 124.0 (C-8), 111.1 (C-10), 47.8 (C-12), 25.6 (C-13); **IR** (ATR): $\tilde{\nu}$ (cm^{-1}) = 3065, 2975, 2955, 2923, 2870, 2845, 2663, 2614, 2446, 2320, 2158, 2041, 1916, 1704, 1635, 1581, 1539, 1483, 1468, 1458, 1450, 1441, 1430, 1400, 1358, 1322, 1294, 1275, 1255, 1235, 1196, 1151, 1126, 1056, 1034, 1001, 964, 952, 946, 927, 863, 826, 807, 791, 771, 750, 738, 720, 694, 682, 638, 631, 580, 547, 539, 528, 523, 506, 494, 489, 485, 473, 466, 457, 441, 433, 429, 424, 414, 406, 402; **HRMS** (**ESI**) calculated for $\text{C}_{17}\text{H}_{17}\text{ClNO}^+ [\text{M}+\text{H}]^+$, m/z : 286.0993; found: 286.0998.

1-(2-Chlorophenyl)-1-(4-(pyrrolidin-1-yl)phenyl)prop-2-yn-1-ol (**20**)^[65]

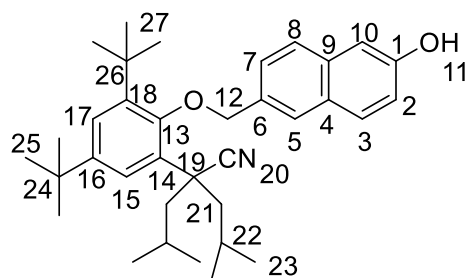


Under nitrogen atmosphere, a solution of trimethylsilylacetylene (0.35 mL, 2.41 mmol, 1.10 equiv.) in THF (10 mL) was added in a 50 ml three-necked flask with an internal thermometer. At $-10\text{ }^\circ\text{C}$, *n*-butyllithium (2.5 M in hexane) (1.14 mL, 2.85 mmol, 1.30 equiv.) was added dropwise over a period of 30 min. The reaction mixture was stirred at $-10\text{ }^\circ\text{C}$ for 1 h. Then 2-chloro-4-pyrrolidinobenzophenone (**17**) (627 mg, 2.19 mmol, 1.00 equiv.) dissolved in abs. THF (4 ml) was added in one portion. The reaction mixture was stirred at room temperature for 4 h. After the TLC control (ethyl acetate / cyclohexane 1:5, R_f = 0.53) indicated complete conversion, the reaction mixture was cooled to $0\text{ }^\circ\text{C}$. Then KOH (246 mg, 4.38 mmol, 2.00 equiv.) dissolved in methanol (2.5 mL) was added and the mixture was stirred at room temperature for 45 min. After further TLC control (ethyl acetate / cyclohexane 1:5, R_f = 0.35) indicated complete deprotection, the reaction mixture was neutralized to pH ~ 7 with acetic acid (0.50 ml) and water (40 ml) was added. The mixture were separated and the aqueous layer was extracted with ethyl acetate (3×50 ml). The combined organic layers were washed with water (2×30 ml) and brine (30 mL), and dried over Na_2SO_4 . The solvent was removed under reduced pressure and purification by column chromatography yielded product **18** (587 mg, 1.88 mmol, 86%) as a grey solid.

R_f = 0.35 (cyclohexane/ ethyl acetate, 10:1); **Mp**: $113\text{ }^\circ\text{C}$; ^1H -NMR (400 MHz, CDCl_3): δ 8.04-8.01 (m, 1H, H-3), 7.38-7.35 (m, 4H, H-2, H-4, H-12), 7.32-7.28 (m, 1H, H-5), 6.54 (d, 3J =8.5 Hz, 2H, H-13), 3.33-3.30 (m, 4H, H-15), 3.06 (s, 1H, H-8), 2.87 (s, 1H, H-10), 2.04-2.00 (m, 4H, H-

16); $^{13}\text{C-NMR}$ (101 MHz, CDCl_3): δ 147.7 (C-14), 141.0 (C-6), 132.6 (C-1), 131.3 (C-2), 129.6 (C-11), 129.2 (C-3), 128.1 (C-5), 127.7 (C-12, C-12'), 126.6 (C-4), 111.2 (C-13), 85.0 (C-9), 75.0 (C-10), 73.6 (C-7), 47.7 (C-15), 25.6 (C-16); **IR** (ATR): $\tilde{\nu}$ (cm^{-1}) = 3237, 2964, 2950, 2876, 2830, 2324, 2112, 2049, 1980, 1895, 1802, 1608, 1570, 1511, 1486, 1465, 1441, 1432, 1402, 1358, 1313, 1286, 1256, 1210, 1181, 1158, 1141, 1130, 1113, 1061, 1038, 1019, 991, 948, 939, 904, 860, 827, 817, 792, 785, 756, 736, 730, 719, 677, 643, 618, 591, 583, 568, 562, 549, 532, 518, 510, 506, 502, 486, 477; **HRMS** (ESI) calculated for $\text{C}_{19}\text{H}_{19}\text{ClNO}^+ [\text{M}+\text{H}]^+$, m/z : 312.1150; found: 312.1144.

2-(3,5-Di-tert-butyl-2-((6-hydroxynaphthalen-2-yl)methoxy)phenyl)-2-isobutyl-4-methylpentanenitrile (23)



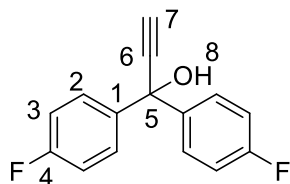
MOM-protected **13** (737 mg, 1.32 mmol, 1 eq.) was taken up in MeCN (35 mL). Aqueous HCl (2 M, 13.2 mL, 20 eq.) was added to the flask and the reaction was warmed to 70 °C for 30 min. The solvent was removed under reduced pressure and water (10 mL) was added. The aqueous layer was then extracted with DCM (3×15 mL). The organic

layer was washed with brine and dried over Na_2SO_4 . The solvent was removed under reduced pressure and purification by column chromatography (pentane/EA = 20:1) to yield a fairly pure product. The product was further purified by re-crystallization from hot pentane/cyclohexane to yield pure **23** (375 mg, 0.73 mmol, 55%) as white-yellow crystals.

R_f = 0.69 (pentane/ ethyl acetate, 5:1); **Mp**: 156 °C; $^1\text{H-NMR}$ (400 MHz, CDCl_3): δ 7.86 (s, 1H, H-5), 7.71 (d, 3J = 8.6 Hz, 1H, H-3), 7.65 (d, 3J = 8.5 Hz, 1H, H-8), 7.47 (dd, 3J = 8.5 Hz, 4J = 1.6 Hz, 1H, H-7), 7.40 (s, 2H, H-17, H-15), 7.06-7.03 (m, 2H, H-2, H-10), 5.31 (br, 1H, H-11, OH), 5.05 (s, 2H, H-12), 2.19-2.17 (m, 2H, H-21), 1.88-1.84 (m, 2H, H-21), 1.77-1.69 (m, 2H, H-22), 1.43 (s, 9H, H-27), 1.34 (s, 9H, H-25), 1.03 (d, 3J = 6.6 Hz, 6H, H-23), 0.75 (d, 3J = 6.6 Hz, 6H, H-23); $^{13}\text{C-NMR}$ (126 MHz, CDCl_3): δ 153.9 (C-13), 153.8 (C-1), 146.2 (C-16), 143.4 (C-18), 134.1 (C-9), 132.2 (C-6), 130.7 (C-14), 129.7 (C-3), 128.7 (C-4), 126.7 (C-8), 125.5 (C-17), 125.3 (C-20), 124.7 (C-5), 124.5 (C-7, C-15), 118.2 (C-2), 109.5 (C-10), 76.9 (C-12), 50.7 (C-21), 45.3 (C-19), 36.3 (C-26), 34.7 (C-24), 32.1 (C-27), 31.5 (C-25), 26.1 (C-22), 24.0 (C-23), 23.7 (C-23); **IR** (ATR): $\tilde{\nu}$ (cm^{-1}) = 3365, 2957, 2241, 1738, 1608, 1468, 1446, 1387 1375, 1271, 1238, 1223,

1203, 1146, 1125, 1048, 1023, 882, 851, 812, 734, 649, 553; **HRMS (APCI)** calculated for $C_{35}H_{48}NO_2^+ [M+H]^+$, m/z: 514.3680; found: 514.3669.

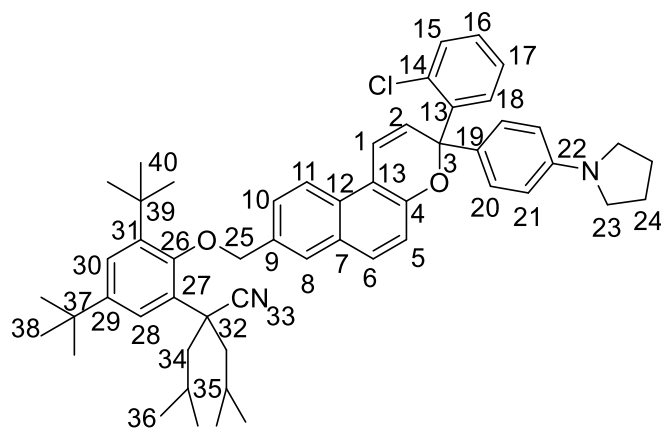
1,1-Bis(4-fluorophenyl)prop-2-yn-1-ol (**25**)^[58]



A 500 mL Schlenk flask was flame dried in vacuo. Then 4,4'-difluorobenzophenone **24** (15.0 g, 68.7 mmol, 1 eq.) and 137 mL THF were added under nitrogen atmosphere. Afterwards, a solution of 230 mL 0.6 M ethynylmagnesium chloride (138 mmol, 2 eq.) was added dropwise within 12 h. After complete addition, the reaction mixture was stirred for further 74 h at r.t. until TLC monitoring indicated a complete conversion of the starting material. The solution was diluted with 500 mL diethyl ether and carefully hydrolysed with a saturated NH_4Cl solution (200 mL). The separated aqueous layer was extracted with diethyl ether (3×300 mL). The combined organic layers was washed with brine (200 mL), dried over Na_2SO_4 and concentrated in vacuo. The crude product was purified by column chromatography (pentane/dichloromethane, 1/5) and yielded alcohol **25** (13.1g, 53.8mmol, 78%) as pale yellow oil.

R_f = 0.48 (pentane/ dichloromethane, 5:1); **1H -NMR** (400 MHz, $CDCl_3$): δ 7.58-7.53 (m, 4H, H-2), 7.04-7.00 (m, 4H, H-3), 2.90 (s, 1H, H-7), 2.80 (s, 1H, H-8); **^{13}C -NMR** (101 MHz, $CDCl_3$): δ 162.5 (d, $^1J_{C-F}$ = 247.3 Hz, C-4), 140.3 (d, $^4J_{C-F}$ = 2.9 Hz, C-1), 128.0 (d, $^3J_{C-F}$ = 8.2 Hz, C-2), 115.3 (d, $^2J_{C-F}$ = 21.0 Hz, C-3), 86.1 (C-6), 76.1 (C-7), 73.5 (C-5); **IR** (ATR): $\tilde{\nu}$ (cm^{-1}) = 3418, 3299, 3074, 2116, 1896, 1602, 1503 1410, 1322, 1300, 1220, 1189, 1156, 988, 903, 831; **HRMS (ESI)** calculated for $C_{15}H_{11}F_2O^+ [M+H]^+$, m/z: 245.0772; found: 245.0776.

2-(3,5-Di-tert-butyl-2-((3-(2-chlorophenyl)-3-(4-(pyrrolidin-1-yl)phenyl)-3H-benzo[f]chromen-8-yl)methoxy)phenyl)-2-isobutyl-4-methylpentanenitrile (N4)



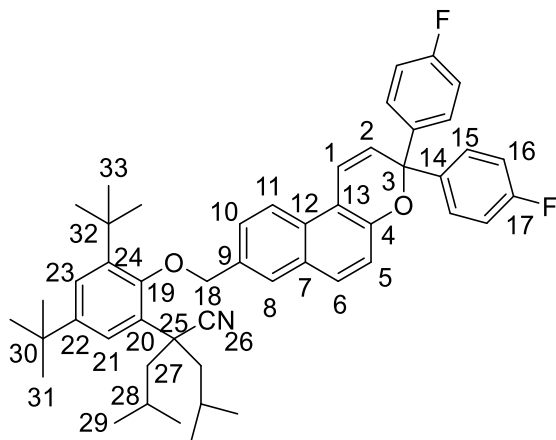
In a 50 mL two-neck flask with reflux condenser, propargyl alcohol **20** (156 mg, 0.5 mmol, 1.00 eq.), compound **23** (257 mg, 0.5 mmol, 1.00 eq.), freshly distilled toluene (6.5 mL) were added under nitrogen atmosphere. At 50 °C, Aluminium oxide (Sigma Aldrich, activated, acidic, Brockman I, pore size 58 Å) (393 mg,

3.85 mmol, 7.70 eq.) was added. The reaction mixture was stirred at 110 °C for 1.5 h. After complete conversion detectable by the thin layer chromatography (TLC) monitoring (ethyl acetate / pentane 1/20, R_f = 0.76), the reaction mixture was filtered and washed with hot toluene (2 × 10 ml). The solvent was removed under reduced pressure to afford the dark green crude product. After purification by column chromatography (silica, ethyl acetate / pentane 1:100), the naphthopyran **N4** (222 mg, 0.275 mmol, 55%) was obtained as a dark blue solid.

R_f = 0.76 (pentane/ ethyl acetate, 20:1); **Mp**: 130 °C; **¹H-NMR** (500 MHz, CD₃CN): δ 8.03 (d, 3J = 8.8 Hz, 1H, H-11), 7.89-7.88 (m, 2H, H-8, H-15), 7.70 (d, 3J = 8.8 Hz, 1H, H-6), 7.61 (dd, 3J = 8.8 Hz, 4J = 1.7 Hz, 1H, H-10), 7.45 (d, 4J = 2.4 Hz, H-30), 7.38 (d, 3J = 9.9 Hz, H-1), 7.38-7.36 (m, 2H, H-28, H-18), 7.33-7.25 (m, 2H, H-16, H-17), 7.18-7.16 (m, 3H, H-20, H-5), 6.60 (d, 3J = 9.9 Hz, 1H, H-2), 6.46 (d, 3J = 8.9 Hz, 2H, H-21), 5.05 (s, 2H, H-25), 3.20-3.18 (m, 4H, H-23), 2.18-2.14 (m, 2H, H-34), 1.94-1.92 (m, 4H, H-24), 1.87-1.82 (m, 2H, H-34), 1.67-1.62 (m, 2H, H-35), 1.39 (s, 9H, H-40), 1.32 (s, 9H, H-38), 0.98 (d, 3J = 6.7 Hz, 6H, H-36), 0.72 (d, 3J = 6.7 Hz, 6H, H-36); **¹³C-NMR** (126 MHz, CD₃CN): δ 154.7 (C-26), 151.2 (C-4), 148.7 (C-22), 147.1 (C-29), 144.1 (C-31), 142.3 (C-13), 134.0 (C-9), 132.4 (C-18), 132.3 (C-7), 132.1 (C-27), 130.6 (C-6), 130.1 (C-16), 130.0 (C-14), 129.8 (C-12), 129.7 (C-15), 129.4 (C-19), 129.3 (C-20), 127.5 (C-17), 127.2 (C-2), 126.4 (C-8), 126.2 (C-30, C-10), 126.1 (C-33), 125.3 (C-28), 122.5 (C-11), 120.9 (C-1), 119.3 (C-5), 115.4 (C-13), 111.8 (C-21), 83.5 (C-3), 77.7 (C-25), 51.3 (C-34), 48.2 (C-23), 45.4 (C-32), 36.7 (C-39), 35.2 (C-37), 32.1 (C-40), 31.5 (C-38), 26.8 (C-35), 26.0 (C-24), 24.0 (C-36), 23.7 (C-36); **IR** (ATR): $\tilde{\nu}$ (cm⁻¹) = 2958, 2869, 2231, 1610, 1520, 1467, 1435, 1374, 1268,

1219, 1178, 1122, 1087, 1052, 1000, 929, 884, 814, 778, 755; **HRMS (APCI)** calculated for $C_{54}H_{64}ClN_2O_2^+$ $[M+H]^+$, m/z : 807.4651; found: 807.4649.

2-(2-((3,3-Bis(4-fluorophenyl)-3H-benzo[f]chromen-8-yl)methoxy)-3,5-di-tert-butylphenyl)-2-isobutyl-4-methylpentanenitrile (N6)



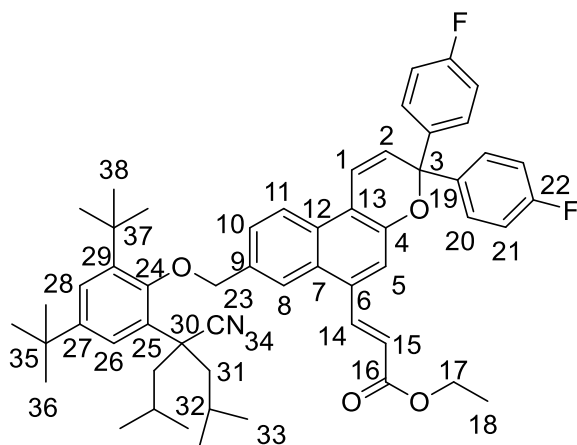
A 50 mL Schlenk flask was flame dried in vacuo and naphthol **23** (257 g, 0.5 mmol, 1.0 eq.), pyridinium tosylate (6.25 mg, 0.025 mmol, 5 mol%) and 12 mL DCE were added under nitrogen atmosphere. The suspension was heated to reflux. Then trimethyl orthoformate (109 μ L, 1.0 mmol, 2.0 eq.) was added in a single portion. To this mixture the propargyl alcohol **25** (171 mg, 0.7 mmol, 1.4 eq.) was added dropwise via syringe. The mixture was heated to

reflux for 48 h until TLC monitoring indicated complete consumption of the starting material. The brown solution was cooled to r.t. and diluted with 10 mL dichloromethane. The organic layer was washed with water (3 \times 10 mL) and with brine (10 mL), dried over Na_2SO_4 and concentrated in vacuo. After purification by column chromatography (silica, ethyl acetate / pentane 1:25), the naphthopyran **N6** (300 mg, 0.405 mmol, 81%) was obtained as a pearl-white solid.

R_f = 0.91 (pentane/ ethyl acetate, 5:1); **Mp**: 93.1-94.5 °C; **¹H-NMR** (500 MHz, $CDCl_3$): δ 7.98 (d, 3J = 9 Hz, 1H, H-11), 7.81 (d, 4J = 1.5 Hz, 1H, H-8), 7.69 (d, 3J = 8.5 Hz, 1H, H-6), 7.56 (dd, 3J = 9 Hz, 4J = 1.5 Hz, 1H, H-10), 7.46-7.42 (m, 2 \times 2H, H-15), 7.41-7.39 (m, 2H, H-21, H-23), 7.33 (d, 3J = 10 Hz, 1H, H-1), 7.18 (d, 3J = 8.5 Hz, 1H, H-5), 7.03-6.98 (m, 2 \times 2H, H-16), 6.18 (d, 3J = 10 Hz, 1H, H-2), 5.02 (s, 2H, H-18), 2.22-2.09 (m, 2H, H-27), 1.85-1.81 (m, 2H, H-27), 1.75-1.67 (m, 2H, H-28), 1.40 (s, 9H, H-33), 1.33 (s, 9H, H-31), 1.01 (d, 3J = 6.5 Hz, 6H, H-29), 0.73 (d, 3J = 6.5 Hz, 6H, H-29); **¹³C-NMR** (126 MHz, $CDCl_3$): δ 162.3 (d, $^1J_{C-F}$ = 247.0 Hz, C-17), 153.8 (C-19), 150.3 (C-4), 146.1 (C-22), 143.3 (C-24), 140.6 (d, $^4J_{C-F}$ = 3.0 Hz, C-14), 133.0 (C-9), 130.6 (C-26), 130.3 (C-6), 129.4 (C-7), 129.2 (C-12), 129.0 (d, $^3J_{C-F}$ = 8.2 Hz, C-15), 127.5 (C-2), 125.5 (C-23), 125.4 (C-8), 125.3 (C-20), 125.1 (C-10), 124.9 (C-21), 121.7 (C-11), 120.1 (C-1), 118.5 (C-5), 115.2 (d, $^2J_{C-F}$ = 21.2 Hz, C-16), 114.1 (C-13), 81.9 (C-3), 76.7 (C-18), 50.3 (C-

27), 45.7 (C-25), 36.2 (C-32), 34.7 (C-30), 32.2 (C-33), 31.5 (C-31), 26.1 (C-28), 24.0 (C-29), 23.5 (C-29); **IR** (ATR): $\tilde{\nu}$ (cm⁻¹) = 2954, 2866, 2232, 1601, 1507, 1467, 1362, 1272, 1222, 1157, 1107, 1087, 1006, 963, 886, 834, 817, 727, 650, 551; **HRMS** (APCI) calculated for C₅₀H₅₆F₂NO₂⁺ [M+H]⁺, m/z: 740.4274; found: 740.4272.

Ethyl (E)-3-(8-((2,4-di-tert-butyl-6-(4-cyano-2,6-dimethylheptan-4-yl)phenoxy)methyl)-3,3-bis(4-fluorophenyl)-3H-benzo[f]chromen-6-yl)acrylate (N7)



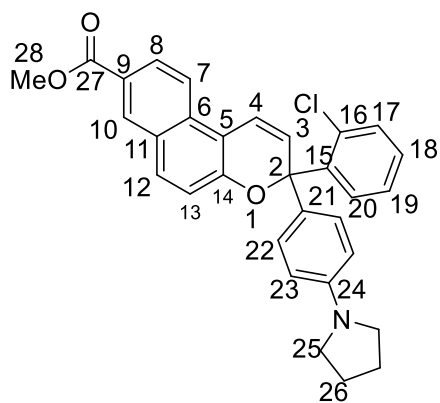
A 10 mL sealed tube (with a Teflon cap) was flame dried and naphthopyran **N6** (74 mg, 0.10 mmol, 1.0 equiv.), Pd(OPiv)₂ (3.4 mg, 0.010 mmol, 10 mol%), AgOPiv (62.7 mg, 0.30 mmol, 3.0 equiv.), ethyl acrylate (22 μ L, 0.20 mmol, 2.0 equiv.) were added. DCE (1.0 mL) was used to wash down the solids on the sides of the tube wall. The tube was then capped and submerged into a preheated 100 °C oil bath. The oil bath was

covered with aluminum foil to stabilize the oil bath temperature and to shield the reaction from light. After one day of stirring, the tube was shaken manually to dislodge the silver salt off the sides of the wall. The reaction was stirred for a total of 48 h and cooled down to room temperature. The reaction mixture was filtered through a pad of Celite and washed with EA (3 \times 3 mL). The solvent was removed under reduced pressure and purified by column chromatography (pentane/EA, 100/1) to yield naphthopyran **N7** (15 mg, 0.017 mmol, 17%) as a yellow solid.

R_f = 0.69 (pentane/ EA, 20:1); **Mp**: 80-81.4 °C; **¹H-NMR** (500 MHz, CDCl₃): δ 8.39 (d, ³J = 16 Hz, 1H, H-14), 8.16 (s, 1H, H-8), 8.05 (d, ³J = 9 Hz, 1H, H-11), 7.68 (dd, ³J = 9 Hz, ⁴J = 1.5 Hz, 1H, H-10), 7.46 (s, 1H, H-5), 7.45-7.41 (m, 2 \times 2H, H-20), 7.39-7.34 (m, 3H, H-1, H-26, H-28), 7.05-6.98 (m, 2 \times 2H, H-21), 6.50 (d, ³J = 16 Hz, 1H, H-15), 6.25 (d, ³J = 10 Hz, 1H, H-2), 5.08 (s, 2H, H-23), 4.27 (q, ³J = 7 Hz, 2H, H-17), 2.17-2.09 (m, 2H, H-31), 1.86-1.81 (m, 2H, H-31), 1.73-1.68 (m, 2H, H-32), 1.42 (s, 9H, H-38), 1.35-1.32 (m, 12H, H-18, H-36), 1.02 (d, ³J = 6.5 Hz, 6H, H-33), 0.73 (d, ³J = 6.5 Hz, 6H, H-33); **¹³C-NMR** (126 MHz, CDCl₃): δ 166.7 (C-16), 162.4 (d, ¹J_{C-F} = 248.2 Hz, C-22), 153.8 (C-24), 149.7 (C-4), 146.3 (C-27), 143.3 (C-29), 140.7 (C-14),

140.3 (C-19), 134.0 (C-9), 133.9 (C-6), 130.8 (C-34), 129.6 (C-12), 129.0 (d, $^3J_{\text{C-F}} = 7.5$ Hz, C-20), 128.9 (C-2), 127.7 (C-7), 125.6 (C-28), 125.5 (C-10), 125.4 (C-25), 124.7 (C-26), 122.4 (C-11), 121.7 (C-15), 120.9 (C-8), 119.9 (C-1), 117.1 (C-5), 116.4 (C-13), 115.3 (d, $^2J_{\text{C-F}} = 21.4$ Hz, C-21), 82.0 (C-3), 76.9 (C-23), 60.7 (C-17), 50.7 (C-31), 45.4 (C-30), 36.3 (C-37), 34.8 (C-35), 32.1 (C-38), 31.5 (C-36), 26.1 (C-32), 24.0 (C-33), 23.6 (C-33), 14.5 (C-18); **IR** (ATR): $\tilde{\nu}$ (cm^{-1}) = 2957, 2869, 2232, 1713, 1633, 1589, 1537, 1507, 1468, 1440, 1396, 1363, 1300, 1273, 1227, 1158, 1124, 1054, 1032, 1006, 928, 864, 828, 750, 683, 637, 581; **HRMS** (APCI) calculated for $\text{C}_{55}\text{H}_{62}\text{F}_2\text{NO}_4^+$ $[\text{M}+\text{H}]^+$, m/z : 838.4641; found: 838.4631.

Methyl 3-(2-chlorophenyl)-3-(4-(pyrrolidin-1-yl)phenyl)-3H-benzo[f]chromene-8-carboxylate (N1)

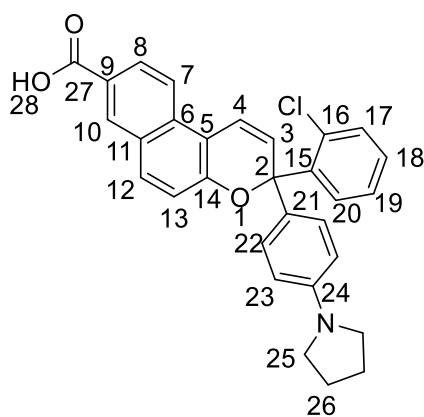


In a 250 mL two-neck flask with reflux condenser, propargyl alcohol **20** (4.00 g, 12.8 mmol, 1.00 eq.), methyl 6-hydroxy-2-naphthoate (2.59 g, 12.8 mmol, 1.00 eq.) in freshly distilled toluene (160 ml) were added under nitrogen atmosphere. At 50 °C, Aluminium oxide (Sigma Aldrich, activated, acidic, Brockman I, pore size 58 Å) (10.07 g, 98.8 mmol, 7.70 eq.) was added. The reaction mixture was stirred at 110 °C for 1.5 h. After complete conversion detectable by the thin layer chromatography (TLC) monitoring (ethyl acetate / pentane 1/10, $R_f = 0.51$), the reaction mixture was filtered and washed with hot toluene (2 × 50 ml). The solvent was removed under reduced pressure to afford the dark green crude product (5.21 g). After purification by column chromatography (silica, ethyl acetate / pentane 1:10), the naphthopyran **N1** (3.41 g, 6.88 mmol) was obtained as a dark blue solid in a yield of 54%.

$R_f = 0.32$ (ethyl acetate / pentane, 1:10); **Mp** : 111 °C; **$^1\text{H-NMR}$** (400 MHz, $\text{CDCl}_3+\text{D}_2\text{O}$): δ 8.46 (s, 1H, H-10), 8.03 (dd, $^3J = 8.8$ Hz, $^4J = 1.9$ Hz, 1H, H-8), 7.97 (d, $^3J = 8.8$ Hz, 1H, H-7), 7.80 (dd, $^3J = 7.6$ Hz, $^4J = 1.9$ Hz, 1H, H-20), 7.75 (d, $^3J = 8.9$ Hz, 1H, H-12), 7.35 (dd, $^3J = 7.2$ Hz, $^4J = 2.0$ Hz, 1H, H-17), 7.29 (d, $^3J = 10.2$ Hz, 1H, H-4), 7.28-7.19 (m, 5H, H-13, H-18, H-19, H-22), 6.62 (d, $^3J = 10.1$ Hz, 1H, H-3), 6.49 (d, $^3J = 8.7$ Hz, 2H, H-23), 3.96 (s, 3H, H-28), 3.27-3.24 (m, 4H, H-25), 1.97-1.94 (m, 4H, H-26); **$^1\text{H-NMR}$** (400 MHz, $\text{MeCN-}d_3$): δ 8.45 (d, $^4J = 1.6$ Hz,

1H), 8.04 (d, $^3J = 9.0$ Hz, 1H), 7.98 (dd, $^3J = 8.9$ Hz, $^4J = 1.8$ Hz, 1H), 7.85-7.82 (m, 2H), 7.38-7.36 (m, 1H), 7.34 (d, $^3J = 10.6$ Hz, 1H, H-4), 7.32-7.25 (m, 2H), 7.22 (d, $^3J = 8.9$ Hz, 1H), 7.16-7.12 (m, 2H, H-22), 6.60 (d, $^3J = 10.1$ Hz, 1H, H-3), 6.45-6.42 (m, 2H, H-23), 3.90 (s, 3H, H-28), 3.18-3.15 (m, 4H, H-25), 1.93-1.90 (m, 4H, H-26); $^{13}\text{C-NMR}$ (101 MHz, $\text{CDCl}_3 + \text{D}_2\text{O}$): δ 167.5 (C-27), 152.6 (C-14), 147.6 (C-24), 141.5 (C-15), 132.3 (C-6), 131.9 (C-16), 131.8 (C-10), 131.7 (C-17), 131.3 (C-12), 129.2 (C-21), 129.0 (C-18, C-20), 128.6 (C-22), 128.4 (C-11), 126.5 (C-19), 126.13 (C-8), 126.10 (C-3), 125.1 (C-9), 121.7 (C-7), 119.4 (C-4), 119.3 (C-13), 113.9 (C-5), 83.5 (C-2), 52.3 (C-28), 47.6 (C-25), 25.5 (C-26); **IR**: $\tilde{\nu}$ (cm^{-1}) = 3061, 2946, 2926, 2843, 1713, 1608, 1587, 1519, 1485, 1466, 1433, 1373, 1338, 1278, 1245, 1208, 1178, 1161, 1125, 1106, 1082, 1051, 1039, 998, 965, 920, 865, 807, 752, 710, 698, 676, 660, 633, 620, 579, 568, 552, 518; **HRMS (ESI)**: calculated for $\text{C}_{31}\text{H}_{27}\text{ClNO}_3$ $[\text{M} + \text{H}]^+$: 496.1674; found: 496.1669;

3-(2-Chlorophenyl)-3-(4-(pyrrolidin-1-yl)phenyl)-3*H*-benzo[*f*]chromene-8-carboxylic acid (**N2**)

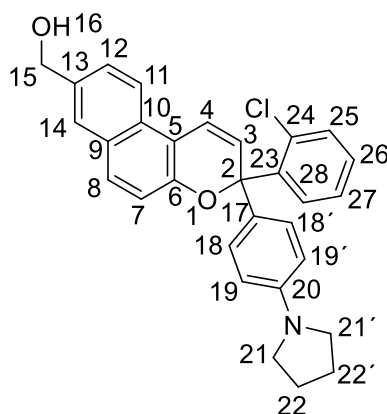


Under nitrogen atmosphere, the naphthopyran **N1** (336 mg, 0.68 mmol.) in abs. tetrahydrofuran (100 mL) and potassium trimethylsilanolate (262 mg, 2.43 mmol.) were added. The reaction mixture was stirred for 22 h at room temperature. Although the TLC analysis (hexane/ethyl acetate = 1/1) indicated no complete conversion at this time, the solvents were removed under reduced pressure. The residue was dissolved in dichloromethane, water was added and the pH was adjusted to pH = 3 with a KHSO_4 (aq) solution (0.1 M). The layers were then separated and the aqueous layer extracted with dichloromethane (2×50 mL). The combined organic layers were dried (Na_2SO_4) and the solvents removed under reduced pressure to afford crude product. After purification by column chromatography (silica, hexane / ethyl acetate = 1/1), the naphthopyran **N2** (142 mg, 0.30 mmol, 44%) was received as a purple solid.

R_f = 0.47 (hexane / ethyl acetate, 1:1); **Mp.** 310 °C; $^1\text{H-NMR}$ (500 MHz, $\text{DMSO}-d_6$): δ 8.33 (s, 1H, H-10), 8.05 (dd, $^3J = 8.7$ Hz, $^4J = 1.3$ Hz, 1H, H-8), 7.97 (d, $^3J = 8.8$ Hz, 1H, H-7), 7.80 (d, $^3J = 8.9$ Hz, 1H, H-12), 7.75 (dd, $^3J = 7.7$ Hz, $^4J = 1.8$ Hz, 1H, H-20), 7.47 (d, $^3J = 10.3$ Hz, 1H,

H-4), 7.41 (dd, $^3J = 7.6$ Hz, $^4J = 1.4$ Hz, 1H, H-17), 7.35 (td, $^3J = 7.5$ Hz, $^4J = 1.6$ Hz, 1H, H-19), 7.31 (td, $^3J = 7.5$ Hz, $^4J = 1.9$ Hz, 1H, H-18), 7.17 (d, $^3J = 8.8$ Hz, 1H, H-13), 7.12 (d, $^3J = 8.8$ Hz, 2H, H-22), 6.55 (d, $^3J = 10.1$ Hz, 1H, H-3), 6.46 (d, $^3J = 8.6$ Hz, 2H, H-23), 3.18-3.16 (m, 4H, H-25), 1.92-1.89 (m, 4H H-26); $^{13}\text{C-NMR}$ (126 MHz, DMSO- d_6): δ 170.2 (C-27), 150.1 (C-14), 147.0 (C-24), 141.2 (C-15), 134.9 (C-9), 131.4 (C-17), 130.9 (C-16), 130.8 (C-12), 129.8 (C-6), 129.3 (C-18), 129.2 (C-10), 128.6 (C-20), 128.5 (C-21), 128.3 (C-11), 128.2 (C-8), 128.0 (C-22), 126.7 (C-19), 125.5 (C-3), 120.2 (C-7), 119.9 (C-4), 117.6 (C-13), 113.4 (C-5), 111.0 (C-23), 82.2 (C-2), 47.1 (C-25), 24.9 (C-26); **IR** (ATR): $\tilde{\nu}$ (cm^{-1}) = 3062, 2928, 1694, 1610, 1609, 1558, 1520, 1467, 1378, 1362, 1329, 1271, 1244, 1222, 1179, 1125, 1084, 1052, 1040, 1000, 966, 925, 868, 809, 754, 710; **HRMS** (ESI) calculated for $\text{C}_{30}\text{H}_{24}\text{ClNO}_3$ $[\text{M}+\text{H}]^+$: 482.1517, found: 482.1502.

(3-(2-Chlorophenyl)-3-(4-(pyrrolidin-1-yl)phenyl)-3*H*-benzo[*f*]chromen-8-yl)methanol (N3)



In a 100 mL three-necked flask with internal thermometer, naphthopyran **N1** (1.20 g, 2.42 mmol, 1.00 eq.) was dissolved in dichloromethane (22 mL) under nitrogen atmosphere and cooled to -78 °C with dry ice. A solution of DIBAL-H in toluene (20% w, 6.90 mL, 8.47 mmol, 3.50 equiv.) was added to this reaction solution dropwise over a period of 60 min. After completion of the addition, the reaction mixture was stirred at -78 °C for an additional 1 h, until TLC (ethyl acetate / pentane, 1: 5, R_f = 0.07)

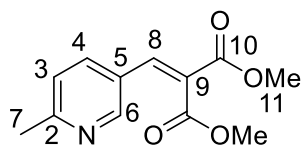
showed complete conversion. Then ethyl acetate (55 mL) was added cautiously at -78 °C to destroy residues of unreacted DIBAL-H. The reaction mixture was warmed to room temperature and then diluted with dichloromethane (150 mL) and washed with saturated NaCl solution (300 mL). The aqueous layer was extracted with dichloromethane (6 x 100 mL). The combined organic layers were washed with water (100 mL), dried over MgSO_4 and the solvent removed under reduced pressure. After purification by column chromatography (silica, ethyl acetate / pentane 2/5), the product **N3** (592 mg, 1.26 mmol) was obtained as a dark blue solid in a yield of 52%.

R_f = 0.26 (ethyl acetate/pentane, 2:5); **Mp**: 120 °C; $^1\text{H-NMR}$ (400 MHz, DMSO- d_6): δ 8.05 (d, $^3J = 8.8$ Hz, 1H, H-11), 7.77-7.72 (m, 3H, H-8, H-14, H-25), 7.48-7.45 (m, 2H, H-4, H-12), 7.42-

7.1 Synthesis

7.39 (m, 1H, H-28), 7.37-7.29 (m, 2H, H-26, H-27), 7.18 (d, $^3J=8.8$ Hz, 1H, H-7), 7.12-7.09 (m, 2H, H-18, H-18'), 6.56 (d, $^3J=10.1$ Hz, 1H, H-3), 6.44 (d, $^3J=8.8$ Hz, 2H, H-19, H-19'), 5.27 (t, $^3J=5.7$ Hz, 1H, H-16), 4.61 (d, $^3J=5.6$ Hz, 2H, H-15), 3.17-3.14 (m, 4H, H-21, H-21'), 1.91-1.88 (m, 4H, H-22, H-22'); $^{13}\text{C-NMR}$ (101 MHz, DMSO- d_6): δ 149.5 (C-6), 147.0 (C-20), 141.2 (C-24), 138.0 (C-13), 131.4 (C-26), 130.9 (C-23), 129.7 (C-25), 129.3 (C-8), 128.8 (C-10), 128.6 (C-28), 128.5 (C-17), 128.3 (C-9), 128.0 (C-18, C-18'), 126.7 (C-27), 126.2 (C-12), 125.7 (C-3), 125.1 (C-14), 121.4 (C-11), 119.9 (C-4), 117.9 (C-7), 113.7 (C-5), 110.9 (C-19, C-19'), 82.1 (C-2), 62.8 (C-15), 47.1 (C-21, C-21'), 24.9 (C-22, C-22'); **IR**: $\tilde{\nu}$ (cm^{-1}) = 3332, 3061, 2836, 2320, 2161, 2047, 2022, 1901, 1608, 1520, 1484, 1469, 1432, 1373, 1287, 1268, 1244, 1222, 1177, 1126, 1086, 1039, 1011, 998, 966, 929, 886, 841, 814, 780, 754, 709, 655, 636, 612, 604, 594, 584, 578, 556, 552, 544, 527, 521, 516, 511; **HR-MS (ESI)**: calculated for $\text{C}_{30}\text{H}_{27}\text{ClNO}_2$ $[\text{M}+\text{H}]^+$: 468.1721; found: 468.1725.

Dimethyl 2-((6-methylpyridin-3-yl)methylene)malonate (**ligand 1**)^[111]



A 10 mL Schlenk tube was flame dried in vacuo and 6-methylnicotinaldehyde (69.1 μL , 0.6 mmol, 1.0 eq.), dimethyl malonate (73.5 μL , 0.63 mmol, 1.05 eq.), piperidine (9 μL , 0.09 mmol, 0.15 eq.), acetic acid (5.2 μL , 0.09 mmol, 0.15 eq.), 3 mL toluene were added under nitrogen atmosphere. The reaction mixture was stirred at 110 $^{\circ}\text{C}$ for 16 h. Then the reaction was cooled down to room temperature and afterwards piperidine (6 μL , 0.06 mmol, 0.1 eq.), acetic acid (3.4 μL , 0.06 mmol, 0.1 eq.) were added under nitrogen atmosphere. The reaction mixture was stirred at 110 $^{\circ}\text{C}$ for additional 2 h. Afterwards the mixture was cooled down to room temperature and diluted with dichloromethane, washed with water (10 mL). The organic layer was dried (Na_2SO_4) and the solvents were removed under reduced pressure to afford the crude product. After purification by column chromatography (silica, ethyl acetate / pentane 1/2), the **ligand 1** (63.5 mg, 0.27 mmol, 45%) as a white solid was received.

R_f = 0.55 (ethyl acetate/pentane, 5:2); **Mp**: 88 $^{\circ}\text{C}$; $^1\text{H-NMR}$ (500 MHz, CDCl_3): δ 8.54 (d, $^3J = 2$ Hz, 1H, H-6), 7.71 (s, 1H, H-8), 7.64 (dd, $^3J = 8$ Hz, $^4J = 2$ Hz, 1H, H-4), 7.19 (d, $^3J = 8$ Hz, 1H, H-3), 3.86 (s, 3H, H-11), 3.85 (s, 3H, H-11), 2.59 (s, 3H, H-7); $^{13}\text{C-NMR}$ (126 MHz, CDCl_3): δ 166.7 (C-10), 164.2 (C-10), 160.8 (C-2), 150.1 (C-6), 139.4 (C-8), 136.3 (C-4), 126.8 (C-9), 126.2 (C-5), 123.6 (C-3), 52.9 (C-11), 24.5 (C-7); **IR**: $\tilde{\nu}$ (cm^{-1}) = 3005, 2955, 2921, 2853, 1724, 1632,

1593, 1560, 1491, 1463, 1443, 1401, 1360, 1307, 1248, 1223, 1197, 1186, 1161, 1142, 1066, 1028, 982, 969, 774, 763, 728, 706, 669, 645, 597, 555, 534, 505;

Procedure for nondirected C-H functionalization of compound **3**

A 10 mL Schlenk tube was flame dried in vacuo and Pd(OAc)₂ (4.5 mg, 0.02 mmol, 10 mol%), **ligand 1** (9.4 mg, 0.04 mmol, 20 mol%), N-acetylglycine (7.0 mg, 0.06 mmol, 30 mol%), AgOAc (100.2 mg, 0.6 mmol, 3.0 eq.), compound **3** (49.3 mg, 0.2 mmol, 1.0 eq.), ethyl acrylate (65.3 μ L, 0.6 mmol, 3.0 eq.), 2 mL HFIP were added under nitrogen atmosphere. The tube was then capped and submerged into a preheated 90 °C oil bath. The oil bath was covered with aluminum foil to stabilize the oil bath temperature and to shield the reaction from light. The reaction was stirred for a total of 24 h and then cooled down to room temperature. The solvent was removed under reduced pressure and purified by column chromatography but the mixture of 5 products could not be separated.

7.2 UV/Vis Absorption Spectroscopy

7.2.1 General Information

The set-up of UV/Vis spectroscopy measurements is displayed in Figure 7.1. All the experiments were carried out with an *Avantes* AvaSpec Dual-channel Fiber Optic Spectrometer, which was equipped with the AvaLight-DH-S-BAL light source (Figure 7.1-1). A cuvette (10 mm, Quartz, Suprasil, Hellma Analytics) was applied to the experiments (Figure 7.1-3). All the LED lights used in this work were bought from Thorlabs (Figure 7.1-5). All the absorption spectra were measured at 273 K in this work unless mentioned specially. Additional air stream cooling was employed (Figure 7.1-7), due to the low efficiency of the temperature regulator (Figure 7.1-6) for cooling down the sample in the sample holder.

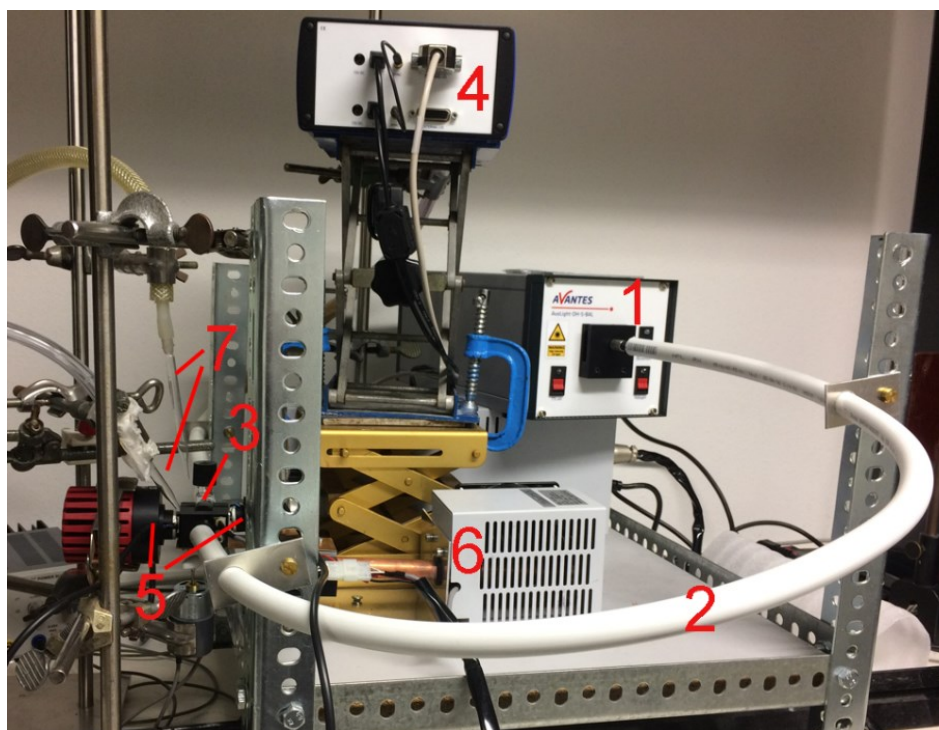


Figure 7.1 The device of UV/Vis experiments: 1) light source; 2) optical fiber in composite pipe; 3) cuvette holder (equipped with a magnetic stirrer below); 4) detector; 5) LED lights; 6) temperature regulator; 7) air stream cooling (picture from the PhD thesis of Marina Vlacjić).

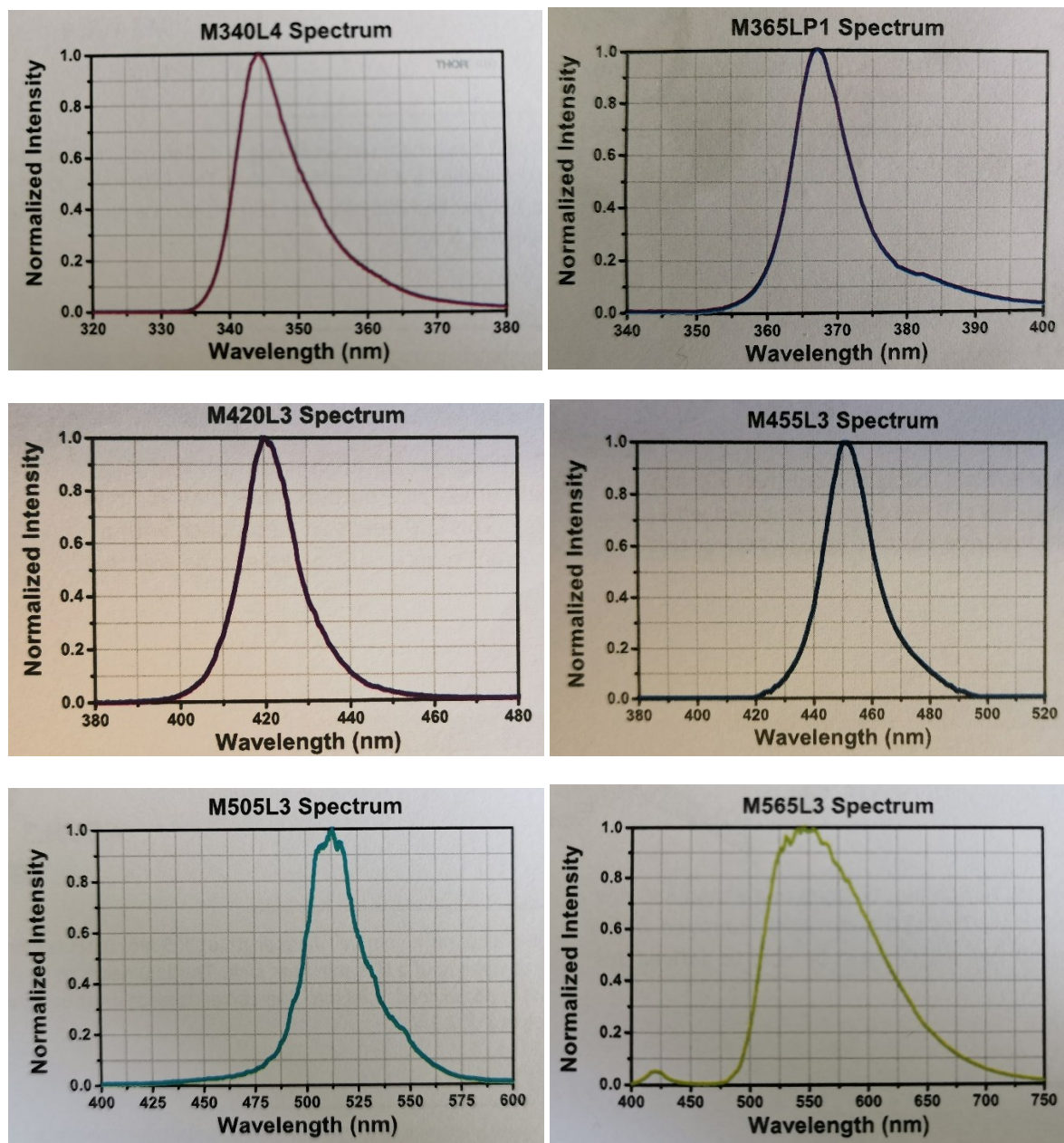


Figure 7.2 Emission spectra of LED lights used in this work (provided by Thorlabs).

The emission spectra of LED lights are exhibited in Figure 7.2. Furthermore, the light intensities of LED lights were detected by a Photometer *International Light IL 1400*. Therein, for the room temperature UV/Vis measurements, they were detected through 1 cm interspace between lights and detector, which is the same distance as the thickness of cuvette holder. For *in-situ* NMR measurements, the light intensities were detected directly from the fiber. Relevant parameters are presented in Table 7.1.

7.2 UV/Vis Absorption Spectroscopy

Besides, two holes of the cuvette holder made it possible to use two LED lights one by one without delay (Figure 7.3). A grey filter (NDUV510B - OD 1.0) was applied between light source and fiber, for reducing the high power of the light source of the detector, which can induce the switching of naphthopyrans. The grey filter is made of fused silica substrate and can absorb around 90 % of the incoming light. Its transmission-spectrum is demonstrated in Figure 7.4.

Table 7.1 The specifications of LED lights applied in this work.

LED	λ_{max} (nm)	Bandwidth (nm)	Power ^a (mW/cm ²)	Power ^b (mW/cm ²)
M340L4	345	11	12	-
M365LP1	367	9	110	3.86
M420L3	420	15	73	8.10
M455L3	452	18	-	4.30
M505L3	512	30	70	2.37
M565L3	550	104	84	3.20

[a] Detected in room temperature UV-Vis spectroscopy. [b] Detected in low temperature *in-situ* NMR measurements.

The samples were prepared with solvents of spectroscopy grade in a 25 mL volumetric flask. The concentration is 1.5×10^{-5} M. All the prepared samples were degassed with argon balloon under ultrasound for 15 min before measurements.

All the absorption spectra were analysed with the software Avasoft 8.5. The applied parameter for recording absorption spectra in this work is as follows: average over 200 spectra, 10 ms integration time, but the shortest time to record a spectrum is less than 1 second (average over 100 spectra, 1 ms integration time).

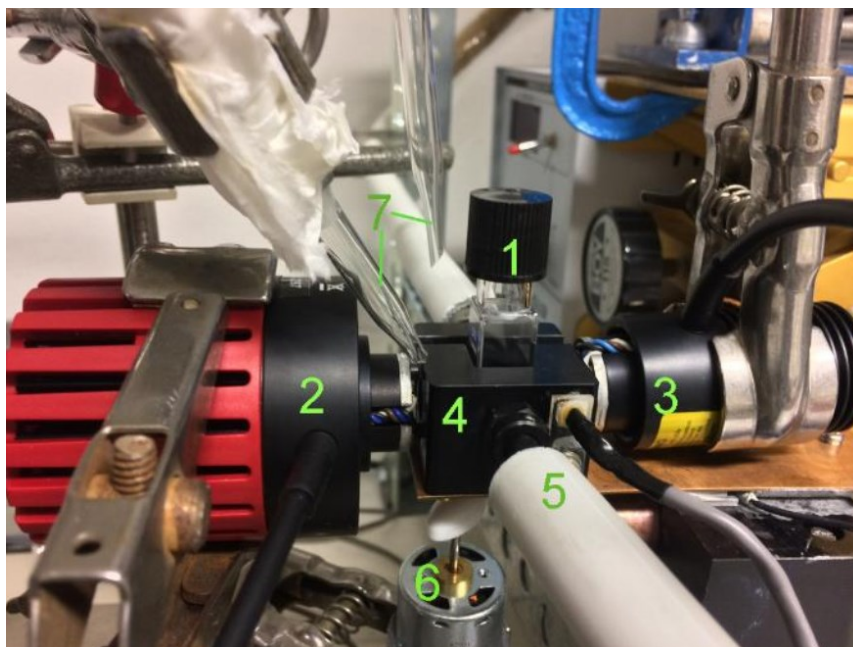


Figure 7.3 The set-up of two LED lights: 1) cuvette with stirring bar; 2) 1st LED light; 3) 2nd LED light; 4) cuvette holder; 5) optical fiber in composite pipe; 6) magnetic stirrer; 7) air stream cooling (picture from the PhD thesis of Marina Vlacjić).

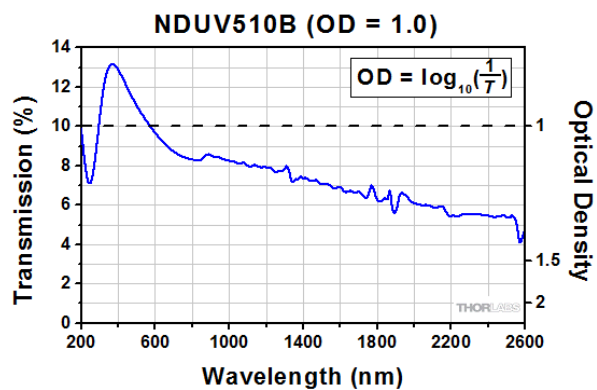


Figure 7.4 Transmission-spectrum of grey filter (provided by Thorlabs).

7.2.2 Time-Resolved Experiments and Exponential Fitting

The TC and TT forms of one naphthopyran were regarded to have the same λ_{\max} , although a deviation of $\lambda_{\max, \text{TC}}$ from $\lambda_{\max, \text{TT}}$ was observed during the thermal back reaction of **N1**, **N2** and **N3** in TCE because of the slow $k_{\text{TT} \rightarrow \text{TC}, \text{thermal}}$ (see Chapter 8.3, Figures 8.3, 8.4 and 8.5). The time resolved absorbance were monitored at λ_{\max} of the open forms. When the system arrived at PSS under UV irradiation, there were three isomers in the equilibrium: CF, TC and TT. Once UV light was switched off, there existed two processes: $\text{TC} \rightarrow \text{CF}$ and $\text{TT} \rightarrow \text{TC} + \text{TC} \rightarrow \text{CF}$ with $k_{\text{TT} \rightarrow \text{TC}, \text{thermal}} < k_{\text{TC} \rightarrow \text{CF}, \text{thermal}}$. The decrease of absorbance was monitored for **N1**, **N2**, **N3** and **N4**, and are exhibited in Figures 7.6 and 7.7. The thermal relaxation kinetics were calculated from time-resolved absorbance at λ_{\max} , by fitting the experimental data to the biexponential decay. Relevant parameters and the coefficients of determination (R^2) are shown in Tables 7.2 and 7.3.

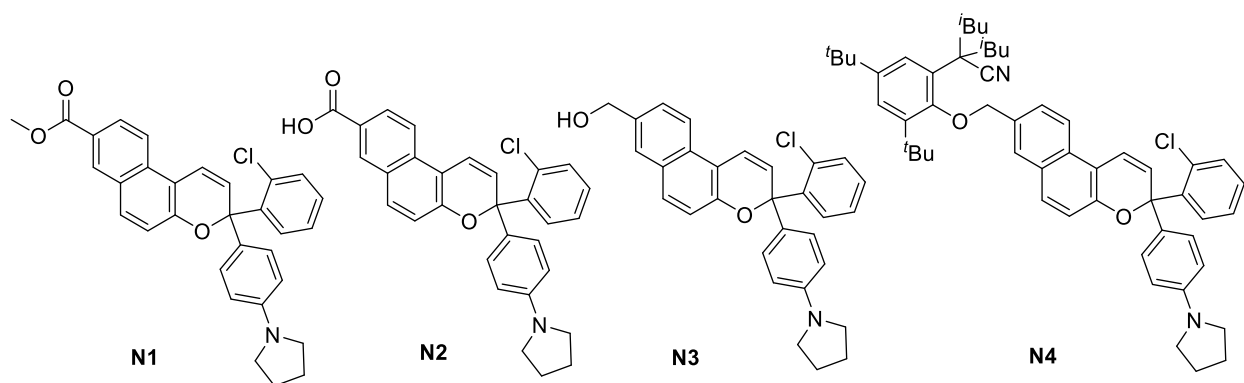


Figure 7.5 The structures of naphthopyrans **N1**, **N2**, **N3** and **N4**.

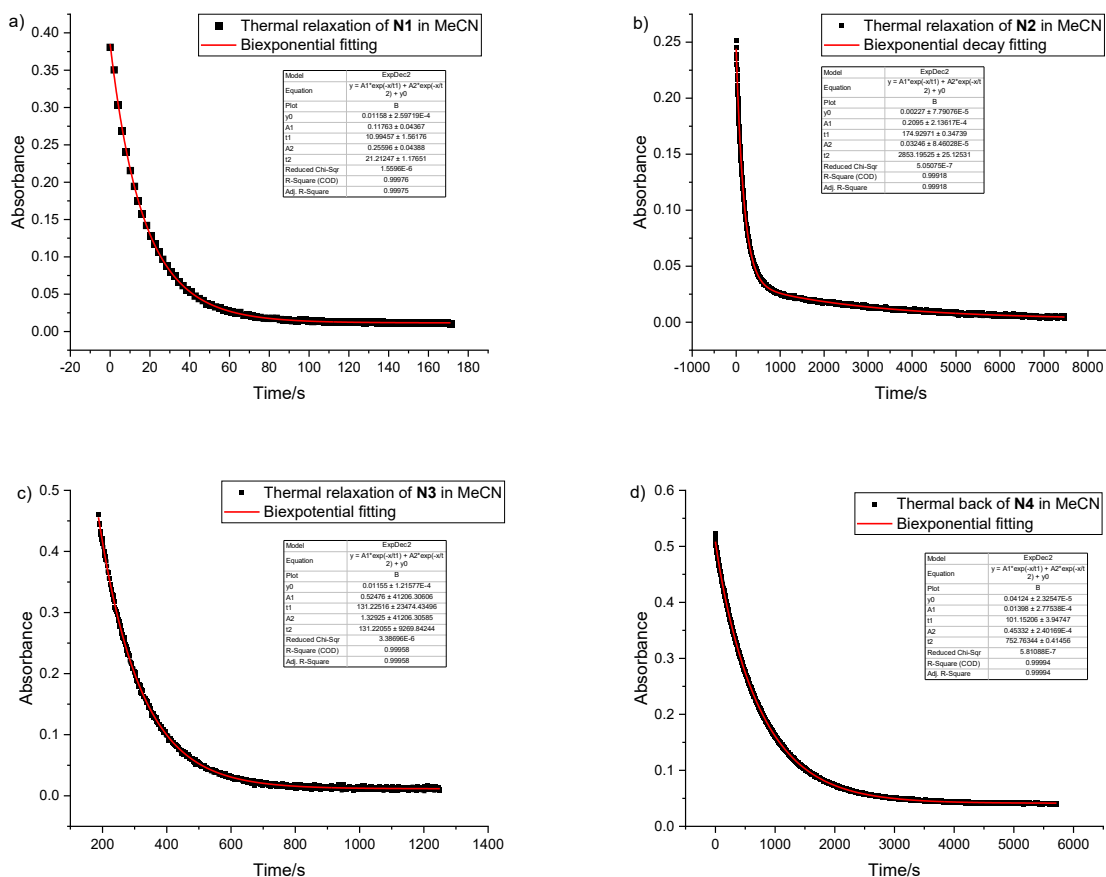


Figure 7.6 The time-resolved absorbance at λ_{max} during thermal relaxation started from PSS (UV) (black dots) and biexponential decay fitting (red line) at 293 K: (a) **N1** in MeCN (data from Chapter 4, Figure 4.5-a), (b) **N2** in MeCN (data from Chapter 4, Figure 4.6-a), (c) **N3** in MeCN (data from Chapter 4, Figure 4.5-b) and (d) **N4** in MeCN (data from Chapter 4, Figure 4.6-b).

Table 7.2 The parameters of biexponential fitting during thermal relaxation of **N1**, **N2**, **N3** and **N4**.^a

	k_1 (10^{-3} s^{-1})	k_2 (10^{-3} s^{-1})	A_1	A_2	A_{th}	R^2
N1	90.9	47.1	0.118	0.256	0.012	0.99
N2	5.72	0.35	0.210	0.032	0.002	0.99
N3	7.62 (7.62076)	7.62 (7.62049)	1.329	0.525	0.012	0.99
N4	9.89	1.33	0.014	0.453	0.041	0.99

[a] $1.5 \times 10^{-5} \text{ M}$ in acetonitrile, 293 K.

7.2 UV/Vis Absorption Spectroscopy

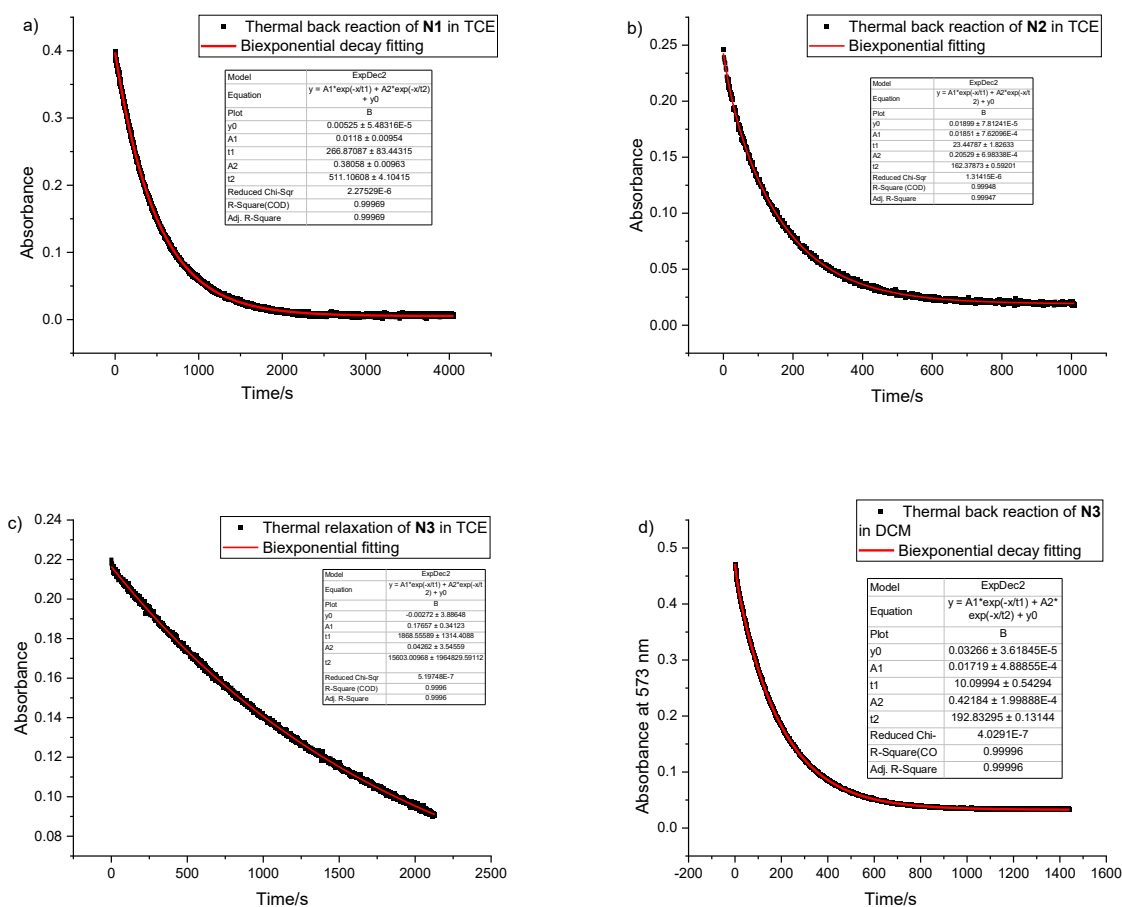


Figure 7.7 The time-resolved absorbance at λ_{\max} during thermal relaxation started from PSS (UV) (black dots) and biexponential decay fitting (red line) at 293 K: (a) N1 in TCE (data from Chapter 4, Figure 4.9-a), (b) N2 in TCE (data from Chapter 4, Figure 4.9-b), (c) N3 in TCE (data from Chapter 4, Figure 4.9-c) and (d) N3 in DCM (data from Chapter 4, Figure 4.9-d).

Table 7.3 The parameters of biexponential fitting during thermal relaxation of N1, N2 and N3.^a

	k_1 (10^{-3} s^{-1})	k_2 (10^{-3} s^{-1})	A_1	A_2	A_{th}	R^2
N1	3.75	1.96	0.012	0.381	0.005	0.99
N2	42.7	6.16	0.019	0.205	0.019	0.99
N3	0.535	0.064	0.177	0.043	-0.002	0.99
N3 ^b	99	5.19	0.017	0.422	0.033	0.99

[a] $1.5 \times 10^{-5} \text{ M}$ in TCE, 293 K. [b] $1.5 \times 10^{-5} \text{ M}$ in DCM.

When the system of **N4** arrived at PSS under UV irradiation, CF, TC and TT isomers existed in the equilibrium. Upon UV light was switched off, 565 nm light was switched on. Two processes were observed in the system: TC→CF and TT→TC + TC→CF. The visible light bleaching kinetics were calculated from time-resolved absorbance at λ_{max} , by fitting the experimental data to the biexponential decay (Figure 7.8). Relevant parameters and coefficients of determination (R^2) are also depicted in Table 7.4.

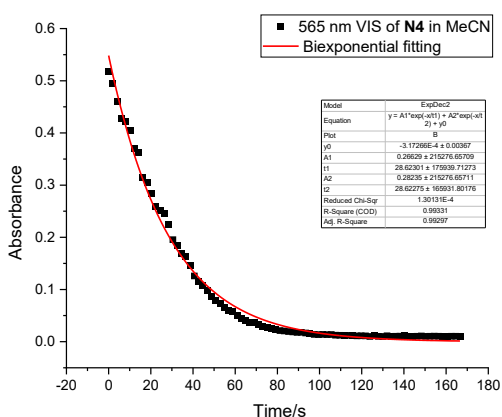


Figure 7.8 The time-resolved absorbance at λ_{max} during visible light irradiation started from PSS (UV) (black dots) and biexponential decay fitting (red line) of **N4** in acetonitrile at 293 K (data from Chapter 4, Figure 4.7).

Table 7.4 The parameters of biexponential fitting of **N4** during irradiation with visible light.^a

	k_1 (10^{-3} s^{-1})	k_2 (10^{-3} s^{-1})	A_1	A_2	A_{th}	R^2
N4	34.9 (34.9372)	34.9 (34.9369)	0.266	0.282	-0.0003	0.99

[a] $1.5 \times 10^{-5} \text{ M}$ in MeCN, 293 K. Visible light: 565 nm, 84 mW/cm².

When the system of **N5**, **N6** and **N7** arrived at PSS under UV irradiation, CF, TC and TT isomers existed in the equilibrium. Upon UV light was switched off, two processes were observed in the system: TC→CF and TT→TC + TC→CF. But the speed of process TT→TC was far slower than the speed of process TC→CF ($k_{\text{TT} \rightarrow \text{TC, thermal}} \ll k_{\text{TC} \rightarrow \text{CF, thermal}}$). The TT form was almost not reduced during the short thermal relaxation time window. Thus, the thermal relaxation kinetics were calculated from time-resolved absorbance measurements at λ_{max} , by fitting the experimental

7.2 UV/Vis Absorption Spectroscopy

data to a monoexponential decay (Figure 7.10). Relevant parameters and coefficients of determination (R^2) are presented in Table 7.5.

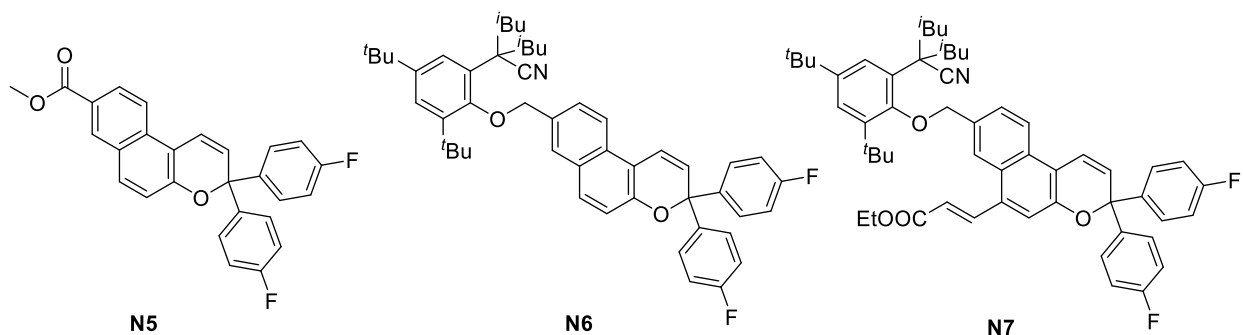


Figure 7.9 The structures of naphthopyrans **N5**, **N6** and **N7**.

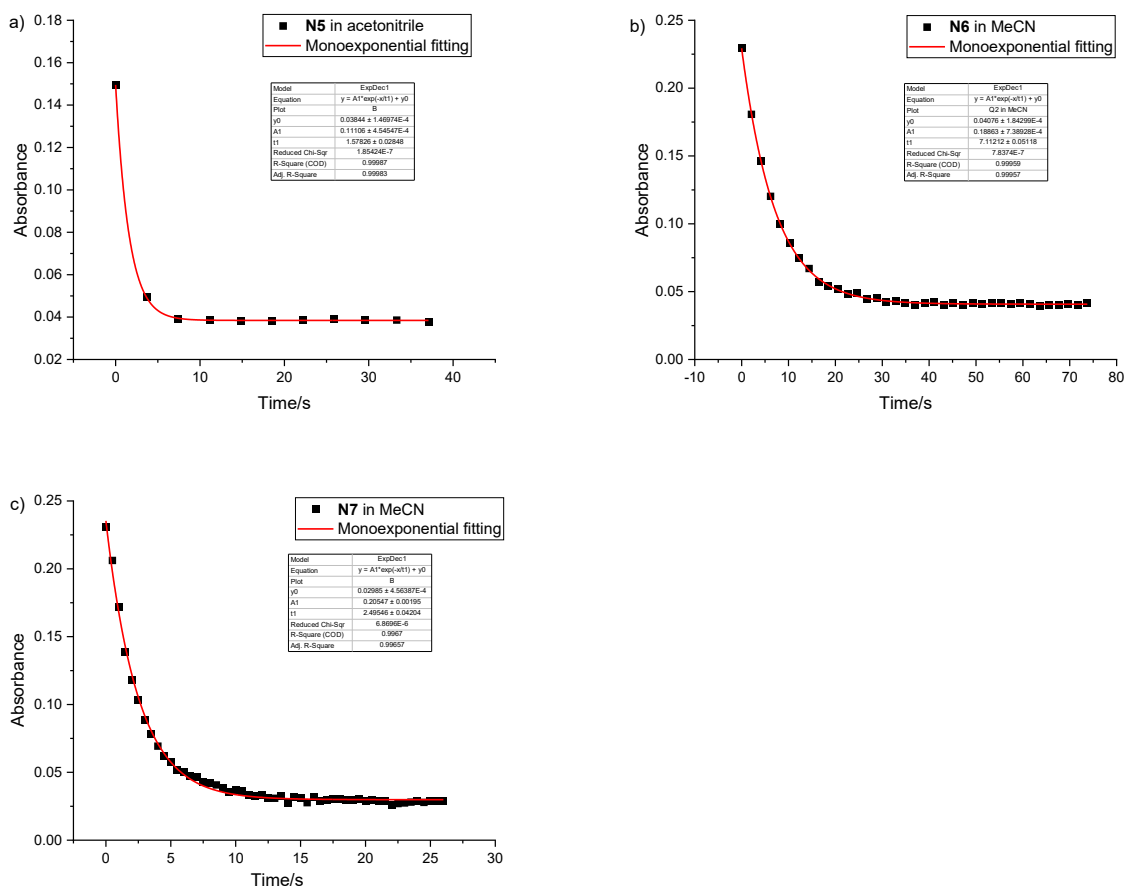


Figure 7.10 The time-resolved absorbance at λ_{\max} during thermal relaxation started from PSS (UV) (black dots) and monoexponential decay fitting (red line) at 293 K: (a) **N5** in MeCN (data from Chapter 4, Figure 4.13-a), (b) **N6** in MeCN (data from Chapter 4, Figure 4.13-b) and (c) **N7** in MeCN (data from Chapter 4, Figure 4.18).

7 Experimental Section

Table 7.5 The parameters of monoexponential fitting of **N5**, **N6** and **N7** during thermal relaxation.^a

	$k_{\text{TC} \rightarrow \text{CF, thermal}}$ (s ⁻¹)	A_{th}	R^2
N5	0.634	0.038	0.99
N6	0.141	0.041	0.99
N7	0.401	0.030	0.99

[a] 1.5×10^{-5} M in acetonitrile, 293 K.

After thermal relaxation in the UV/Vis measurements, there were only two isomers, TT and CF, in the system of **N5**, **N6** and **N7**. Upon visible light (420 nm for **N5** and **N6**; 505 nm for **N7**) was switched on, the process, TT→TC→CF existed in the system. Wherein the process TT→TC was the rate determining step because of the faster speed of TC→CF. Accordingly, the time-resolved absorbance at λ_{max} was studied by using a monoexponential decay model during visible light irradiation (Figure 7.11). Relevant parameters and coefficients of determination (R^2) are presented in Table 7.6.

Table 7.6 The parameters of monoexponential fitting of **N5**, **N6** and **N7** during irradiation with visible light.^a

	$k_{\text{TT} \rightarrow \text{TC, Vis}}$ (s ⁻¹)	A_{th}	R^2
N5^b	0.150	0.023	0.97
N6^b	0.106	0.022	0.98
N7^c	0.149	0.008	0.94

[a] 1.5×10^{-5} M in acetonitrile, 293 K. [b] Visible light: 420 nm, 73 mW/cm². [c] Visible light: 505 nm, 70 mW/cm².

7.2 UV/Vis Absorption Spectroscopy

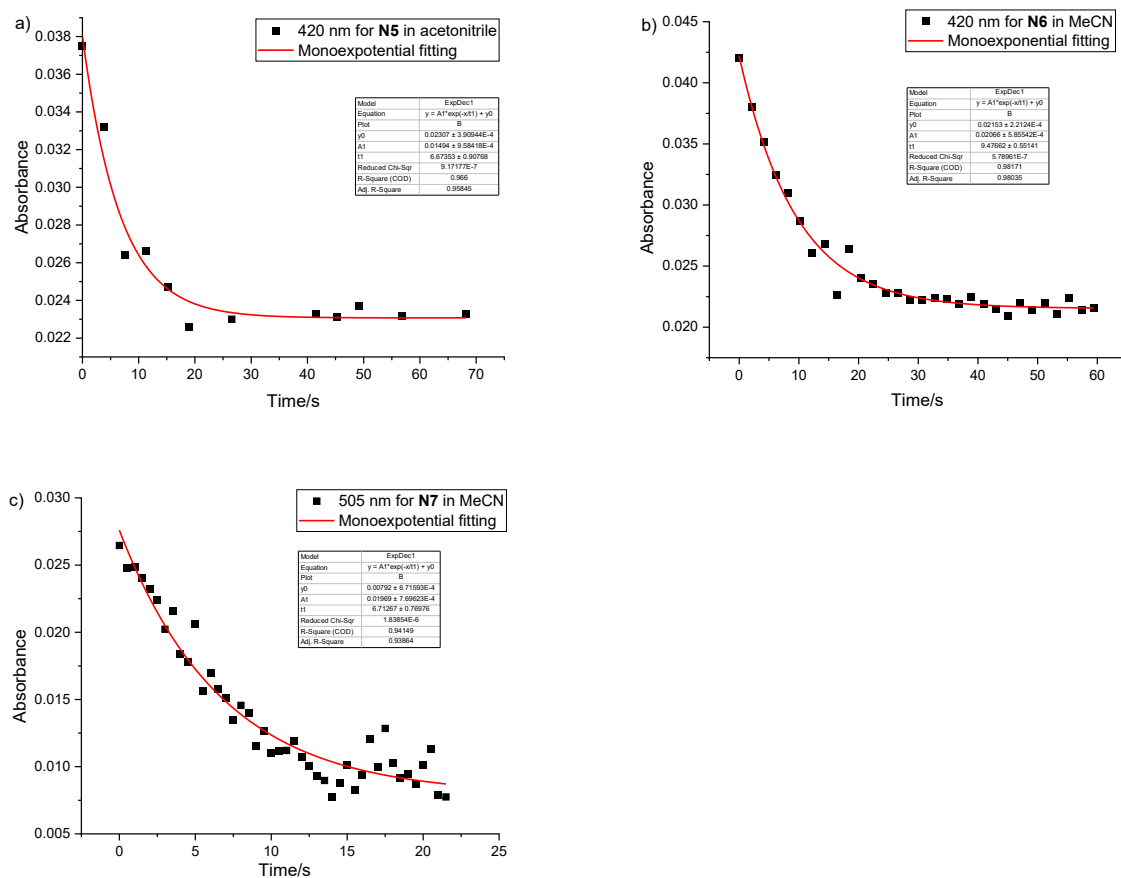


Figure 7.11 The time-resolved absorbance at λ_{\max} during visible light irradiation (black dots) and monoexponential decay fitting (red line) at 293 K: (a) **N5** in MeCN (data from Chapter 4, Figure 4.13-a), (b) **N6** in MeCN (data from Chapter 4, Figure 4.13-b) and (c) **N7** in MeCN (data from Chapter 4, Figure 4.18).

7.3 *In-situ* NMR Measurement

The set-up of *in-situ* NMR measurements is depicted in Figure 7.12. A 6 m optical fibre was used for transmitting light. The light source were LED lights, which were connected with an attachment to the fiber (Figure 7.12 right). The other tip of the fiber was prepared based on the literature^[139] and inserted into the NMR tube with the samples (Figure 7.12 left).



Figure 7.12 The device of *in-situ* NMR measurements.

As demonstrated in Figure 7.13, the cladding of 5 cm of the fiber was removed from one end of the fiber, which will be inserted into the NMR tube. Then the top 3 cm fiber was sand blasted to make sure the light is distributed over the whole distance of the NMR sample (Figure 7.11 middle). At last, the prepared end of the fiber was put into a NMR-tube insertion made from quartz glass with an absorption <300 nm. Now the other tip of fiber, which will be inserted into the NMR tube, was prepared well.

The NMR samples were prepared with acetonitrile- d_3 in a concentration of 1×10^{-2} M. At first, 0.4 mL prepared sample were transferred into an amber NMR tube (absorption spectrum demonstrated in Figure 7.14). At second, the prepared NMR-tube insertion with a cap was put into the NMR tube. At last, the NMR tube was carefully inserted into the *Bruker Avance III* 500 MHz NMR spectrometer, which was already cooled down to 238 K. After one spectrum of the closed form was measured, UV light was switched on and the NMR spectra were measured one by one with the same delay time, and all the spectra were analysed by *Topspin 3.5pl7* software.

7.3 *In-situ* NMR measurement

For ^1H NMR measurements, 8 scans were detected per spectrum. Every spectrum was obtained in 46 s and there was 1 s delay time between two spectra. For ^{19}F NMR measurements, 32 scans were detected per spectrum. Every spectrum was obtained in 66 s and there was 1 s delay time between two spectra.

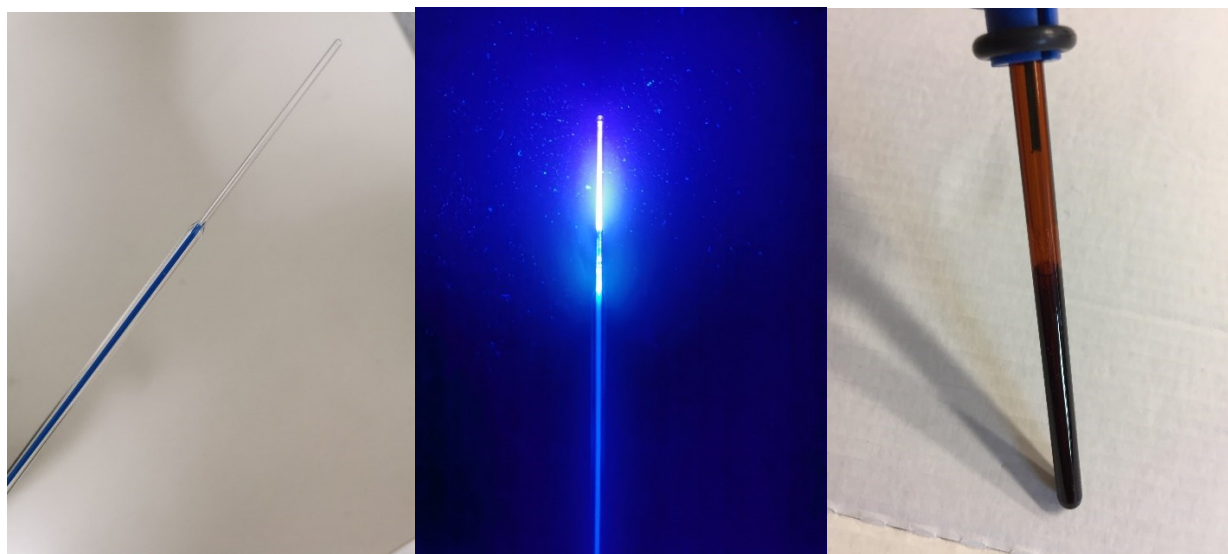


Figure 7.13 The prepared NMR-tube insertion with roughened fiber inside (left); the NMR-tube insertion when UV light was switched on (middle); the brown NMR tube with prepared insertion inside (right).

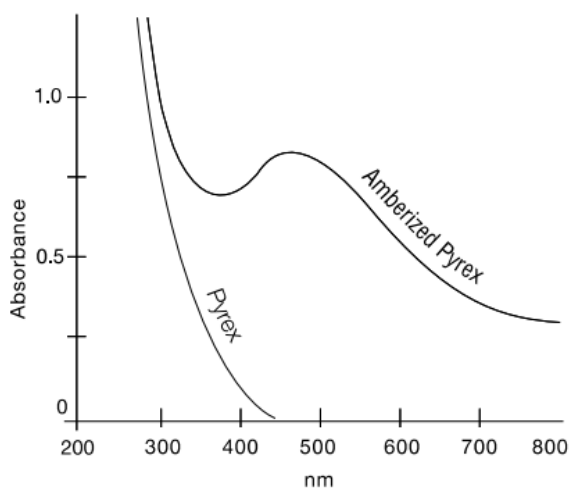
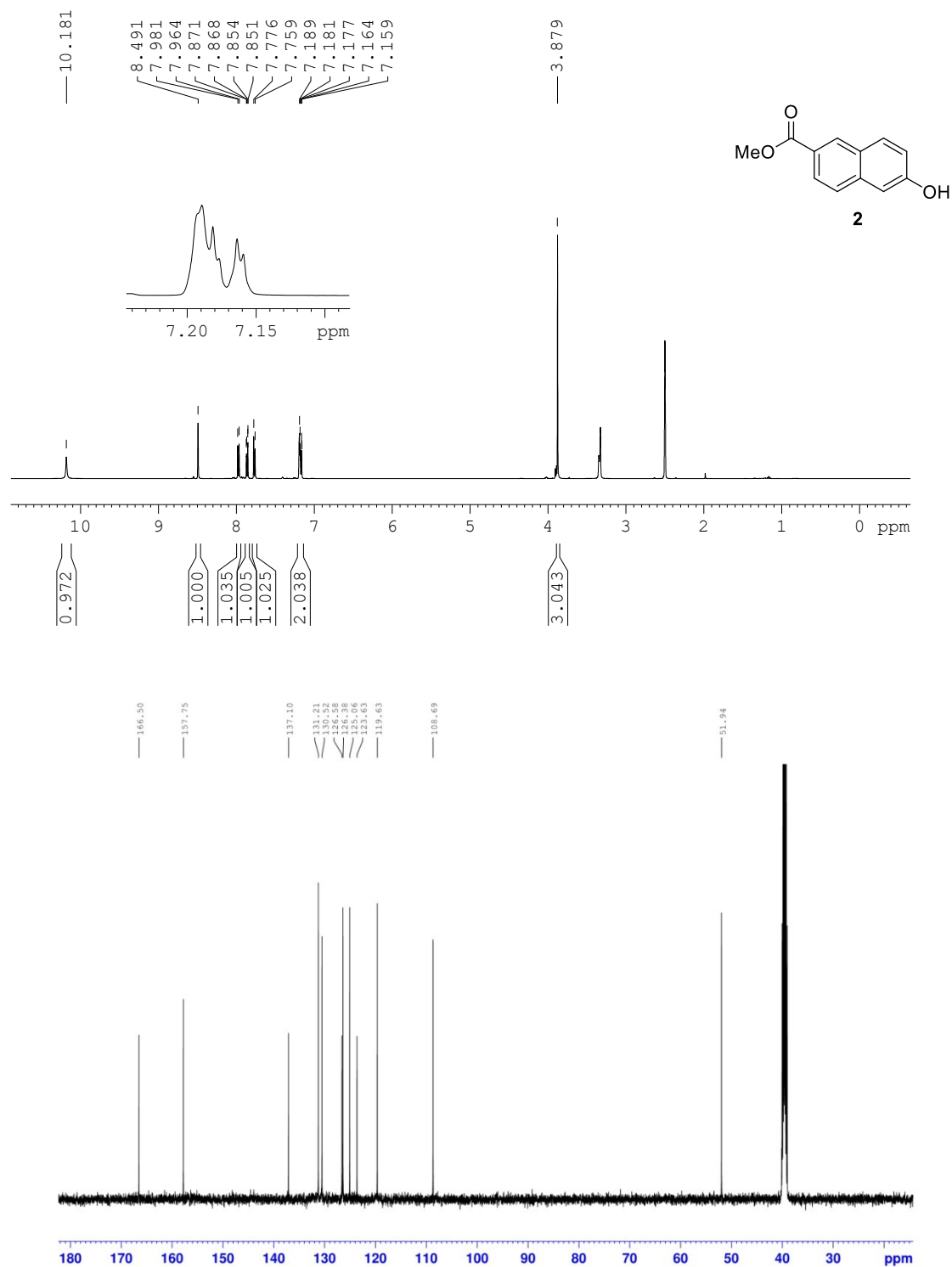
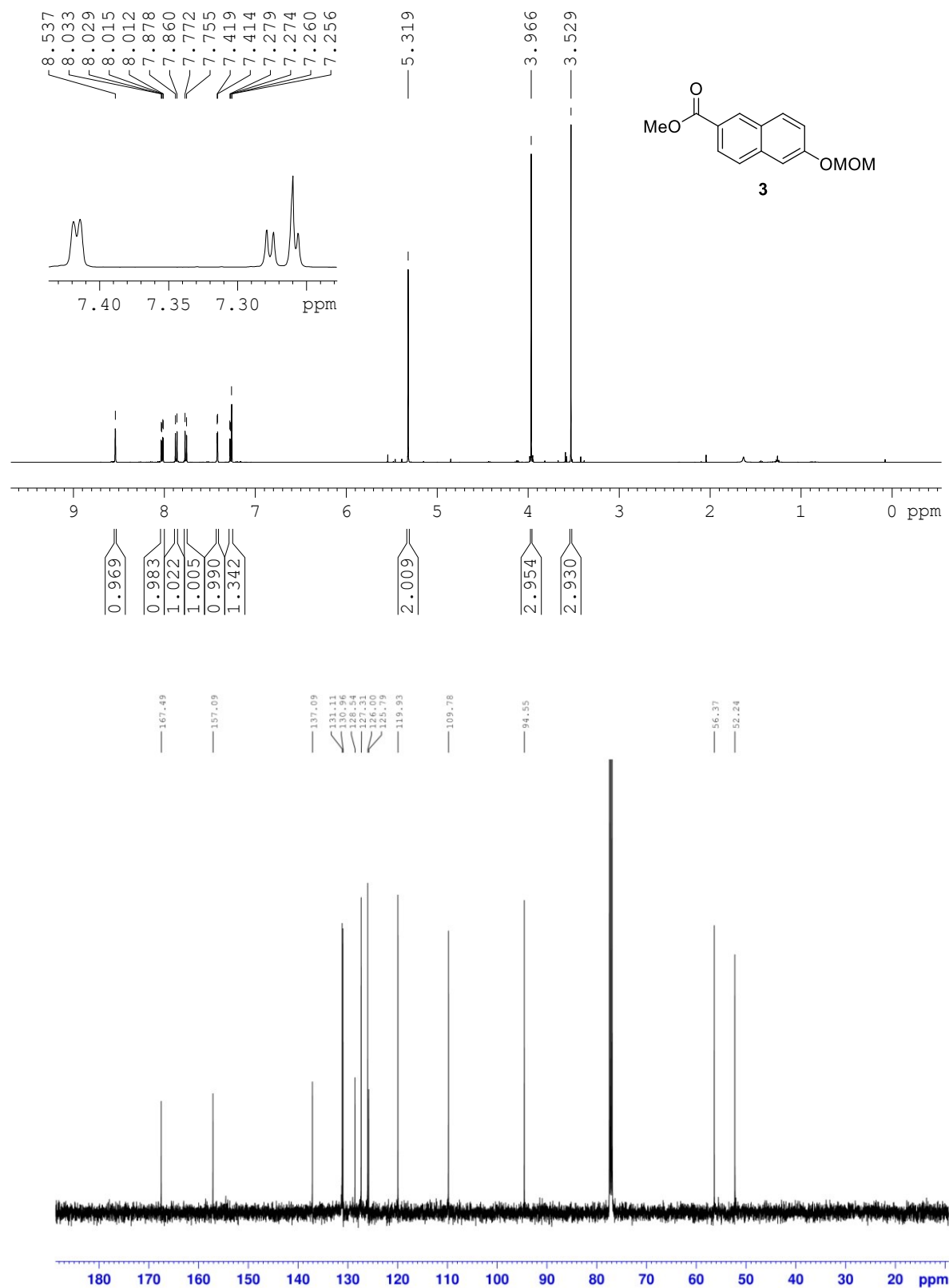


Figure 7.14 The absorption spectrum of amberized Pyrex NMR tube (provided by Deutero).

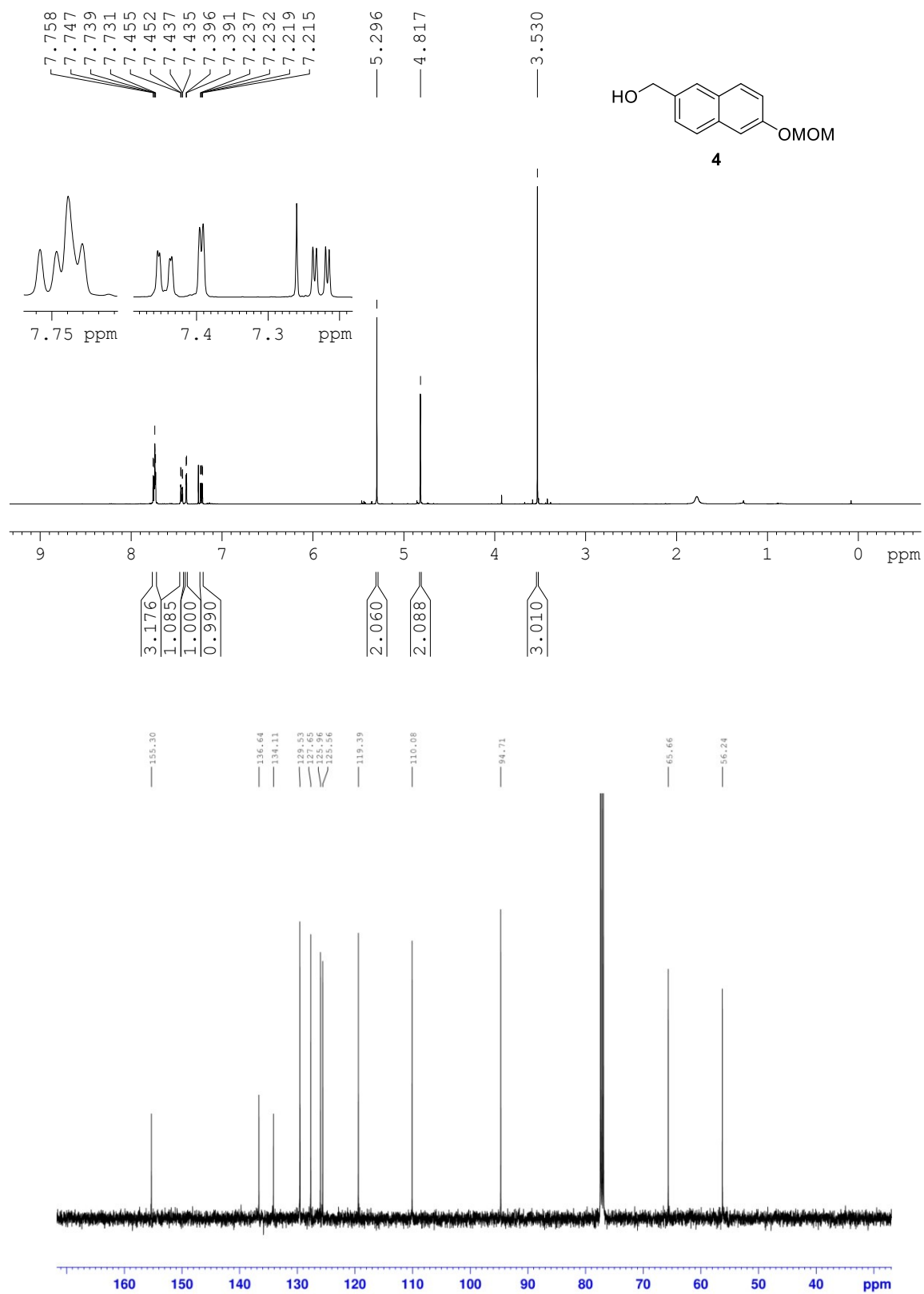
8. Appendix

8.1 ^1H and ^{13}C NMR Spectra

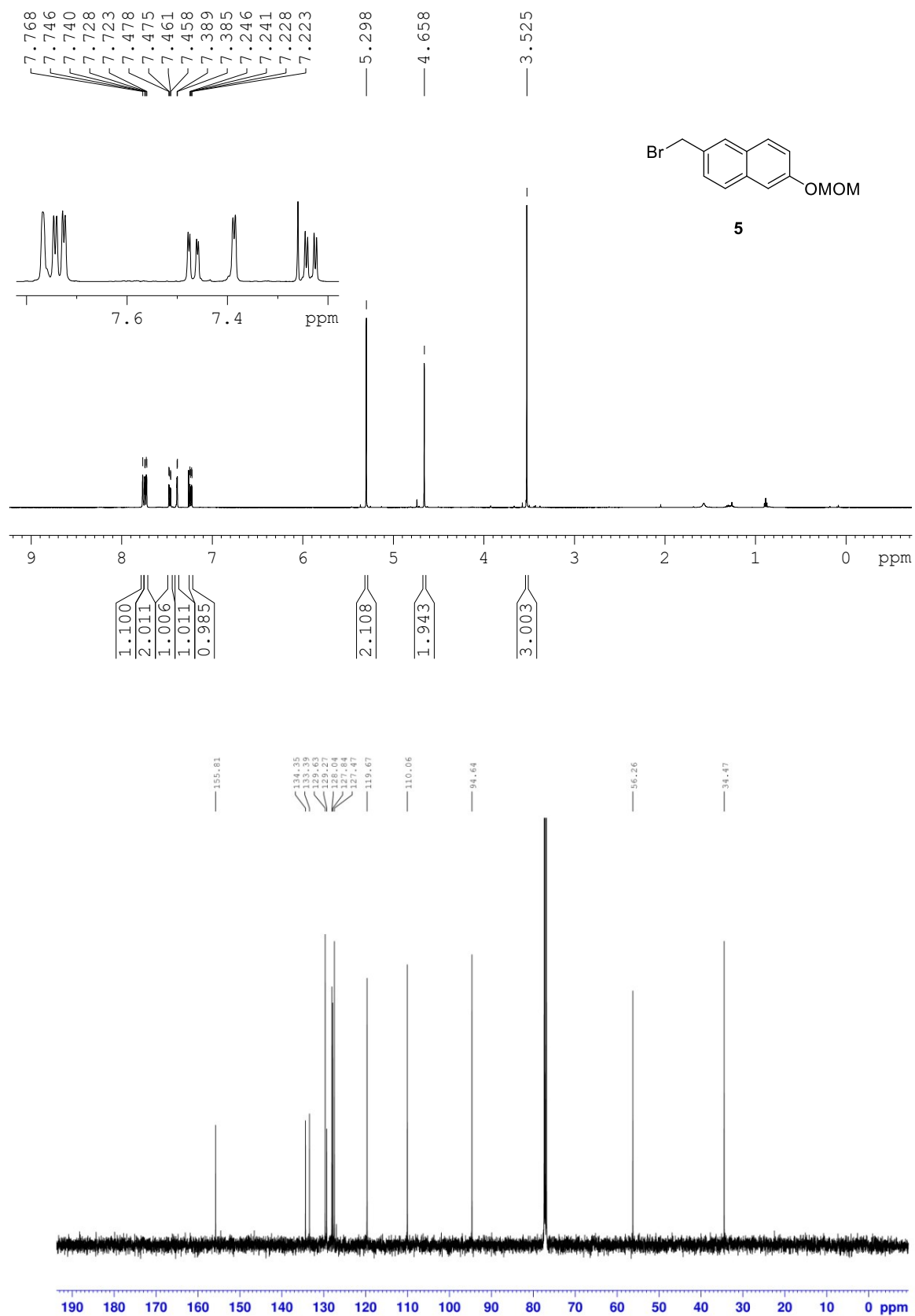
8.1 ^1H and ^{13}C NMR Spectra



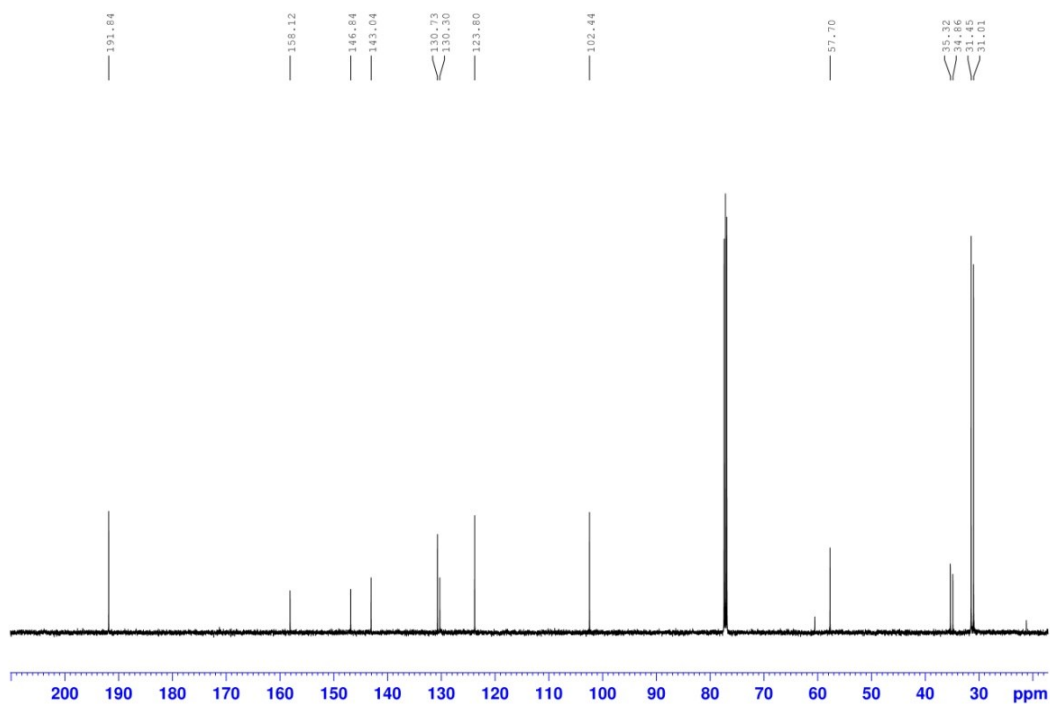
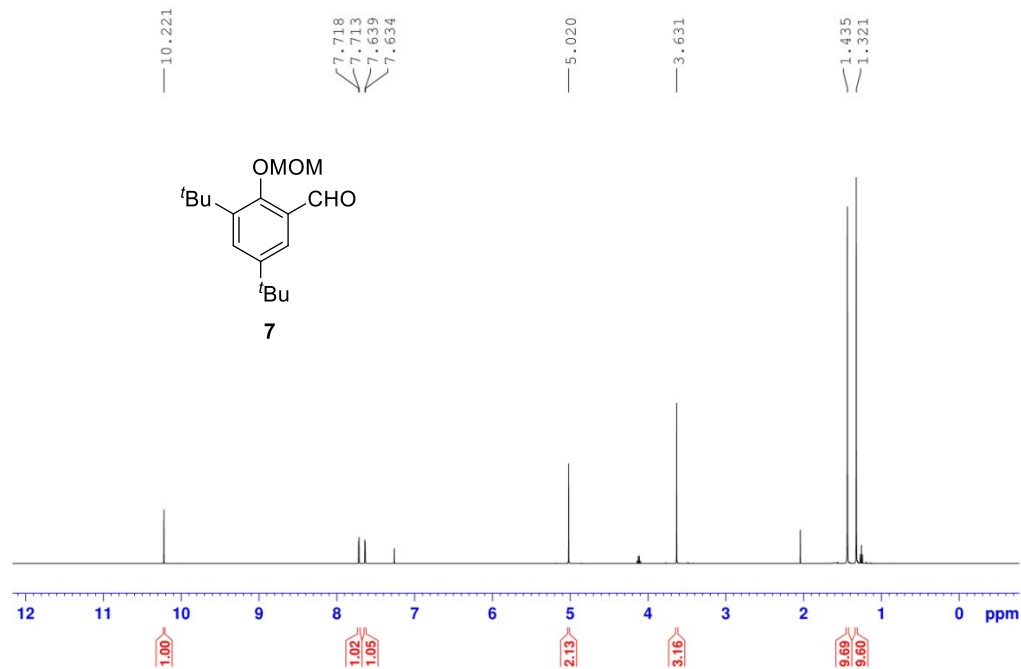
8 Appendix



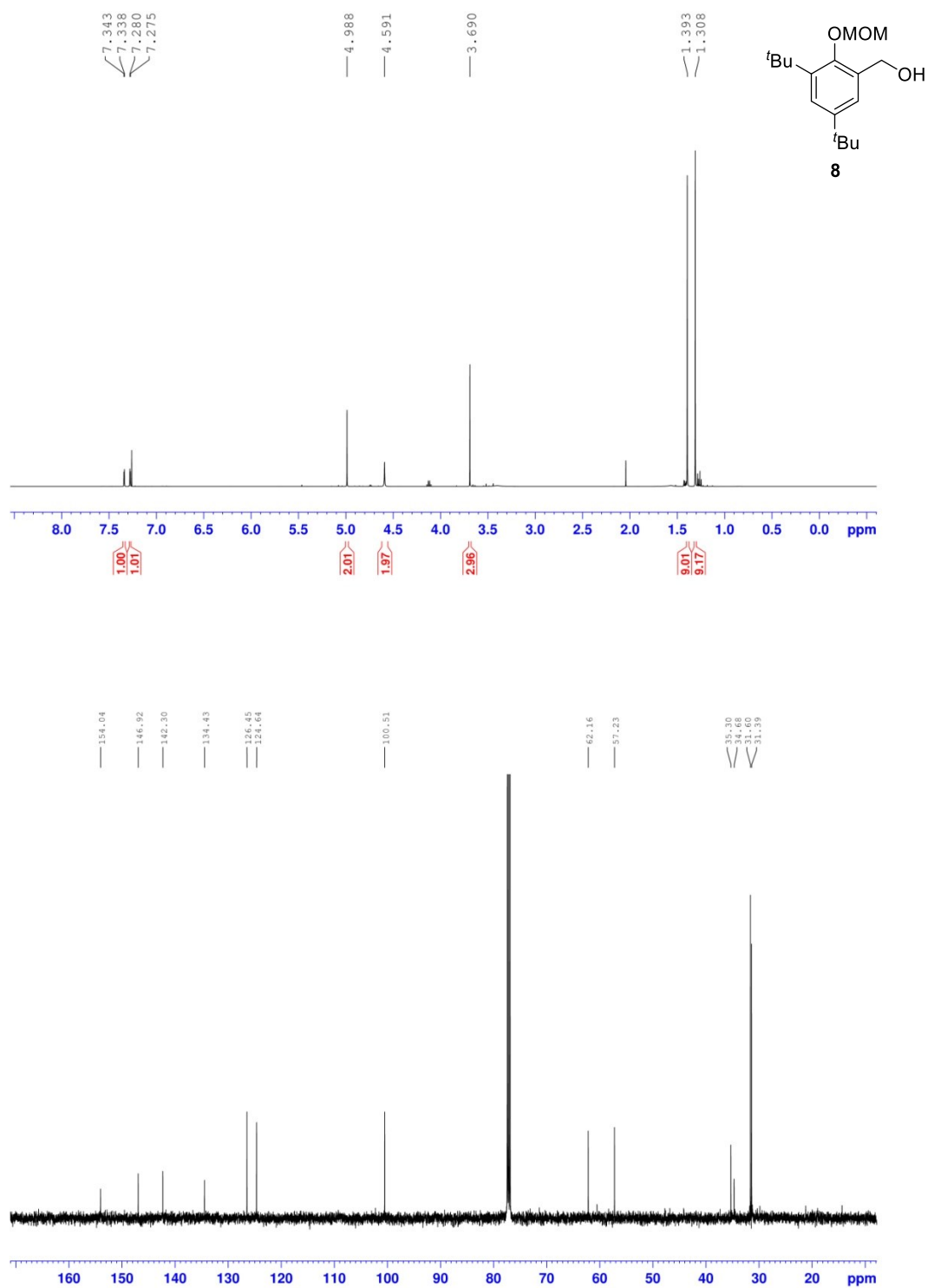
8.1 ^1H and ^{13}C NMR Spectra



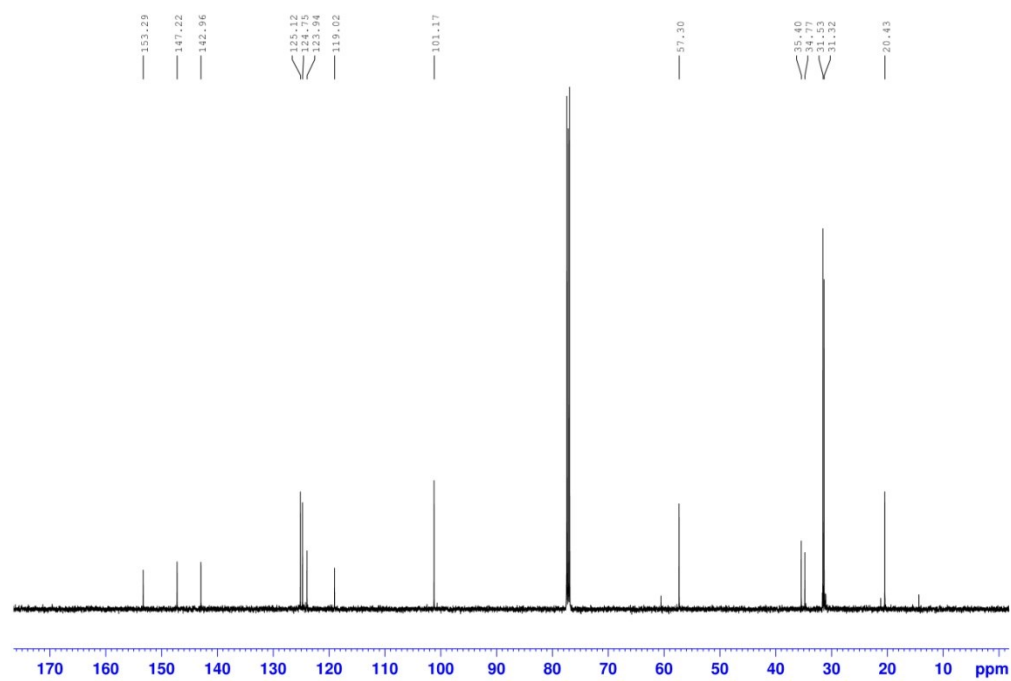
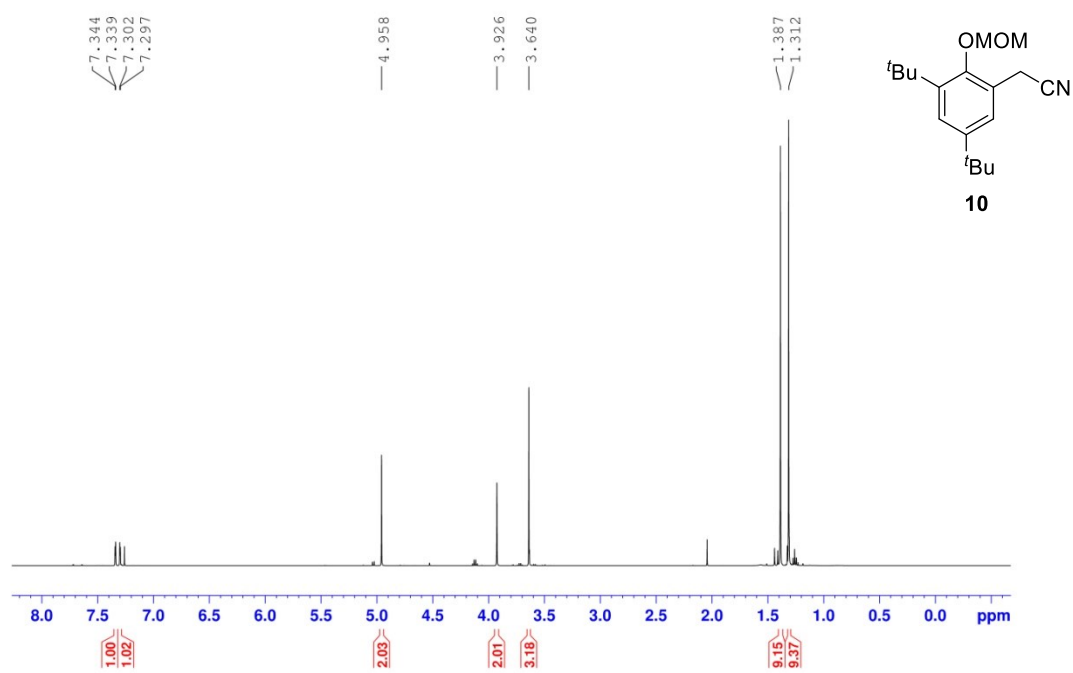
8 Appendix



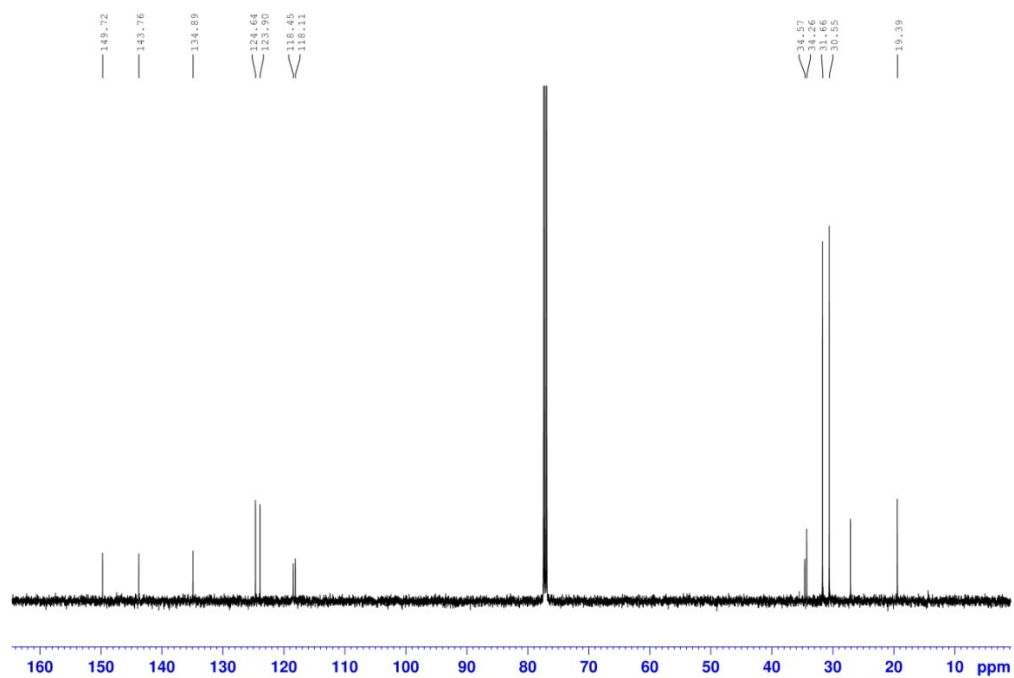
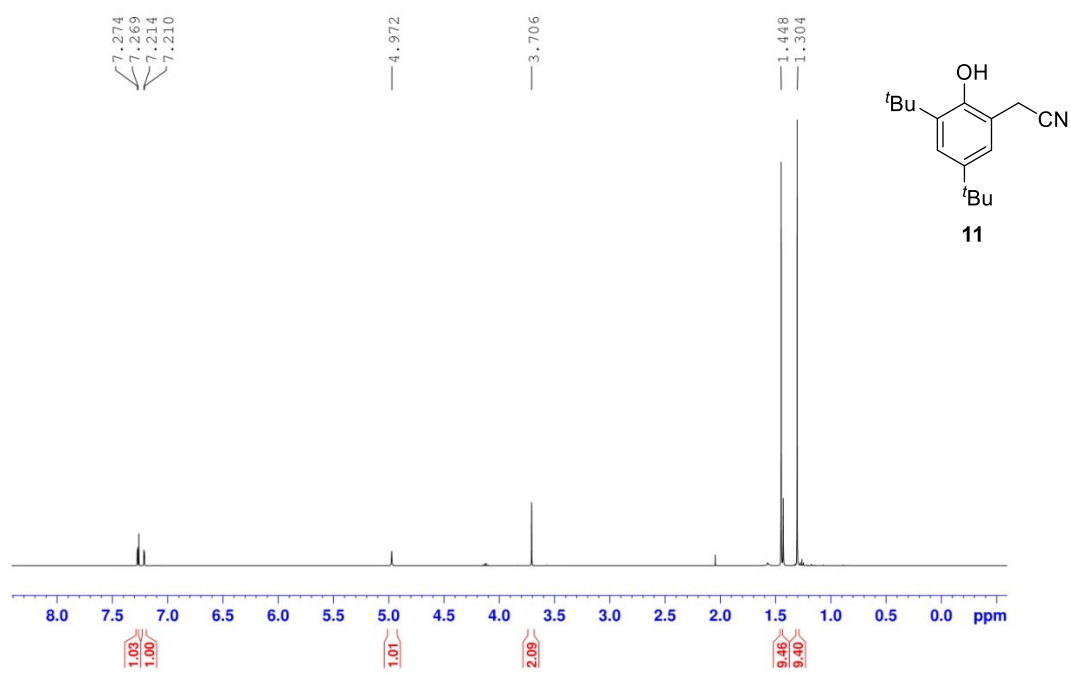
8.1 ^1H and ^{13}C NMR Spectra

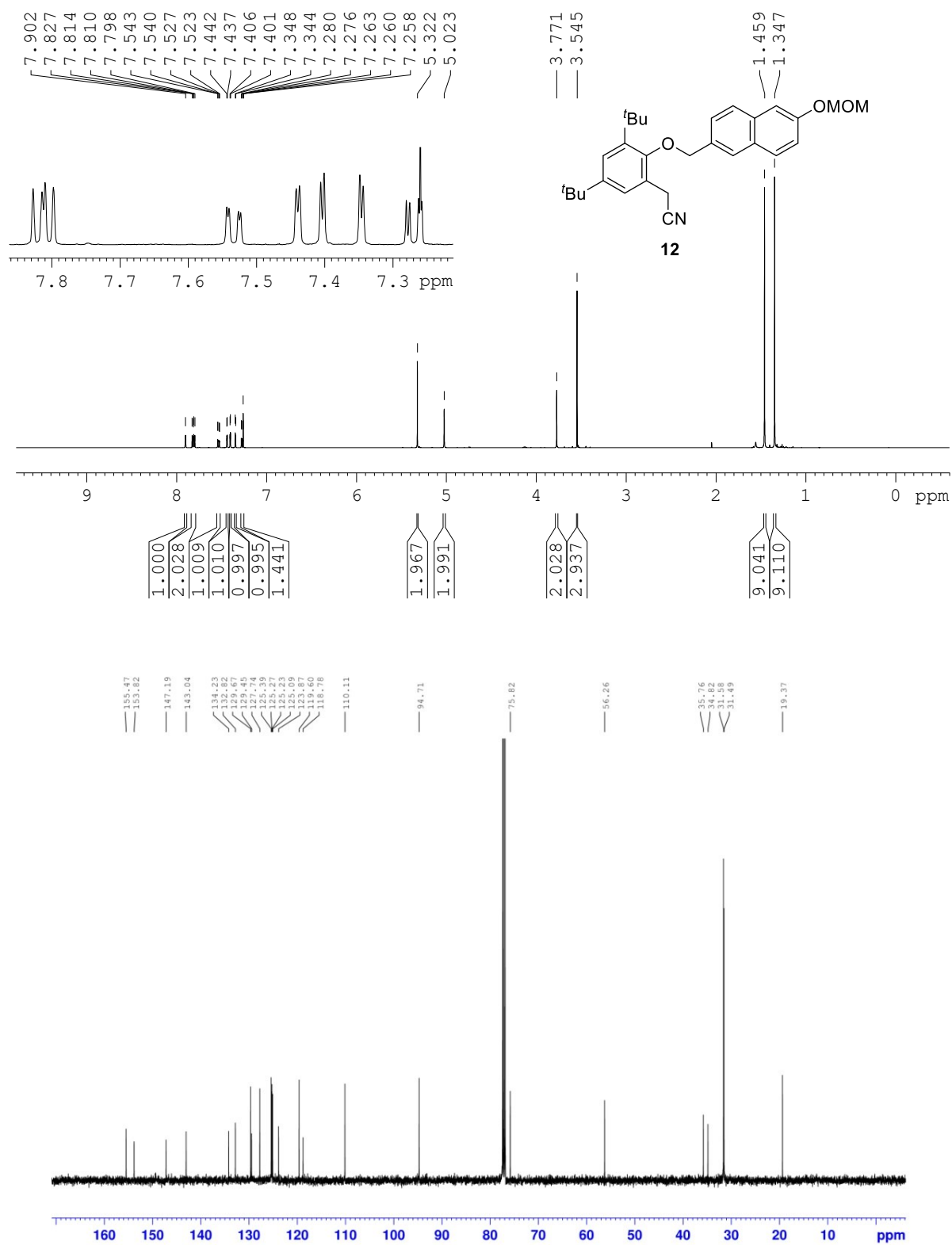


8 Appendix

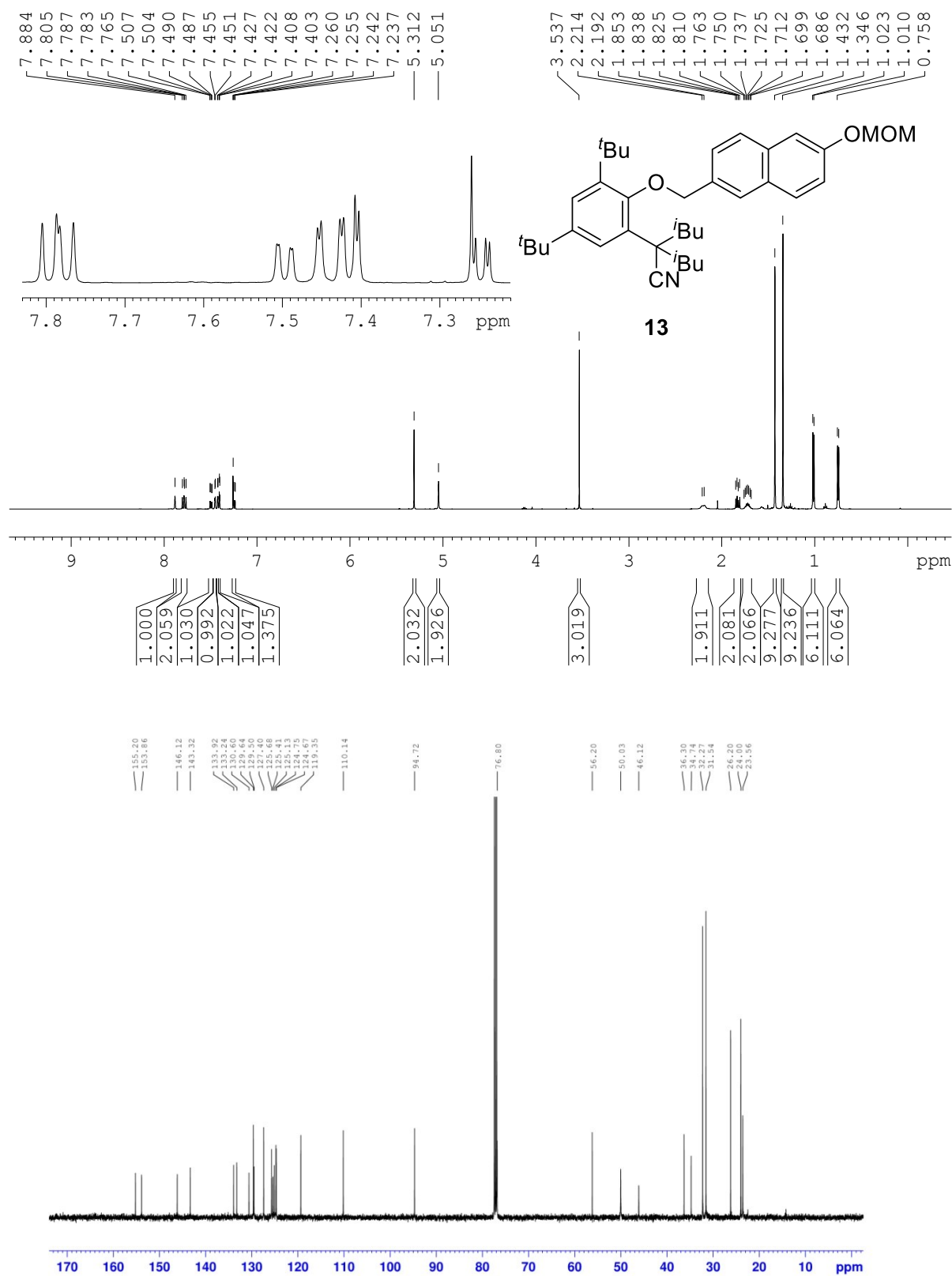


8.1 ^1H and ^{13}C NMR Spectra

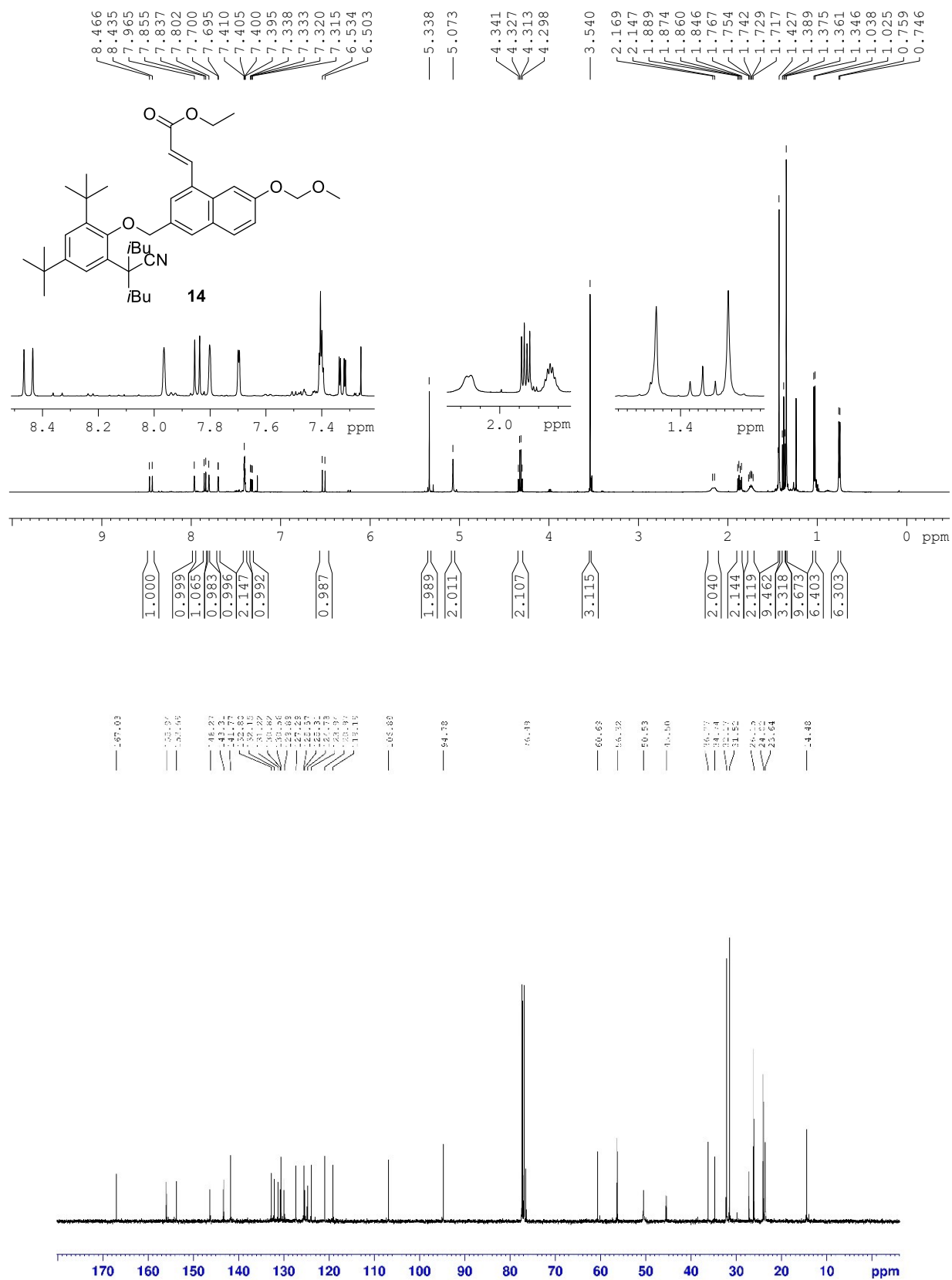




8.1 ^1H and ^{13}C NMR Spectra

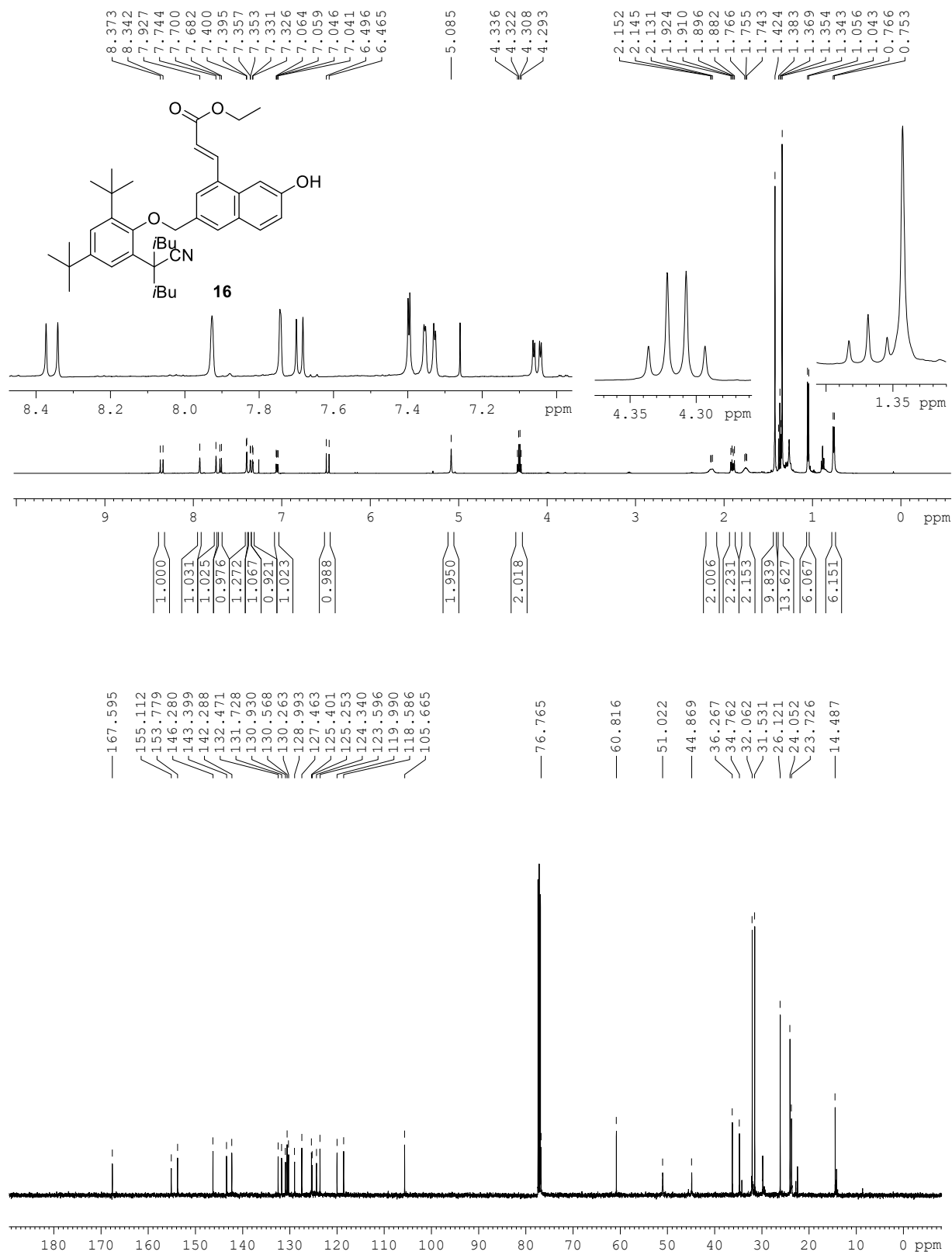


8 Appendix

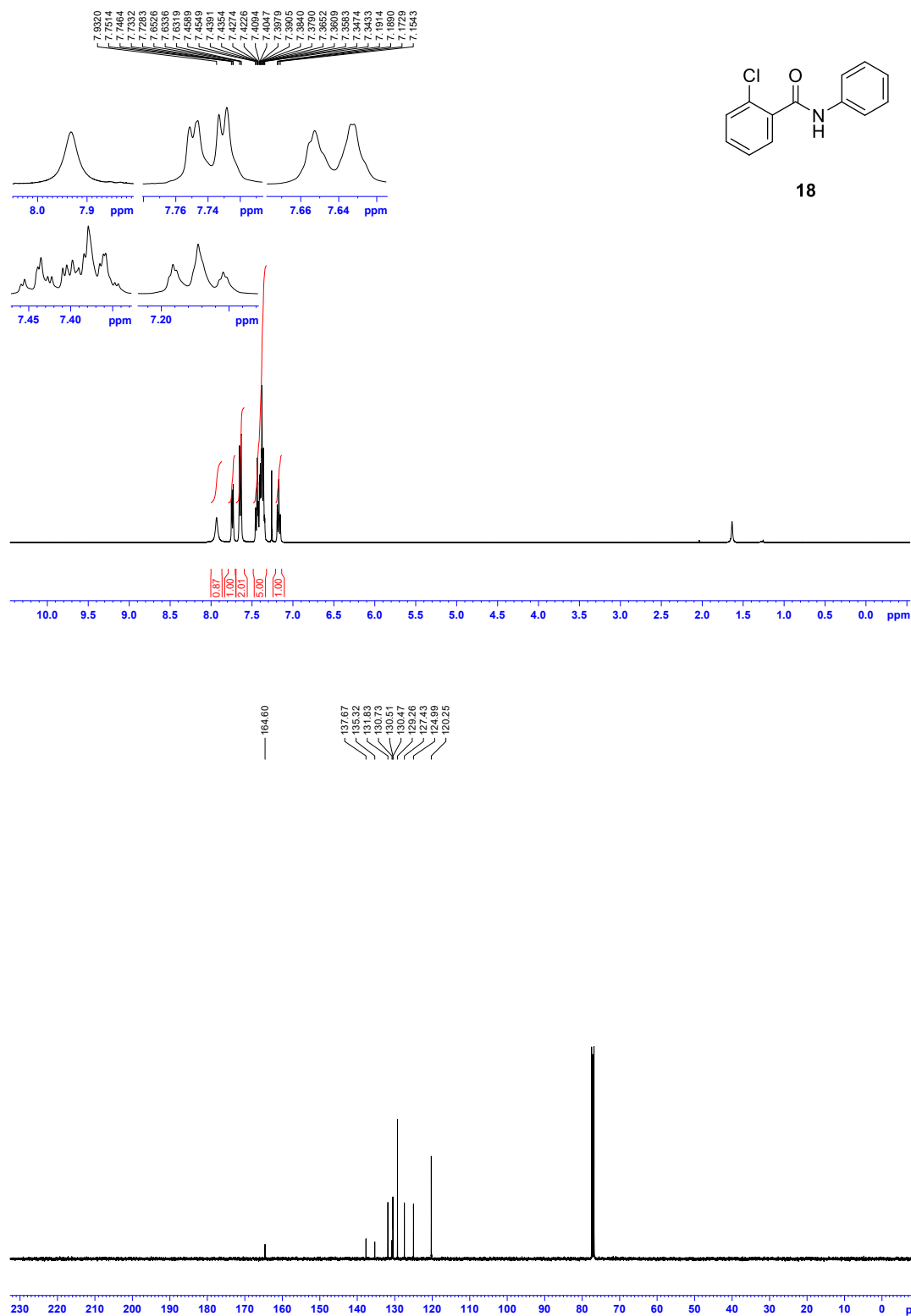




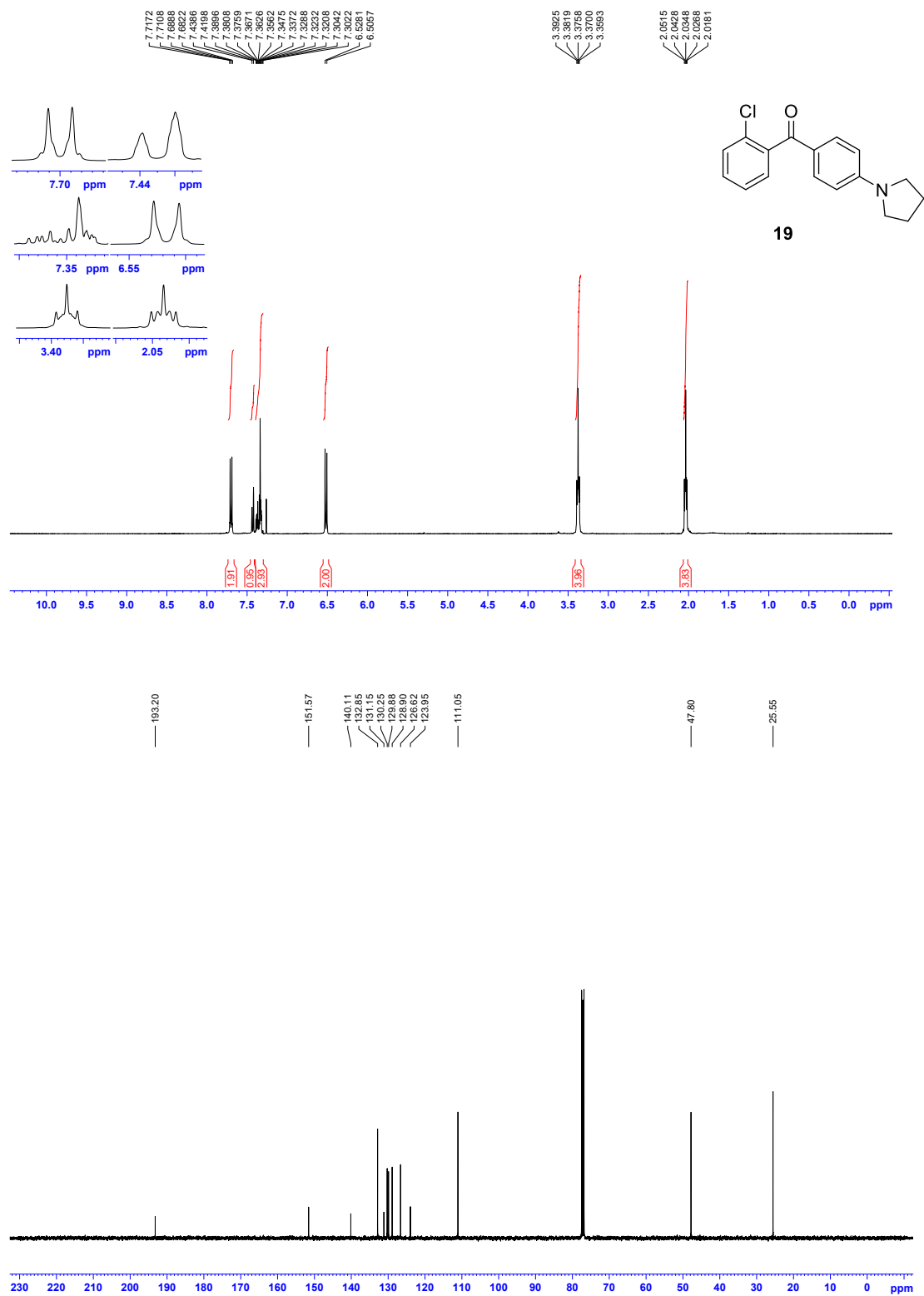
8 Appendix



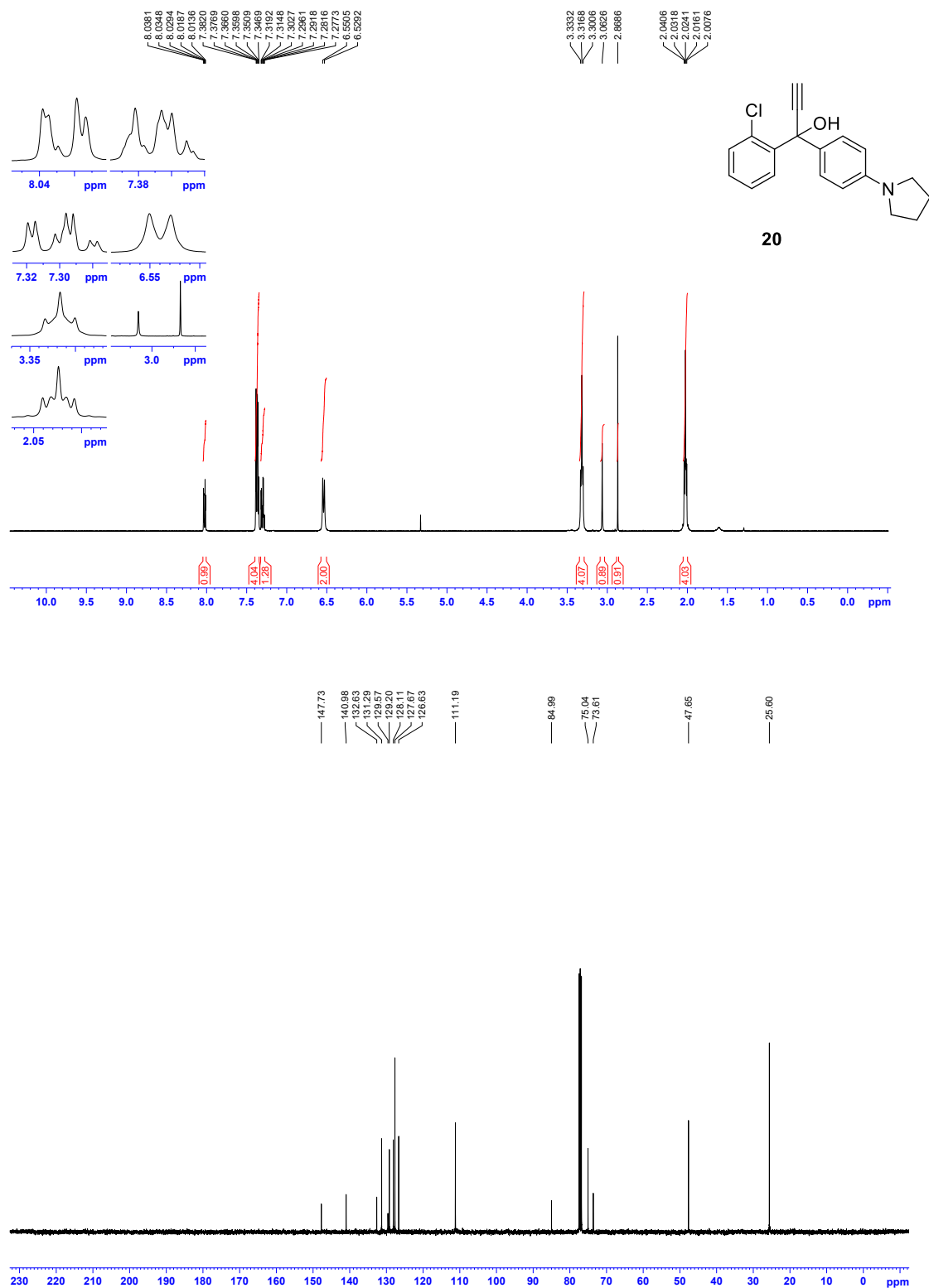
8.1 ^1H and ^{13}C NMR Spectra



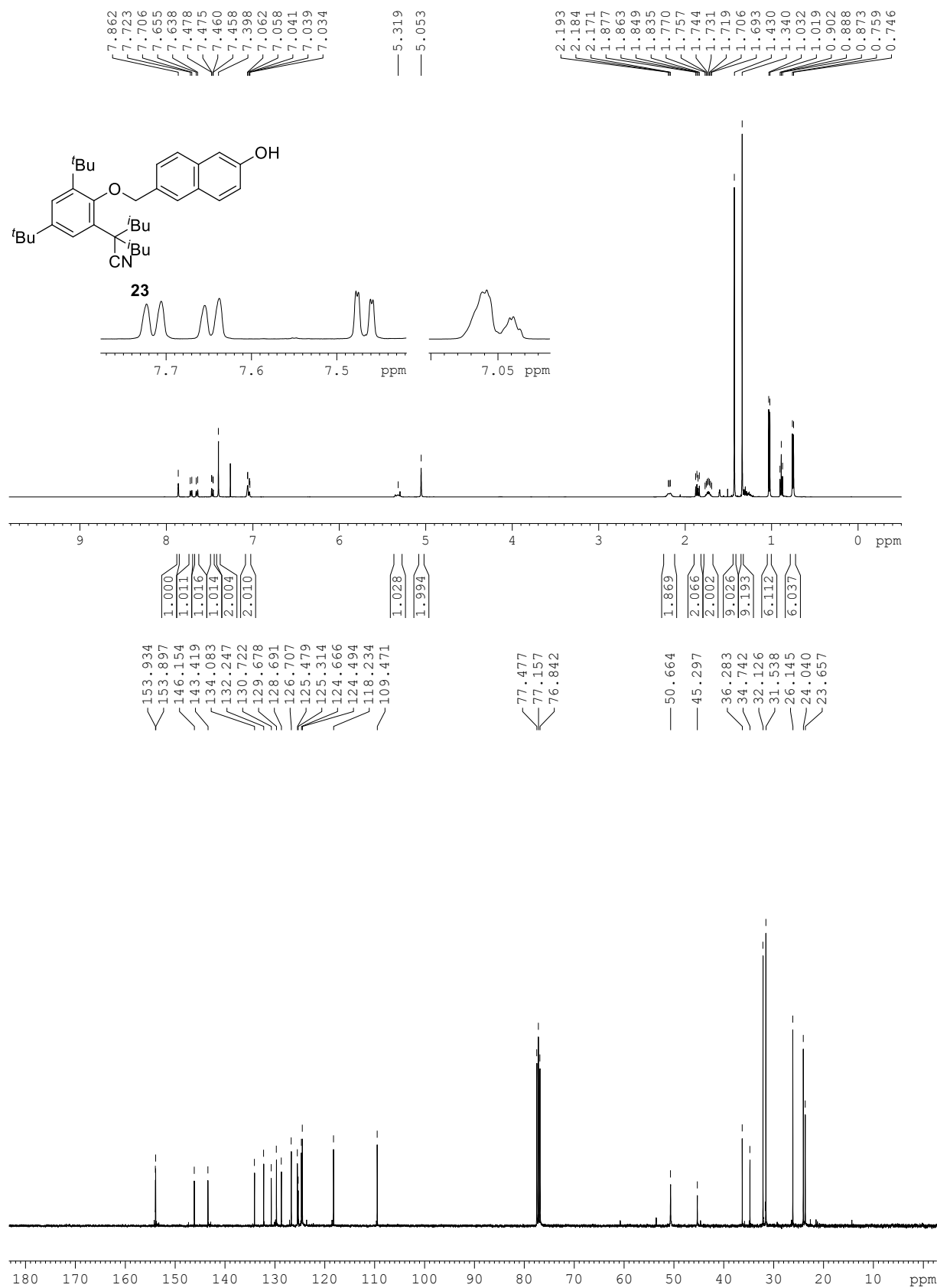
8 Appendix



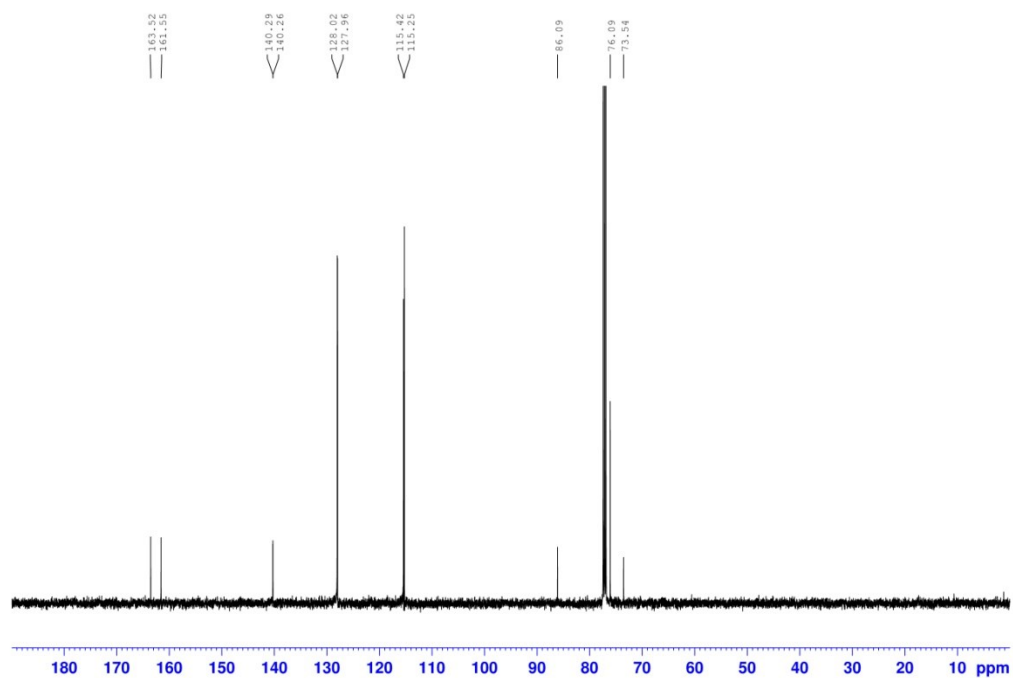
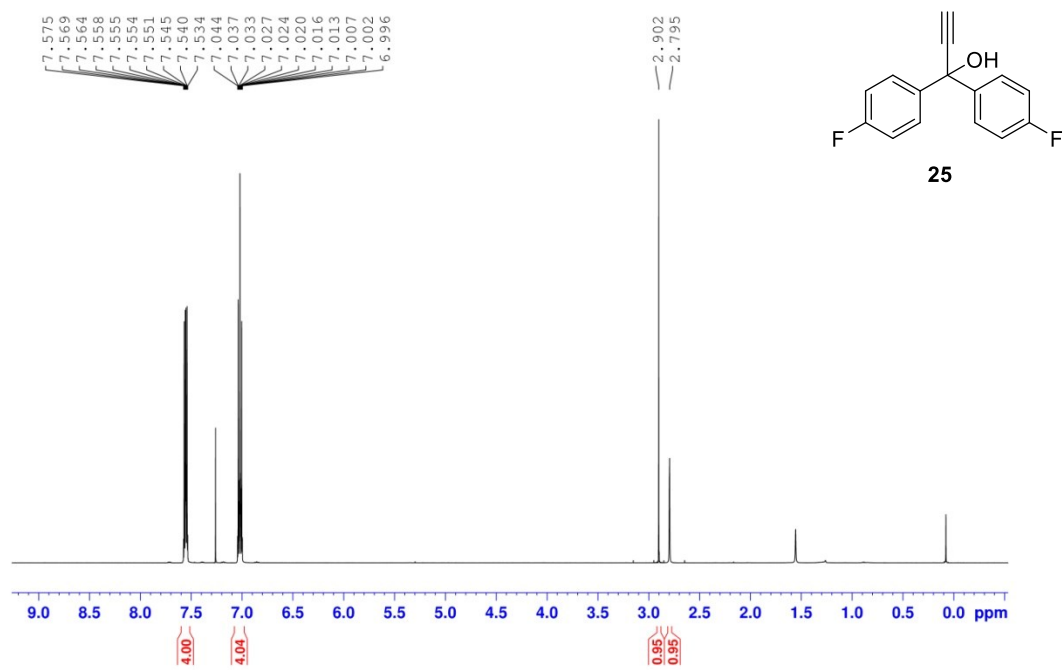
8.1 ^1H and ^{13}C NMR Spectra

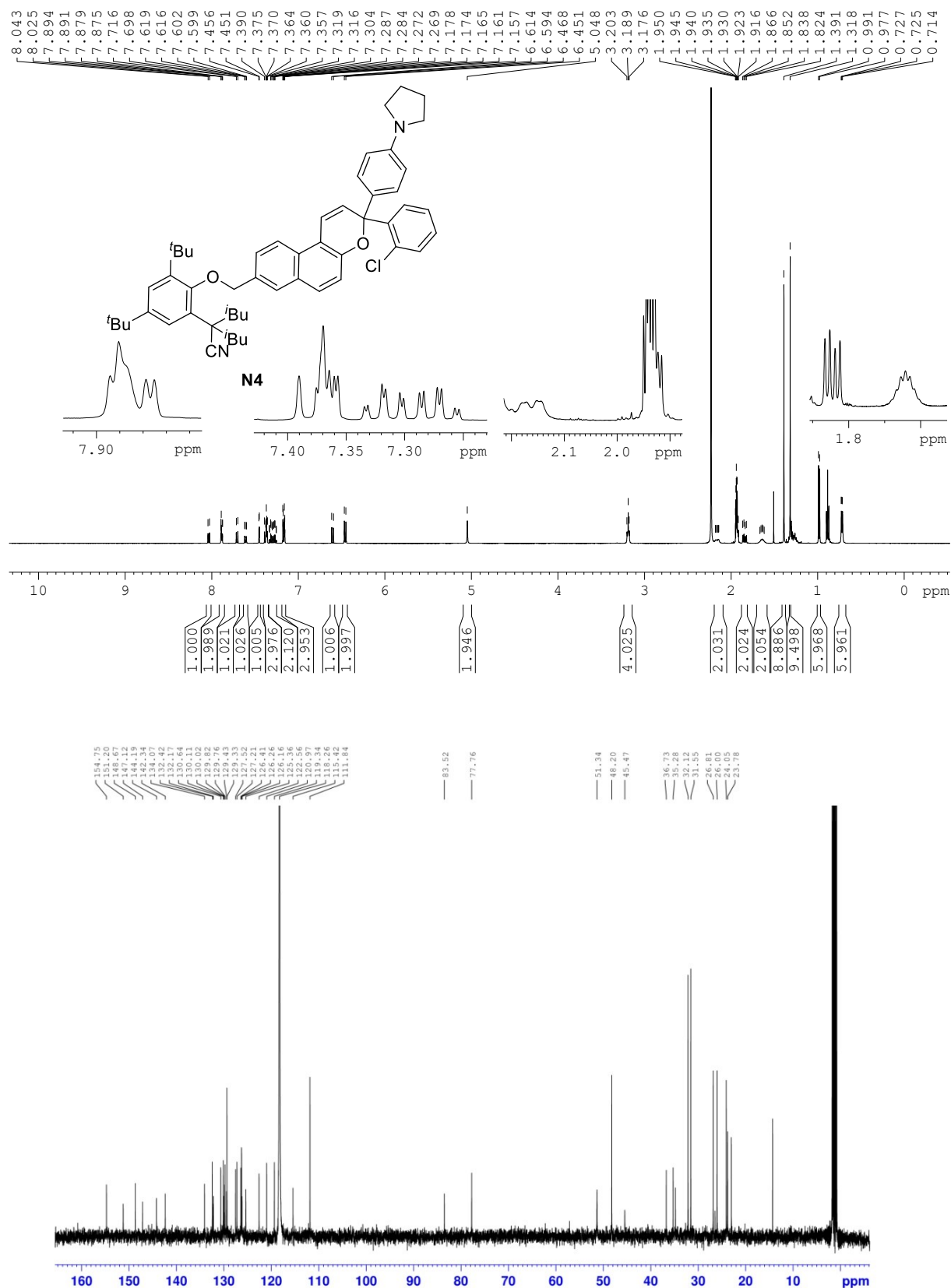


8 Appendix

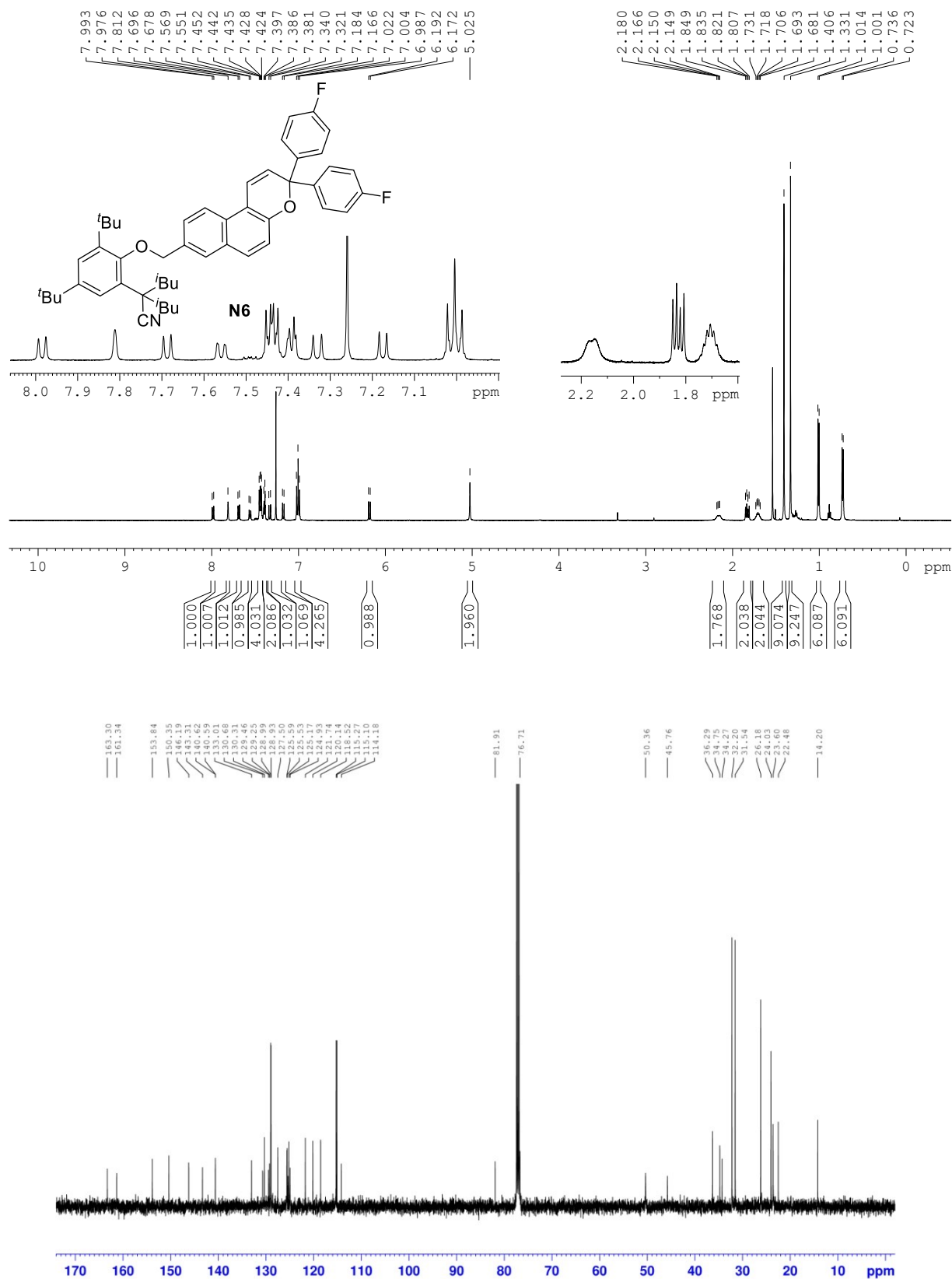


8.1 ^1H and ^{13}C NMR Spectra

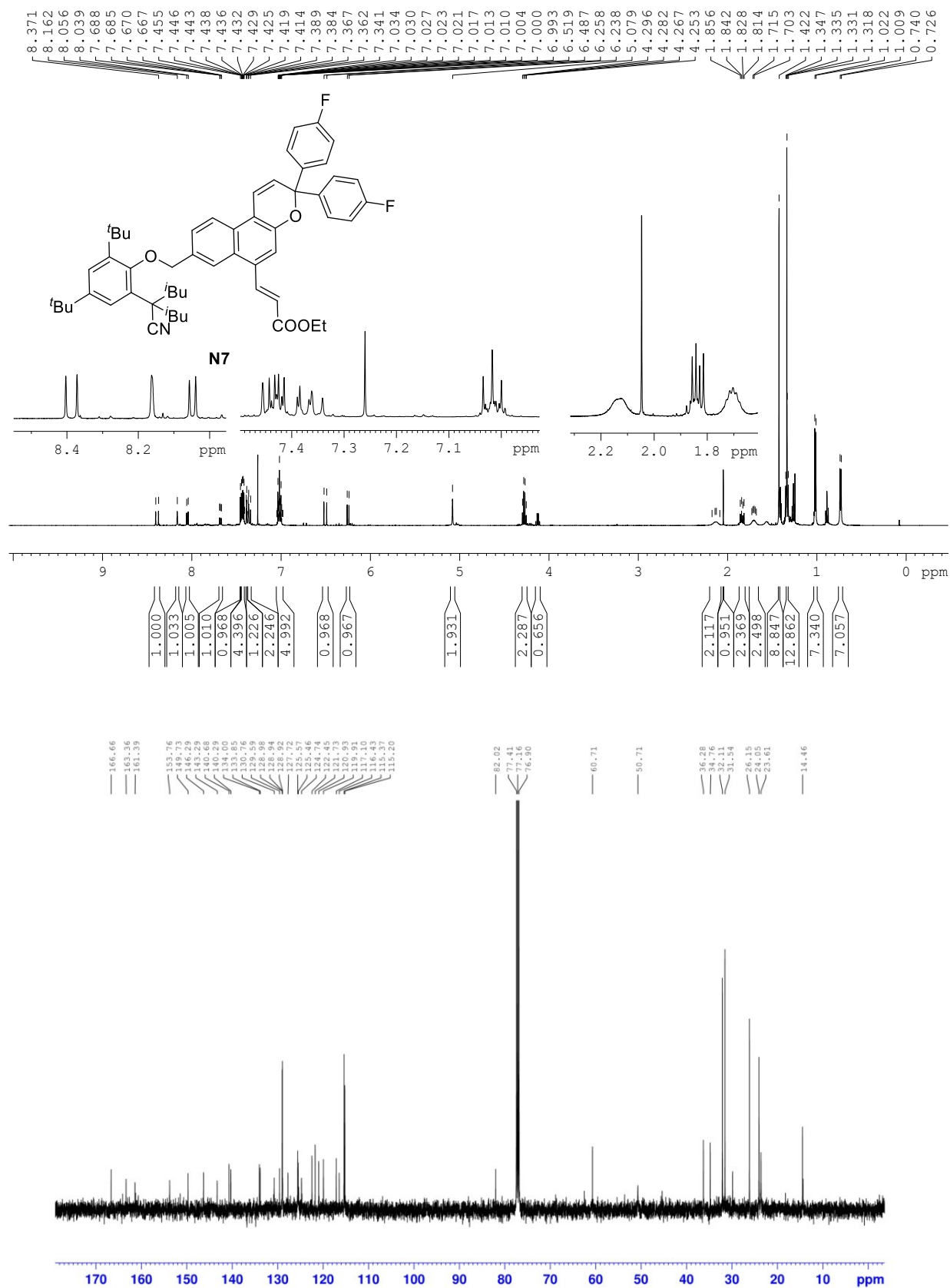




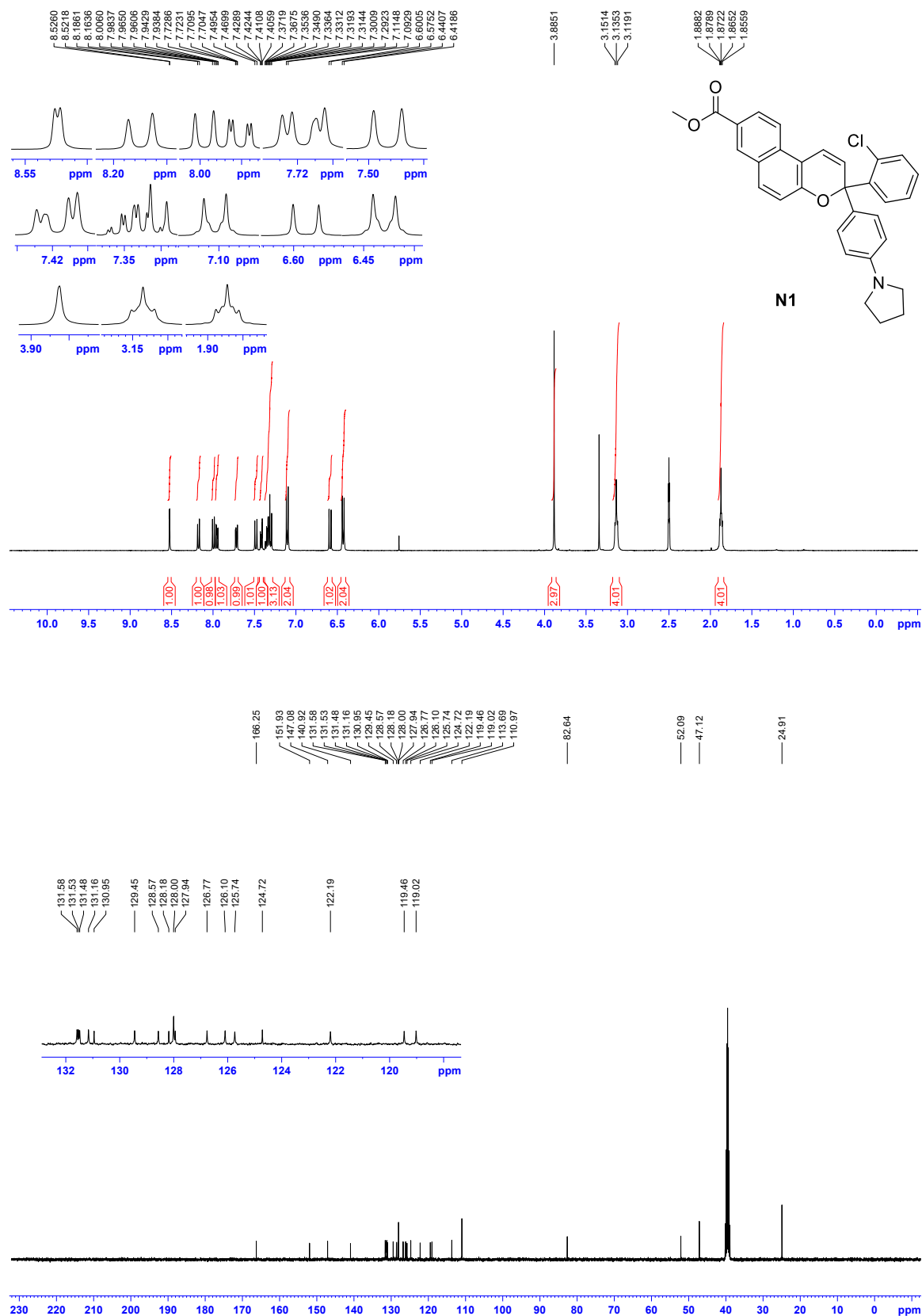
8.1 ¹H and ¹³C NMR Spectra



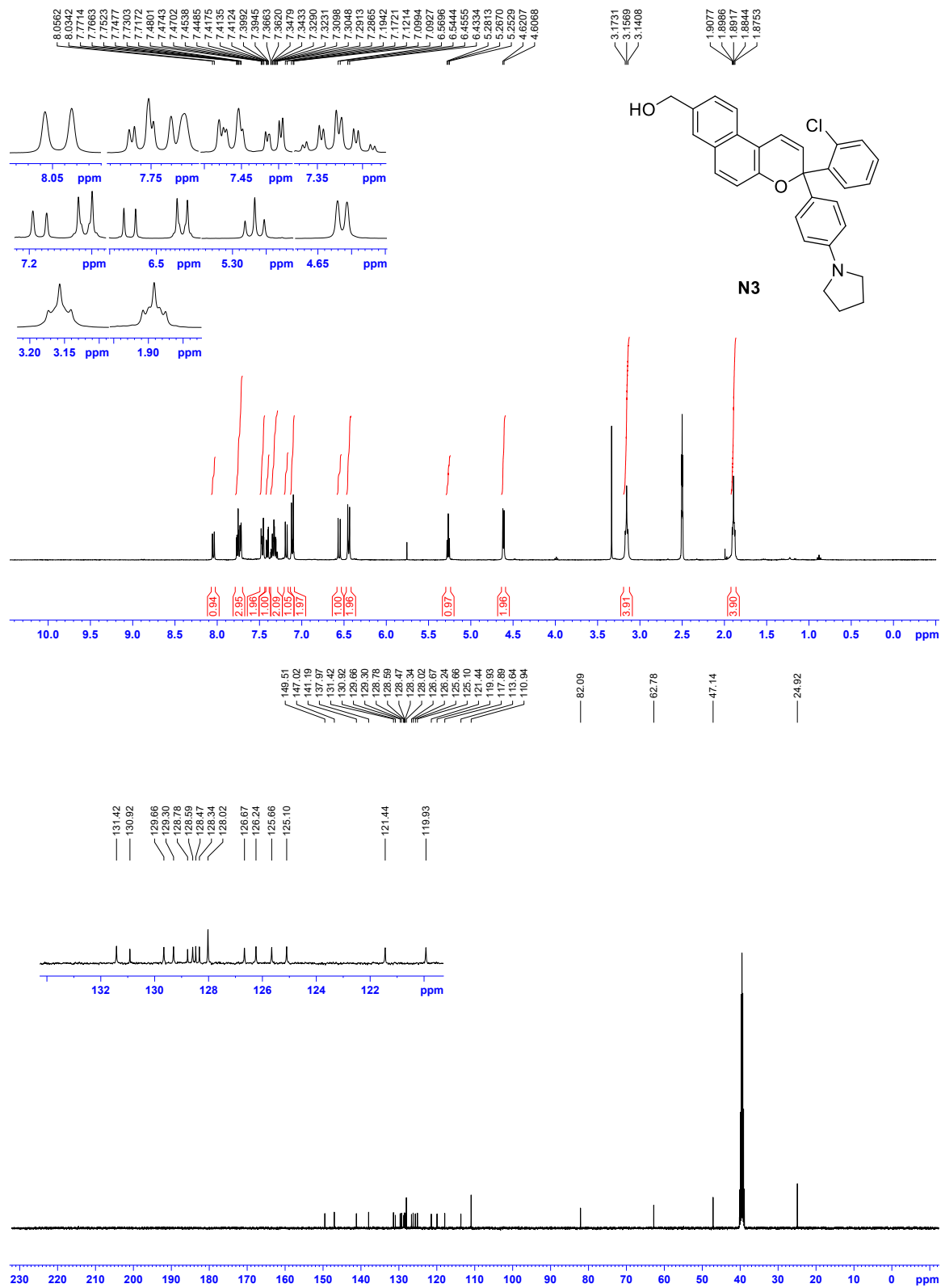
8 Appendix



8.1 ^1H and ^{13}C NMR Spectra



8 Appendix



8.1 ^1H and ^{13}C NMR Spectra

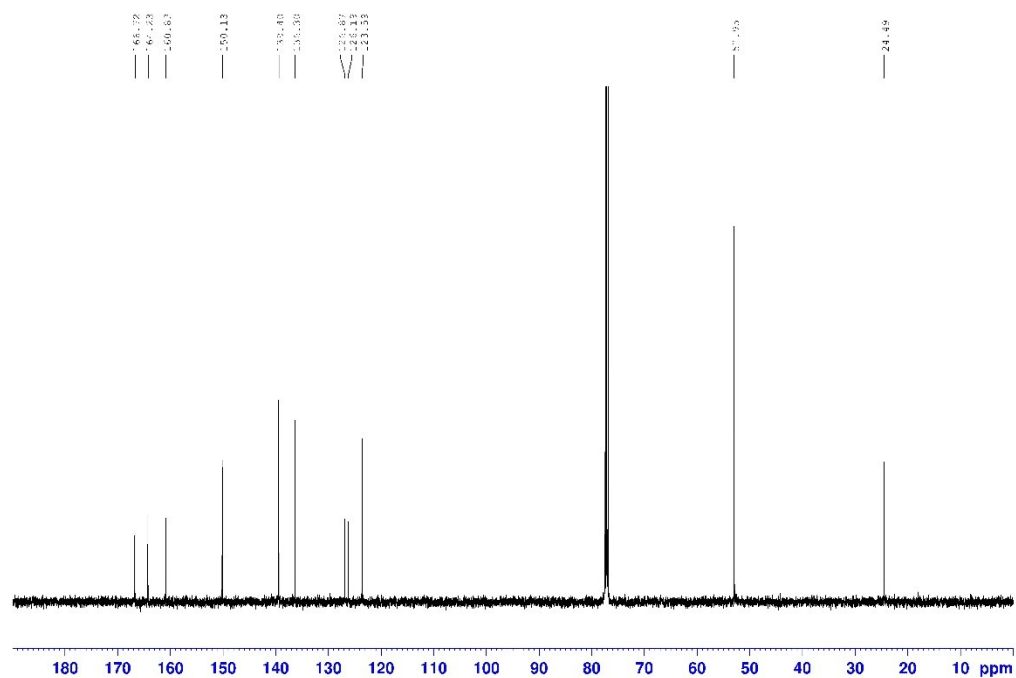
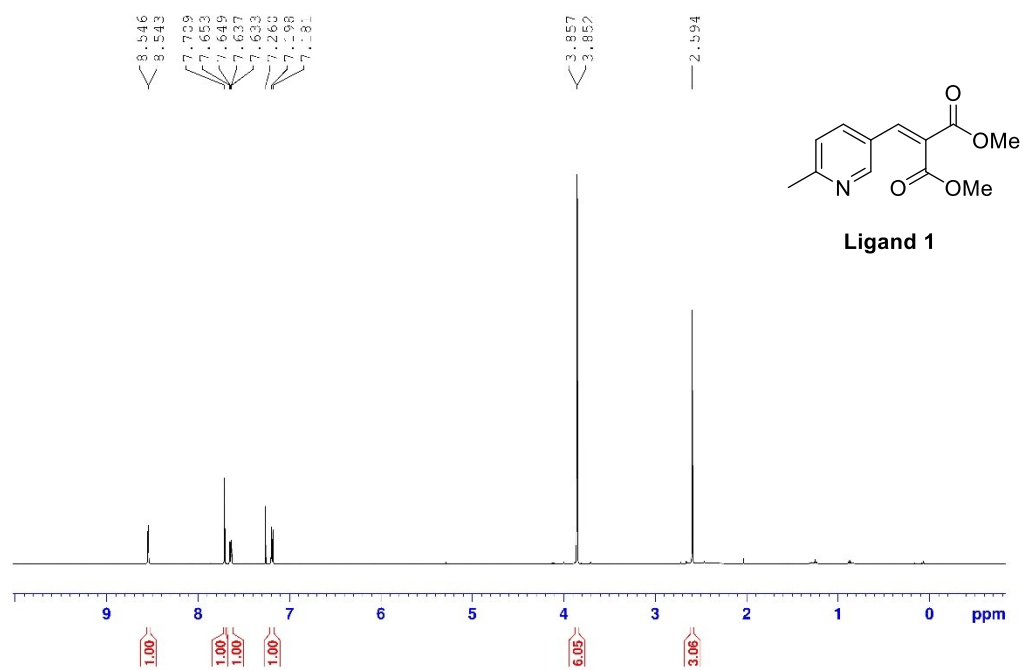
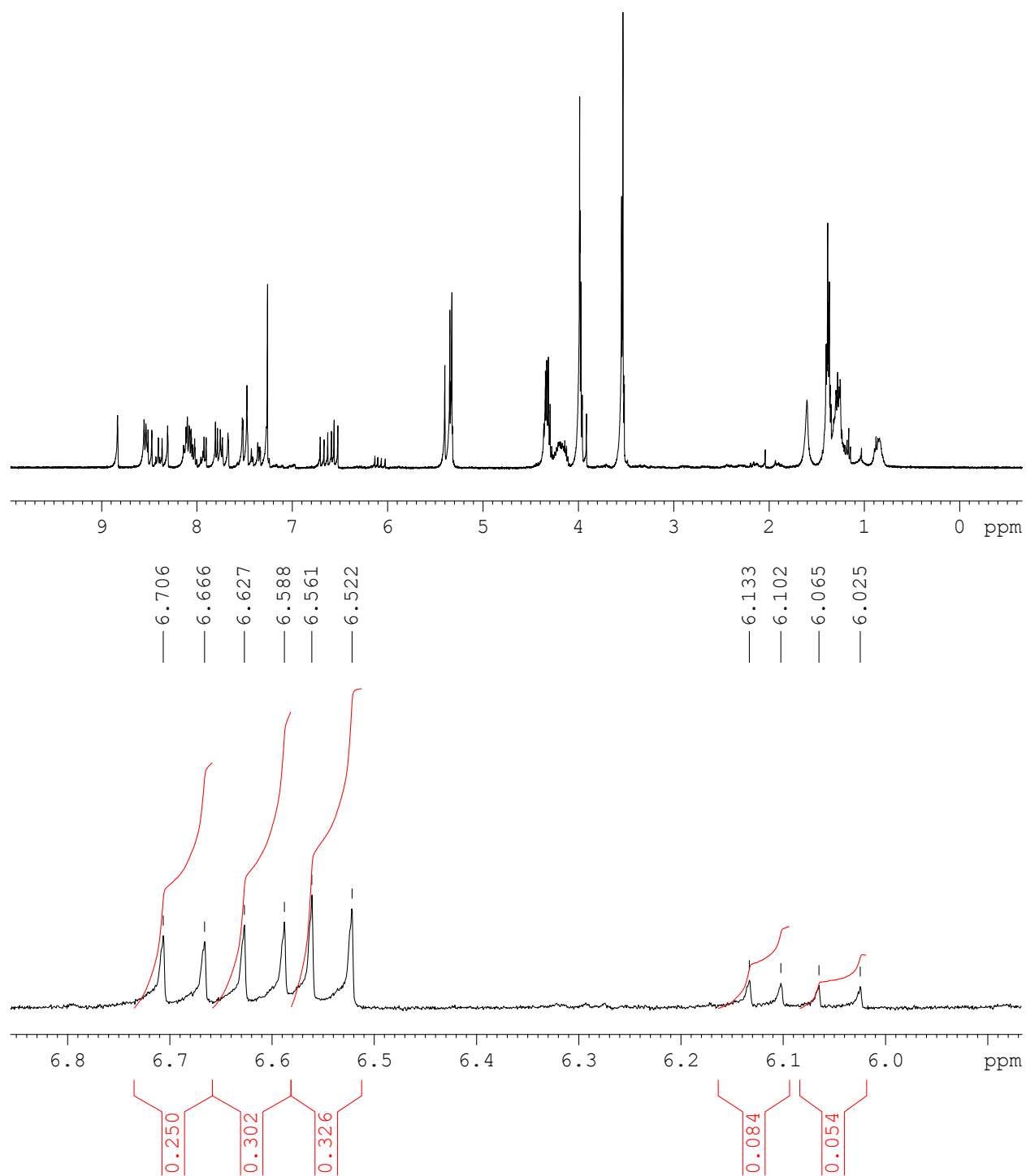
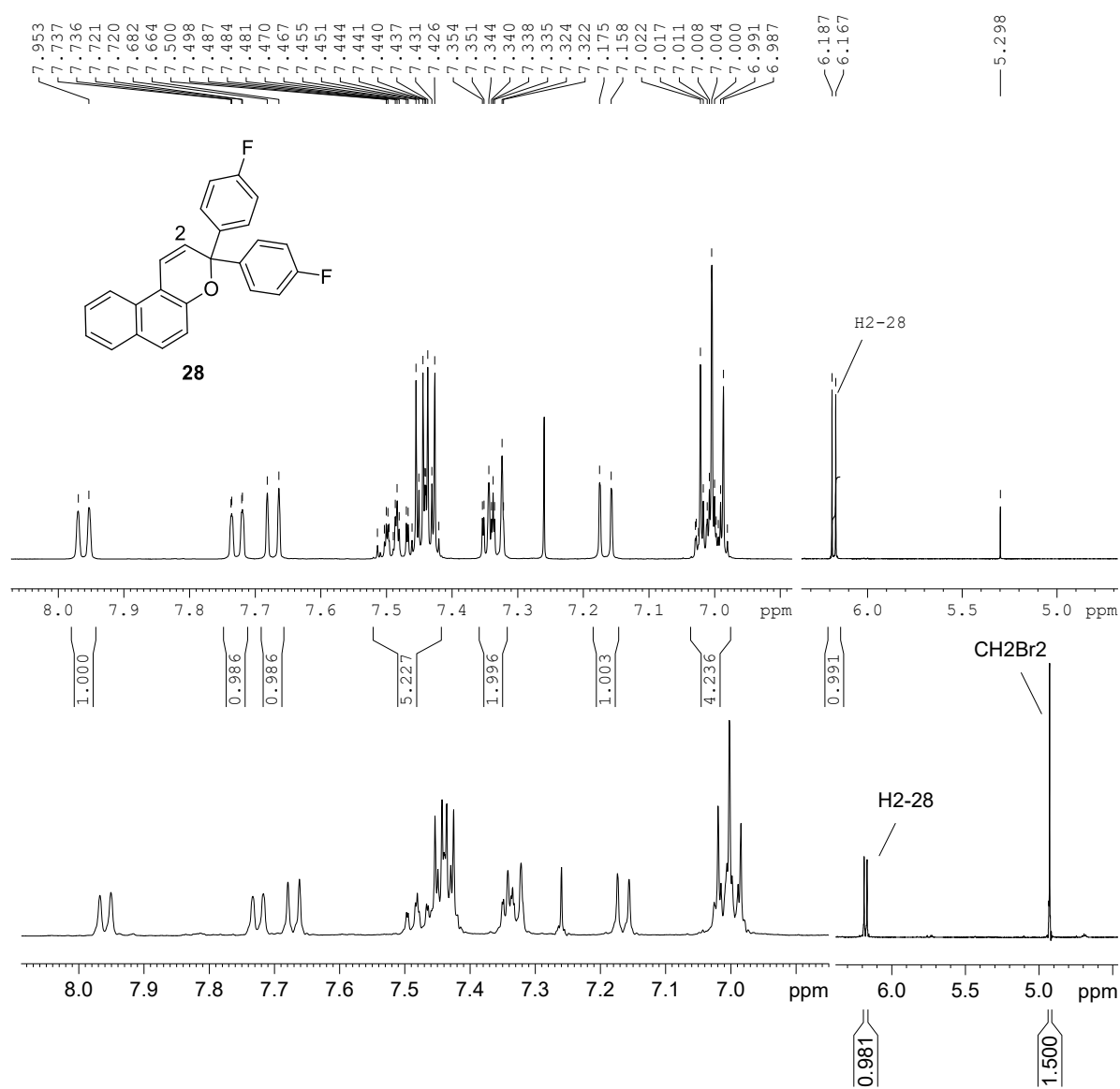


Figure 8.1 The ^1H NMR spectrum of nondirected C-H functionalization products and their ratios (Chapter 3, Table 3.2-entry 1).



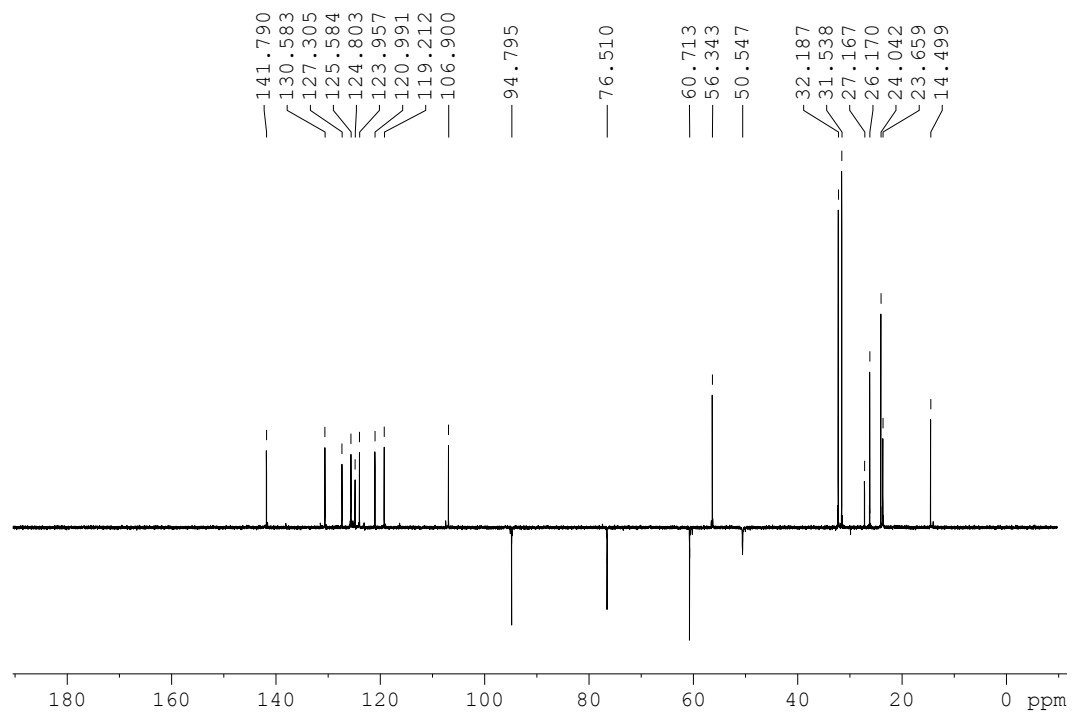
8.1 ^1H and ^{13}C NMR Spectra

Figure 8.2 The ^1H NMR spectrum of naphthopyran **28** (up) and the crude ^1H NMR spectrum of reaction (0.17 mmol scale) in Figure 3.25 (Chapter 3) using CH_2Br_2 (0.13 mmol) as the internal standard (down).

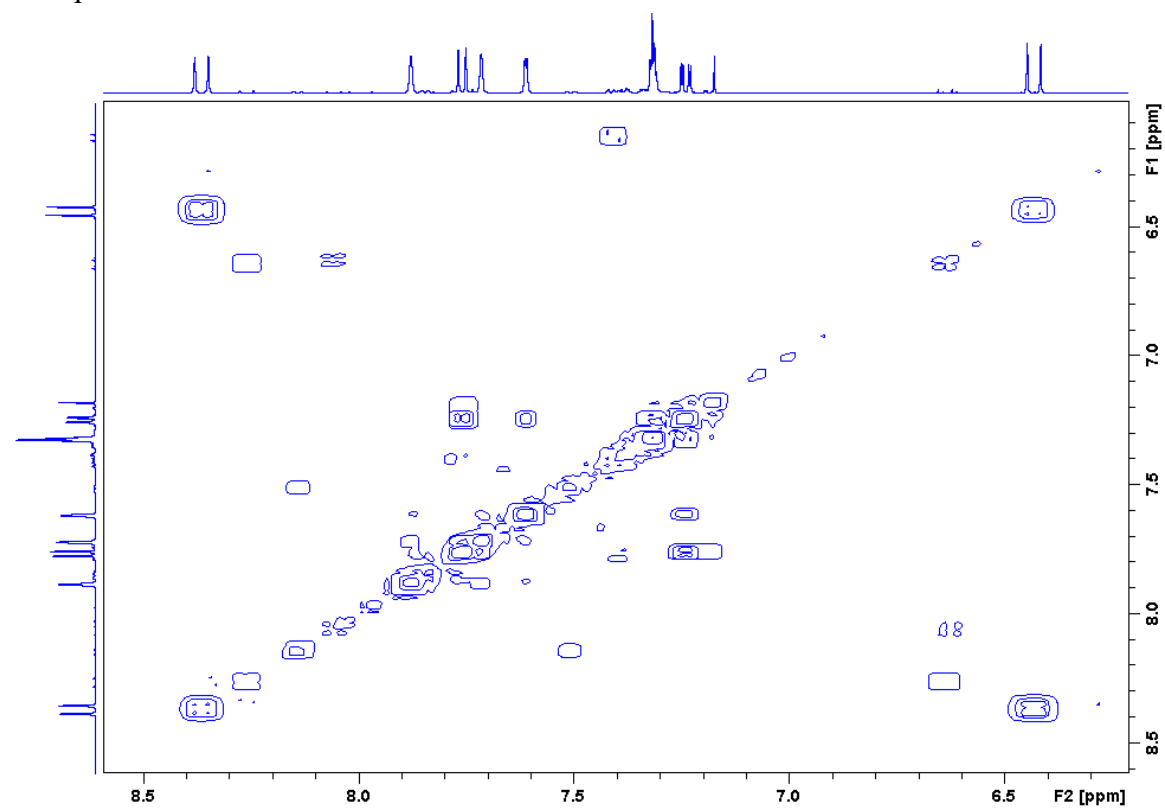


8.2 2D NMR Spectra

Compound **14**- ^{13}C -DEPT

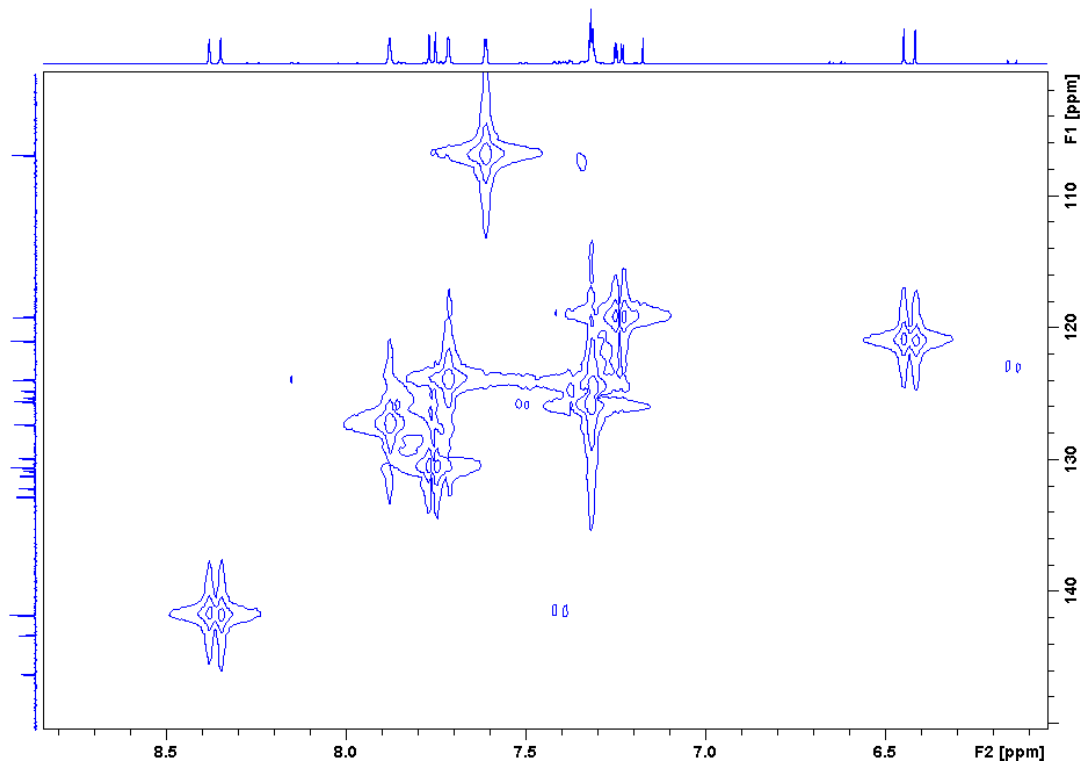


Compound **14**-HH-COSY

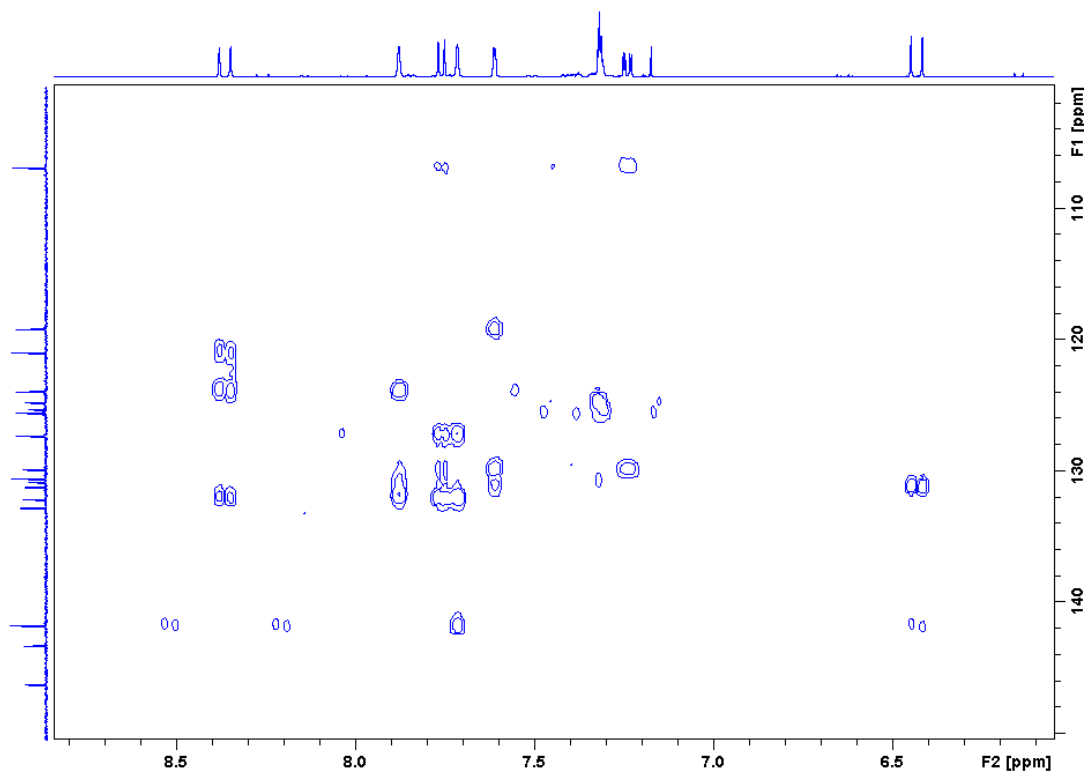


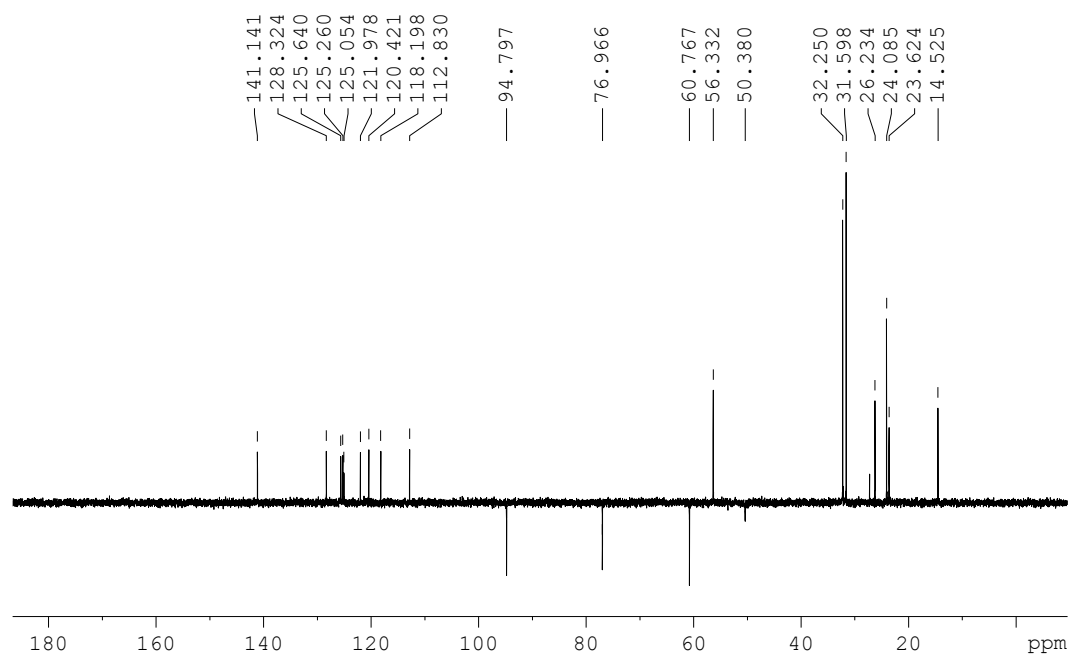
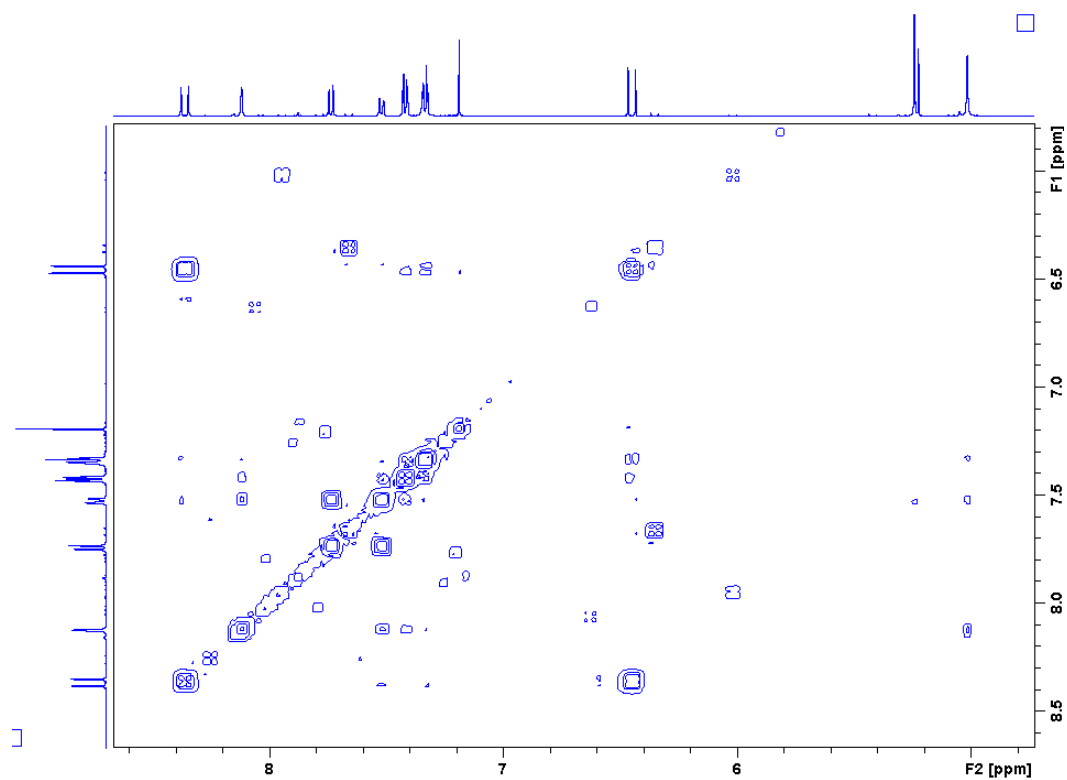
8.2 2D NMR Spectra

Compound **14**-HC-HMQC



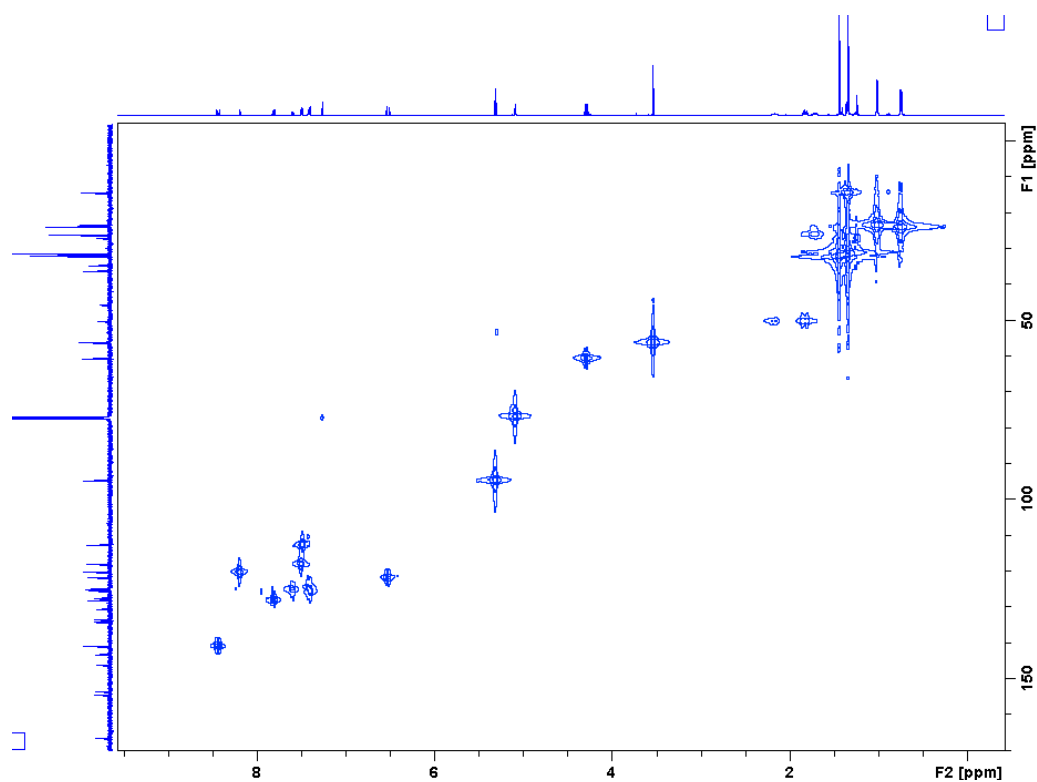
Compound **14**-HC-HMBC



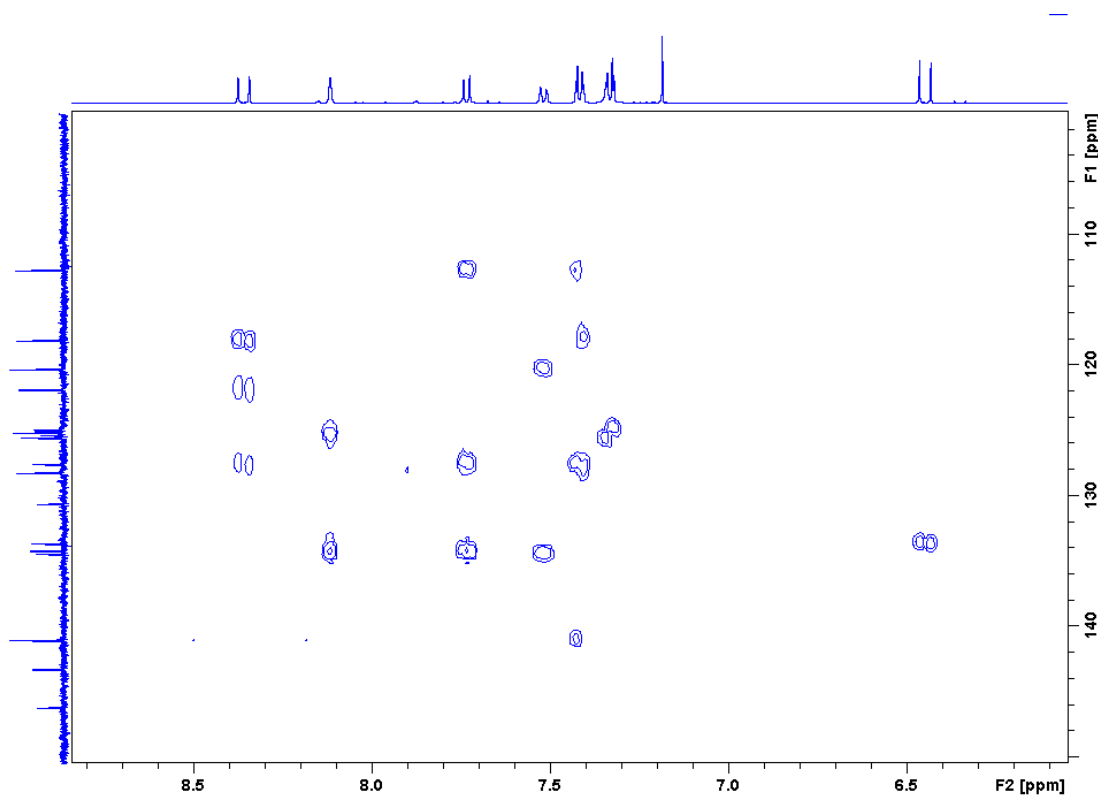
Compound **15**- ^{13}C -DEPTCompound **15**-HH-COSY

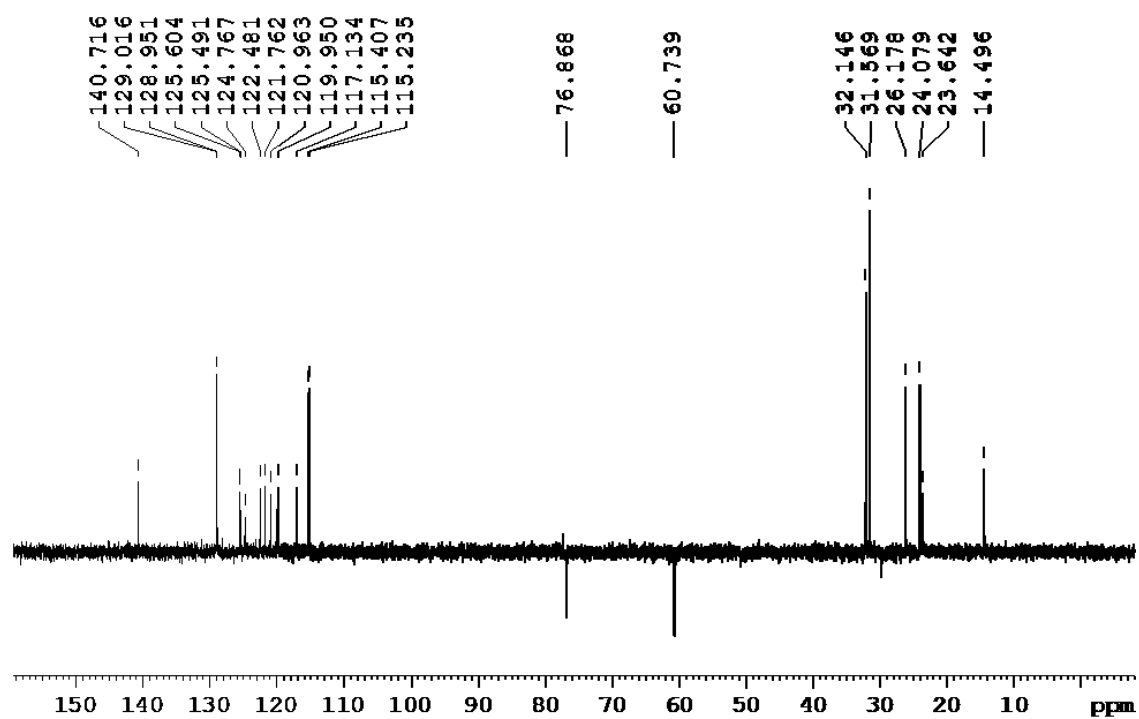
8.2 2D NMR Spectra

Compound **15**-HC-HMQC

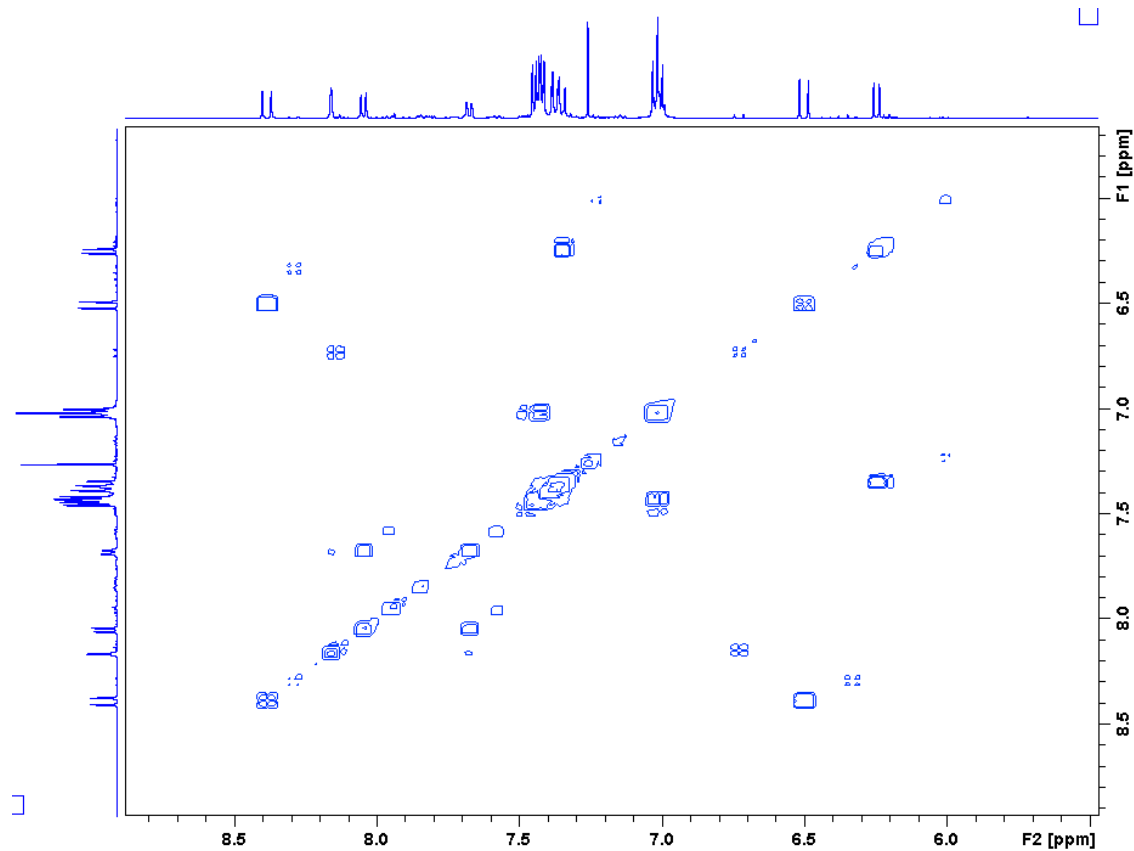


Compound **15**-HC-HMBC



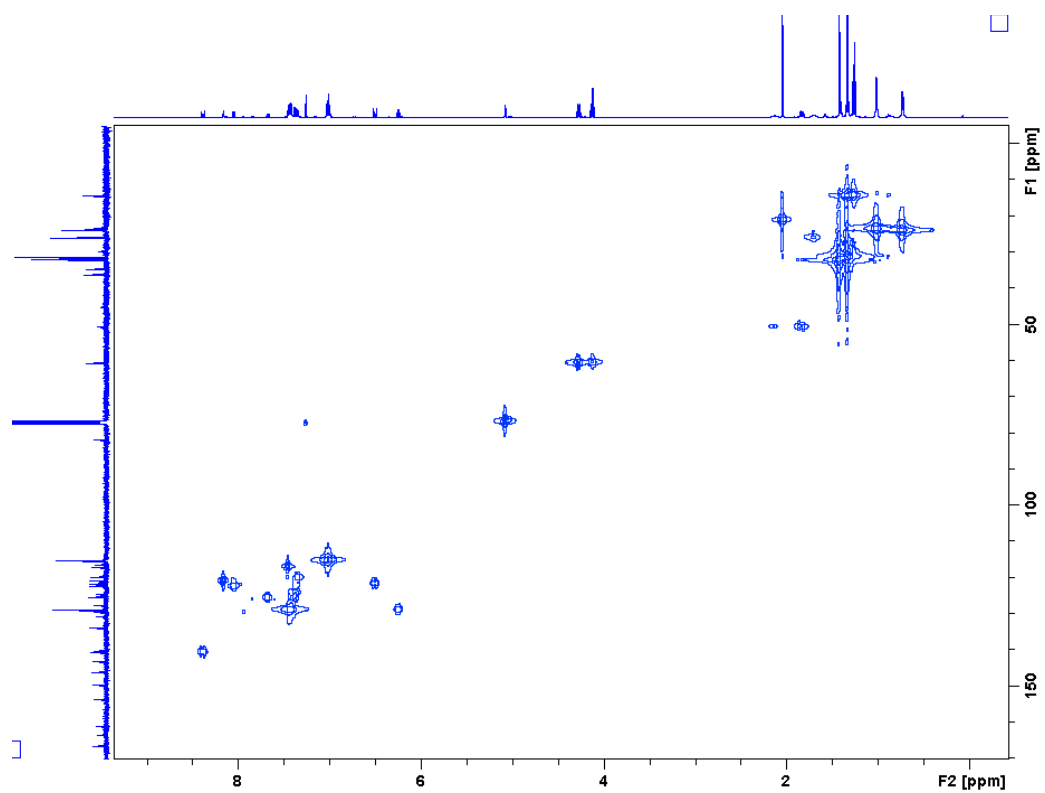
Compound N7- ^{13}C -DEPT

Compound N7-HH-COSY

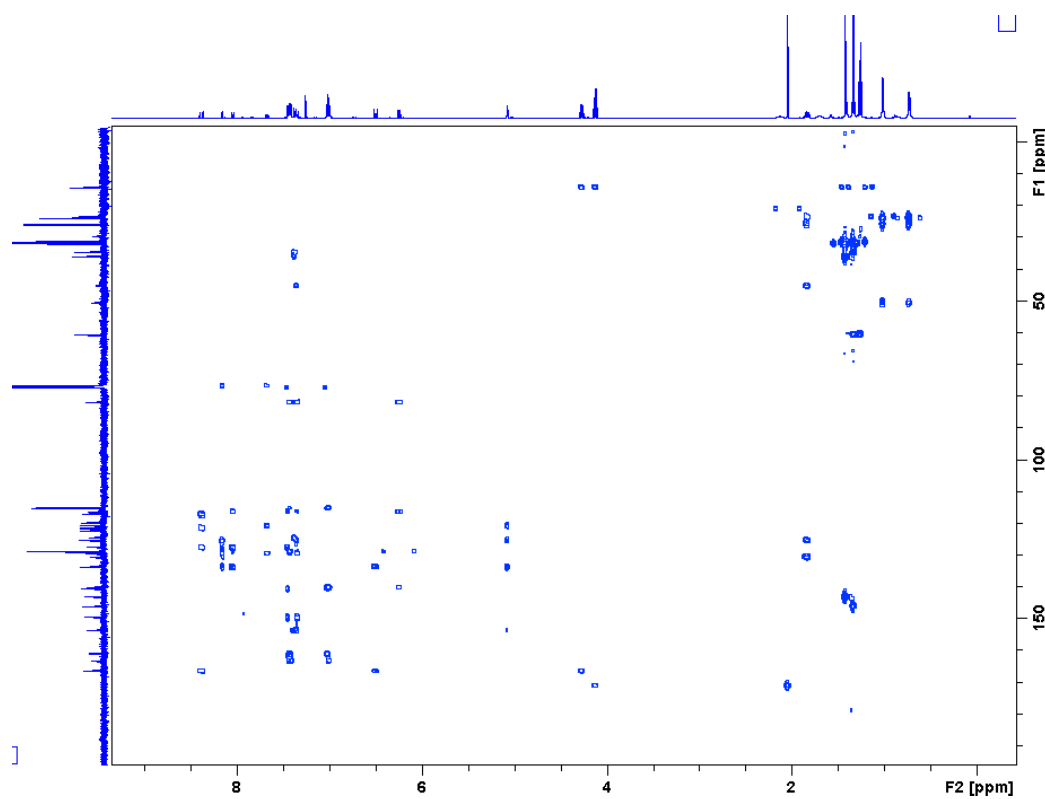


8.2 2D NMR Spectra

Compound N7-HC-HMQC



Compound N7-HC-HMBC



8.3 UV Absorption Spectra

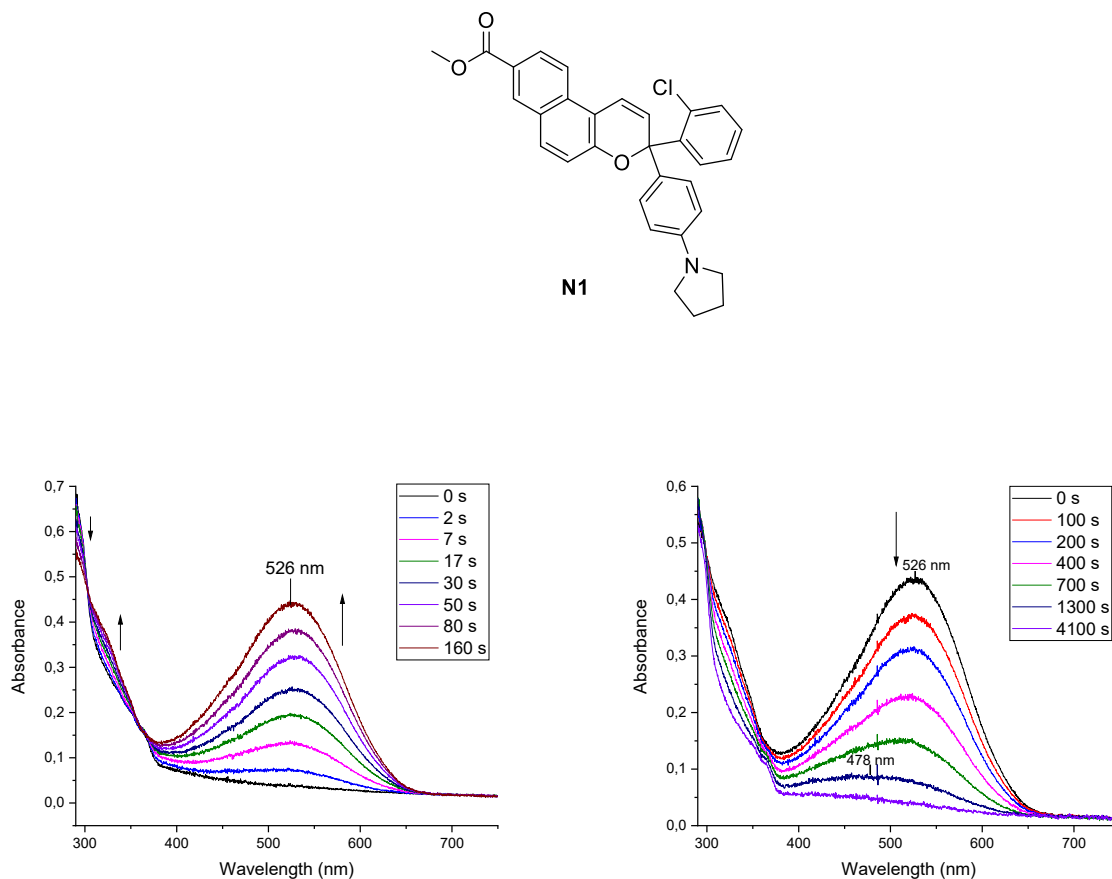


Figure 8.3 Absorbance changes of **N1** during (a) UV irradiation (left) and (b) thermal relaxation in the darkness (right) in tetrachloroethylene ($c = 1.5 \times 10^{-5}$ M) at 293 K. (340 nm, 12 mW/cm². The arrows are presented to guide the eye through the changes in the absorbance, PSS: reached after 160 s, a shift of λ_{\max} was observed during the thermal back reaction).

8.3 UV Absorption Spectra

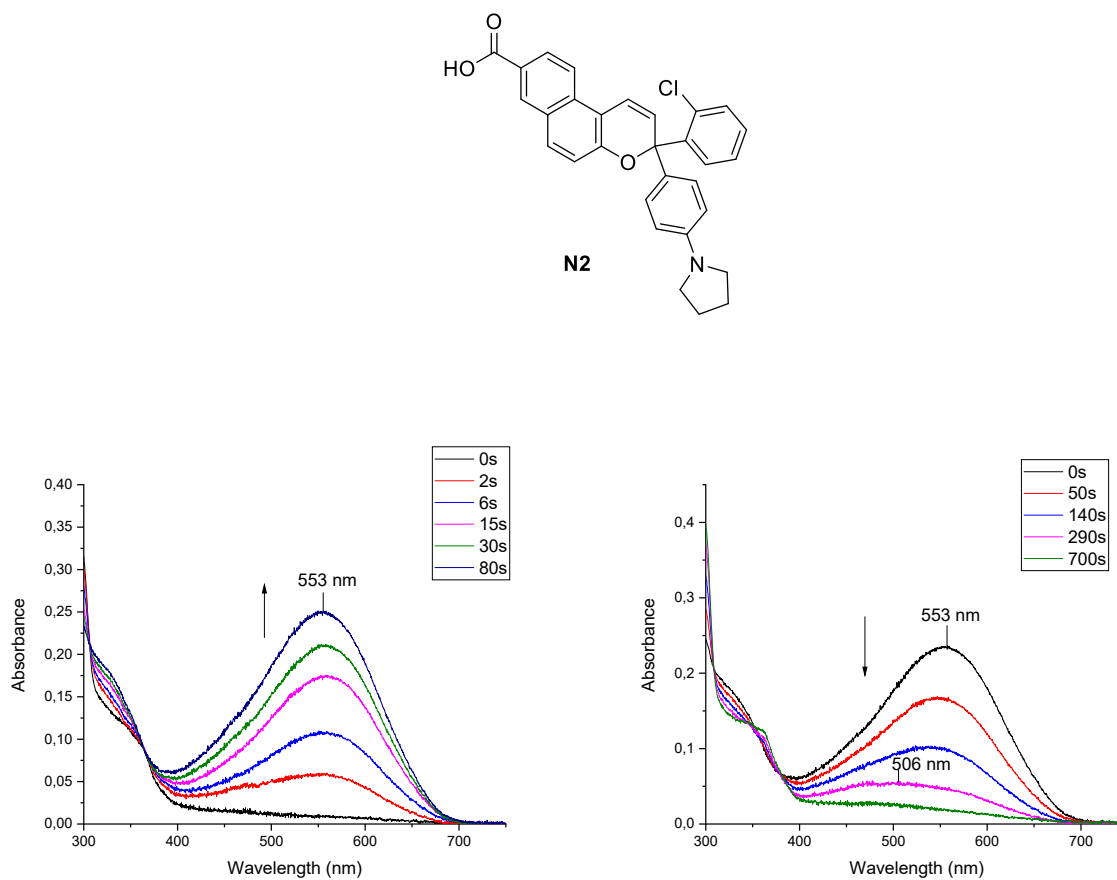


Figure 8.4 Absorbance changes of **N2** during (a) UV irradiation (left) and (b) thermal relaxation in the darkness (right) in tetrachloroethylene ($c = 1.5 \times 10^{-5}$ M) at 293 K. (340 nm, 12 mW/cm². The arrows are presented to guide the eye through the changes in the absorbance, PSS: reached after 80 s, a shift of λ_{\max} was observed during the thermal back reaction).

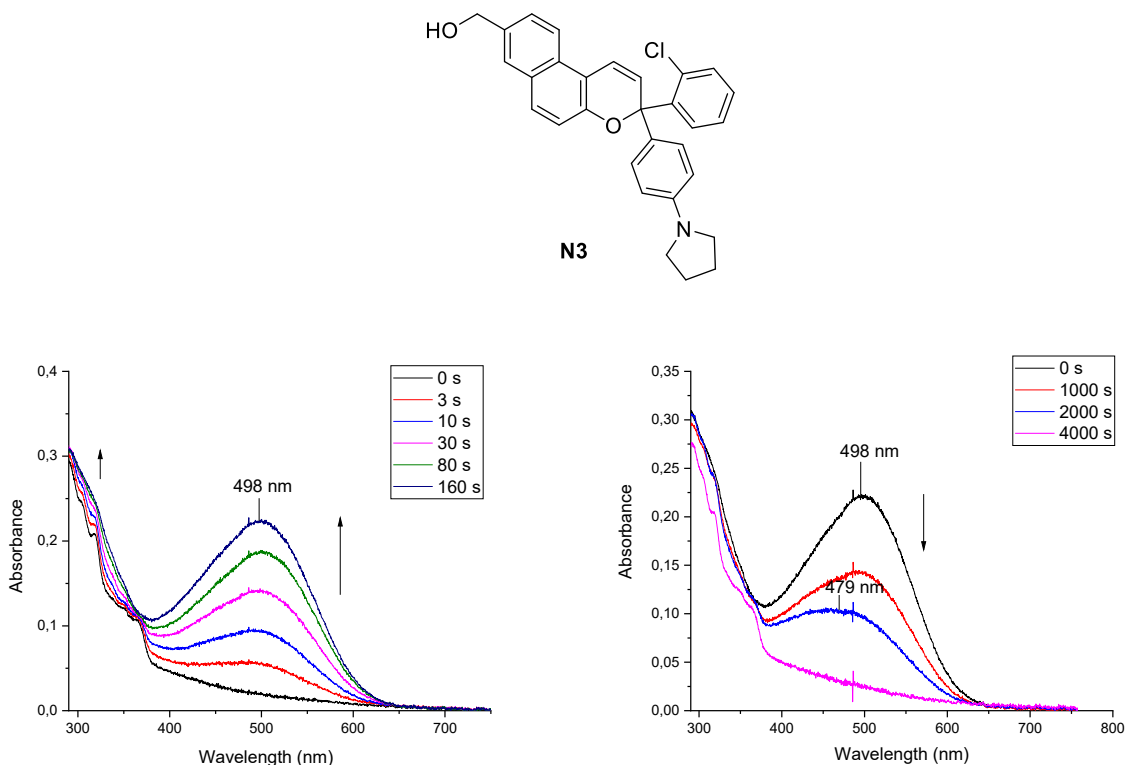


Figure 8.5 Absorbance changes of N3 during (a) UV irradiation (left) and (b) thermal relaxation in the darkness (right) in tetrachloroethylene ($c = 1.5 \times 10^{-5}$ M) at 293 K. (340 nm, 12 mW/cm². The arrows are presented to guide the eye through the changes in the absorbance, PSS: reached after 160 s, a shift of λ_{\max} was observed during the thermal back reaction).

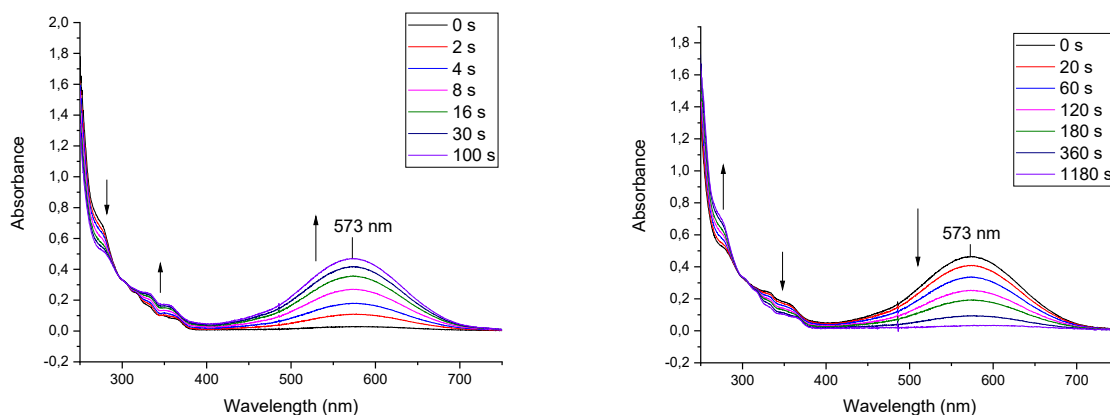


Figure 8.6 Absorbance changes of N3 during (a) UV irradiation (left) and (b) thermal relaxation in the darkness (right) in DCM ($c = 1.5 \times 10^{-5}$ M) at 293 K. (340 nm, 12 mW/cm². The arrows are presented to guide the eye through the changes in the absorbance, PSS: reached after 100 s.)

8.3 UV Absorption Spectra

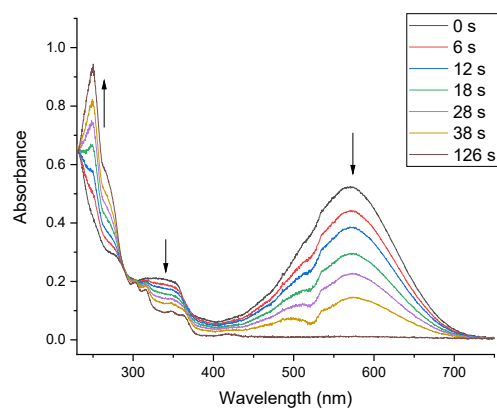
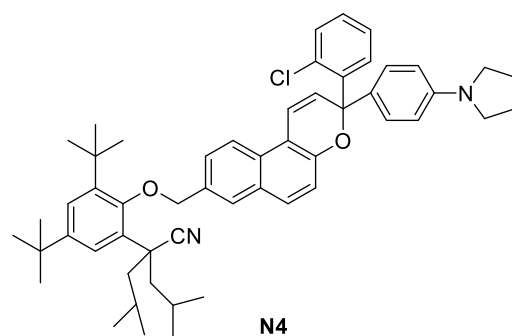


Figure 8.7 Absorbance changes of **N4** during visible light bleaching (565 nm, 84 mW/cm²) in MeCN ($c = 1.5 \times 10^{-5}$ M) at 293 K. (The arrows are presented to guide the eye through the changes in the absorbance, PSS: reached after 24 s.)

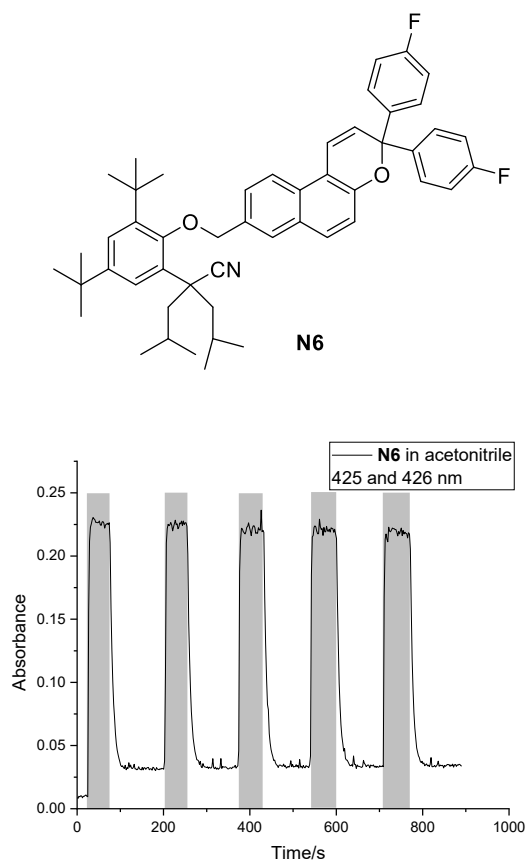


Figure 8.8 UV irradiation/dark cycles for **N6** in MeCN ($c = 1.5 \times 10^{-5}$ M) at 293 K. The grey regions signal the period when the sample was irradiated with UV light (365 nm, 110 mW/cm²); non-marked regions present the periods when the sample was in the dark in the short time window and totally thermal back to the initial state will be found if the sample is in the dark for long enough time (monitoring wavelength is between 425 and 426 nm).

8.3 UV Absorption Spectra

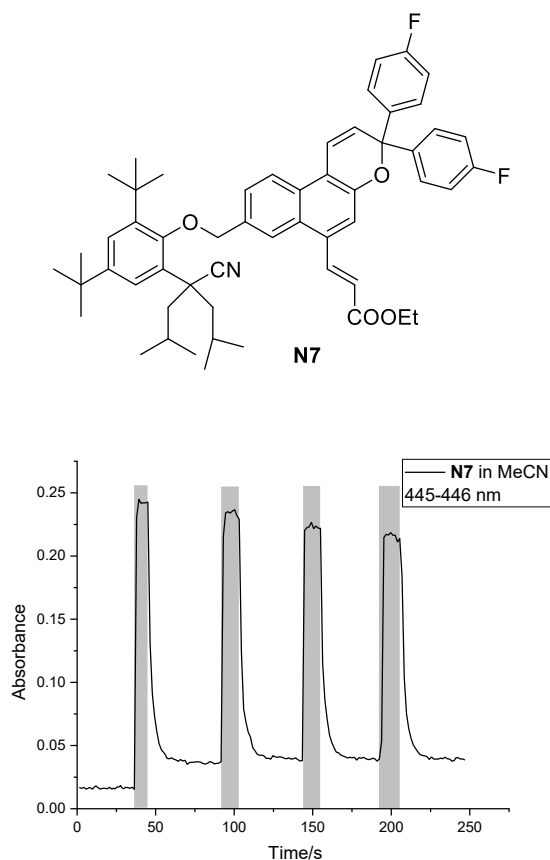


Figure 8.9 UV irradiation/dark cycles for **N7** in MeCN ($c = 1.5 \times 10^{-5}$ M) at 293 K. The grey regions signal the period when the sample was irradiated with UV light (365 nm, 110 mW/cm²); non-marked regions present the periods when the sample was in the dark in the short time window and totally thermal back to the initial state will be found if the sample is in the dark for long enough time (monitoring wavelength is between 445 and 446 nm).

Table 8.1 Some physical properties of the solvents used in this thesis.

Solvent	Permittivity ϵ (25°C)	n	Viscosity, η /mPa· s (25°C)	b.p./ °C
TCE	2.5	1.49	0.829	121
DCM	8.93	1.42	0.41	39.7
MeCN	35.7	1.34	0.37	81.6

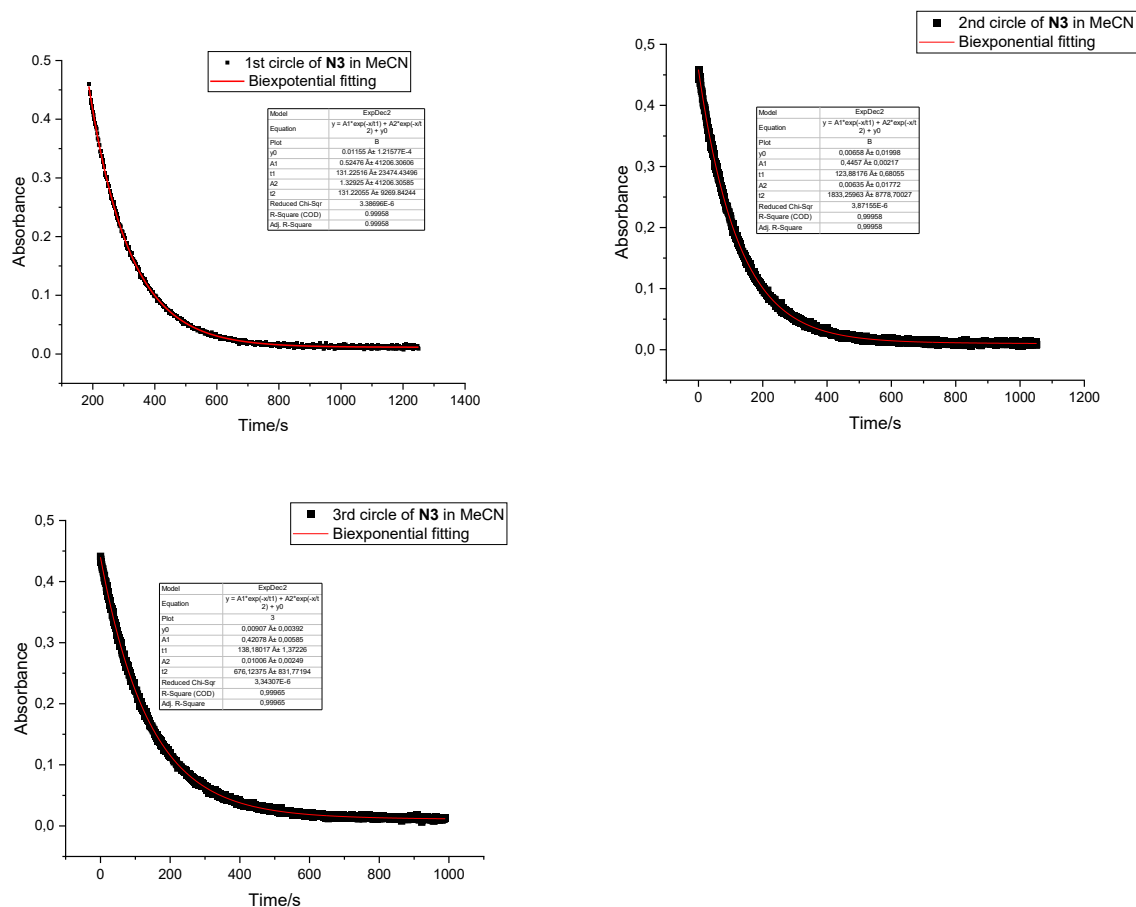


Figure 8.10 The time-resolved absorbance at λ_{\max} during thermal relaxation (black dots) and biexponential decay fitting (red line) in MeCN (1.5×10^{-5} M) at 293 K: (a) N3 in the 1st circle, (b) N3 in the 2nd circle and (c) N3 in the 3rd circle. (Data from Chapter 4, Figure 4.5-b)

Table 8.2 The parameters of biexponential fitting of N3 during thermal back reaction (Chapter 4, Figure 4.5-b).^a

	k_1 (10^{-3} s^{-1})	k_2 (10^{-3} s^{-1})	A_1	A_2	A_{th}	R^2
1 st circle	7.62	7.62	0.223	0.221	-0.0003	0.99
2 nd circle	8.07	0.55	0.446	0.006	0.0066	0.99
3 rd circle	7.24	1.48	0.421	0.010	0.0090	0.99

[a] 1.5×10^{-5} M in MeCN, 293 K.

8.3 UV Absorption Spectra

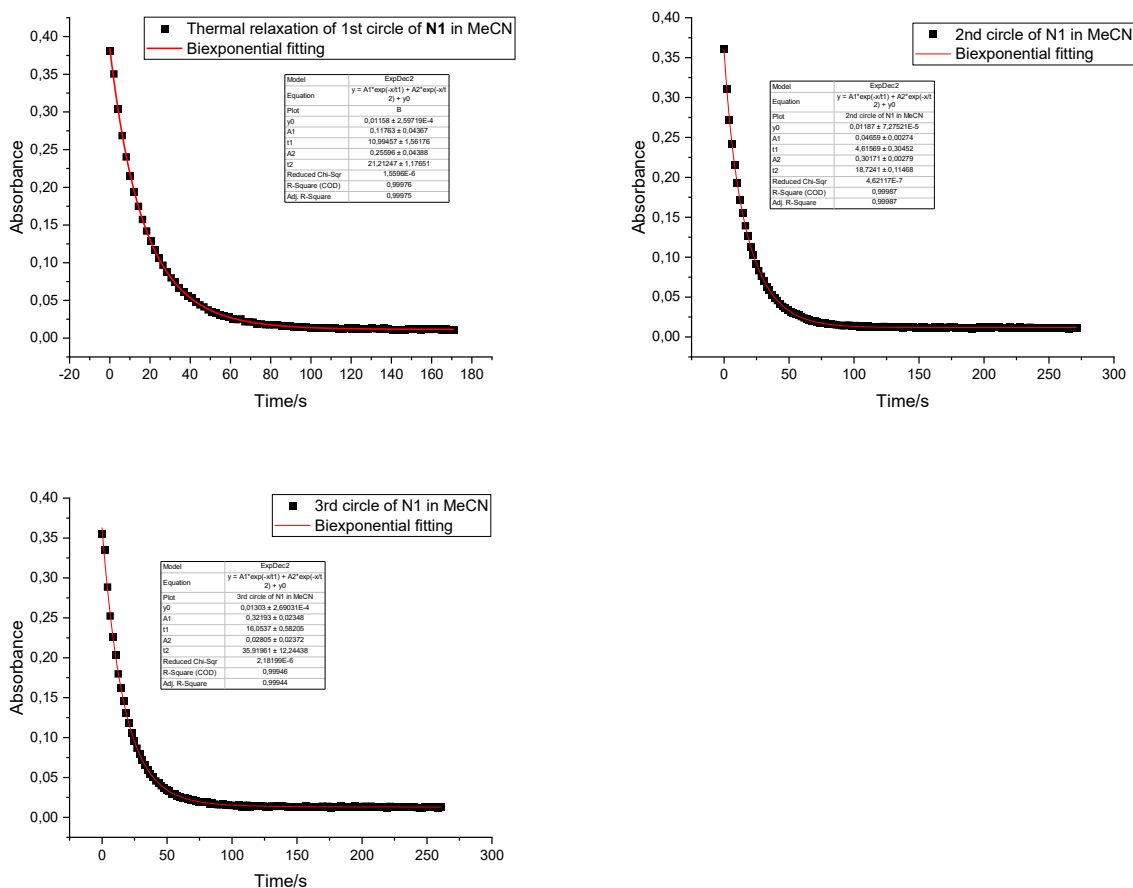


Figure 8.11 The time-resolved absorbance at λ_{\max} during thermal relaxation (black dots) and biexponential decay fitting (red line) in MeCN (1.5×10^{-5} M) at 293 K: (a) N1 in the 1st circle, (b) N1 in the 2nd circle and (c) N1 in the 3rd circle. (Data from Chapter 4, Figure 4.5-a)

Table 8.3 The parameters of biexponential fitting of N1 during thermal back reaction (Chapter 4, Figure 4.5-a).^a

	k_1 (10^{-2} s^{-1})	k_2 (10^{-2} s^{-1})	A_1	A_2	A_{th}	R^2
1 st circle	9.09	4.71	0.118	0.256	0.012	0.99
2 nd circle	21.6	5.34	0.047	0.302	0.013	0.99
3 rd circle	6.23	2.78	0.322	0.028	0.012	0.99

[a] 1.5×10^{-5} M in MeCN, 293 K.

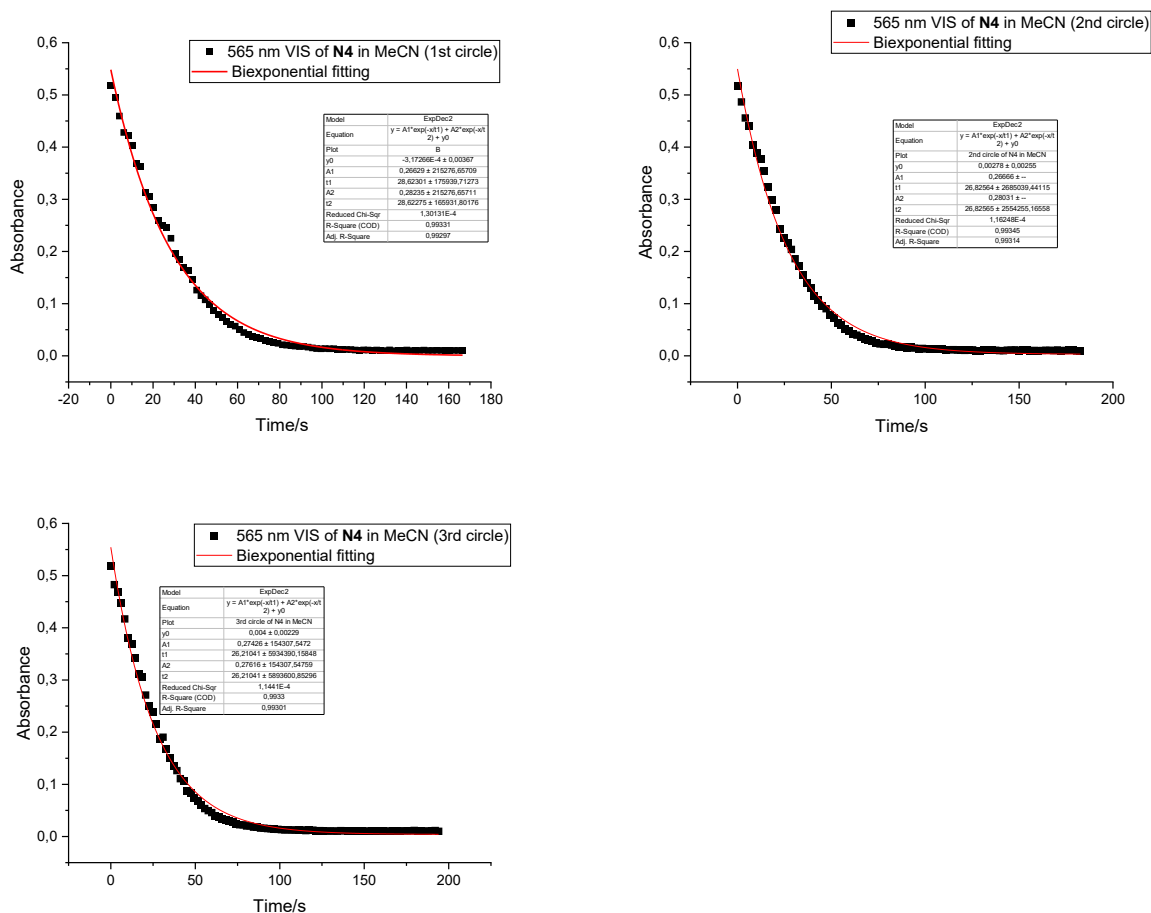


Figure 8.12 The time-resolved absorbance at λ_{\max} during irradiation with visible light (black dots) and biexponential decay fitting (red line) in MeCN (1.5×10^{-5} M) at 293 K: (a) N4 in the 1st circle, (b) N4 in the 2nd circle and (c) N4 in the 3rd circle. (Visible light: 565 nm, 84 mW/cm², data from Chapter 4, Figure 4.7)

Table 8.4 The parameters of biexponential fitting of N4 during irradiation with visible light (Chapter 4, Figure 4.7).^a

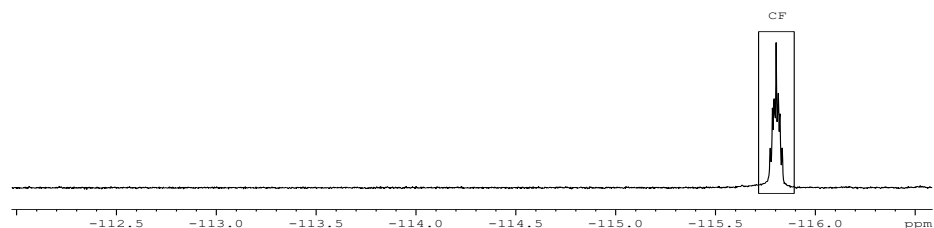
	k_1 (10^{-3} s^{-1})	k_2 (10^{-3} s^{-1})	A_1	A_2	A_{th}	R^2
1 st circle	3.49	3.49	0.266	0.282	-0.0003	0.99
2 nd circle	3.72	3.72	0.267	0.280	0.002	0.99
3 rd circle	3.82	3.82	0.274	0.276	0.004	0.99

[a] 1.5×10^{-5} M in MeCN, 293 K. Visible light: 565 nm, 84 mW/cm²,

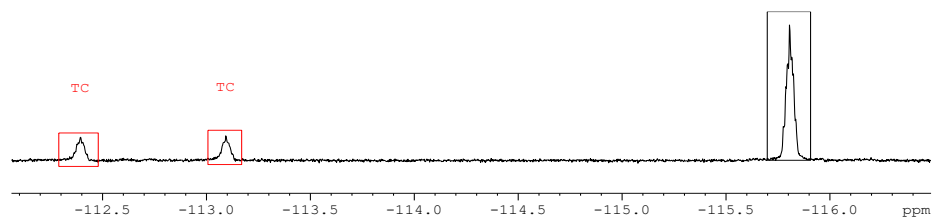
8.4 *In-situ* NMR Spectra

Figure 8.13 470 MHz ^{19}F NMR spectra of **N5** in CD_3CN ($c = 1 \times 10^{-2}$ M) at 238 K. (UV light: 365 nm, $3.86 \text{ mW}/\text{cm}^2$, 500 MHz Bruker NMR spectrometer, 2.5 h measurements, 120 spectra were obtained.)

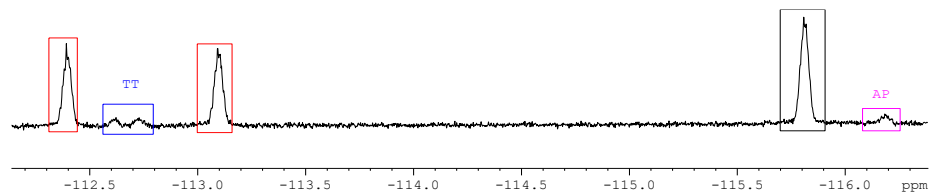
a. Initial state:



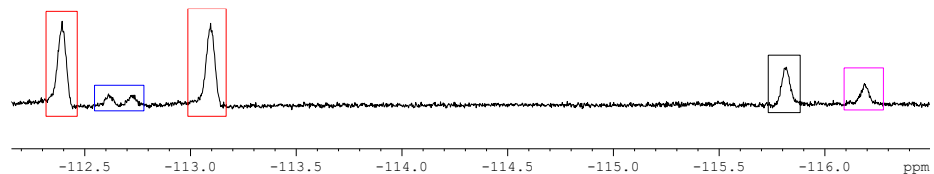
b. After 1 min of 365 nm irradiation:



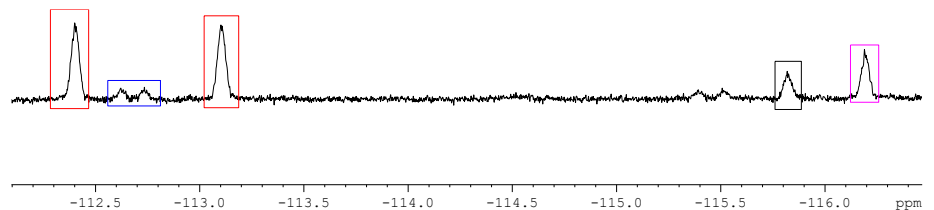
c. After 3 min of 365 nm irradiation:



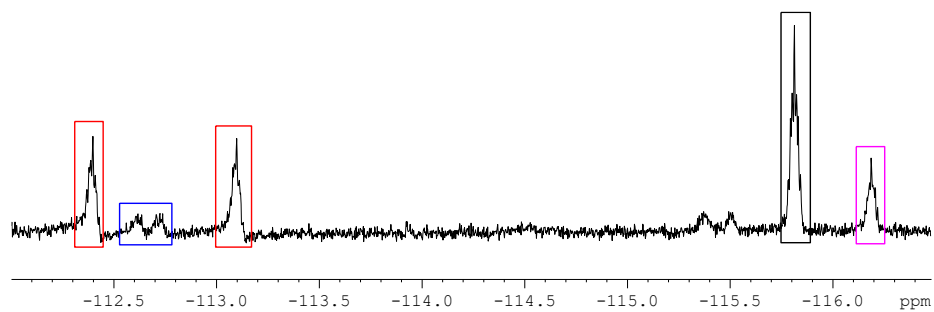
d. After 10 min of 365 nm irradiation:



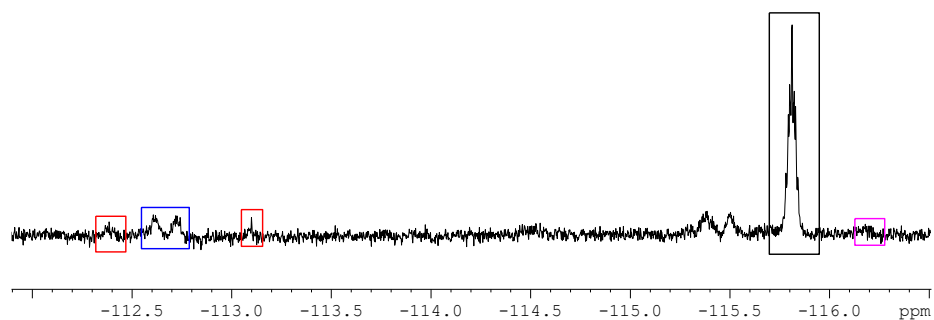
e. PSS (after 32 min of 365 nm irradiation, CF : TC : TT : AP = 10:60:8:22, peaks at around -115.4 ppm are decomposition products after long time irradiation):



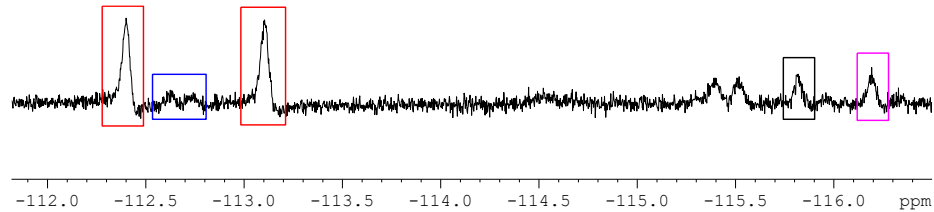
f. after 11 min in the dark (CF : TC : TT : AP = 38:37:9:16):



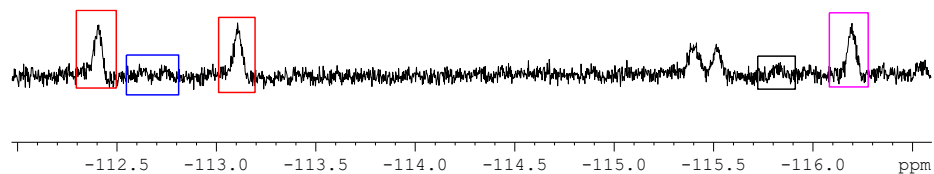
g. after 70 min in the dark (CF : TC : TT : AP = 67:9:17:7):



h. After 3 min of 365 nm irradiation (CF : TC : TT : AP = 12:64:11:13):



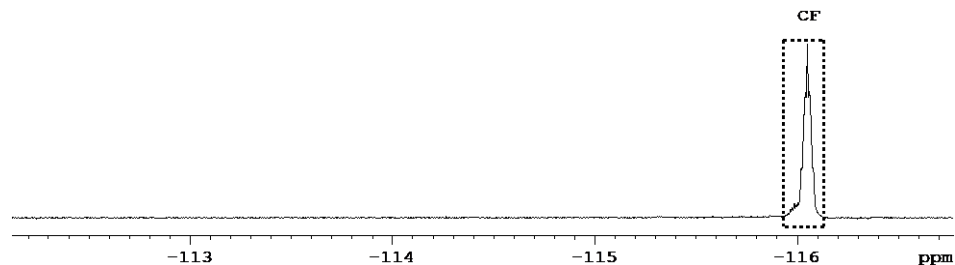
i. After 22 min of 365 nm irradiation (CF : TC : TT : AP = 9:53:11:27):



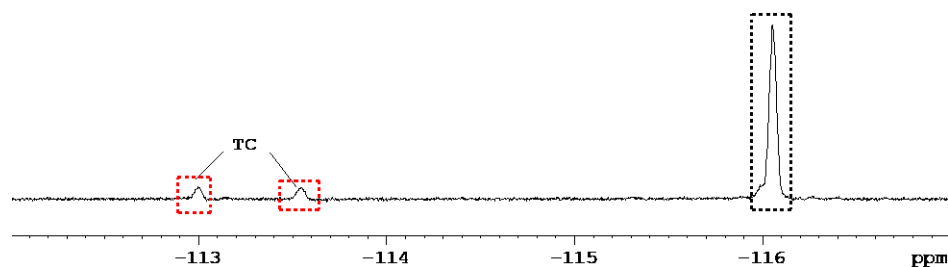
8.4 *In-situ* NMR Spectra

Figure 8.14 470 MHz ^{19}F NMR spectra of **N6** at 238 K in CD_3CN . ($c = 1 \times 10^{-2}$ M. UV: 365 nm, 3.86 mW/cm 2 . 420 nm light: 8.10 mW/cm 2 . 500 MHz Bruker NMR spectrometer. 4 h measurements, 200 spectra were obtained.)

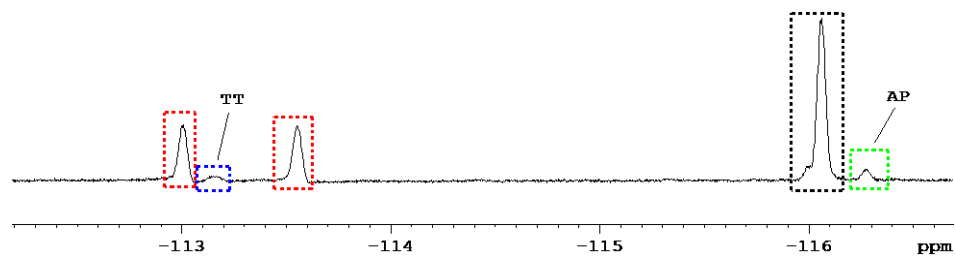
a. Initial state:



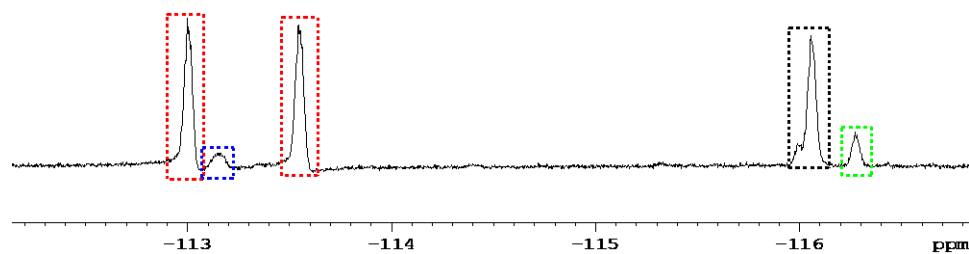
b. After 1 min of 365 nm irradiation:



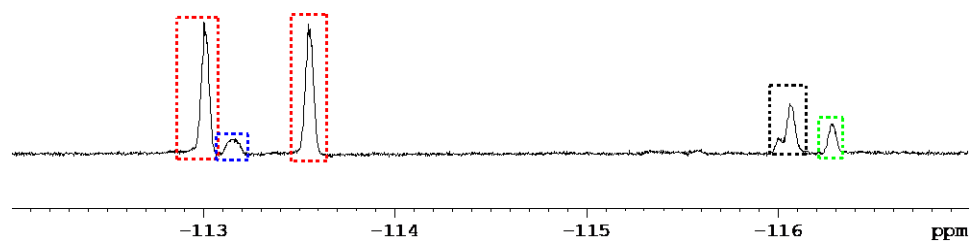
c. After 4 min of 365 nm irradiation:



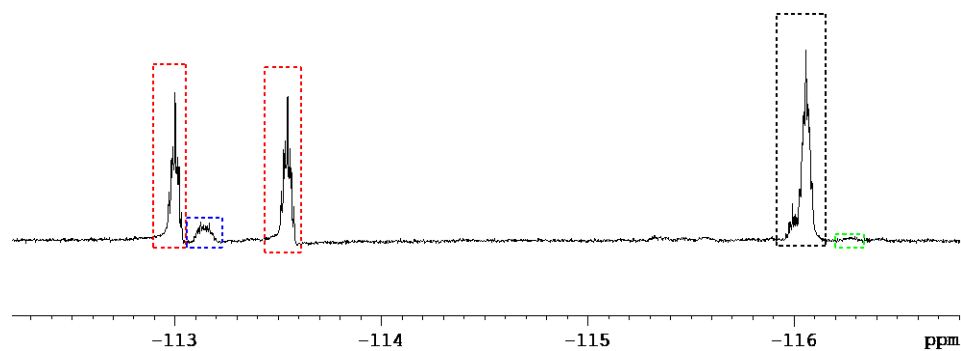
d. After 11 min of 365 nm irradiation:



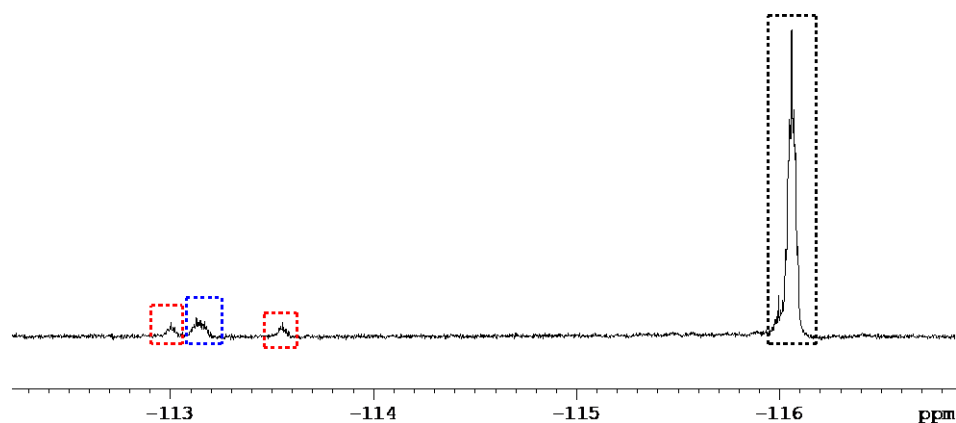
e. PSS (after 30 min of 365 nm irradiation, CF : TC : TT : AP = 15:72:5:8):



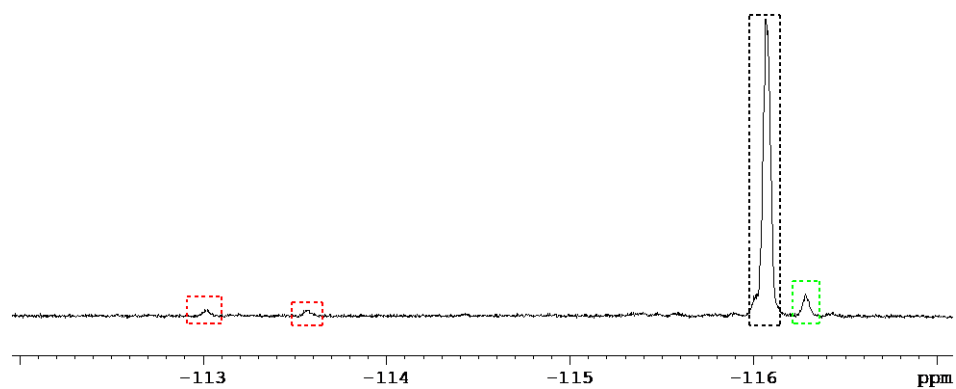
f. after 22 min in the dark (CF : TC : TT : AP = 42:52:5:1):



g. after 130 min in the dark (CF : TC : TT : AP = 87:6:7:0):



h. PSS (after 26 min of 420 nm irradiation, CF : TC : TT : AP = 92:3:0:5)



8.4 *In-situ* NMR Spectra

i. after 19 min in the dark (CF : TC : TT : AP = 94:6:0:0):

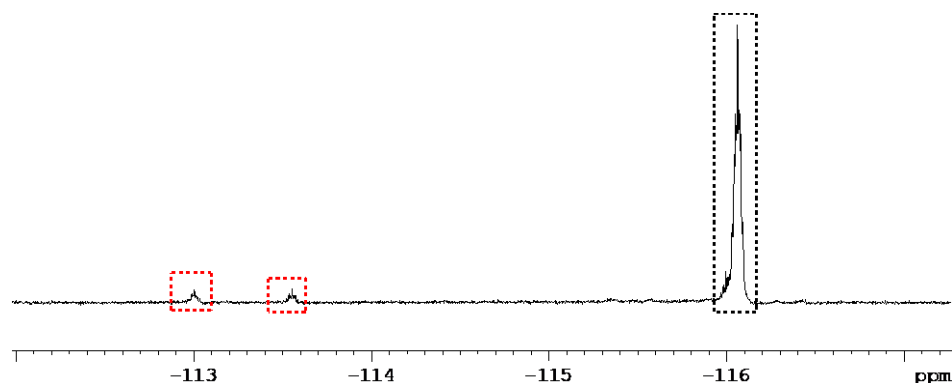
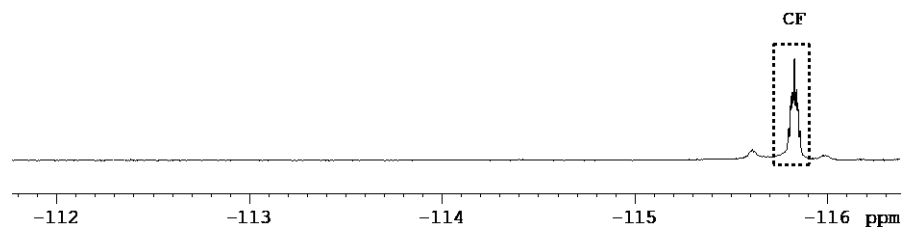
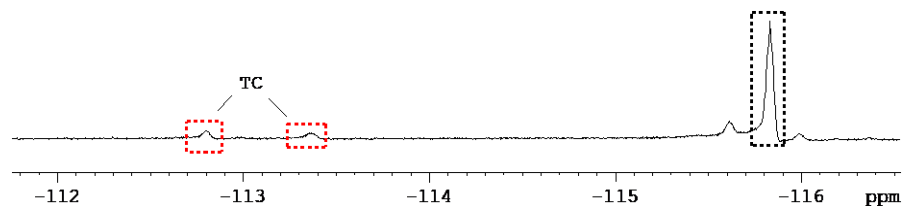


Figure 8.15 470 MHz ^{19}F NMR spectra of **N7** at 238 K in CD_3CN . ($c = 1 \times 10^{-2}$ M, LED light: 365 nm, 3.86 mW/cm 2 . 420 nm, 8.10 mW/cm 2 . 455 nm, 4.30 mW/cm 2 . 505 nm, 2.37 mW/cm 2 . 500 MHz Bruker NMR spectrometer. 3 h measurements, 142 spectra were obtained.)

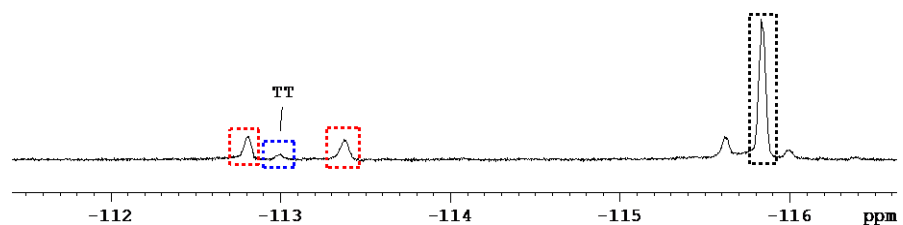
a. Initial state (peaks at around -115.6 and -116.0 ppm are byproducts from the synthesis):



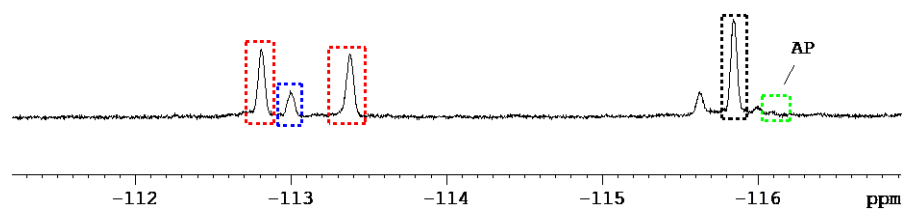
b. After 1 min of 365 nm irradiation:



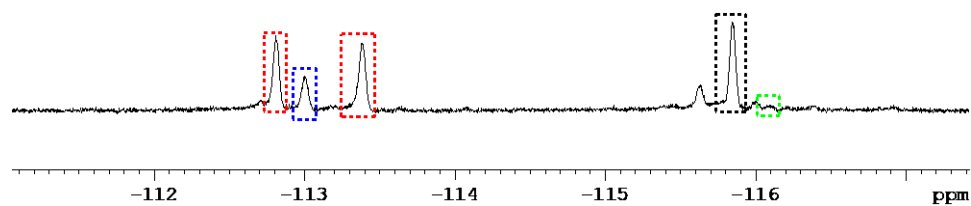
c. After 2 min of 365 nm irradiation:



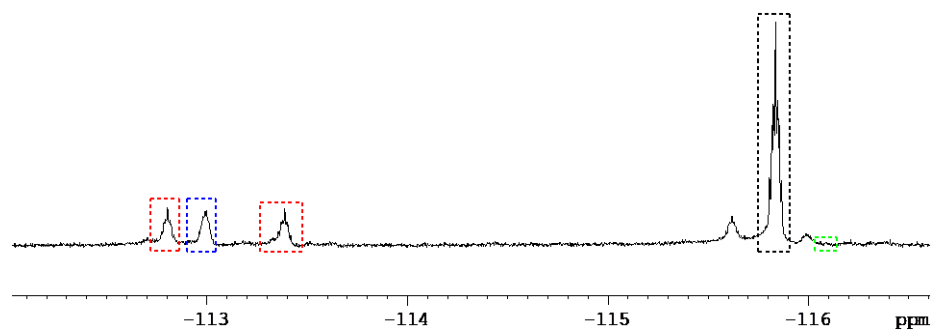
d. After 10 min of 365 nm irradiation:



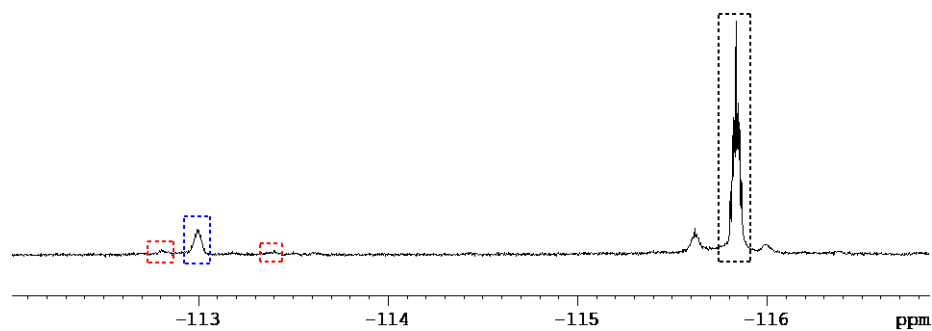
e. PSS (after 24 min of 365 nm irradiation, CF : TC : TT : AP = 32:53:13:2):

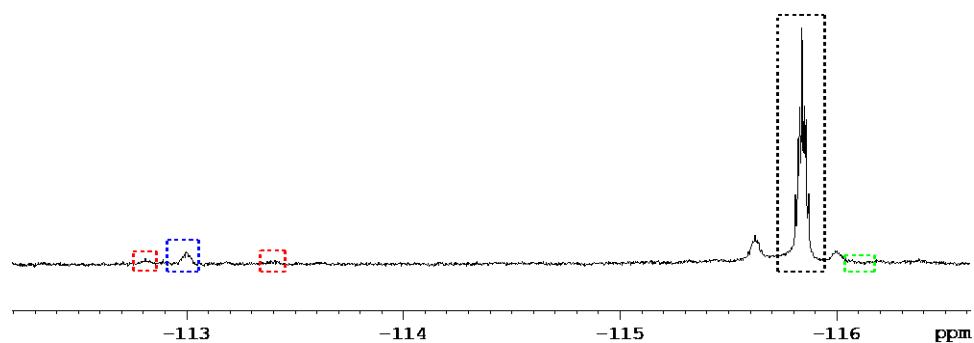
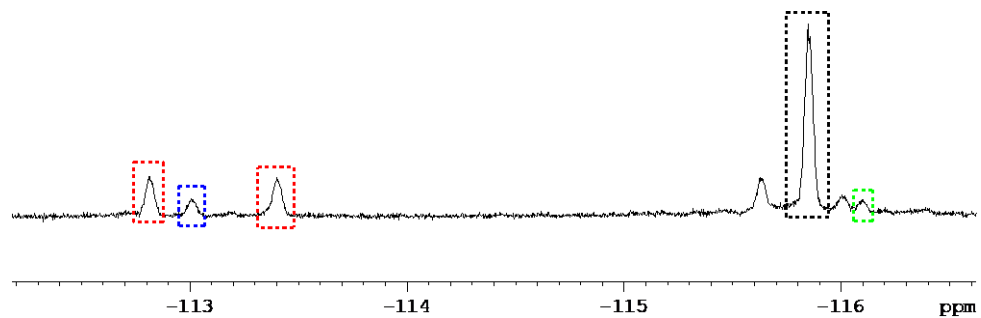
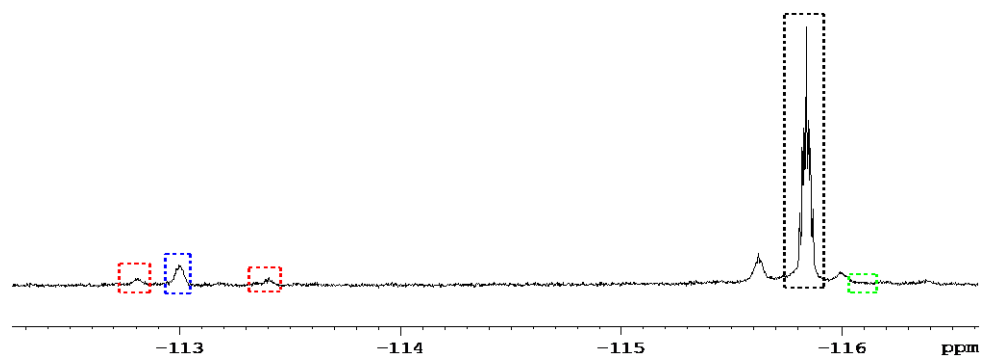
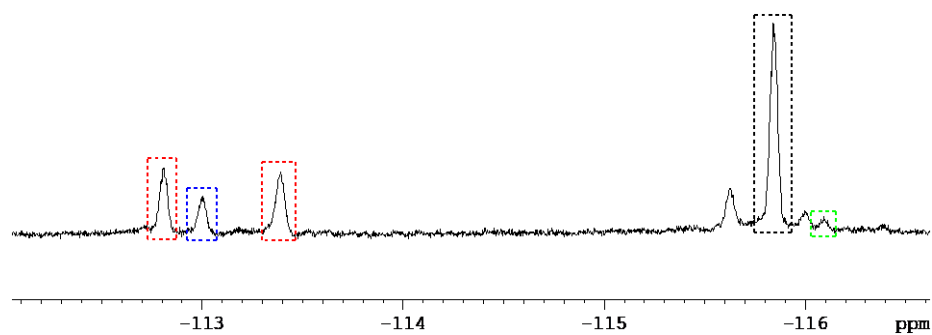


f. After 11 min in the dark (CF : TC : TT : AP = 61:25:13:1):

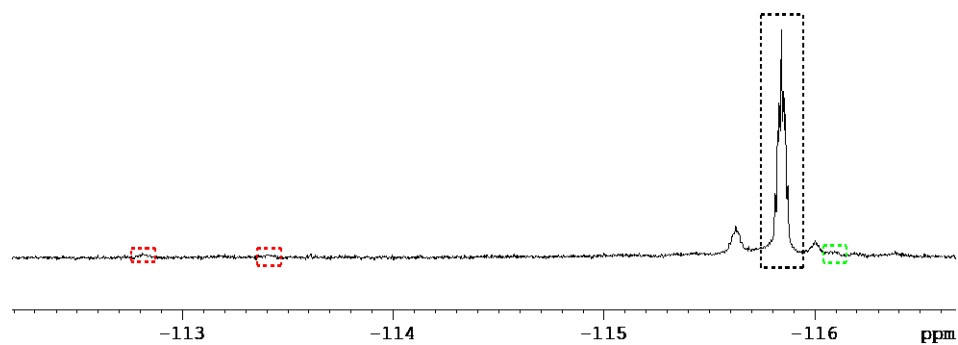


g. After 40 min in the dark (CF : TC : TT : AP = 80:6:14:0):





1. After 11 min of 505 nm irradiation (CF : TC : TT : AP = 92:4:0:4):



9. Reference

- [1] Y. Hirshberg, *Compt. Rend. Acad. Sci., Paris* **1950**, 231, 903.
- [2] H. Bouas-Laurent, H. Dürr, *Pure Appl. Chem.* **2001**, 73, 639.
- [3] J. Fritzsche, *Comptes Rendus Acad. Sci., Paris* **1867**, 69, 1035.
- [4] M. Hänsel, C. Barta, C. Rietze, M. Utecht, K. Rück-Braun, P. Saalfrank, P. Tegeder, *J. Phys. Chem. C* **2018**, 122, 25555.
- [5] S. Kitzig, K. Rück-Braun, *J. Pept. Sci.* **2017**, 23, 567.
- [6] S. Kitzig, M. Thilemann, T. Cordes, K. Rück-Braun, *Chemphyschem* **2016**, 17, 1252.
- [7] M. Vlajić, W. Unger, J. Bruns, K. Rueck-Braun, *Appl. Surf. Sci.* **2019**, 465, 686.
- [8] C. H. de Villeneuve, F. Michalik, J. N. Chazalviel, K. Rück-Braun, P. Allongue, *Adv. Mater.* **2013**, 25, 416.
- [9] H. Tian, Z. Junji (Eds.) *Photochromic materials. Preparation, proprieties and applications*, Wiley, Weinheim (Germany), **2016**.
- [10] H. Dürr, H. Bouas-Laurent (Eds.) *Photochromism. Molecules and Systems*, Elsevier, Amsterdam, Oxford, **2003**.
- [11] R. S. Becker, J. Michl, *J. Am. Chem. Soc.* **1966**, 88, 5931.
- [12] S.-H. Kim, *Functional dyes*, Elsevier, Amsterdam, Boston, **2006**.
- [13] T. T. Herzog, G. Ryseck, E. Ploetz, T. Cordes, *Photochem. Photobiol. Sci.* **2013**, 12, 1202.
- [14] S. Brazevic, S. Nizinski, R. Szabla, M. F. Rode, G. Burdzinski, *Phys. Chem. Chem. Phys.*, **2019**, 21, 11861.
- [15] J. Aubard, F. Maurel, G. Buntinx, O. Poizat, G. Levi, R. Guglielmetti, A. Samat, *Mol. Cryst. Liq. Cryst.* **2000**, 345, 215.
- [16] A. Mukhopadhyay, J. N. Moorthy, *J. Photochem. Photobiol., C* **2016**, 29, 73.
- [17] S. Delbaere, G. Vermeersch, *J. Photochem. Photobiol. A: Chem.*, **2003**, 159, 227.
- [18] S. Delbaere, G. Vermeersch, *Tetrahedron Lett.* **2003**, 44, 259.
- [19] J. Cottam, R. Livingstone, *J. Chem. Soc.*, **1964**, 5228.
- [20] W. D. Cotterill, R. Livingstone, M. V. Walshaw, *J. Chem. Soc. C*, **1970**, 1758.
- [21] R. Livingstone, D. Miller, S. Morris, *J. Chem. Soc.*, **1960**, 5148.
- [22] J. J. Talley, *Synthesis* **1983**, 1983, 845.
- [23] H. G. Heller, J. R. Levell, D. E. Hibbs, D. S. Hughes, M. B. Hursthouse, *Mol. Cryst. Liq. Cryst.* **1997**, 297, 123.
- [24] M. Uchida, M. Irie, *Chem. Lett.* **1991**, 20, 2159.
- [25] M. Uchida, M. Irie, *Chem. Lett.* **1992**, 21, 2257.
- [26] M. Uchida, M. Kume, M. Irie, *BCSJ* **1996**, 69, 1023.
- [27] I. IWAI, J. IDE, *Chem. Pharm. Bull.* **1962**, 10, 926.
- [28] I. IWAI, J. IDE, *Chem. Pharm. Bull.* **1963**, 11, 1042.
- [29] Barry V. Gemert, Maria P. Bergomi, US Patent 5066818, **1991**.
- [30] Tanaka, Aoki, Hosomi, Ohba, *Org. Lett.* **2000**, 2, 2133.
- [31] C. D. Gabbutt, B. M. Heron, A. C. Instone, D. A. Thomas, S. M. Partington, M. B. Hursthouse, T. Gelbrich, *Eur. J. Org. Chem.* **2003**, 2003, 1220.

- [32] C. Moustrou, N. Rebière, A. Samat, R. Guglielmetti, A. E. Yassar, R. Dubest, J. Aubard, *HCA* **1998**, *81*, 1293.
- [33] L. M. Carvalho, A. M.S. Silva, C. I. Martins, P. J. Coelho, A. M.F. Oliveira-Campos, *Tetrahedron Lett.* **2003**, *44*, 1903.
- [34] W. Zhao, E. M. Carreira, *Org. Lett.* **2003**, *5*, 4153.
- [35] P. Appriou, R. Guglielmetti, F. Garnier, *J. Photochem.* **1978**, *8*, 145.
- [36] S. Delbaere, B. Luccioni-Houze, C. Bochu, Y. Teral, M. Campredon, G. Vermeersch, *J. Chem. Soc., Perkin Trans. 2* **1998**, 1153.
- [37] R. Demadrille, A. Rabourdin, M. Campredon, G. Giusti, *J. Photochem. Photobiol. A: Chem.*, **2004**, *168*, 143.
- [38] Z. Wang, Q. Meng, Z. Zhang, D. Fu, W. Zhang, *Tetrahedron* **2011**, *67*, 2246.
- [39] P. J. Coelho, M. A. Salvador, M. M. Oliveira, L. M. Carvalho, *J. Photochem. Photobiol. A: Chem.*, **2005**, *172*, 300.
- [40] S. Han, Y. Chen, *J. Mater. Chem.* **2011**, *21*, 4961.
- [41] M. Zhang, D. Li, Y. He, G. Wang, *Spectrochim. Acta Part A* **2015**, *151*, 525.
- [42] T. Ubukata, Y. Ozawa, M. Saito, K.-i. Hiwatari, Y. Yokoyama, *BCSJ* **2018**, *91*, 563.
- [43] Y. Inagaki, Y. Kobayashi, K. Mutoh, J. Abe, *J. Am. Chem. Soc.* **2017**, *139*, 13429.
- [44] H. Kuroiwa, Y. Inagaki, K. Mutoh, J. Abe, *Adv. Mater.* **2019**, *31*, e1805661.
- [45] F. Ortica, P. Smimmo, G. Favaro, U. Mazzucato, S. Delbaere, D. Venec, G. Vermeersch, M. Frigoli, C. Moustrou, A. Samat, *Photochem. Photobiol. Sci.* **2004**, *3*, 878.
- [46] B. A. Versaw, M. E. McFadden, C. C. Husic, M. J. Robb, *Chem. Sci.* **2020**, *11*, 4525.
- [47] G. Harié, A. Samat, R. Guglielmetti, D. de Keukeleire*, W. Saeyens, I. van Parys, *Tetrahedron Lett.* **1997**, *38*, 3075.
- [48] S. Delbaere, G. Vermeersch, *J. Photochem. Photobiol., C* **2008**, *9*, 61.
- [49] S. Delbaere, J.-C. Micheau, Y. Teral, C. Bochu, M. Campredon, G. Vermeersch, *Photochem. Photobiol.* **2001**, *74*, 694.
- [50] X. Sallenave, S. Delbaere, G. Vermeersch, A. Saleh, J.-L. Pozzo, *Tetrahedron Lett.* **2005**, *46*, 3257.
- [51] D. Venec, S. Delbaere, J. C. Micheau, M. Frigoli, C. Moustrou, A. Samat, G. Vermeersch, *J. Photochem. Photobiol. A: Chem.*, **2006**, *181*, 174.
- [52] D. Venec, S. Delbaere, J. C. Micheau, M. Frigoli, C. Moustrou, A. Samat, G. Vermeersch, *J. Photochem. Photobiol. A: Chem.*, **2006**, *183*, 70.
- [53] J. Berthet, P. J. Coelho, L. M. Carvalho, G. Vermeersch, S. Delbaere, *J. Photochem. Photobiol. A: Chem.*, **2009**, *208*, 180.
- [54] M. Frigoli, F. Maurel, J. Berthet, S. Delbaere, J. Marrot, M. M. Oliveira, *Org. Lett.* **2012**, *14*, 4150.
- [55] O. A. Fedorova, A. N. Sergeeva, P. A. Panchenko, Y. V. Fedorov, F. G. Erko, J. Berthet, S. Delbaere, *J. Photochem. Photobiol. A: Chem.*, **2015**, *303-304*, 28.
- [56] Diana Liebmman, *PhD Thesis*, Technischen Universität Berlin, Germany, **2014**.
- [57] S. Aldoshin, I. Chuev, A. Utenyshev, O. Filipenko, J. L. Pozzo, V. Lokshin, R. Guglielmetti, *Acta Cryst. C* **1996**, *52*, 1834.
- [58] C. D. Gabbutt, T. Gelbrich, J. D. Hepworth, B.M. Heron, M. B. Hursthouse, S. M. Partington, *Dyes and Pigments* **2002**, *54*, 79.
- [59] H.-M. Huang, Y. Ding, P.-L. Chen, J.-B. Meng, *Acta Cryst. C* **2004**, *60*, o709.

- [60] B. P. Birukov, B. V. Unkovskij, *kristallokhimia* **1976**, *11*, 132.
- [61] A. C. Instone, *Ph.D Thesis*, University of Leeds, UK, **2004**.
- [62] C. Böttcher, G. Zeyat, S. A. Ahmed, E. Irran, T. Cordes, C. Elsner, W. Zinth, K. Rueck-Braun, *Beilstein J. Org. Chem.* **2009**, *5*, 25.
- [63] K. Arai, Y. Kobayashi, J. Abe, *Chem. Commun.* **2015**, *51*, 3057.
- [64] J. Griffiths, *Dye & pigment chemistry*, Dept. of Colour Chemistry, Leeds, **1999**.
- [65] B. Mark Heron, C. D. Gabbutt, A. C. Instone, *HETEROCYCLES* **2003**, *60*, 843.
- [66] C. D. Gabbutt, B. M. Heron, A. C. Instone, P. N. Horton, M. B. Hursthouse, *Tetrahedron* **2005**, *61*, 463.
- [67] J. C. Crano, T. Flood, D. Knowles, A. Kumar, B. Van Gemert, *Pure Appl. Chem.* **1996**, *68*, 1395.
- [68] X. Sallenave, S. Delbaere, G. Vermeersch, J.-L. Pozzo, *J. Phys. Org. Chem.* **2007**, *20*, 872.
- [69] P. Bamfield, M. G. Hutchings, *Chromic phenomena. Technological applications of colour chemistry / Peter Bamfield and Michael G. Hutchings*, Royal Society of Chemistry, Cambridge, **2018**.
- [70] S. Kobatake, M. Irie, *Annu. Rep. Prog. Chem., Sect. C* **2003**, *99*, 277.
- [71] S. Nigel Corns, S. M. Partington, A. D. Towns, *Color. Technol.* **2009**, *125*, 249.
- [72] I. Kahle, O. Tröber, H. Richter, S. Spange, *New J. Chem.* **2013**, *37*, 1479.
- [73] A. Yassar, F. Garnier, H. Jaafari, N. Rebière-Galy, M. Frigoli, C. Moustrou, A. Samat, R. Guglielmetti, *Appl. Phys. Lett.* **2002**, *80*, 4297.
- [74] S. V. Paramonov, V. Lokshin, O. A. Fedorova, *J. Photochem. Photobiol., C* **2011**, *12*, 209.
- [75] M. J. Robb, T. A. Kim, A. J. Halmes, S. R. White, N. R. Sottos, J. S. Moore, *J. Am. Chem. Soc.* **2016**, *138*, 12328.
- [76] I. Kahle, O. Tröber, S. Trentsch, H. Richter, B. Grünler, S. Hemeltjen, M. Schlesinger, M. Mehring, S. Spange, *J. Mater. Chem.* **2011**, *21*, 5083.
- [77] S. A. Ahmed, X. Sallenave, F. Fages, G. Mieden-Gundert, W. M. Müller, U. Müller, F. Vögtle, J.-L. Pozzo, *Langmuir* **2002**, *18*, 7096.
- [78] R. Pardo, M. Zayat, D. Levy, *Chem. Soc. Rev.* **2011**, *40*, 672.
- [79] M. Frigoli, G. H. Mehl, *Chem. Commun.* **2004**, 2040.
- [80] J. N. Moorthy, S. Mandal, A. Mukhopadhyay, S. Samanta, *J. Am. Chem. Soc.* **2013**, *135*, 6872.
- [81] J. Yang, *Org. Biomol. Chem.* **2015**, *13*, 1930.
- [82] A. Dey, S. Agasti, D. Maiti, *Org. Biomol. Chem.* **2016**, *14*, 5440.
- [83] R. J. Phipps, M. J. Gaunt, *Science (New York, N.Y.)* **2009**, *323*, 1593.
- [84] D. Leow, G. Li, T.-S. Mei, J.-Q. Yu, *Nature* **2012**, *486*, 518.
- [85] Y.-F. Yang, G.-J. Cheng, P. Liu, D. Leow, T.-Y. Sun, P. Chen, X. Zhang, J.-Q. Yu, Y.-D. Wu, K. N. Houk, *J. Am. Chem. Soc.* **2014**, *136*, 344.
- [86] M. Bera, S. Agasti, R. Chowdhury, R. Mondal, D. Pal, D. Maiti, *Angew. Chem. Int. Ed.* **2017**, *56*, 5272.
- [87] M. Bera, A. Maji, S. K. Sahoo, D. Maiti, *Angew. Chem. Int. Ed.* **2015**, *54*, 8515.
- [88] M. Bera, A. Modak, T. Patra, A. Maji, D. Maiti, *Org. Lett.* **2014**, *16*, 5760.
- [89] G.-J. Cheng, Y.-F. Yang, P. Liu, P. Chen, T.-Y. Sun, G. Li, X. Zhang, K. N. Houk, J.-Q. Yu, Y.-D. Wu, *J. Am. Chem. Soc.* **2014**, *136*, 894.
- [90] H.-X. Dai, G. Li, X.-G. Zhang, A. F. Stepan, J.-Q. Yu, *J. Am. Chem. Soc.* **2013**, *135*, 7567.
- [91] Z. Fan, K. L. Bay, X. Chen, Z. Zhuang, H. S. Park, K.-S. Yeung, K. N. Houk, J.-Q. Yu, *Angew. Chem. Int. Ed.* **2020**, *59*, 4770.

- [92] S. Lee, H. Lee, K. L. Tan, *J. Am. Chem. Soc.* **2013**, *135*, 18778.
- [93] S. Li, L. Cai, H. Ji, L. Yang, G. Li, *Nat. Commun.* **2016**, *7*, 10443.
- [94] S. Li, H. Ji, L. Cai, G. Li, *Chem. Sci.* **2015**, *6*, 5595.
- [95] A. Maji, B. Bhaskararao, S. Singha, R. B. Sunoj, D. Maiti, *Chem. Sci.* **2016**, *7*, 3147.
- [96] R.-J. Mi, J. Sun, F. E. Kühn, M.-D. Zhou, Z. Xu, *Chem. Commun.* **2017**, *53*, 13209.
- [97] R.-J. Mi, Y.-Z. Sun, J.-Y. Wang, J. Sun, Z. Xu, M.-D. Zhou, *Org. Lett.* **2018**, *20*, 5126.
- [98] A. Modak, A. Mondal, R. Watile, S. Mukherjee, D. Maiti, *Chem. Commun.* **2016**, *52*, 13916.
- [99] T. Patra, R. Watile, S. Agasti, T. Naveen, D. Maiti, *Chem. Commun.* **2016**, *52*, 2027.
- [100] R.-Y. Tang, G. Li, J.-Q. Yu, *Nature* **2014**, *507*, 215.
- [101] T. Truong, O. Daugulis, *Angew. Chem. Int. Ed.* **2012**, *51*, 11677.
- [102] L. Wan, N. Dastbaravardeh, G. Li, J.-Q. Yu, *J. Am. Chem. Soc.* **2013**, *135*, 18056.
- [103] H.-J. Xu, Y.-S. Kang, H. Shi, P. Zhang, Y.-K. Chen, B. Zhang, Z.-Q. Liu, J. Zhao, W.-Y. Sun, J.-Q. Yu et al., *J. Am. Chem. Soc.* **2019**, *141*, 76.
- [104] H.-J. Xu, Y. Lu, M. E. Farmer, H.-W. Wang, D. Zhao, Y.-S. Kang, W.-Y. Sun, J.-Q. Yu, *J. Am. Chem. Soc.* **2017**, *139*, 2200.
- [105] J. Xu, J. Chen, F. Gao, S. Xie, X. Xu, Z. Jin, J.-Q. Yu, *J. Am. Chem. Soc.* **2019**, *141*, 1903.
- [106] G. Yang, P. Lindovska, D. Zhu, J. Kim, P. Wang, R.-Y. Tang, M. Movassaghi, J.-Q. Yu, *J. Am. Chem. Soc.* **2014**, *136*, 10807.
- [107] Y.-F. Yang, G.-J. Cheng, P. Liu, D. Leow, T.-Y. Sun, P. Chen, X. Zhang, J.-Q. Yu, Y.-D. Wu, K. N. Houk, *J. Am. Chem. Soc.* **2014**, *136*, 344.
- [108] J. Luo, S. Preciado, I. Larrosa, *J. Am. Chem. Soc.* **2014**, *136*, 4109.
- [109] O. Saidi, J. Marafie, A. E. W. Ledger, P. M. Liu, M. F. Mahon, G. Kociok-Köhn, M. K. Whittlesey, C. G. Frost, *J. Am. Chem. Soc.* **2011**, *133*, 19298.
- [110] M. T. Mihai, H. J. Davis, G. R. Genov, R. J. Phipps, *ACS Catal.* **2018**, *8*, 3764.
- [111] H. Chen, P. Wedi, T. Meyer, G. Tavakoli, M. van Gemmeren, *Angew. Chem. Int. Ed.* **2018**, *57*, 2497.
- [112] B. Large, D. Prim, *Synthesis* **2020**, *52*, 2600.
- [113] P. Jiang, F. Li, Y. Xu, Q. Liu, J. Wang, H. Ding, R. Yu, Q. Wang, *Org. Lett.* **2015**, *17*, 5918.
- [114] S. Prévost, *ChemPlusChem* **2020**, *85*, 476.
- [115] S. Okumura, S. Tang, T. Saito, K. Semba, S. Sakaki, Y. Nakao, *J. Am. Chem. Soc.* **2016**, *138*, 14699.
- [116] Y. Nakao, S. Okumura, T. Ebara, K. Semba, *HETEROCYCLES* **2019**, *99*, 1128.
- [117] M. Zhang, A. Luo, Y. Shi, R. Su, Y. Yang, J. You, *ACS Catal.* **2019**, *9*, 11802.
- [118] H. A. Duong, R. E. Gilligan, M. L. Cooke, R. J. Phipps, M. J. Gaunt, *Angew. Chem. Int. Ed.* **2011**, *50*, 463.
- [119] B. Li, S.-L. Fang, D.-Y. Huang, B.-F. Shi, *Org. Lett.* **2017**, *19*, 3950.
- [120] G. Li, P. Gao, X. Lv, C. Qu, Q. Yan, Y. Wang, S. Yang, J. Wang, *Org. Lett.* **2017**, *19*, 2682.
- [121] P.-X. Ling, K. Chen, B.-F. Shi, *Chem. Commun.* **2017**, *53*, 2166.
- [122] H. Shi, P. Wang, S. Suzuki, M. E. Farmer, J.-Q. Yu, *J. Am. Chem. Soc.* **2016**, *138*, 14876.
- [123] Z. Jin, L. Chu, Y.-Q. Chen, J.-Q. Yu, *Org. Lett.* **2018**, *20*, 425.
- [124] J. Wu, D. Zhang, L. Chen, J. Li, J. Wang, C. Ning, N. Yu, F. Zhao, D. Chen, X. Chen et al., *J. Med. Chem.* **2013**, *56*, 761.

- [125] X. Chen, J. Klöckner, J. Holze, C. Zimmermann, W. K. Seemann, R. Schrage, A. Bock, K. Mohr, C. Tränkle, U. Holzgrabe et al., *J. Med. Chem.* **2015**, *58*, 560.
- [126] N. Furukawa, T. Inoue, T. Aida, S. Oae, *J. Chem. Soc., Chem. Commun.* **1973**, 212a.
- [127] K. Omura, D. Swern, *Tetrahedron* **1978**, *34*, 1651.
- [128] H.-X. Dai, G. Li, X.-G. Zhang, A. F. Stepan, J.-Q. Yu, *J. Am. Chem. Soc.* **2013**, *135*, 7567.
- [129] L. Zhang, Y. Wang, Y. Shi, Y. Wu, J. Lan, W. Ma, J. You, *ACS Catal.* **2019**, *9*, 5358.
- [130] S. Swaminathan, K. V. Narayanan, *Chem. Rev.* **1971**, *71*, 429.
- [131] W. Zhao, E. M. Carreira, *Org. Lett.* **2003**, *5*, 4153.
- [132] B. A. Versaw, M. E. McFadden, C. C. Husic, M. J. Robb, *Chem. Sci.* **2020**, *11*, 4525.
- [133] A. J. A. Aquino, D. Tunega, G. Haberhauer, M. H. Gerzabek, H. Lischka, *J. Phys. Chem. A* **2002**, *106*, 1862.
- [134] D. Venec, S. Delbaere, J. C. Micheau, M. Frigoli, C. Moustrou, A. Samat, G. Vermeersch, *J. Photochem. Photobiol. A: Chem.*, **2006**, *183*, 70.
- [135] F. Maurel, S. Delbaere, S. L. Truong, T. Couesnon, R. Dubest, G. Vermeersch, J. Aubard, *J. Phys. Org. Chem.* **2007**, *20*, 944.
- [136] S. Delbaere, J.-C. Micheau, G. Vermeersch, *J. Org. Chem.* **2003**, *68*, 8968.
- [137] M. Vlajić, J. Schmidt, A. Thomas, K. Rück-Braun, *ChemPhotoChem* **2018**, *2*, 952.
- [138] K. Endo, R. H. Grubbs, *J. Am. Chem. Soc.* **2011**, *133*, 8525.
- [139] C. Feldmeier, H. Bartling, E. Riedle, R. M. Gschwind, *J. Magn. Reson.* **2013**, *232*, 39.

Acknowledgements

First and foremost I would like to thank my supervisor Prof. Dr. Karola Rück-Braun, for providing me an opportunity to undertake interesting research in her group. She always gave me instructive advice and helpful suggestions during the whole study period. I thank her for her patient guidance and prompt response to my questions. I am so lucky to be a PhD student of her and I will benefit a lot from her profound knowledge and this experience.

I thank Prof. Dr. Bernd Schmidt for accepting the role of the second examiner.

I thank Prof. Dr. Michael Gradzielski for accepting the role of the chairman of the examination committee.

I would also like to thank all employees of the analytic centers of the Institut für Chemie, Technische Universität Berlin for their excellent work and strong support. I would like to thank Dr. Sebastian Kemper and Ms. Samantha Voges for their professional help with the NMR spectrometer. I thank Dr. Maria Schlangen and Mr. Marc Griffel for the measurements on Mass analysis. In addition, I would like to thank Ms. Barbara-Cornelia Fischer and Ms. Juana Krone for the IR and elemental analysis measurements.

I would like to thank all the members of the Rück-Braun group for their support and help. I thank Gregor, Tino, Sebastian and Pierre for useful discussion, friendly help and interesting chatting. I thank Miro for the introduction of the institute. I thank Nandor and Marina for the introduction of the UV/Vis measurements. I thank Junjie for chatting with me in Chinese and having fun together after work. I would also like to thank Christoph for his introduction of naphthopyrans. I thank my master students: Philipp and Toan. Moreover, I am grateful to have memorable lunch time with Gregor, Tino, Sebastian, Nandor, Philipp, Marie, Vale und Pierre®. I will miss the happy parties together with them before Coronavirus, and I hope I can drink Glühwein with them again during the Christmas after the disappearance of Coronavirus.

I would like to thank my family, my friends and my wife. 感谢我的爸爸，祁勇；感谢我的妈妈，丁继武；感谢我的老婆许聪慧的支持与陪伴，爱你么么哒。另外，我还要感谢我的其他亲戚朋友的支持和帮助，谢谢你们。

Finally, I would like to thank the China Scholarship Council (CSC) for the financial support with grant No. 201606360126. I would also like to thank the financial support from the STIBET program of Technische Universität Berlin and the DAAD.